UNIVERSITY OF SOUTHAMPTON

ABSTRACT

FACULTY OF ENGINEERING, SCIENCE & MATHEMATICS
SCHOOL OF CHEMISTRY

Doctor of Philosophy

SUPRAMOLECULAR APPROACHES TO CRYORELAXORS FOR BIOLOGICAL NMR STUDIES

Francesco Cuda

The work reported in this thesis concerns the development of Cryorelaxors having potential applications in very low temperature NMR studies of biological materials. Two approaches have been explored, namely calixarene host-guest complexes incorporating rotationally labile methyl groups, and endohedral fullerene complexes.

The first chapter provides an overview of the background of the project and of potential approaches to the problem of low temperature relaxation agents, particularly those based on supramolecular systems. The next chapter describes the preparation, characterization, and studies of the behaviour of calixarene complexes incorporating potentially freely rotating guests. Ten calixarene complexes have been prepared and characterised by X-ray structural studies and their relaxation behaviour has been investigated using a variety of techniques including MAS and Field Cycling NMR experiments and Inelastic Neutron Scattering spectroscopy. Crystallographically disordered methyl-group environments have been identified in a number of cases and their proton spin-lattice relaxation behaviour has been shown to be strongly dependent on the thermal history of the sample. NMR studies of samples of partially deuterated calixarene complexes reveal a systematic reduction in T_1 at low temperatures with higher levels of deuteration of the system studied, the p-*iso*-propylcalix[4]arene (2:1) p-xylene complex has been shown to have the best relaxation properties. Synthetic strategies towards calixarene and fullerenes complexes bearing active biological anchors are also discussed. The third chapter describes an investigation of the Komatsu route to the endohedral fullerene complex $H_2@C_{60}$ and the structural characterization of one of the key intermediates in this process. The fourth chapter give a brief overview the results obtained and the final chapter details of the experimental work undertaken. Appendices are also included containing full details of the X-ray structural studies and mathematical models.

Acknowledgments

In my country (Italy) a PhD is a dream not possible for all so, to get a PhD position for 4 years was an amazing experience for me. Firstly, Thank you Martin, always kind and ready to give useful advices and encouragement, this project was not easy.

Special thanks to Malcolm and all is staff: Salvatore, Marina, Ole, Peppe, Maria, Sergey and Michael to wait the preparation of my samples and give me useful advices. Special thanks to Tony Horsewill from Nottingham and Panesar Kuldeep to provide Field Cycling measurements.

Thanks to all the other members of the Cryo-MAS consortium; Prof. Peter Henderson and Simon Patching for the biological tests and all the engineering staff. Thanks to the many friendly faces around the department who have helped me during my PhD (in various different ways): John Langley, Julie Herniman to spend a long time listen my problems, Neil Wells and John Street.

To all those in the Martin's group: special thanks to my post-doc, Alain Danquigny he was always kind and patience with me; Alex, Georgie, Jon, Alan, Polski, Andrew, and Richard. Special thanks to Mark Light, it was really a nightmare for him to resolve my structure. Tanks a lot to Dr. James Orton to resolve my deuterated crystal structures a real challenge.

Apologies to all that I have missed, I am sure that there are many but before I move on I'd like to offer special thanks to my old supervisor in Dr. Stefano Roelens who teaching me for a long time in Florence. Thanks a lot to my Prof. Armando De Cicco who follows me during my undergraduate studies as special tutor. Special thanks to my secondary school Prof. Brandolini Edwige that put the chemistry in my heart, giving the knowledge and the force to arrive at this level: she is still my reference.

With loving thanks to my Mum and sister to understanding and support me during my time at University....a really long journey. Lastly, special thank to my wife Michela for its patience and to get sense in my life in a *very* special way.

Table of Contents

Additional supporting data

Appendix A: Crystallographic data

X-ray crystallographic data

p-*tert*-butylcalix[4]arene (1:1) toluene complex

p-*tert*-butylcalix[4]arene (1:1) picoline complex

p-*tert*-butylcalix[4]arene (1:1) 4-fluorotoluene complex

p-*tert*-butylcalix[4]arene (1:1) 4-chlorotoluene complex

p-*tert*-butyl_d_{36} calix[4]arene toluene (1:1) complex [only CIF]

p-*iso*-propylcalix[4]arene (2:1) p-xylene complex

p-*iso*-propylcalix[4]arene (1:1) iodomethane complex

p-*iso* -propylcalix[4]arene (1:1) 2-butyne complex

p-*tert*-butylcalix[4]arene-tetracarbonate (1:1)
nitromethane complex

p-*tert*-butylcalix[4]arene-Biscrown3 (1:1)
acetonitrile complex

Open-cage 13-membered-ring SO_3 (H_2@13mSO_3)

Appendix B: Other compounds

p-*tert*-butyl-[25,27-bis(maleonylmethylcarbonyl-aminoethoxy
ethyl]-26,28-dihydroxycalix[4]arene

p-*tert*-butyl-[25,27-bis(2,6-pyridine-acetamidobutoxy)dihydroxy
calix[4]arene methylpyridinium

Appendix C: The rationale behind the deuteration of calixarene molecule

Appendix D: Field–cycling NMR experiments

Field-cycling NMR technique

Mono-exponential and bi-exponential models

Effect of thermal history on T1

Appendix E: Solid state NMR spectrum

Appendix F: Publications, presentation and prices

1 Introduction

1.1 Background to project

Nuclear magnetic resonance, is a powerfull spectroscopical technique discovered by Bloch and Purcell in 1946[1], used in different fields of contemporary science, medicine and industry. The NMR represents an excellent tool in the investigation of fundamental and applied chemistry, from simplest organic molecules to complex molecular systems such as proteins. Among these techniques, magic-angle-spinning solid-state NMR is a primary tool for molecular structural studies of the many important systems which can neither be crystallized nor dissolved. Solid state NMR[2] has made many technological advances recently, and is now able to provide detailed molecular structural information on a wide range of complex solid systems, such as complete protein structures[3] (e.g. a study of the molecular structure of the protein fibrils responsible for plaque formation in Alzaheimer's disease[4]) and relaxometry NMR studies for the molecular dynamics of supramolecular systems in the solid state[5]. Unfortunately, solid state NMR is greatly limited by its poor sensitivity. At ordinary temperatures solid state NMR requires at least 100 nanomoles of substance and, in many cases, this material must be labelled with NMR active isotopes such as ^{13}C and ^{15}N. For a protein of typical size (40 kDa) this requires the preparation of at least 4 mg of isotopically-labelled material. Although the synthesis of this amount of substance is feasible for some systems it is always laborious and expensive and can be impossible for most interesting proteins which don't express well in bacterial media. A 10-fold increase in signal would require the preparation of 10 times less material, leading approximate 100-fold increase in the applicability of the method. Many methods have been proposed for increasing the sensitivity of NMR. There are numerous *hyperpolarization* schemes available which can generate nuclear spin polarization far excess of their thermal equilibrium state values, but most of them are highly system-specific. For example, optical pumping of noble gas atoms is widely applied for the NMR imaging[6] of gas-filled cavities, but transfer of polarization from noble gas nuclei to other systems has proved to be exceedingly difficult. The most general method is *dynamic nuclear polarization (DNP)*[7] which involves doping of material of interest with paramagnetic agents. This method is capable of large nuclear spin polarizations, but has strong magnetic field limitations; at the moment DNP has

been demonstrated at magnetic fields up to 9 tesla, which is generally insufficient to resolve the spectra of most macromolecules.

However, the equilibrium nuclear spin magnetization obeys the Curie law and is proportional to the inverse of the absolute temperature. The sensitivity of NMR can be enhance by factor of around 30 cooling the sample from room temperature to cryogenic temperature[8]. At this temperature the relaxation process of the nuclear spin magnetization become much less efficient and in extreme cases the magnetization-build up can became so sluggish that experiments cannot be performed in a reasonable time. As discussed before, one method for enhancing nuclear spin relaxation is by paramagnetic doping[9], but this produces undesirable line-broadening effects, and their behaviour is highly field and temperature-dependent. This problem could be resolved by new classes of molecules called Cryorelaxors[10] which have hydrogen or methyl groups capable of rapid rotation at cryogenic temperatures. This rapid motion acts as an agent for the relaxation of the molecular surroundings.

1.1.1 Cryorelaxors

Cryorelaxors are robust agents that can be brought into intimate contact with the molecules of interest and which enhance their relaxation rates at cryogenic temperatures. One potentially ideal molecular system would be a fullerene C_{60} cage inside which hydrogen molecules (H_2) have been introduced which are free to rotate.

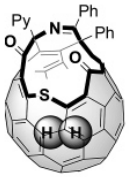

Figure 1 H_2@ATOCF

Figure 2 $H_2@C_{60}$

Hydrogen molecules have lowest moment of inertia of any molecule and rotate very rapidly even at cryogenic temperatures. This rapid motion acts as an agent for the relaxation of the molecular surroundings, while the robust cage protects the molecular rotor from external interference. Levitt and co-workers[11] have demonstrated that the relaxation of hydrogen is very rapid at cryogenic temperatures, so this data strongly supports the cryorelaxor concept. Supramolecular complexes in which a series of

methyl-substituted arene derivatives are contained within a molecular bucket/cavity such as calixarene could also be potential cryorelaxors[12] (Figure 3).

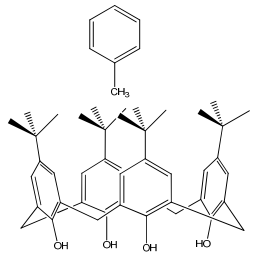

Figure 3 p-*tert*-butylcalix[4]arene (1:1) toluene complex

In this case the cavity rotor will act as a cryorelaxor for neighbouring molecules. For this complex Caciuffo and co-workers have shown that, at low temperatures, the torsional motions of the toluene methyl group is very close to the limit of a quantum free rotor[12] Alternative systems involving methyl-group based cryorelaxors include a scaffold in which a molecular group such as methyl substituent is located in a robust molecular cavity thereby providing an environment in which rapid rotation can occur. Dimethylanthracene derivatives (e.g. Fig. 4) reported from Toda and co-workers[13] are also expected to have interesting properties in this context.

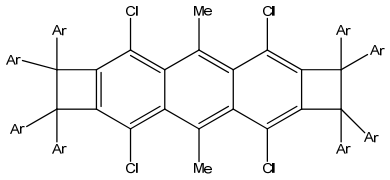

Figure 4 Dimethylanthracene derivatives [ref. 13]

In this case the central methyl groups are expected to rotate freely and act as cryorelaxors since they are screened from the external environment by the large terminal aryl groups. 4-Methyl-pyridine forms a similar cavity-rotor in the solid state [14](Figure 5).

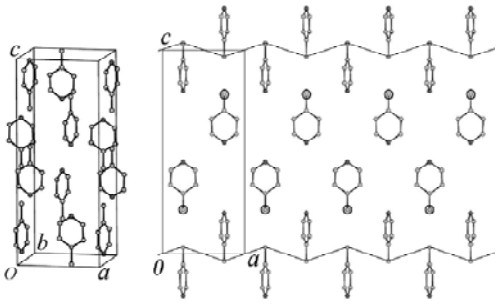

Figure 5 Crystal structure of 4-methylpyridine [ref. 14]

Here the methyl rotors are organized in multiple chains with rotational axes parallel to the *c* crystal axis[14]. The crystal symmetry inhibits coupling between equivalent chains parallel to either the *a* or *b* axis. In such situations an additional NMR signal enhancement is observed at cryogenic temperatures called *Haupt effect* (see section 1.1.3.8) and this has indeed been reported for this structure.

1.1.2 Other approach to cryorelaxors problem

1.1.2.1 Supramolecular architectures

Substantial progress has been made during these years involving the design of new molecular architectures able to recognize metal cations and/or neutral molecules by artificial cavity. Complexation of specific target by high selectivity is the major challenge for the scientists, opening a new development in supramolecular chemistry: "chemistry inside the cage". Other systems with internal cavities able to accommodate neutral and charged molecules include larger fullerenes[15], cyclodextrins[16], cucurbituril cages[17], calixpyrroles[18,19] and other artificial cages[20,21].

Larger fullerenes: the Hydrogen Fullerene C_{70} complex

Recently Komatsu and co-workers[15] using a chemical surgery have prepared a complex in which one and two hydrogen molecules are trapped inside the cage of fullerenes C_{70} (Figure 6).

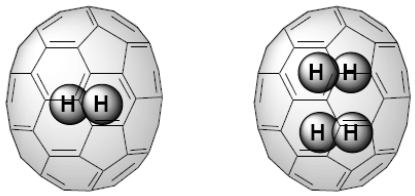

Figure 6 Hydrogen fullerene C_{70} complex [ref. 15]

Recent studies of the T_1 relaxation time of the hydrogen molecule inside a larger fullerene cage (e.g. fullerene C_{70}) is very rapid and shorter rather than inside fullerene C_{60} at cryogenic temperature[22] .

Cyclodextrins

Cyclodextrins are cyclic oligosaccharides composed of 6 to 8 α-D-glucopyranoside units linked by 1,4 bond, as in amylose. The production of these involves treatment of ordinary starch with a set of enzymes (e. g. *Bacillus Macerans*), containing the *cyclodextrin glycosyltransferase* (CGTase)[16]. CGTase is able to synthesize all different cyclodextrins α, β, γ, but the ratios are strictly dependent on the enzyme used (Figure 7).

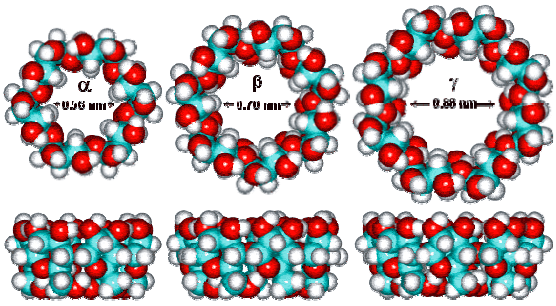

Figure 7 α, β, and γ-Cyclodextrin structures [ref. 16]

Cyclodextrins have a typical basket shape bearing on the larger and smaller openings cavity respectively secondary and primary hydroxyl groups. These hosts are water soluble as a result of the oxygen-rich external surface. The internal cavity of the basket is not entirely hydrophobic, but is significantly less hydrophilic than the aqueous environment and thus is able to host other hydrophobic molecules (Figure 8).

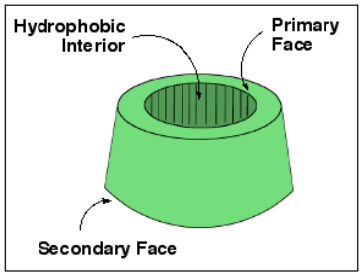

Figure 8 Cyclodextrin structure [ref. 16]

The physical and chemical properties of the guest molecule are deeply modified by the inclusion inside the cavity, principally in terms of water solubility. This property has speedup the interest in many fields, especially in development of pharmaceutical formulations, because are able to penetrate body tissues. These can release biologically active compounds under specific conditions. However significant studies on crystalline cyclodextrin inclusion compounds formed with aromatic guests have

been have been reported from Tonelli and co-workers[23]. They have studied a series of solid γ-cyclodextrin complexes containing the aromatic guests aniline, benzene, ethyl-benzene, phenol p-xylene styrene and toluene. γ-Cyclodextrin can be divided in two classes of crystal motifs: a *"cage"* and a *"channel"* (Figure 9)[24].

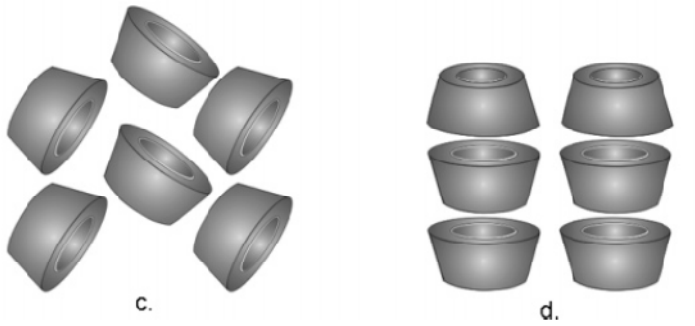

Figure 9 γ-cyclodextrin (c) Cage structure (d) channel structure [ref. 23]

In the "*cage"* structure the γ-CD molecules have a herringbone arrangement where each γ-CD cavity is blocked by a neighboring γ-CD Fig (c). In the "*channel"* structure the molecules are stacked on top of each other to form extensive cylindrical channels in which guest molecules can reside. They have found that all the aromatic guest γ-CD complex favour a channel-type crystal structure with (1:1) molar ratio inclusion complex for p-xylene and toluene. Torre and co-workers[25] have reported an inclusion complex of γ-CD with 4-methylpyridine.

Cucurbiturils

Cucurbituril is a particular name given to the pumpkin-shaped macrocyclic hexamer obtained formed by the condensation reaction between glycoluril and formaldehyde[17] These compounds are also molecular containers that are capable of binding other molecules within their cavities (Figure 10)

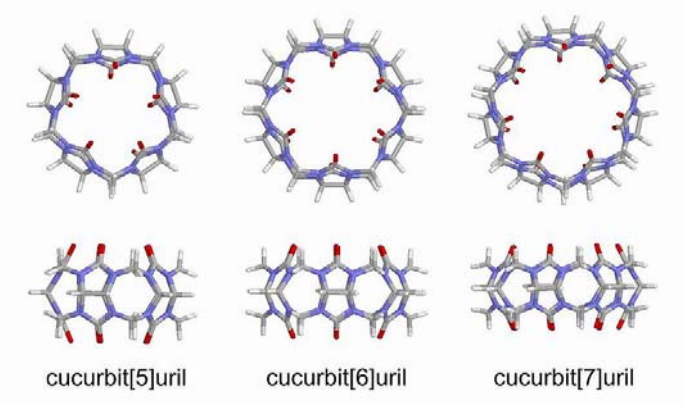

Figure 10 Cucurbituril structures [ref. 17]

In 1984 Freeman published[26,27] the crystal structure of the first host-guest complex of cucurbit[6]uril which incorporated the p-xylenediammonium cation into the macrocycle's cavity (Figure 11a).

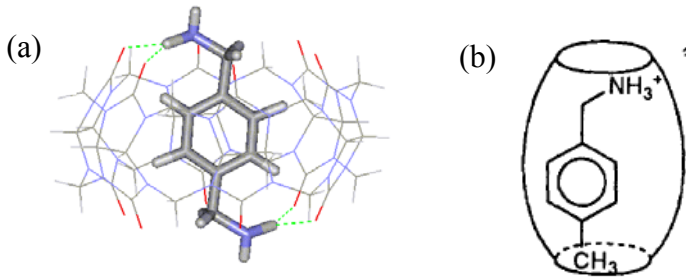

Figure 11 Cucurbituril complexes a) with p-xylenediammonium cation b) with 4-methylbenzylammonium ion [ref. 26,27]

Knoche and co-workers[28] have also reported a cucurbituril complex with 4-methylbenzylammonium ion (Figure 11b). In this study two different complexes were explored: i) An association complex where the ammonium group binds the one of the polar portals of cucurbituril and the hydrophobic part extends into the solvent; ii) an inclusion complex where the hydrophobic part extends into the cavity of cucurbituril.

Calix[4]pyrroles

Calixpyrroles are macrocycles formed of pyrrole rings connected through the pyrrolic 2 and 5 positions by sp^3 carbon atoms (Figure 12). Although known for over a century, their binding properties only recently were recognized and extensively explored by Sessler and co-workers[18,29]

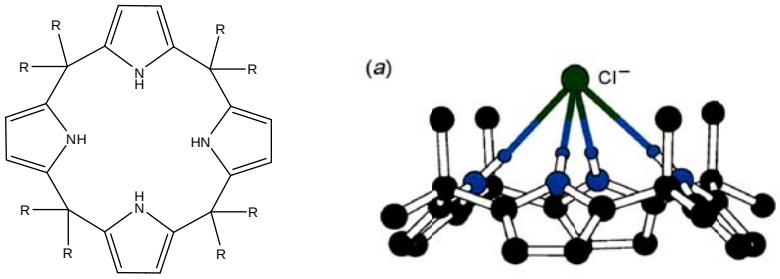

Figure 12 Calixpyrrole and crystal structure complexed with chlorine ion [ref. 30]

In this system there is no possibility to create hydrogen bonding between the different pyrrolic NH group, thus in absence of an added substrate there is no propensity for the free macrocycles to adopt the cone conformation, a motif prevalent in calix[4]arene chemistry. Octamethylcalix[4]pyrrole form complexes in solid state with chloride (Figure 12) or fluoride with the four pyrrole NH groups forming hydrogen bonds to the bound chlorine ion. Neutral species includes short chain alcohols, amides and other oxygen-containing neutral species can be coordinated. The same authors[29,30] have used p-*tert*-butylcalix[4]arene as template around which a calix[4]pyrrole can form the cylindrical calix[4]arene-calix[4]pyrrole pseudo-dimer (Figure 13).

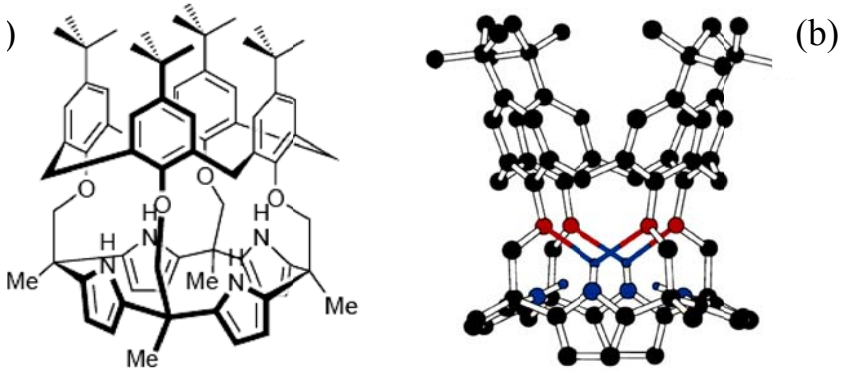

Figure 13 Calix[4]arene-calix[4]pyrrole pseudo-dimer; b) Crystal structure [ref. 30]

The X-ray structure (Figure 13b) revealed that the calixarene adopts a cone conformation in which two of the pyrrole NH groups are able to create hydrogen bonds to the phenolic oxygen atoms at the lower rim of the calixarene. This structure could be an interesting system to explore the inclusion and the physical behaviour of different guest molecules bearing potentially labile methyl groups in crystalline solid state.

Other potential cages

Several cage systems including capsules and modified calix[4]arenes have been reported from many authors[20,21,31]. Rebek and co-workers[20] have prepared capsules based on resorcinarene derivatives (Figure 14) able to accommodate simultaneously different guest molecules e.g methane and anthracene molecules (Figure 14).

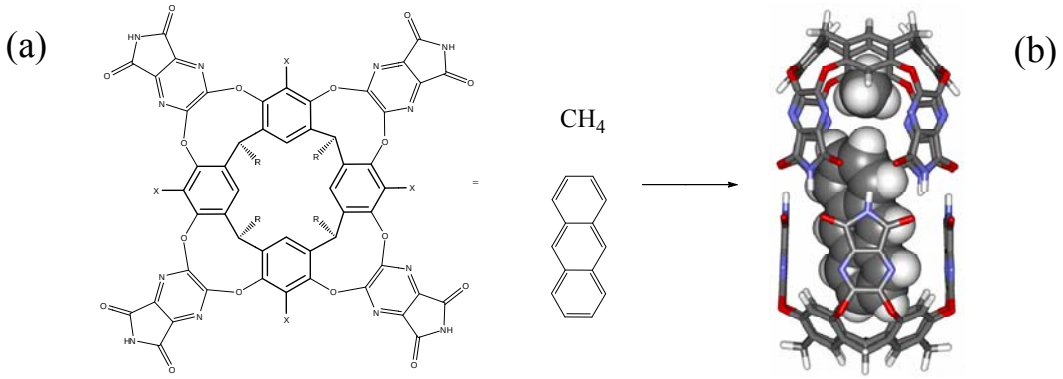

Figure 14 a) Cylindrical capsules with methane and anthracene guests; b) Crystal structure [ref. 20]

Ripmeester and co-workers[21]have prepared calix[4]arene derivatives able to encapsulate nitroxide guests (TEMPO, DEPN) in crystalline solid state (Figure 15).

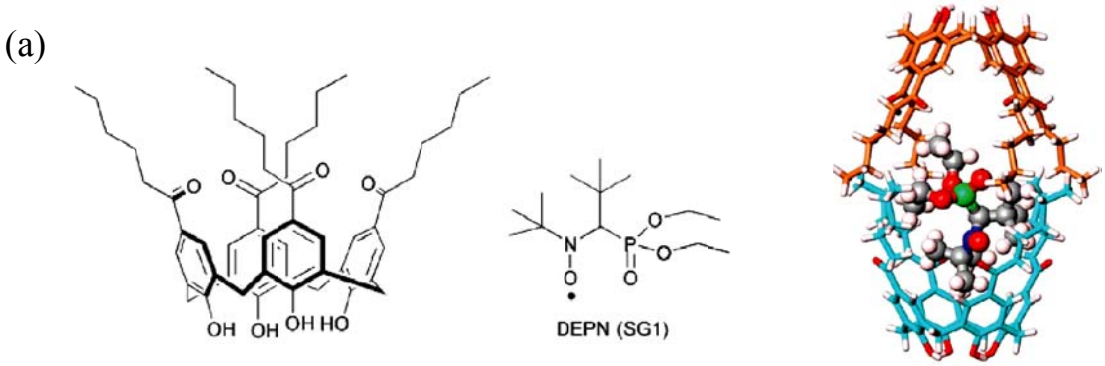

Figure 15 Capsular complex of p-*hexanoyl*-calix[4]arene with DEPN and crystal structure [ref. 21]

The isolation of stable complexed radicals is of significant importance in nuclear magnetic resonance in order to enhancing nuclear spin relaxation (see section 1.1.2.4).

1.1.2.2 Molecular architecture shielding methyl groups

The rotation of methyl groups in molecular crystal structures is a fascinating and much studied phenomenon. Several literature examples of molecular architecture shielding methyl groups have been reported. Dance and co-workers[32] have studied the crystal motifs of four different isomeric tritolylamines. Crystal packing of *N,N*-bis-(3-methylphenyl)-*N*-(4-methylphenyl)amine [334TTA] is shown in (Figure 16).

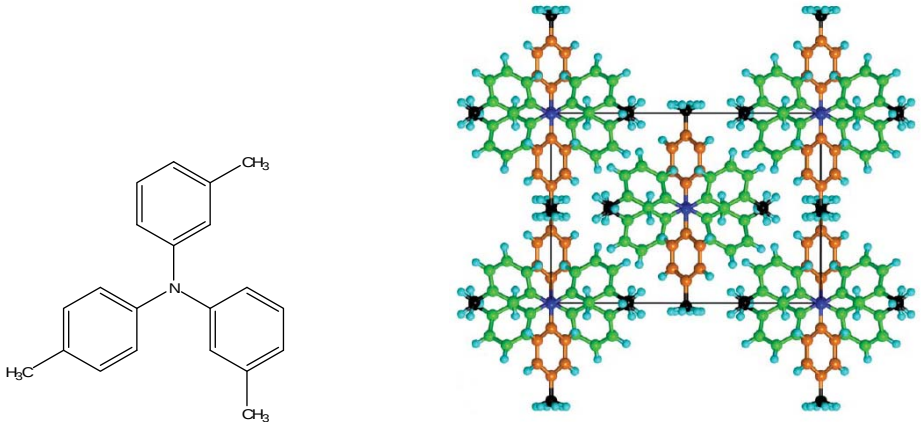

Figure 16 334TTA structure and crystal packing [ref. 32]

In this crystal the point symmetry of the molecule is C_2 with the twofold axis through the 4-tolyl group for which the methyl group is twofold rotationally disordered. Hart and co-workers[33] have reported in several studies a class of new peculiar compounds in which arenes are fused together through the bicycle[2.2.2]octane framework called an Iptycene skeleton. To describe the extended iptycene structure, a prefix is added to indicate the number of independent arenes present. Iptycenes involving five arenes are called pentiptycenes (Figure 17).

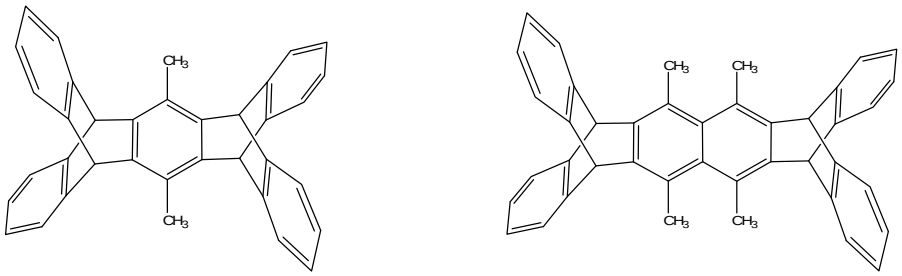

Figure 17 pentiptycenes structure with one and two methyl rotors [ref. 33]

These are two important examples with one or two central benzene rings bearing methyl rotors which are sterically shielded. Recently another interesting system has appeared in the literature called an *in*-methylcyclophane[34] in which the methyl groups are forced into the centers of basal aromatic rings with attractive spectroscopic and structural behaviour as shown in (Figure 18).

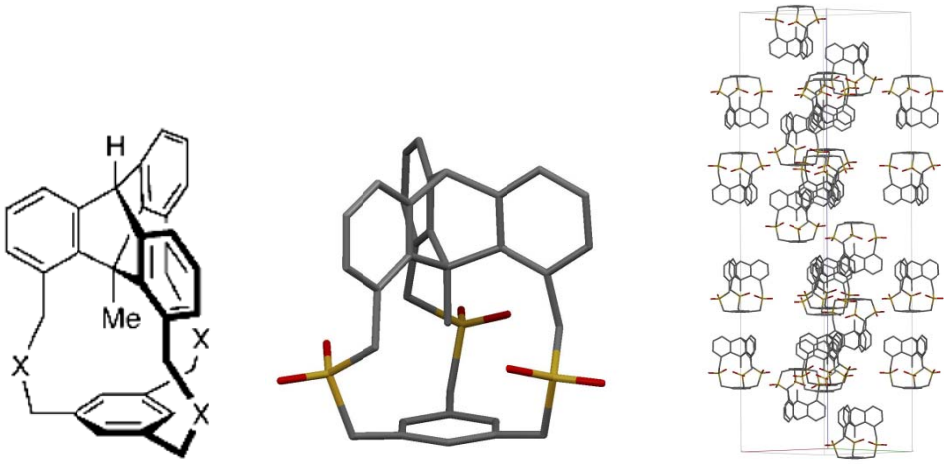

Figure 18 *in*-methylcylclophane crystal structure and packing [ref. 34]

The ^{1}H-NMR of this system exhibits an *in*-methyl resonance shifted significantly upfield shifted because the methyl protons lie above the inside edge of the basal aromatic ring[35].

Garcia-Garibay and co-workers[36] have investigated by ^{2}H-NMR and single crystal X-ray diffraction, the effect of molecular structure and crystalline environment on the rotational dynamics of methyl groups in 1,4-dimethylanthrone and 1,4-dimethylanthraquinone[36] (protonated and deuterated) (see Figure 19).

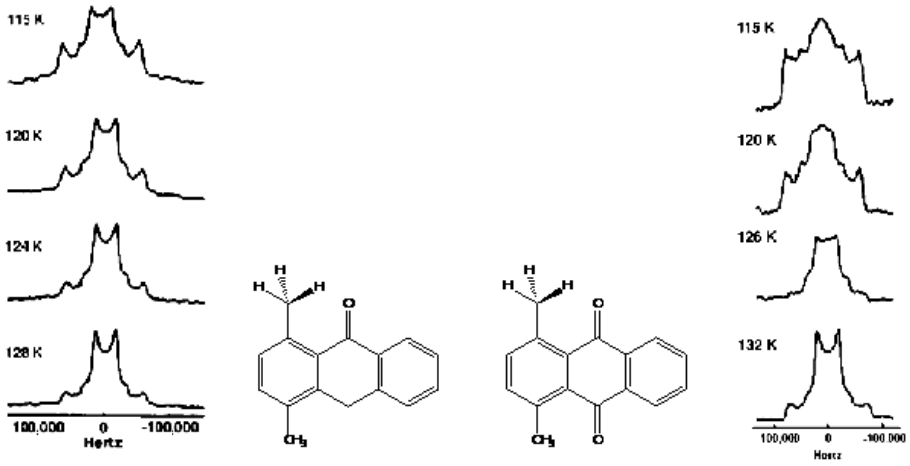

Figure 19 Spectra between 128-111K of 1,4-dimethylanthrone and 1,4-dimethylanthraquinone [ref. 36]

Spectra measured between 128 and 111K revealed clear broadening and an increased intensity for signals corresponding to the aromatic deuterons, which have a shorter spin-lattice relaxation time at lower temperatures[36]. The ^{13}C CP-MAS NMR spectrum for 1,4-dimethylanthraquinone clearly shows two distinct methyl groups with different relaxation times 1.18 and 1.21s suggesting either a non-symmetric conformation (Figure 19).

1.1.2.3 Crystal architecture

Crystal architecture is a system in which molecules are join together by weak physical bonding such as van der Waals forces, dipole-dipole bonds, or hydrogen bonding as opposed to chemical bonding like ionic or metallic bonds. Several examples of crystal architecture bearing methyl groups have been reported in the literature[14,37]. Fillaux and co-workers[38] have reported the tunnelling behaviour of methyl groups confined in crystal architecture of 2,6-dimethylpyrazine (Figure 20).

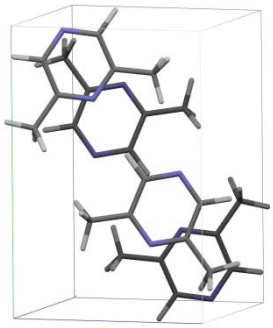

Figure 20 2,6-Dimethylpyrazine crystal packing [ref. 38]

Prager and co-workers[39] have reported the crystal structure of 2-butyne (Fig. 21) and its tunnelling behaviour of the methyl groups by INS (see section 2.2.3.3 of this thesis).

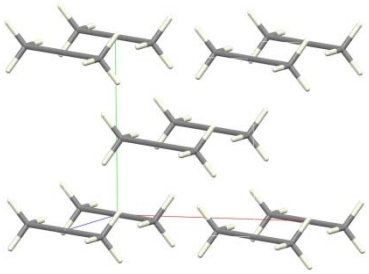

Figure 21 2-Butyne crystal packing [ref. 39]

1.1.2.4 Paramagnetic agents

Paramagnetic doping is a method able to enhance nuclear spin relaxation[9]. The paramagnetic materials enhance proton relaxation (thereby decreasing T_1, the spin-lattice relaxation time) by varying the local magnetic environment. By definition, paramagnetic substances have a permanent magnetic moment. In absence of magnetic field these magnetic moments are randomly aligned. However, in an externally applied magnetic field, magnetic moments are aligns preferentially with the field. The local magnetic field produced by paramagnetic substances shortens the relaxation times (T_1 and T_2) of neighboring hydrogen nuclei, a phenomenon referred to as "*proton relaxation enhancement"*.

Substances are paramagnetic, in quantum mechanical terms, because of the presence of an unpaired spin (proton, neutron, or electron). The magnetic moment of unpaired electrons is substantially greater than that of neutrons and protons; thus, agents that possess unpaired electron spin have received great attention as potential NMR relaxation agents. The strength of interaction between paramagnetic centre and the hydrogen nuclei depends on several factors as shown in equation *I*, a relation first described by Bloembergen and co-workers[40] and subsequently expanded by others[41]

.

$$\Delta\left(\frac{1}{T_1}\right) = \frac{12\pi^2\gamma^2\varepsilon\mu^2 N}{5kT} \quad (I)$$

Where: μ is effective magnetic moment, $\mathcal{E}$ is the viscosity of the solvent, k is Boltzman's constant, T is absolute temperature, γ is the giromagnetic ratio (for the hydrogen nucleus) and N is the number of ions per unit volume (concentration) [ref. 41]

From this equation it is apparent that decrease in T_1 is directly dependent on the concentration of the paramagnetic agents and the square of their effective magnetic moment. Compounds that decrease T_1 will increase signal intensity in NMR spectra and thus will act as effective relaxation agents. Three types of relaxation agents for use in NMR can be considered:

- paramagnetic metal ions,
- paramagnetic chelates and metallic complexes
- nitroxide stable free radicals (NSFR).

A large number of chemical species are paramagnetic and a partial list of these is presented below

Metallic ion-based relaxation agents suitable include: Transition metals include: titanium (Ti^{3+}), iron (Fe^{3+}), vanadium (V^{4+}), cobalt (Co^{3+}), chromium (Cr^{3+}), nickel (Ni^{2+}), manganese (Mn^{2+}), copper (Cu^{2+}). An example is the Cr $(acac)_3$ illustrated in Figure 22.

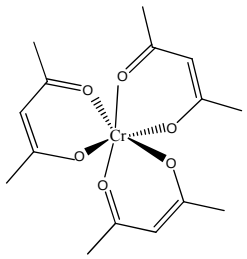

Figure 22 $Cr(acac)_3$ complex [ref. 9]

Suitable lanthanides includes: praseodynium (Pr^{3+}), gadolinium (Gd^{3+}), europium (Eu^{3+}), dysprosium (Dy^{3+}). Most important is Gd and an example is Gd chelates of the tripodal ligand[42,43] illustrated in Figure 23.

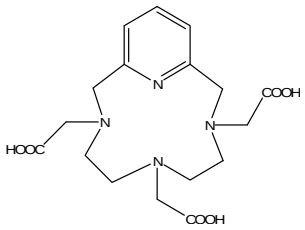

Figure 23 Gd chelates of the tripodal ligand [ref. 42, 43]

Organic relaxation agents These include two important classes: pyrrolidine and piperidine nitroxide derivatives[44] such as those shown in Figure 24.

Figure 24 Pyrrolidine and piperidine derivatives [ref. 44]

Other relaxation agents include in particular molecular oxygen O_2

1.1.3 Methyl rotors (NMR data)

In this section some fundamental concepts of nuclear magnetic resonance (NMR), quantum mechanics and inelastic neutron scattering (INS) relevant for to this thesis will be reviewed. The existing theoretical framework of spin-lattice relaxation via tunnelling of methyl groups (the so-called Haupt model) will be discussed shortly, as will the motivation behind using the field-cycling NMR relaxometry as a technique to study rotational dynamics of methyl groups confined in a calixarenes cavity as discussed in section 2.2.

1.1.3.1 NMR fundamentals[8, 2, 45, 46]

An NMR experiment involves the excitation of nuclear spin by radio frequency pulses and the subsequent acquisition of free induction decay (FID) (Figure 25)

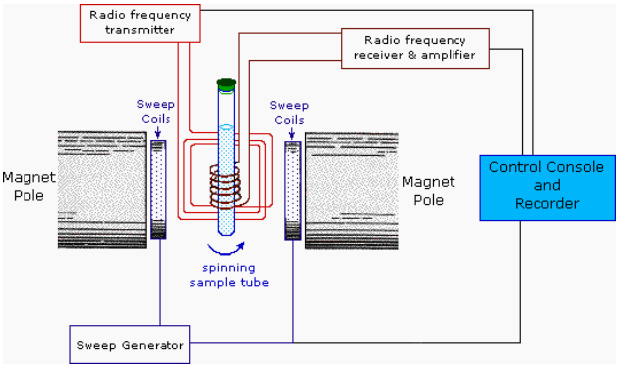

Figure 25 Schematic NMR experiment [ref 46]

Many nuclei possess an intrinsic spin angular momentum. Rather than being due to an actual physical rotation, spin angular momentum is an intrinsic property of the nucleus, as the mass and the charge. Spin angular momentum is quantised, and since it is a vector quantity, there are two quantum numbers associated with it; these are the nuclear spin quantum number I, and the azimuthal quantum number m_I. I determines the magnitude of the spin angular momentum vector S by

$$|S| = \hbar\sqrt{I(I+1)} \qquad (II)$$

and may have integer or half-integer values. The azimuthal quantum number m_I defines the allowed orientations of the spin angular momentum, relative to a reference

axis, conventionally defined as the z-axis. m_I may take on any of the $(2I + 1)$ values allowed by the following expression (*III*);

$$m_I = -I, (-I + 1) \ldots I. \qquad (III)$$

When a nucleus with non-zero spin is exposed to a static magnetic field B_0, the interaction between the field and the nuclear magnetic moment μ, causes the degeneracy of the spin angular momentum states to be lifted. (Figure 26)

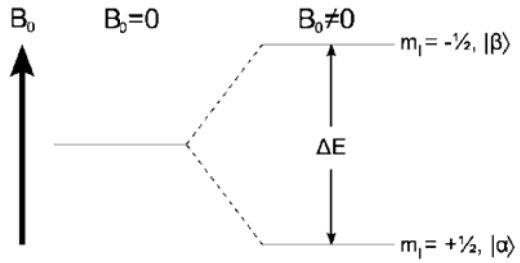

Figure 26 Zeeman splitting for spin ½ nucleus [ref. 45]

The nuclear magnetic moment μ is proportional to the spin angular momentum (*IV*):

$$\mu = \gamma S \qquad (IV)$$

The constant of proportionality γ is known as the magnetogyric ratio. The energy of a magnetic moment in the presence of a magnetic field is given by the expression (*V*):

$$E = -\mu B_0 \qquad (V)$$

If the B_0 field is considered to be aligned with the z-axis, using equations (*II*) and (*III*), equation (*V*) can be rewritten as

$$E = -\gamma \hbar m_I B_z \qquad (VI)$$

For a spin I nucleus, the $(2I + 1)$ spin states become separated by an energy

$$\Delta E = \hbar \gamma B_z \qquad (VII)$$

This splitting of the energy of the spin states caused by exposure to a magnetic field is known as Zeeman splitting. Figure 26 illustrates the case for a nucleus with spin I =

1/2 (e.g. ^{1}H, ^{13}C, ^{15}N). The $m_I = +1/2$ state is referred also as $|\alpha\rangle$, and $m_I = -1/2$ is the $|\beta\rangle$. The component γB_z is indicated ω_L and so-called *Larmor frequency*

$$\omega_L = \gamma B_z \qquad (VIII)$$

Re-examination of equation (*VII*) reveals that $\hbar\omega_L$ is exactly equal to the Zeeman splitting of the spin states. ω_L is the rate of precession of spins about the applied magnetic field, and also the frequency of RF (radio frequency) electromagnetic radiation required to induce transitions between the spins states. Application of a perpendicular RF field at resonant frequency has the effect of introducing an additional torque, which as an axis of rotation orthogonal to the B_0 field (Figure 27)

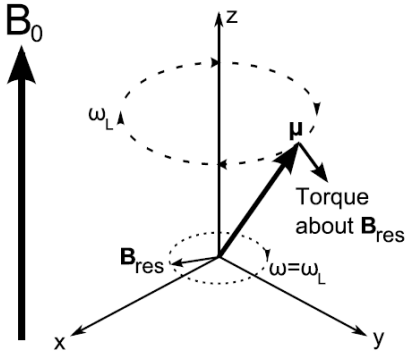

Figure 27 Interaction between a magnetic moment and a resonant RF magnetic field [ref. 45]

The torque acts to increase the angle subtended by **μ** with B_0. This introduces an additional precession that superimposes itself on the Larmor precession, referred to as *nutation.* If the magnetic moment vectors of a set of nuclei are quantized towards the external magnetic field, they have definite projections on the z-axis but randomly distributed in the XY-plane. There is a small excess of lower energy projections aligned parallel to the field over the anti-parallel projection, indicates as net magnetization in the Z direction. The net magnetization vector is so-called bulk magnetization and labelled ***M***. The bulk magnetization at thermal equilibrium $\boldsymbol{M_0}$ aligns itself with the B_0 field. The equilibrium which produces $\boldsymbol{M_0}$ is a dynamic equilibrium and that thermal energy constantly causes transitions between nuclear spin states.

The magnetization is proportional to magnetic field strength, an inversely proportional to temperature following the Curie law.

$$|\boldsymbol{M}_0| = \frac{1}{4}N(\hbar\gamma)^2\frac{B_z}{k_BT} \qquad (IX)$$

The equilibrium between the nuclear spin states is determined by the Boltzmann distribution:

$$\frac{N_\alpha}{N_\beta} = \exp\left(\frac{-\Delta E}{k_BT}\right) \qquad (X)$$

If the system is perturbed from equilibrium by application of an RF pulse, the magnetization of a sample will be in a non-equilibrium state. The system may not persist in this state, and must return to the state of thermal equilibrium. The process by which the magnetization ***M*** returns to the thermal equilibrium value is known as *relaxation*. Two different types of relaxation occur with its own time constant. Relaxation of ***M*** on the z-axis take place each with time constant T_1; this is refereed to as *spin-lattice relaxation, or longitudinal relaxation*. As the name suggests spin-lattice relaxation is caused by spins interacting with the various degrees of freedom of the surrounding *lattice*; energy exchange between the spin system and lattice is necessary to drive the spins toward equilibrium. Measurement of T_1 may reveal information about the molecular motion. T_2 characterises the decay of the components of the magnetisation that are perpendicular to the applied field; this is referred to as *spin-spin relaxation,* or *transverse relaxation.* Spin-spin relaxation is caused by spins interacting with each other, which results in a dephasing of the spin precession and therefore a decay in the transverse magnetisation.

1.1.3.2 Spin-lattice relaxation

Relaxation of longitudinal magnetisation $\boldsymbol{M_z}$ towards equilibrium magnetisation $\boldsymbol{M_0}$ in an NMR sample occurs due to the existence of mechanisms for the exchange of energy between the nuclear spin system and thermal energy sinks or reservoirs. Examples of such thermal energy reservoirs include the motional modes of the molecule, i.e. translation, vibration and rotation. The reservoirs are collectively

referred to as the lattice; hence relaxation due to interaction with the lattice is referred to as spin-lattice relaxation. Without the lattice, transitions from higher Zeeman energy levels $|\beta\rangle$ to lower ones $|\alpha\rangle$ would not be possible, as the spontaneous emission transition rate is negligible. Attainment of thermal equilibrium following, for example, a 90º RF pulse or a decrease in temperature is achieved through stimulated emission via interactions with the lattice. In a system of non-interacting spin 1/2 nuclei, in the presence of a static B_0 field we can define two transition rates, $W_\uparrow$ and $W_\downarrow$ which are probabilities per unit time for transitions to occur between energy levels.

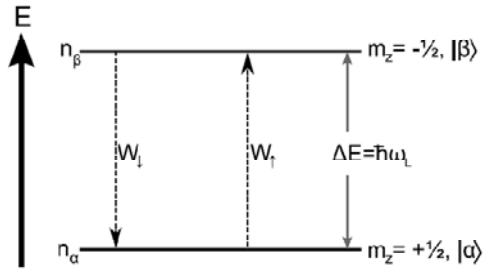

Figure 28 Zeeman splitting of spin states for spin 1/2 nucleus with transition probabilities [ref. 46]

$W_\downarrow$ is a downward transition ($|\beta\rangle \rightarrow |\alpha\rangle$) and $W_\uparrow$ is an upward transition ($|\alpha\rangle \rightarrow |\beta\rangle$) (Figure 28). The mechanism may be a time-varying magnetic field, or randomly fluctuating molecular interaction. In matter the random Brownian motion of molecules causes random fluctuations of internuclear distances and angles, which results in a random fluctuation of internuclear interactions. In spin-relaxation, it is the fluctuation of the magnetic dipole-dipole interaction that drives relaxation. The following expression of T_1 is found to reveal information about motional processes that are central to causing spin-lattice relaxation process.

$$T_1^{-1} = S^2\left(\frac{\tau_c}{1+\omega^2\tau_c} + \frac{4\tau_c}{1+4\omega^2\tau_c^2}\right) \qquad (XI)$$

S is a strength factor dependent on whether the sample is a powder or a single-crystal. In the case of a single-crystal sample S has an angular dependency, as the magnitude of a dipole-dipole interaction is dependent on the angle among the internuclear vector and the reference field; for a powder sample S is constant.

1.1.3.3 Quantum Tuneling phenomenon

In molecular crystals, the constituent molecules and moieties experience electrostatic interactions with surrounding atoms, which give rise to potential barriers that hinder motional processes such as rotation and translation[47]. At low temperatures it is often the case that the molecules do not have enough kinetic energy to overcome these barriers. However, in certain systems, it is possible for motion to persist even at the lowest of temperatures, due to either the molecule being very weakly hindered, or the ability of the molecule to penetrate the barrier via quantum tunnelling. Quantum tunneling (or the *tunnel effect*) is a phenomenon in which a particle can violate the principles of classical mechanics by passing through the barrier due to its wave character (dashed line Figure 29)[48]. In classical mechanics this process can occur only if the particle has enough kinetic energy ($W > E_0$) to overcome the barrier by a classical process (solid line Figure 29). Several biological systems like enzymes use quantum tunnelling as mechanism to increase reaction rates by transfering electrons and nuclei such as hydrogen and deuterium[49]. It has even been proved, that in enzyme like glucose oxidase, oxygen nuclei can tunnel under physiological conditions[50].

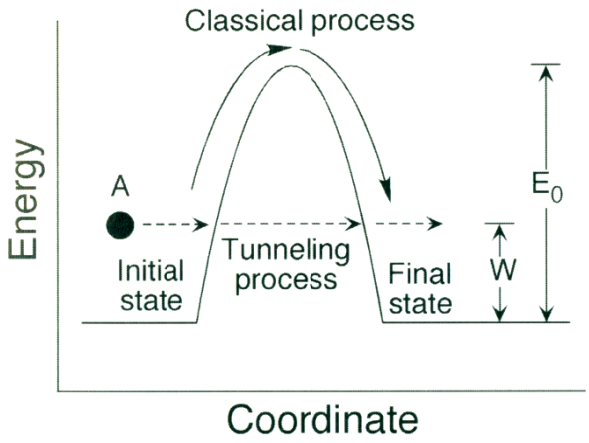

(Figure 29) Diagram comparing quantum tunneling to classical movement [ref. 48]

Tunnelling is a very small-scale effect, generally only being observed when dealing with particles of atomic size, that potential when dealing with all forces becomes considerably more complex, and that particles cannot tunnel "upward". However Tunnelling occurs in many systems much larger than atoms for example in some transistor types. For tunnelling to occurs the wavefuctions describing the two states must simply overlap[51-52]. This effect can *only* occur from a higher-energy to a lower-

energy state, in agreement with the second law of thermodynamics[52]. As shown in (Fig. 29) classically, to reach the lowest state, additional energy must be supplied. Under the laws of quantum mechanics, however, the object can occasionally "tunnel" to a lower state. Protons in hydrogen-bonds and methyl-groups are two such examples of systems that exhibit quantum-tunnelling in the solid-state, and both have been studied extensively in the Quantum Molecular Dynamics laboratory of Prof. A.J. Horsewill at the University of Nottingham[53-55].

The rotation of methyl-groups in molecular crystals is a fascinating, much studied phenomenon. It is a model system for studying the complementarities between quantum and classical mechanics, and the transition between these two regimes. The rotational motion of methyl-groups in molecular crystals was first inferred from anomalies in the measurements of bulk macroscopic properties such as heat capacity and the dielectric constant[52]. The first studies of methyl group rotation in solids using NMR centred on observing changes in the profile of the proton NMR absorption peak, as a function of temperature. One of the primary causes of line-width broadening is the interaction of nuclear spins with a local magnetic field, which has its origins in dipole-dipole interactions with surrounding magnetic nuclei. Molecular motion can average out the local magnetic fields to zero, thus causing the line-width to narrow significantly. This effect is known as motional narrowing, and was first described by Bloembergen, Purcell and Pound in their seminal paper "*Relaxation effects in NMR absorption*"[40,56,57]. A more complete model of methyl-group tunnelling, in which the spin and rotational degrees of freedom are coupled to lattice phonons, was developed further by Haupt[58,59]. The emergence of high resolution neutron scattering spectrometers in the latter half of the 1970s allowed direct measurement of tunnelling spectra via inelastic neutron scattering. The first publications on rotational tunnelling using INS techniques appeared around 1975[60]. The effects of temperature, pressure, isotopic replacement (H-D), and change of environment are discussed within the single particle model. It was soon realized that, in the solid state, rotational tunnelling influences proton relaxation in nuclear magnetic resonance experiments (NMR-T_1) and is "a widely used technique". NMR investigations of methyl-group rotation have been complemented with INS measurements, and vice-versa.

1.1.3.4 Rotational Tunneling and methyl groups

Rotational tunneling is a phenomenon that describes the librational states of a molecule in which rotating atoms are indistinguishable. The splitting between the substrates is called tunnel splitting. The inertial properties of the molecule and the rotational potential are produced by the size of the tunnel splitting. Large tunnel splittings are found for light molecules in weak potentials. The molecule with the largest rotational constant, *B,* is the hydrogen H_2 $B(H_2)$ = 7.3 meV[47]. The rotors with the next largest rotational constants are the ammonium ion NH_4^+, ammonia NH_3 $B(NH_4^+)$ = $B(NH_3)$ = 0.782 meV, and the hydrocarbons CH_4 and $-CH_3$ $B(CH_4)$ = $B(CH_3)$ = 0.655 meV[60].

Methyl group moieties that are attached to larger molecules have only a rotational degree of freedom. At room temperature the vibrational degrees of freedom can be neglected, therefore the CH_3 group can be considered as a rigid rotor that moves about the covalent bond between the carbon atom and the rest of the molecule. In the simplest case the rotational motion of a methyl group is defined in one dimension in terms of angle ϕ with three-fold symmetry axis (Figure 30).

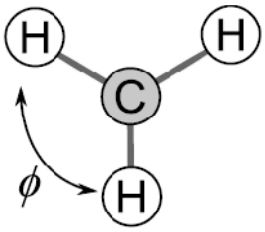

Figure 30 Schematic Methyl Rotor with angle ϕ describing its position from [ref. 53]

The hindering potential V(ϕ) indicated as a Fourier series incorporating three-fold, six-fold and higher harmonics (equation *XII*) is given by intermolecular and intramolecular contributions of valence and non-bonding interactions between the methyl group atoms and the molecular environment[53].

$$V(\phi) = \sum \frac{V_{3l}}{2} \left[1 - \cos\left(3l(\phi + \chi_{3l})\right)\right] \qquad (XII)$$

The three minima coincide with the three preferred orientations of the methyl rotor minima which are separated by interceding hindering barrier defining also the

potential well regions. In general barrier heights measured experimentally are typically in the range between approximately 0.2 and 20 kJ mol^{-1}.

The methyl group has symmetry C_3 so according irreducible representations the eigenstates may be classified as A, E_a and E_b (Figure 31).

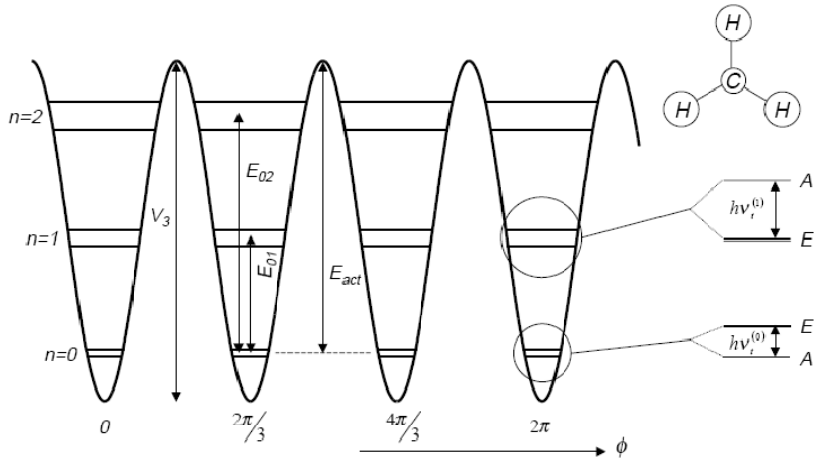

Figure 31 Energy levels of a methyl group under the influence of a three-fold hindering potential of magnitude V_3 [ref 53]

The torsional states are labelled by n^{th} and the torsional excitations involving the ground state are defined E_{on}. Every torsional state exhibits a tunnel splitting $hv_t^{(n)}$ with symmetry *A* and *E*. It is the quantum tunnelling bearing the tunnelling frequency of the n^{th} torsional level able to generate the *A*-*E* splitting $hv_t^{(n)}$. E_{act} is the activation energy from the ground torsional state to the top of the barrier[53]. At low temperatures the motional spectrum of a methyl group is characterised by three peaks, two *A*–*E* peaks centred at ω_t and an *E*–*E* peak at zero frequency (Figure 32)[53].

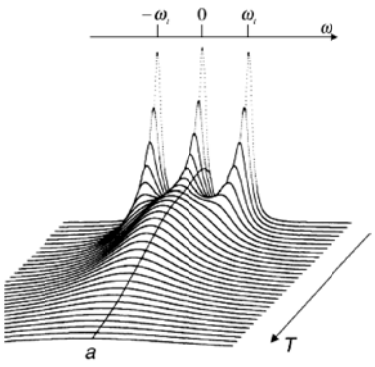

Figure 32 Motional spectrum of a methyl group at low temperature [ref. 53]

The system evolves slowly into a quasi-classical dynamics at higher temperature. The three peaks become indistinguishable, broad and the tunnelling frequency diminishes forming a single broad line centred at zero. Tunnelling frequencies of methyl groups

have been measured in several systems with very dissimilar chemical nature[60,61]. The techniques used include mainly nuclear magnetic resonance (NMR) methods, neutron scattering infrared or hole burning optical spectroscopy, calorimetry and electron nuclear double resonance. Typical range of the lowest librational transitions E_{01}, E_{02} are between 10-60 meV and by INS can also be directly detected as resolution-width inelastic peaks. Some important parameters namely the crystal structure space group, tunnelling frequency (ν_t) and hindering potentials (V_3) and (V_6) of different methyl rotors discussed in section 2 of this thesis are showed in (Table 1).

Compound name	Compound formula	Crystal structure	ν_t (μeV)	V_3 (meV)	V_6 (meV)	Technique
Toluene	$C_6H_5CH_3$	$P2_1/c$	28.5 26.0	14.8 19.3	-1.2 -9.6	INS
Toluene(1:1) t-Bc4			160/200/ 360/630			INS/NMR
4-fluorotoluene	$C_6H_4FCH_3$		17.6			INS
p-xylene*	$(CH_3)C_6H_4$	$P2_1/n$	0.97	50 53.8	0 1.1	INS/NMR NMR
p-xylene(1:2) t-Bc4			626			INS
4-methylpyridine	$CH_3C_5NH_4$		520	7.3		INS
dimethylacetylene	$CH_3C_2CH_3$	$P2_12_12_1$	1.74	27.9	2.26	INS
methyl iodide	CH_3I	*Pnma*	2.44	41.0	1.9	INS
acetone	CH_3COCH_3		0.4			MW/FC/LC
nitromethane	CH_3NO_2	$P2_12_12_1$	> 0.01 35.1	25.2	15.4	INS

* NMR studies reported for p-xylene confined in zeolite [ref. 62]

(Table 1) Methyl Rotors table adapted [ref. 60]

V_6 represents a Fourier component of the resultant potential. The V_6 components modulates the V_3 component, but the resultant barrier is never negative (i.e. $V = V_3$ component + V_6 component and is greater than zero for all values of ϕ)[47]. As shown in table 1 only the p-*tert*-butylcalix[4]arene (1:1) toluene complex has been studied in detail by NMR relaxometry in solid state[12]. In order to investigate further behaviour of the methyl rotors confined in calixarene cavity, several complexes have prepared in the present study and the spin-lattice relaxation rate T_1^{-1} has been measured by field-cycling NMR (see section 2 of this thesis).

1.1.3.5 Spin-lattice relaxation of rotating methyl groups

A model for the spin-lattice relaxation time of rotating methyl groups has been developed by Haupt[53,59]. In this model it is assumed that relaxation between librational levels is driven by phonons modulating the potential. The rapid transitions between librational levels ensure that thermal equilibrium is maintained between the lattice and the librational levels. The energy levels of a methyl group in the ground torsional state are indicate by two spins *A* and *E* as showed in (Figure 33).

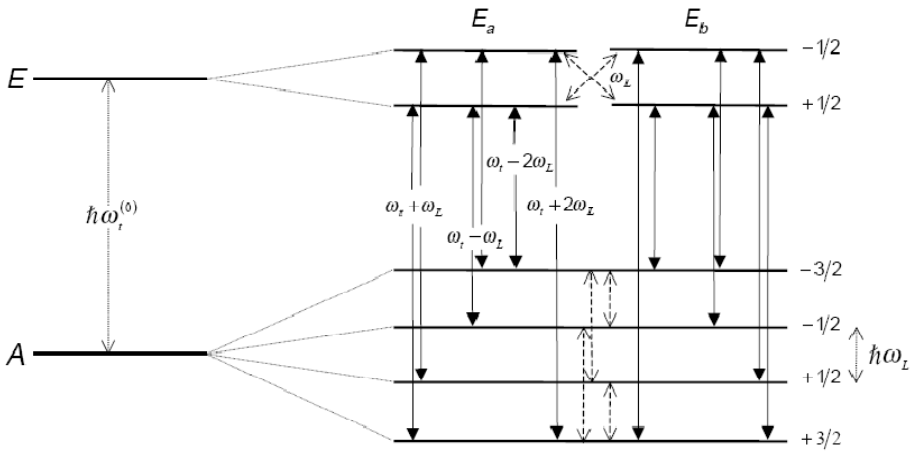

Figure 33 Energy levels of the ground state and Zeeman splitting of a methyl group [ref. 53]

Under the influence of an applied magnetic field the two spin levels show the Zeeman splitting phenomenon. The rotational *A*-state is a nuclear spin quartet with $m_I = 3/2$ and the rotational *E*-state (E_a and E_b) species are nuclear spin doublet with $m_I = 1/2$. By summing up the probabilities of the individual transitions, Haupt has obtained the following expression for the spin-lattice relaxation rate (*XIII*)[61] :

$$\begin{aligned}\frac{1}{T_1} &= C_{AE} f(\omega_t, \omega_L, \tau_c) + C_{EE} g(\omega_L, \tau_c) \\ &= C_{AE} \sum_{n=1}^{2} \left(\frac{n^2 \tau_c}{1 + (\omega_t + n\omega_L)^2 \tau_c^2} + \frac{n^2 \tau_c}{1 + (\omega_t - n\omega_L)^2 \tau_c^2} \right) \\ &+ C_{EE} \sum_{n=1}^{2} \frac{n^2 \tau_c}{1 + n^2 \omega_L^2 \tau_c^2}\end{aligned} \qquad (XIII)$$

where C_{AE} and C_{EE} are the intermolecular and the intramolecular dipolar interactions, respectively, and τ_c is the correlation time, which is characteristic of the motion of the methyl group. In the low temperature limit τ_c is given by Arrhenius rate law:

$$\tau_c^{-1} = \tau_0^{-1} \exp(-E_{01} / k_B T) \qquad (XIV)$$

where E_{01} is the energy difference between the ground and first excited librational state. Equation (*XIII*) describes the spectral density function of the dipole-dipole interaction in powder samples with rotating methyl groups. The relaxation rate is dependent on ω_L and the correlation time τ_c. These variables are themselves dependent on the magnetic field strength and temperature, respectively (equation *XIV*). This dictates the experimental approach for studying the methyl group dynamics. T_1 is measured as a function of temperature and also as a function of magnetic field, in order to determine the spectral density function of the magnetic dipolar interaction.

In general we observe a T_1 minima at low temperature, due to the weakly hindered methyl groups, and minima at high temperatures due to the strongly hindered t-butyl/iso-propyl groups. The reason we observe minima is because we make measurement at fixed field, and as the temperature range changes the value of the spectral density at particular field goes through a maximum value. So the reason the T_1 changes as a function of temperature is due to a change in the correlation time of the motion[47,53,63]. Examples of spin-lattice relaxation studies of methyl rotors confined in different materials (calixarenes, zeolite) are described in the next section.

1.1.3.6 NMR relaxometry measurements of p-*tert*-butylcalix[4]arene (1:1) complex

In 1999 Horsewill and co-workers[12] reported NMR relaxometry measurements on p-*tert*-butylcalix[4]arene and the p-*tert*-butylcalix[4]arene (1:1) toluene complex in solid state. The dynamics of the p-*tert*-butyl groups of the host cage with variation apported on the activation energy by toluene guest molecule in the reorientation of the methyl groups are explored. The spin lattice relaxation time T_1^{-1} is measured as a function of the inverse temperature as showed in (Figure 34).

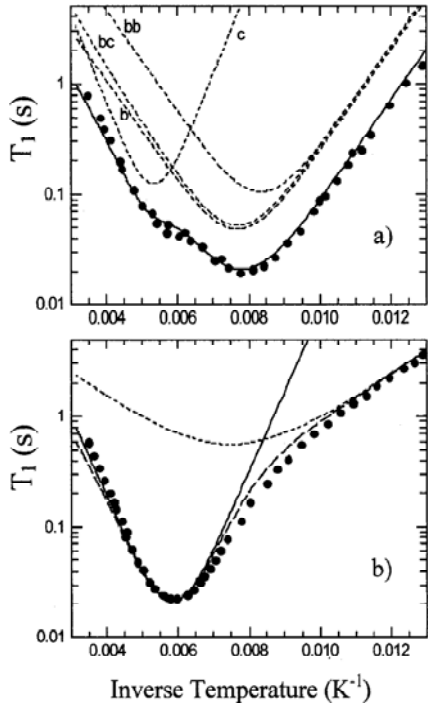

Figure 34 Spin-lattice relaxation time as function of the inverse temperature for p-*tert*-butylcalix[4]arene system a) empty b) toluene (1:1) complex [ref. 12]

The observed spin-lattice relaxation times T_1 are presented for the empty calixarene (a) and the (1:1) toluene complex, respectively. There are two overlapping minima for T_1 at 127 and 170 K in the empty basket. A single minimum is observed at 172 K for the calixarene (1:1) toluene complex, with a different slope from 60 and 100 K, confirming the existence of an additional type of motion. The relaxation process over 100 K is governed by the rotational motions of the *tert*-butyl groups, $C(CH_3)$, of the host cage. Reorientation of the three methyl groups and the rotation of entire *tert*-butyl group create the total motion for this supramolecular host-guest complex.

1.1.3.7 NMR relaxometry measurements of p-xylene confined in crystalline zeolite host

An interesting study of a methyl rotor confined in a crystalline nanoporous material has been reported from the same author[62]. In this paper p-xylene molecules are absorbed in a zeolite matrix as showed in (Figure 35).

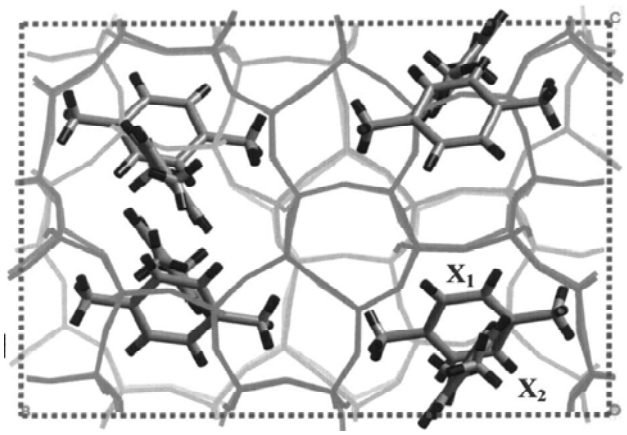

Figure 35 Zeolite lattice and p-xylene absorbed in the crystal [ref. 62]

This material is able at room temperature to encapsulate eight p-xylene molecules per unit of cell (see Figure 35). The p-xylene molecules are identically allocated in two different inclusion sites denominated X_1 and X_2 molecules as the single crystal diffraction studies suggestes at room temperature.

This system is characterized by four distinct environments for the methyl groups attached to the C_6 rings, because there are two methyl groups for each p-xylene molecules. In this situations the contact of p-xylene with the silicate framework decreases the space group of the crystal structure from *Pnma* to $P2_12_12_1$, changing the symmetry correlation of the two methyl groups on the same p-xylene. The spin-lattice relaxation time T_1 of protons as function of the temperature has been measured using the NMR technique (Fig. 36). A zeolite sample was poured in contact with p-xylene vapour and then cooled down to 14 K (in the NMR probe) to prevent any possible loss of p-xylene molecules from the crystal structure and subsequently the spin-lattice relaxation time was measured in a range from 14 K to 180 K. The same measurement was repeated at low temperature (in a range from 14 to 4 K) cooled down the sample again to 14 K. As shown in Figure 36 a broad minimum centred at ~ 8 K appeared together with a sharper drop in T_1 within the 20-50 K range. Minima in the

temperature dependence of T_1 are observed when the time scale of a molecular motion involving the protons matches the time scale of the NMR frequency (42.6 MHz).

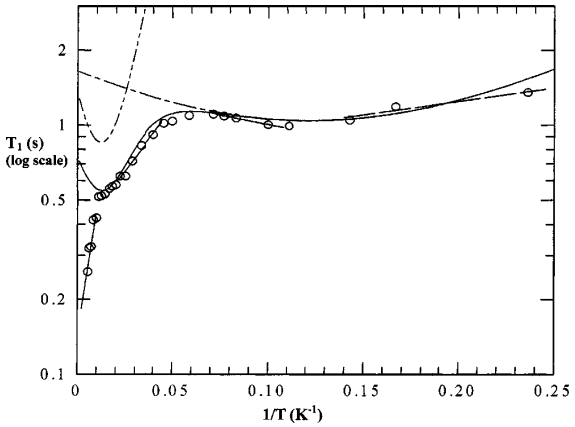

Figure 36 Temperature dependence of the proton spin-lattice T_1 relaxation time (42.6 MHz) from [ref. 62]

These motions at low temperatures correspond to methyl rotational tunnelling in which the aromatic rings of the p-xylene molecules are frozen in their absorption sites[62]. Beyond 50 K the relaxation time drops steeply as the temperature increases, so that the minimum at intermediate temperatures (20-50 K) appears.

1.1.3.8 4-Methyl pyridine and Haupt effect

The 4-methyl pyridine molecule, also called γ-picoline, consists of a pyridine ring and a methyl group opposite to the nitrogen atom (Figure 37).

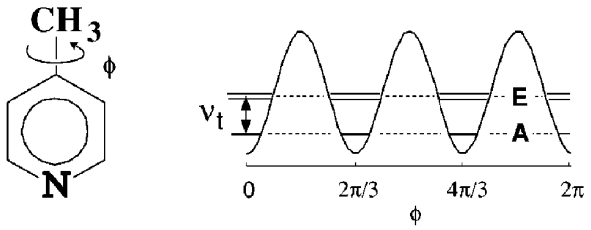

Figure 37 γ-picoline structure and schematic diagram of CH_3 potential [ref. 64]

It is liquid at room temperature and becomes solid at + 3ºC. In 1972 J. Haupt changing the temperature "sudden jump" from 8ºK to 30ºK in a polycrystalline γ-picoline sample observed a particular proton NMR spectrum of dipolar type, characterized by an enhancement factor of 10^4, hundred times bigger than the equilibrium Zeeman signal. The build up of the dynamic polarization started at zero

instantly after the temperature changed, reached a maximum after 4 minutes and then disappered slowly[64]. Reversal of the temperature jump changed the phase of the signal by 180º. The enhancement factors became smaller if less temperature changes were applied. This result can be described in terms of quantum mechanics properties of the methyl rotor[55]. Rotating methyl groups in solid state as discussed before can exist in three different proton-spin isomers: A, E_a and E_b with molecular nuclear-spin quantum numbers of respectively, 3/2, ½, and ½ (Figure 38)[61,64].

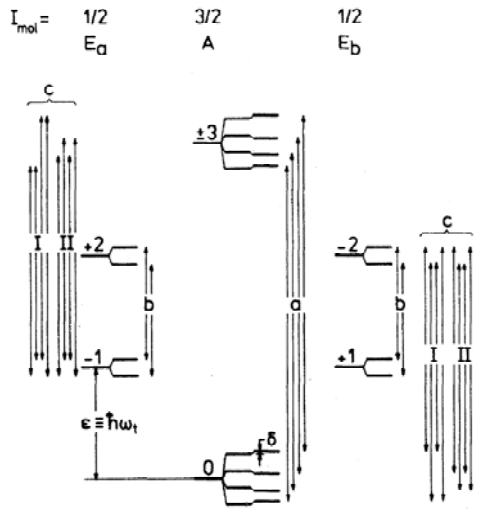

Figure 38 Energy-level scheme of the three species of a CH_3 rotor without and with magnetic field [ref. 64]

The differences ε between the rotational energy of the two degenerate E species is reprensented by $\hbar\omega_t$, where ω_t is the tunnel frequency. For a sample placed in a magnetic field with a temperature jump, very fast nonmagnetic phonon-assisted transitions restore almost immediately a thermal-equilibrium distribution inside each of the three subsets consisting of all the rotational levels of one species. The system characterised by different population between the A and E state, evolve into its thermal-equilibrium condition very slowly, because these transitions are not only phonons dependent but involve also dipolar and magnetic interactions. The final transitions, giving rise to nuclear-spin conversion, also generate dipolar polarization. Two groups represents all the A-E conversion transitions I and II: I, to and from upwards-shifted levels, and II, to and from downwards shifted levels. Each transition generates a modification in dipolar polarization. Haupt[59]showed that there is a net change in dipolar energy upon A-E conversion because the sum of the transition

probabilities weighted by the changed in dipolar energy is not zero. The growth of the dipolar polarisation and the observation of significantly enhanced dipolar signal can be explaned by the coupling between the tunnelling and the dipolar reservoir. Recently Tomaselli and co-workers[64] have estimated the proton polarization enhancement by Haupt effect in their 220 MHz NMR apparatus as shown in (Figure 39).

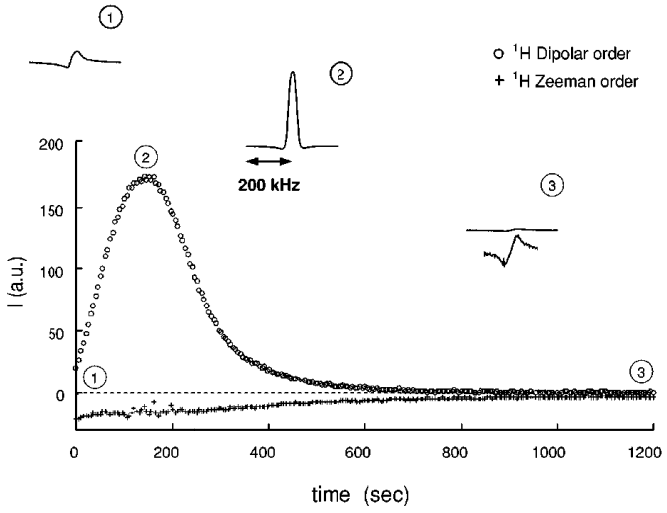

Figure 39 ^{1}H magnetization intensity traces in γ-picoline at 55K following a temperature jump [ref. 64]

In (Figure 35) is displayed the γ-picoline dynamic ^{1}H magnetization following a temperature jump from 4K to 55K after 40 min of thermal equilibration at 4K. A maximum enhancement factor of ~ 70 is observed compared to the equilibrium Zeeman signal at 55K and an enhancement of ~ 9 with respect to the equilibrium Zeeman signal at 4K. ^{1}H spectra at three different times (1), (2) and (3) are shown in the corresponding insets. (Figure 35)

1.1.3.9 Neutron Scattering Techniques[65]

The structure and dynamics of condensed matter can be explored by using neutrons. Main reasons are summarized by three major features: i) neutrons have typical wavelengths of few Å, which match to the characteristic distance between atoms, ii) neutrons distinctive energies are of the range of a few meV, which match to the energy scale of a representative excitations in condenser matter, iii) neutrons, are able to penetrate the sample providing structure details because they haven't electric charge instead particles like electrons are important probes to explore the external surface. In the neutron scattering two quantities are very important and needs to be measured: (*i*) the energy transfer, $\hbar^2\omega = \hbar^2(k^2 - k_0{}^2)/2m$, correspond to the difference between the final and the initial neutron energy; and (*ii*) the momentum transfer, $\hbar Q = \hbar k - \hbar k_0$, where k and k_0 are correspondingly to the final and initial neutron vectors (Figure 40).

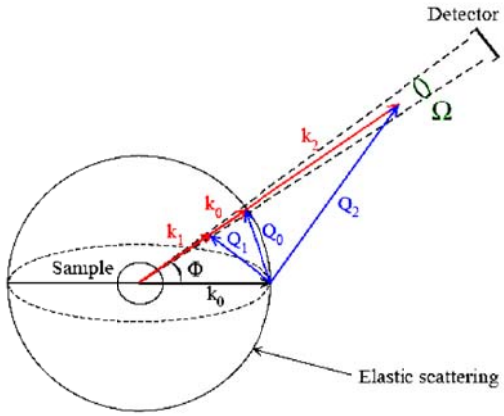

Figure 40 Neutron scattering [ref. 65]

Three different types of scattering processes are used to characterize the dynamic interaction with the matter. These are the elastic, quasielastic and inelastic scattering. When the neutron exchanges energy with sample excitations two resolution-width lines of finite energy appear in the spectrum so, this is called *inelastic neutron scattering* (INS). If the neutron energy remains constant, *elastic scattering* occur and a resolution-width elastic line appear in the spectrum. In the end, *quasielastic neutron scattering* (QENS, generate from the Doppler Effect) is connected with the amount of energy transfered when a neutron interacts elastically with moving particles giving a broad line in the region of the elastic line. If the energy changes is smaller compairing

to the instrumental energy resolution inelastic or quasielastic processes giving an further contribution to the experimental elastic line. The ranges for quasielastic and inelastic processes usually are between $|\hbar\omega| < 2\,\text{meV}$ and $|\hbar\omega| > 2\,\text{meV}$ respectively, the last corresponding to characteristic vibrational excitations in condensed matter. In methyl group tunnelling mesurements they have orders of μeV. For molecules that are in the liquid state, they can move by diffusion from the original position and lose memory of their initial positions, and no elastic component in neutron scattering spectra appeared. If a group of particles can move in a restrict region, as the rotation of a methyl group in a crystalline structure, in addition to the eventual inelastic and quasielastic peaks the neutron spectrum can shown, an elastic component. This peak is drived by a Q-dependent quantity called the elastic-incoherent-structure-factor (EISF). The EISF accounts can provide via Fourier transform to give informations about the geometry of the motion. An example of spectrum for methyl group motion in crystalline systems at different temperature is show (in Figure 41).

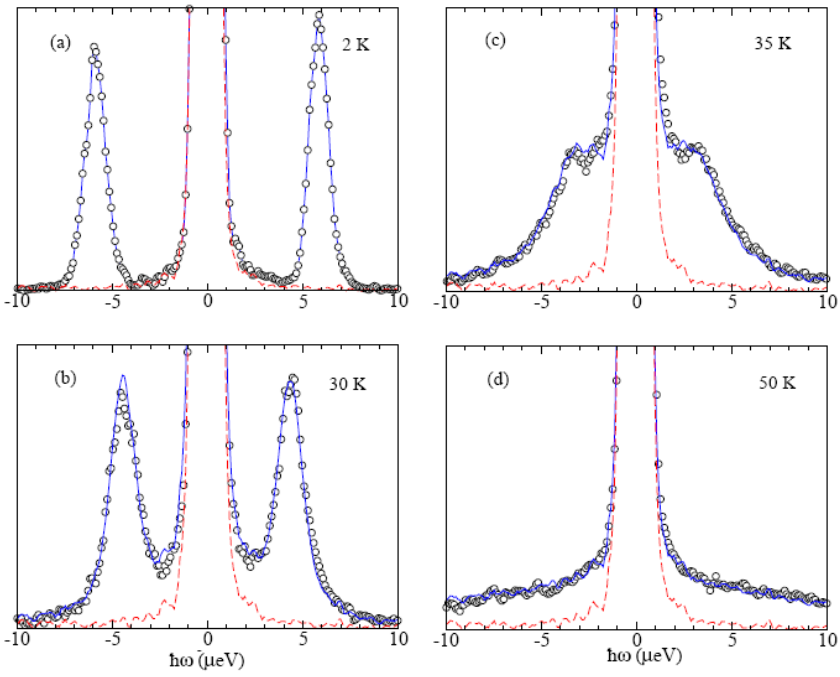

Figure 41 Experimental spectra for methyl group dynamics in crystalline sodium acetate trihydrate [ref. 65]

The spectrum (Figure 41) at T~1K is characterized by a central elastic peak and two inelastic peaks of resolution width. The inelastic peaks correspond to the two transitions $A \leftrightarrow E$ within the ground librational state. The elastic peak includes the ground-state transitions $E_a \leftrightarrow E_b$ and the transitions without symmetry change. At higher temperature, the inelastic peaks gradually become broad and move to the

elastic peak. At the same time, a quasielastic component appears around the elastic peak, and this broadens with increasing temperature (b, c). The quasielastic and inelastic components in a restrict temperature interval (ΔT~7K), join into a single quasielastic line (d). Inelastic neutron scattering spectrum of several methyl rotors confined in calixarene cavity and in some endohedral fullerenes will be discussed in section 3 of this thesis.

1.1.4 The supramolecular approach

1.1.4.1 Background

Supramolecular chemistry is an interdisciplinary science that brings together chemistry, physics and biology. In 1967 Charles J. Pedersen discovered a novel class of molecules that he dubbed the crown ethers[66,67]. Pedersen demonstrated the ability of these electrically-neutral, ring-shaped molecules to form stable complexes with a variety of metal ions via an ion-dipole interaction between the metal ion and the oxygen atoms of the poly-ether framework (Figure 42).

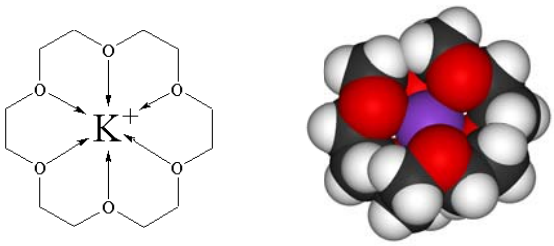

Figure 42 Complexation of 18-Crown ether with potassium cation [ref 67]

This pioneering work signified a paradigm-shift in the world of chemistry. Having mastered chemistry of the molecule and 'hard' covalent bonds, chemists began to address the chemistry of complexes held together by non-covalent 'soft' interactions. It is for this reason that supramolecular chemistry is often described as '*chemistry beyond the molecule*'[68]. Taking inspiration from the myriad of poly-molecular systems and structures in nature that owe their function or architecture to reversible, non-covalent bonding (e.g. substrate-protein binding, enzymatic reactions, antigen-antibody binding, hydrogen-bonding in DNA), synthetic chemists have developed a number of molecular classes that exploit intermolecular interactions in order to form host-guest complexes (e.g. Figure 43)[69].

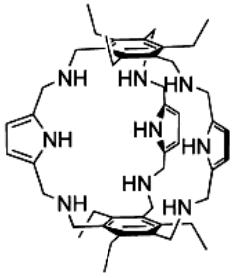

Figure 43 Pyrrolic cage receptor for carbohydrates [ref. 69]

Supramolecular host-guest complex is a system formed by a molecule (host) binding another molecule (guest). The host could be an aggregate or a cyclic molecule (e.g. macrocycles) bearing a cavity in which defined binding sites are able to form chemical interactions with the guest molecule (e.g. hydrogen bonds, etc.). Donald Cram (1986)[70,71] define the host-guest system as as follows:

Complexes are composed of two or more molecules or ions held together in unique structural relationships by electrostatic forces other than of full covalent bonds….molecular complexes are usually held together by hydrogen bonding, by ion pairing, by π-acid to π-base interactions, by metal-to-ligand binding, by van der Waals attractive forces, by solvent reorganising, and by partially made and broken covalent bonds (transition states)…….

1.1.4.2 Classification of supramolecular host-guest compounds

In 1948 H.M. Powell[72,73] proposed for a cage like host-guest the term of clathrate. This is a system in which which two or more components are linked without usual chemical union. It is possible to classify the host-guest systems into *Cavitands* bearing intramolecular cavities and *Clathrands* having extramolecular cavities as shown in (Figure 44)[74].

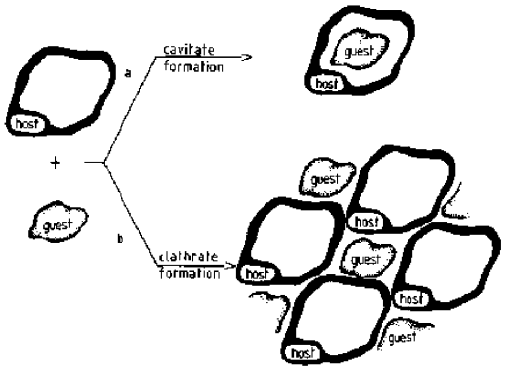

Figure 44 Differences between cavitates and clathrates [ref. 74]

Another way to classify these systems is based on different forces involved in the host-guest complex formations. For systems in which van der Waals or crystal close packing effects are predominat the term cavitate and clathrate is used; but for systems

in which ion-dipole, hydrogen bonding or dople-dipole are involved the term complex is more correct. Some examples are shown in (table 2).

Host	Guest	Interaction	Class	Example
Crown ether	Metal cation	Ion-dipole	Complex	$[K^+$ [18]crown-6]
Spherand	Alkyl ammonium	Hydrogen bond	Complex	Spherand (CH_3NH_3)
Cyclodextrin	Organic molecule	Hydrophobic/ van der Waals	Cavitate	(α-cyclodextrin)/p-hydroxybenzoic acid)
Calixarene	Organic molecule	Van der Waals/ crystal packing	Cavitate	(p-tert-butylcalix[4]arene/ Toluene)
Cyclotriveratrylene	Organic molecule	Van der Waals/ crystal packing	Clathrate	(CTV)/acetone

Table 2 Classification of common host-guest compounds [ref. 70]

1.1.4.3 Nature of Supramolecular interactions

Supramolecular chemistry involves weak bonding interactions. A variety of non-covalent or supramolecular interactions are readily available to facilitate synthetic molecular assembly, the majority of which arise from the variation of electron density around molecules. These can include: hydrogen bonding, dipole-dipole interactions, ion-ion, ion-dipole, van der Waals and hydrophobic interactions and cation-π and π-π interactions. A list of typical bond energies involved their formation is listed in (Scheme 1).

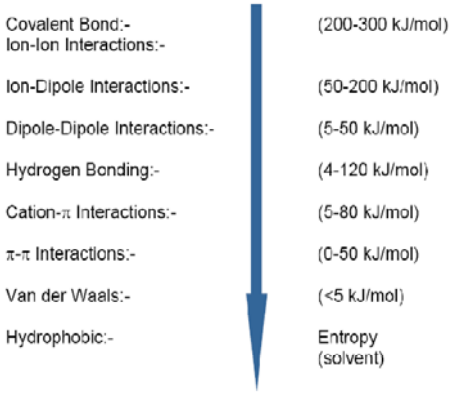

Scheme 1 Chemical interaction energies [ref 75]

The quantification of non-covalent forces is of paramount importance for the design of variety of systems such as: synthetic host-guest complexes; new drugs and new materials; enzyme analogue catalysts for active-site directed mutagenesis; and many other applications.

Ion-ion interactions A typical example of ion-ion interactions is sodium chloride in which a sodium atom bind six Cl^- anions to form a cubic lattice structure (Figure 45).

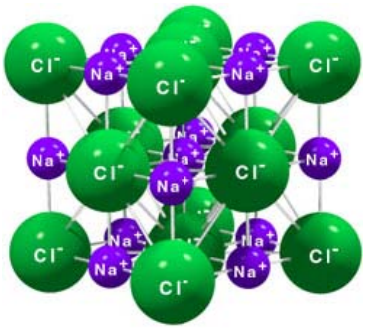

Figure 45 Sodium chloride structure [ref 76]

In water the solvatation process occurs because this structure is broken to form an octahedral species called $Na(H_2O)_6^+$. Anslyn and co-workers[77] have reported a synthetic receptor selective for citrate operating by ion-ion interactions. A noticeable specificity of electrostatic binding of tricarboxylates with tris-guanidinium receptor (Figure 46) may find even application for citrate determination in orange juice. This example demonstrates that even directionless interionic interactions can provide noticeable shape selectivity upon complexation (Figure 46)[77].

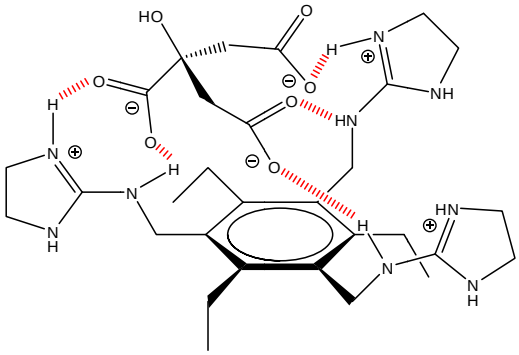

Figure 46 Trisguanidinium receptor for citrate ions recognition [ref. 77]

Ion-dipole interactions are formed when a polar molecule such as carbonyl group (with partial negative charge on the oxygen) interact an ion species like Na^+ (Figure 47).

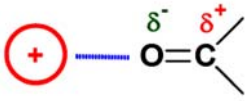

Figure 47 Ion-dipole interactions [ref. 78]

In the crown ethers the oxygen atoms play the role similar to that of the polar water moderate to form complexes with alkali metal cations, the oxygen ion pairs being attracted to the cations is positive charge (Figure 48).

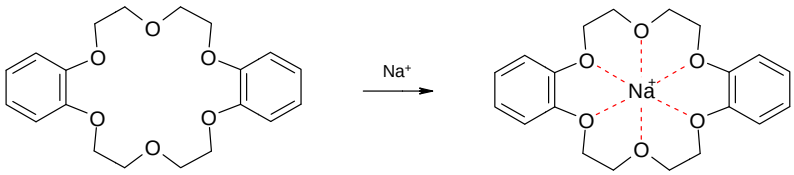

Figure 48 Crown ether sodium complex [ref 70]

Ion-dipole interactions also include coordinative bonds, with a significant covalent component as in $[Ru(bpy)_3]^{2+}$.

Dipole-dipole interactions these systems called also Keesom interactions take origin from the dipole-dipole interactions between two molecules. Organic carbonyl groups for example show this behaviour (Fig. 49).

Figure 49 Dipole-dipole interactions [ref 79]

Alignment of one dipole with another can result in a significant attractive interaction from matching either a single pair of dipoles on adjacent molecules (Type I) or opposing alignment of one dipole with respect to the other (type II)[80].

Hydrogen bonding This is a particular interaction that occurs when an hydrogen attached to electronegative atom interacts with an electronegative atom of a different molecule. It normally results from dipole-dipole interactions involving a hydrogen atom bonded to nitrogen, oxygen or fluorine. Other interactions involve for example carbon atoms with hydrogens near electronegative groups. As result of this environment the C-H proton can increase significantly the acidity and a dipole system

is generates. An elegant example of six-point hydrogen bonding between the hosts and guests has been reported by Hamilton and co-workers (Figure 50)[81].

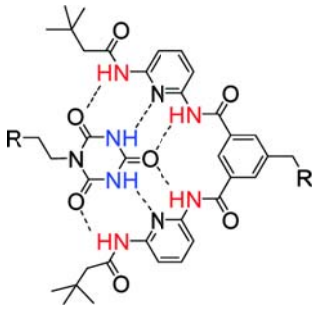

Figure 50 Host-guest receptor with six-point hydrogen bonds [ref. 81]

The most important hydrogen bonding contact occurs between a single donor D and an acceptor A atom. However, one hydrogen atom can also interact with two acceptor A atoms in a three-center, often called bifurcated, contact and less frequently in other types (Figure 51)

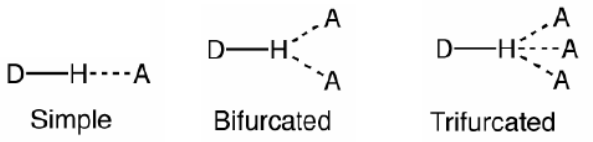

Figure 51 Hydrogen bonding examples [ref. 80]

In many proteins hydrogen bonds contribute to generate the shape and the spatial conformation. They are also able to create specific binding sites in enzyme systems and in the DNA structure to form the double helix motif.

Cation-π interaction This involves a non-covalent bonding between the face of an electronic-rich π system (e.g. benzene) with an adjacent cation (e.g. Na^+) (Figure 52).

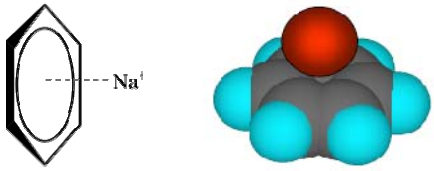

Figure 52 Cation-π interaction [Ref. 82]

This unusual interaction is an example of non-covalent bonding between a monopole (cation) and a quadrupole (π system). There is no permanent dipole moment in a

molecule like benzene, but in electron-rich π systems a partial negative charge can be measured. This gives a situation in which the positive charges in order to counterbalance the negative charges forms an association on the plane in which all benzene atoms are situated, generating an electric quadrupole (a pair of dipole). The cation-π interactions are of important to stabilize the three dimensional structure of proteins. An example is represented by nicotinamide-acetylcholine receptor whose molecular recognition mechanism of its substrate acetylcholine almost entirely relies on cation-π interactions. Examples of different synthetic cyclophanic tetraester receptors able to bind acethylcoline based on pure cation-π interactions have been reported recently by Roelens and co-workers[83].

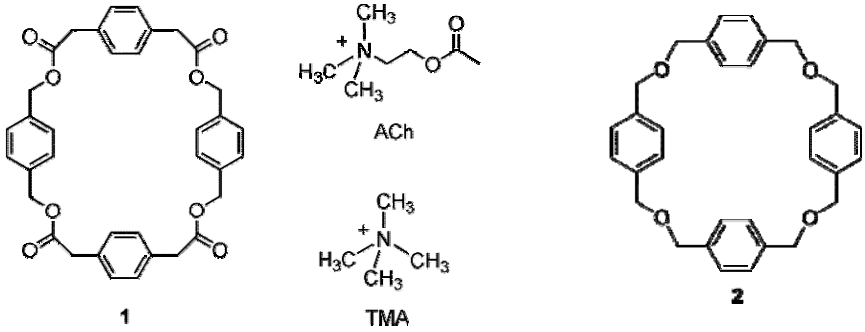

Figure 53 Cyclophane macrocycles [ref. 83]

π-π interactions This weak interaction occurs in two aromatic rings, in which one is moderately electron rich and one is electron poor. There are two types of π-stacking involving face-to-face and edge-to-face contacts (Figure 54).

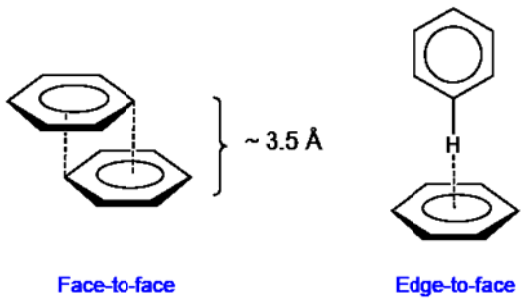

Figure 54 π-π Interactions examples [ref 84]

A face-to-face π-stacking interaction generates the slippery behaviour of the graphite and also determs its lubricant properties. The π-stacking interactions between the aryl rings also have an important role into the stabilization process between the

nucleobases pairs inside DNA double helix[84]. In order to clarify the geometry differences studied for π-π stacking interactions, Sanders and Hunter[84] have developed a simple model by using competing electrostatic van der Waals interactions (Figure 55).

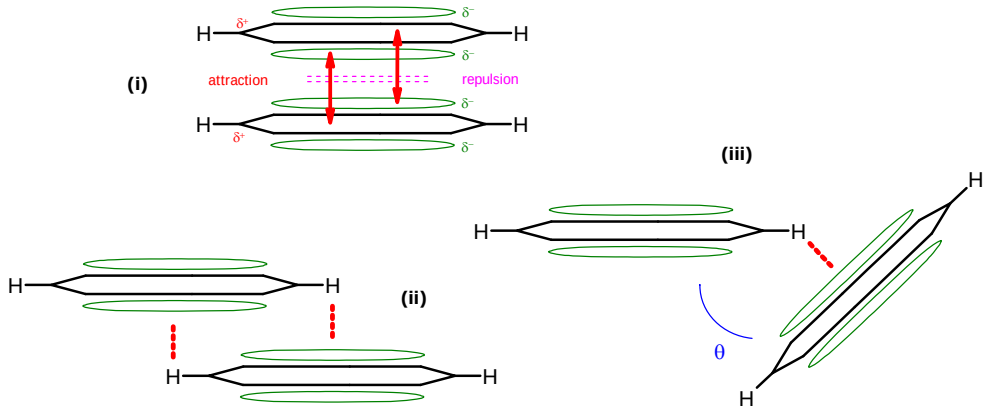

Figure 55 Geometries of π-π stacking interactions [ref. 84]

The van der Waals interaction results from the size of the contact surface area of the two π-systems. In this process the driving forces between the negative charge π-cloud of one molecule and the positive charge of an adjacent molecule correspond to the attractive energy involved in the the π-π stacking interaction. Furthemore electrostatic repulsions between the two negatively charged π-systems determ the relative orientation of the two interacting molecules.

Van der Waals interactions These are attractive forces generated by non permanent dipoles between single molecules that can interact positively giving a further enthalpic stabilisation in the organization process of hydrophobic guest into a hydrophobic cavity.

They are nondirectional and provide a classical attractive interaction for most soft (polarisable) species. These forces play a fundamental role during the inclusion compounds process in which molecules (usually organic), are complexed inside the crystalline lattices or molecular cavities. An example is the complexation of the

toluene within the molecular cavity of p-*tert*-butylcalix[4]arene (discussed in detail in section 2.2.1 of this thesis) (see Figure 56)[85].

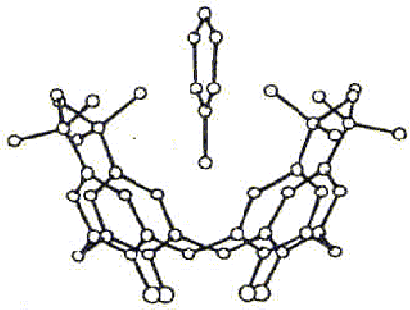

Figure 56 p-*tert*-butylcalix[4]arene (1:1) toluene complex [ref. 85]

The van der Waals interactions can be divided in two main categories: dispersion and exchange-repulsion. The dispersion is an attractive interaction originated from the contacts between fluctuating multipoles between adjacent molecules while the exchange-repulsion describes the molecular shape and balances dispersion at short range[85].

1.1.4.4 CH-π interactions

Among intermolecular interactions, the hydrogen bond is the most representative, especially in the dynamic processes involved in biological reactions. In recent years, it has gradually become accepted that a still weaker attractive force, the CH-π interaction, exists in a variety of chemical and biochemical phenomenon. We may regard the CH-π interaction as the weakest hydrogen bond occurring between a soft acid (CH) and a soft base (π-electrons). In 1960 the interactions of acetone with benzene was studied by Schaefer and co-workers[86] by means of NMR measurements. Fujiwara and Simizu[87] suggested from the results of NMR that the methyl groups in acetic acid, acetonitrile, nitromethane and toluene derivatives interact with the solvent benzene. In the late 1970[88] the existence of an attractive interaction between alkyl groups and π-bases was suggested on the grounds of a conformational study of a series of compounds. In many cases the alkyl group has been shown to position itself close to the π-group (e.g Phenyl). Comparison of the experimental results with those obtained from molecular mechanics calculations led the authors to propose that a

weak but attractive force, the CH-π interaction, was working between an alkyl group and π-system. The suggestion found theoretical support in MO calculations for several supramolecular systems. These indicated that a CH···π linear geometry should be the most stable (Figure 57).

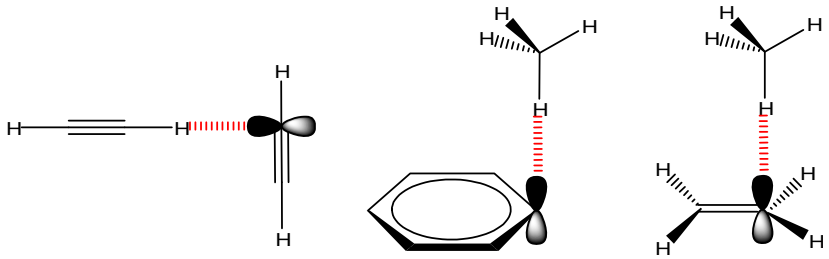

Figure 57 Preferred geometries for CH-π [ref. Nishio et al *The CH/π Interaction* Wiley-VCH]

In this system, one of the C-H bonds orients itself on the sp^2 carbon to give maximum overlap between the relevant orbitals. Using the hard-soft-base principle, Klopman[89] correlated the interaction between acids and bases to the LUMO energies of acids and HOMO energies of bases. The LUMO energies of CH acids were obtained by MO calculations; those of methane and chloroform are + 0.8ev and -1.2eV respectively. These values are within the range of soft acids. The HOMO energies of aromatics are in the range from -6.61eV (pentacene) to -9.25eV (benzene), and those of ethylene, tetramethylene and acetylene are -10.5ev, -8.27ev together with delocalized electron distribution in these molecules and -11.4eV, respectively. The orbital data strongly support the fact that the CH-π interaction may be considered as a soft acid/soft base type interaction in which the Coulombic component is less important than the charge transfer interaction. The specificity of an interaction is determined by the differences in the free energy ($\Delta G°$ or $\Delta\Delta G*$) of the two competing states (ground or transition state). In view of this, it is pertinent to point out that a difference in free energy of ca 4 kCal mol^{-1} is sufficient for bringing about 1000: 1 specificity.

A suggestion for a possible role of the CH-π interaction in supramolecular chemistry was made in 1984, by Ungaro and co-workers[90] in X-ray crystallographic study of a toluene complex of p-*tert*-butylcalix[4]arene (see section 1.1.5.3 of this thesis). In this complex a methyl group bering by the guest was shown to be surrounded by four phenyl rings of p-*tert*-butylcalix[4]arene, while aromatic ring of the toluene is chelated by two *tert*-butyl groups of the host.

The study was also enlarged to include a pyridine complex in view of involvement of the CH-π interaction[91]. The experimental results have been shown to be best reproduced in Molecular Mechanics Calculations by introducing parameters for CH-π interaction in force fields. Kobayashi and co-workers[92] using resorcinares as host system have explored the substrate specificity of several alkyl-ammonium chlorides (Figure 59).

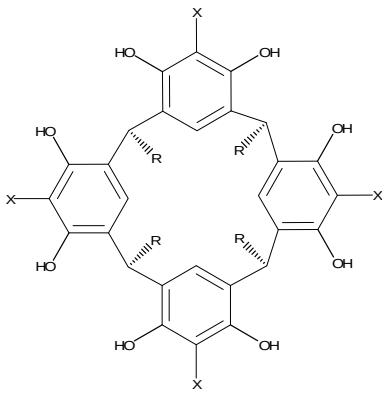

Figure 58 Resorcinarene host system [ref. 92]

Addition of methyl groups on the ammonium chloride guest results in increasing of the stability of the inclusion complex (Table 3).

	N^+H_4	MeN^+H_3	$Me_2N^+H_2$	Me_3N^+H	Me_3N^+	Me_3COH
X = H	1	1	3	30	160	4
X = CH_3					1500	19
X = OH					1800	24

Tab 3 Binding constants of different ammonium chloride guests [ref. 92]

This phenomenon supports that the force of a CH-π interaction becomes larger if the π-electron density of the aromatic ring increases. This result, with the findings reported by Ungaro and co-workers[93] show the importance of CH-π interactions during host-guest molecular systems. Specific inclusion using a similar type of host molecule (e.g. p-*tert*-butylcalix[4]arene and p-*iso*-propylcalix[4]arene) with aromatic guests such as γ-picoline, p-xylene, halo-toluenes and non-aromatic methyl guests will be discussed in more detail in section 2 of this thesis. In these systems the methyl groups are localized inside the cavity of the host to form CH-π interaction with the aromatic rings and stabilise the entire complex.

1.1.5 Calixarenes (Background)

Calixarenes are cyclic oligomers formed by the reaction of p-alkylphenols and formaldehyde in basic catalytic conditions. The basket shape gives the reason of the name "calix" (in Latin means "beaker"). These compounds are able to trap inside the cavity different guest molecules (Figure 60)[94-97].

Figure 59 p-*tert*-butylcalix[4]arene and a greek calix [ref 96]

The history of these amazing molecules start in the nineteenth century by Adolph von Bayer[98]. Bayer (Nobel Prize in Chemistry in 1905) explored different ares of organic chemistry including reaction of phenols with formaldehyde. He described in different papers (*i.e. Chemische Berichte*) the results of experiments mixing aldehydes and phenol under strong acids conditions[94]. In these studies a thick mass (resin) is reported as results of the reaction mixing aldehydes and phenols that he calls "Kittartige Sustanz" ("a cement-like substance"). In successive studies these reactions were discussed in more detail in which the reaction between benzaldehyde and pyrogallol, gave a different red-brown resin. After this time a long delay due probably that in 1872 formaldehyde was a rare chemical not easily available, opened a new field in phenol-formaldehyde chemistry. However Baeyer was able to prepare the formaldehyde by reducing iodoform with HI and red phosphorus to methylene diiodide and replacing the iodide atoms with oxygen moieties by treatment with silver acetate in acetic acid[94]. By this strategy, Bayer proved that the reaction between formaldehyde, synthesized as described above, and phenol produced a resinous material. Some years later Leo Baekeland[94] realized that a new material prepared by reaction of phenol and formaldehyde called "Velox" could be used for photographic area. Years later several other hard cement-like substances described by Baeyer founded different applications. Baekeland in 1907 pubblished a patent in which described that mixing phenol and formaldehyde by using controlled amount of base gave a new material that he called Bakelite starting the most innovative age of modern

synthetic plastics. The great success of the Bakelite process described in over 400 patents issued to Baekeland constituted the first large scale production of synthetic plastic. In 1942 Alois Zinke[94] had a great idea to use p-substituted phenols instead of normal phenol in order to avoid both the *ortho* and *para* positions to form a highly cross-linked polymer in the condensation reaction with formaldehyde (Figure 61). Using this strategy the *para*-substituted phenol can react only at the two *ortho*-positions, thereby reducing the cross-linking possibilities (Figure 62).

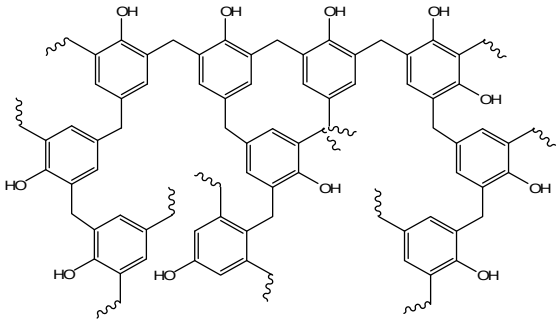

Figure 60 Cross-linked phenolic polymer [ref. 94]

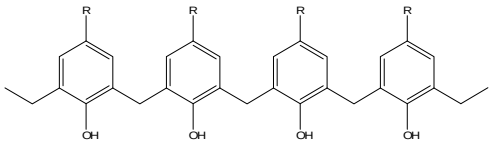

Figure 61 linear phenolic polymer [ref. 94]

The solid obtained from p-*tert*-butylphenol appeared as plates with high melting point above 300ºC, with poor solubility in organic solvents that impede the molecular-weight determination. However, the use of p-octylphenol gave a solid enough soluble in organic solvent giving a molecular-weight that resulted compatible with a cyclic tetramer. From this, tetrameric structures were inferred for all of the compounds obtained by Zinke from reaction of para-substituted phenols with formaldehyde, including those from p-*tert*-butylphenol, p-*tert*-amylphenol, p-octylphenol, p-cyclohexylphenol, p-benzylphenol and p-phenylphenol.

Subsequently Cornforth and co-workers[94,97] divided the products from p-*tert*-butylphenol and p-octylphenol with formaldehyde into higher-melting and lower-melting compounds hypothesizing the presence of conformational isomers. The model of conformational isomers for the cyclic tetramers contained four discrete forms which years later Gutsche refered to as the cone, partial cone, 1,2-alternate and 1,3-alternate conformations. Moreover Gutsche realized that the Zinke cyclic tetramers could be possible candidates as molecular baskets. The fundamental idea was to create an enzyme-mimicing receptor able to encapsulate a guest molecule by specific physical-chemistry interactions. In 1972 a research program[99] was initiated in order to

explore the Zinke compounds as appropriate host bearing a cavity capable of molecular recognition. The result of the studies of the product using p-*tert*-butylphenol and formaldehyde was a colorless substance that melted at 360-375ºC, and displayed very simple ^{1}H-NMR spectra. In order to further differentiate the linear and the cyclic oligomer a powerful NMR technique like ^{13}C-NMR spectra appeared the most useful tool showing a characteristic peaks for the cyclic tetramer[100]. The osmometric molecular weight determination gave a value of 1330, also in agreement with a cyclic octamer. Moreover an interesting result came from mass spectroscopy analysis with a strong signal at m/e 648 gave reason of the cyclic tetramer existence. Actually appear relatively easy to prepare the cyclic tetramer, hexamer and octamer from *tert*-butylphenol using the one-step procedure due the efforts involving changes in solvents, bases, reactants and other reaction variables developed by Gutsche and co-workers.

The same authors[101,102] for convenience of written and verbal discussion called the cyclic tetramer derived from p-*tert*-butylphenolic and methylene units (n = 4) p-*tert*-butyl-calix[4]arene. However this compound is more systematically named as 5,11,17,23-tetra-*tert*-butyl-25,26,27,28 tetrahydroxycalix[4]arene (Figure 64).

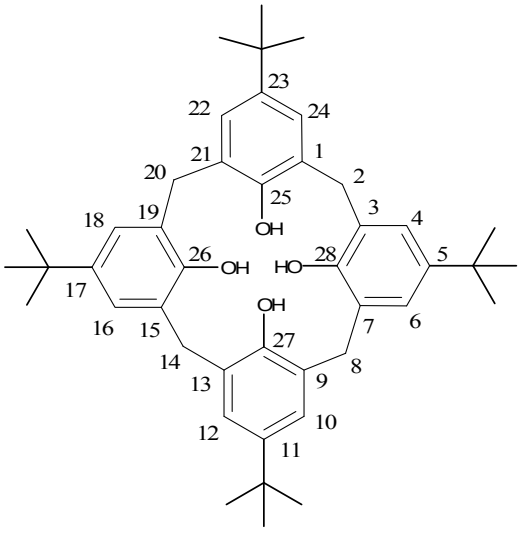

Figure 62 p-*tert*-butylcalix[4]arene nomenclature [ref. 94, 102]

Two regions can be distinguished in calixarenes: (i) the phenolic OH group region; and (ii) the *para* substituted positions of the aromatic rings; these are called respectively the “lower rim” and the “upper rim” of the calix. In the crystalline state p-*tert*-butylcalix[4]arene can exist in the vase-like conformation that provides the basis for the generic name of the entire class. This conformer has been designed by

Gutsche and co-workers[94,103] as the "cone" form (u,u,u,u) to distinguish it from the "partial cone" (u,u,u,d), "1,2-alternate (u,d,u,d), and 1,3-alternate" (u,u,d,d) forms (Figure 63). All those conformations are accessible by rotations of the aryl groups around the axis that passes through the *meta* carbon atoms bonded to the bridging methylene group.

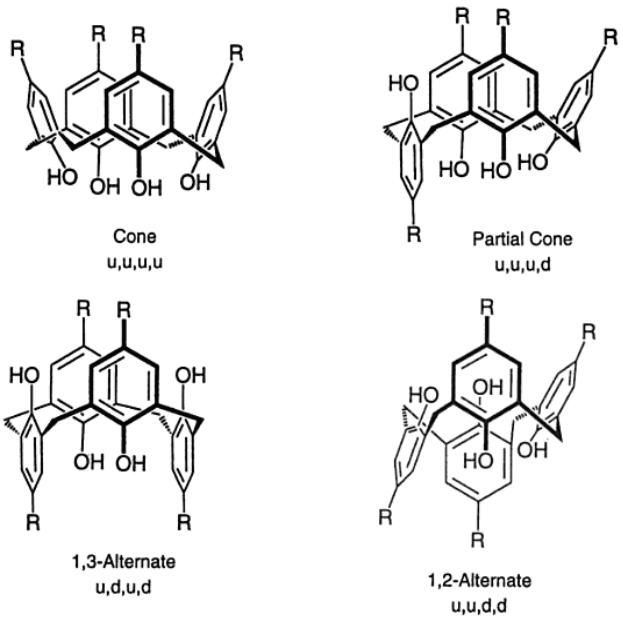

Figure 63 calixarenes conformations "u" upward or "d" downward [ref. 94]

The magnitude of the barrier to this rotation was overestimated by Gutsche and co-workers for p-*tert*-butylcalix[4]arene to be at 52ºC in chloroform at $\Delta G^{\#}$ = 15.7 kcal/mol[104]. Moreover the same author has reported the barriers for conformational inversion in different solvents for different calix[4]arenes as shown in (Table 4).

			Methylene shifts, Hz		
p-substituent	**deuterated solvent**	**T_c ºC**	**H(A)**	**H(B)**	**$\Delta G^{\#}$ Kcal/mol**
tert-butyl	chloroform	52	425	350	15.7
	toluene	39	425	324	14.9
	Carbon disulfite	36	427	351	14.9
	benzene	35	423	336	14.8
	pyridine	15	472	360	13.7
iso-propyl	chloroform	33	426	350	14.8
	toluene	30	428	322	14.4

Table 4 Coalescence temperature, Methylene Shift positions and Free Energies of Activation for calix[4]arenes [ref. 104]

In more polar solvents an appreciable decrease in the inversion barrier is observed which becomes even greater in the basic, hydrogen bonding solvent pyridine. Gutsche and co-workers[94] postulated that the major effect of these solvents, particularly pyridine, is to disrupt the intramolecular hydrogen bonding which is the primary force responsible for the preference of the calixarene to assume the cone conformation. For conformational inversion to occur it is necessary that the intramolecular hydrogen bonding be interrupted to some extent. This mechanism, which is called the broken chain pathway, requires the total disruption of the hydrogen bonding in the circular array of the initial cone conformation, although it can be recovered between two of the hydroxyl groups when the 1,3 alternate conformation has been achieved. The ^{1}H-NMR spectrum of the p-*tert*-butylcalix[4]arene (in the cone conformation) is uncomplicated at room temperature. The resonances from the aromatic protons, the *tert*-butyl protons, and the hydroxyl protons are singlets, and that of the CH_2 protons is a pair of doublets because of their inequivalence in the cone conformation which results in an AB quartet splitting pattern (Figure 65)[94].

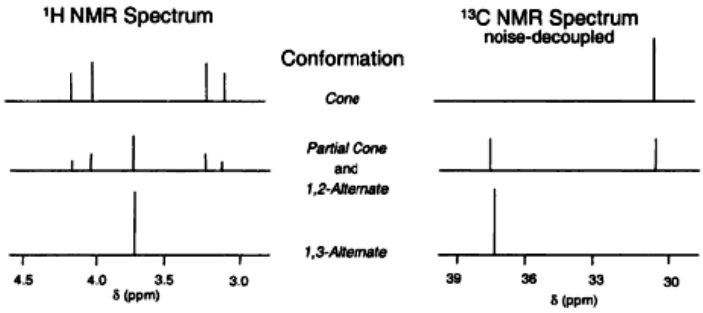

Figure 64 Calix[4]arenes splitting pattern [ref. 96]

As Kammerer first showed[105] the spectrum of the calix[4]arene in chloroform at ca. 20 °C displays a pair of doublets which collapse to a singlets when the temperature is raised to ca. 60 °C. These observations are rationalized in terms of conformational inversion (i.e., cone-cone, cone-1.2-alternate, and/or cone-1,3-alternate transformations) which, if slow on the NMR time scale, will show the CH_2 hydrogens being non equivalent and coupled to each other but which, if rapid on NMR scale, will result in the CH_2 hydrogens being observed in time-averaged environment[106]. On the basis of NOE experiments and the shift induced by pyridine as a solvent, Ungaro and co-workers[107] assigned the higher field doublet to the equatorial protons (closer to the aromatic rings) and the lower field doublet to the axial protons (closer to the

hydroxyl groups). The position of the singlet arising from the OH groups varies with the ring size of the calixarene: for calix[4]arene δ_{OH} = 10.2 ppm; wherease for calix[8]arene δ_{OH} = 9.6 ppm in $CDCl_3$. These compounds have the same NMR spectroscopical behaviour in $CDCl_3$ and bromobenzene-d_5 solutions figure 66 (1-A), (1-B), (1-C) and (1-D), that are undistinguishable also at different temperatures giving a complicated puzzle to resolve[108].

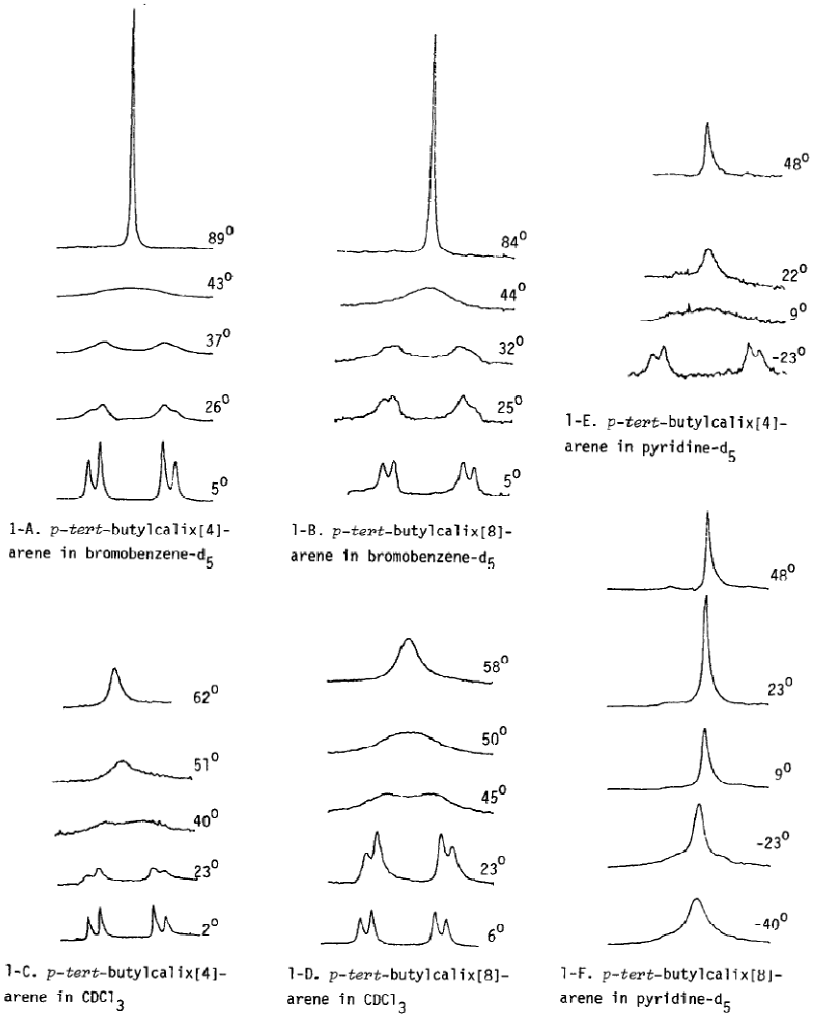

Figure 65 Temperature-dependent ^{1}H-NMR spectra of p-*tert*-butylcalix[4]arene and p-*tert*-butylcalix[8]arene, showing the CH_2 resonance behaviour at δ 3.9 [ref. 108]

A solution to this problem came by the use of pyridine-d_5 as solvent in which the coalescence temperature of the CH_2 resonance (Dynamic Nuclear Magnetic Resonance) for the p-*tert*-butylcalix[4]arene is lowered from 42-52 ºC to about 15 ºC as showed in Fig 65 (1-E). In this solvent the p-*tert*-butylcalix[8]arene spectrum reveal any resolution of CH_2 resonance into doublets down to -53°C in pyridine-d_5 as

illustrated in Fig. 65 (1-F)[108]. The rationalization behind this behaviour is attributing to the ability of pyridine to act as a hydrogen bonding solvent. With the exception of calix[8]arene, which shows peculiar conformational behaviour, the increase in the number of phenolic units in the cyclic array, increases the conformational mobility of calixarenes in solution, and allows the macrocycle to adopt new shapes (Figure 66).

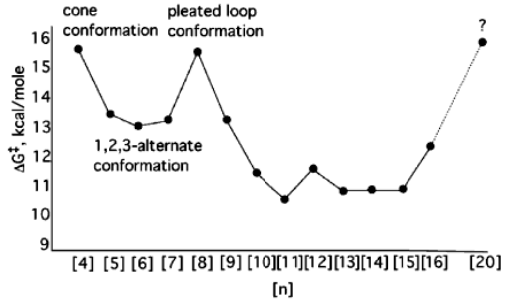

Figure 66 p-alkyl-calix[n]arenes conformation [ref 96 calixarenes revisited book]

As the number of aryl groups increases in the macrocycle, the number of possible stereoisomers also increases and their designation and representation becomes difficult. For example in the solid state the conformation of p-*tert*-butylcalix[6]arene is often referred to as "*pinched cone"* or "*winged"*[109] and that of p-*tert*-butylcalix[8]arene as "*pleated loop"* (Figure 67)[110].

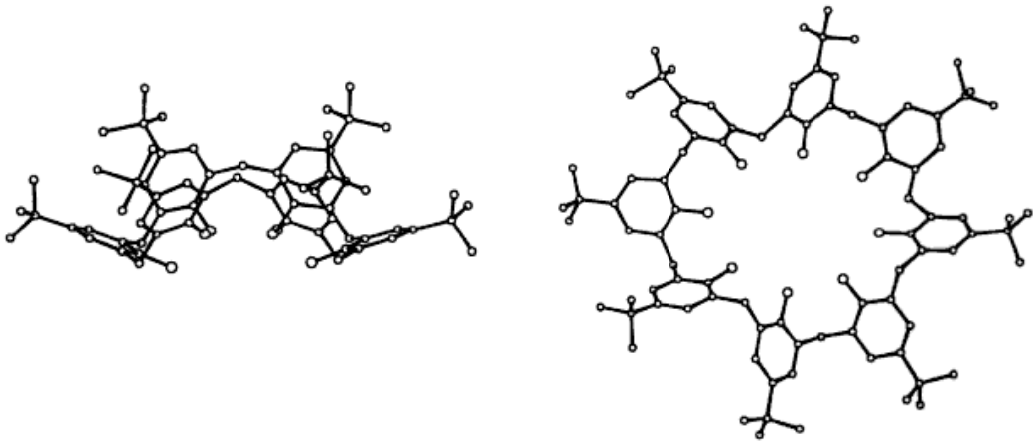

Figure 67 p-*tert*-butylcalix[6]arene and p-*tert*-butylcalix[8]arene conformations [ref. 109, 110]

For a calix[8]arene there are sixteen 'up-down' forms, as well as others in which one or more aryl group assumes the 'out' alignment. In this way the calix[8]arene maximizes intramolecular hydrogen bonding by assuming a conformation in which the OH groups lie above and below a plane. For this reason the solubility of

calix[8]arenes in the various solvents is lower than the corresponding values for the calix[4]arenes in the same solvent as illustrated in (Table 5)[111].

p-*tert*-butylcalix[4]arene			
Solvent	**Solubility/mol dm^{-3}**	**Δ_s/KJmol^{-1}**	**Δ_s/KJmol^{-1}**
MeOH	(5.90±0.13) x 10^{-4}	18.43	-6.26
EtOH	(3.30±0.11) x 10^{-4}	19.87	-4.82
DMF	(1.10±0.01) x 10^{-3}	16.89	-7.80
AN	(4.73±0.23) x 10^{-5}	24.69	0
$CHCl_3$	(4.34±0.04) x 10^{-3}	13.48	-11.21
p-*tert*-butylcalix[8]arene			
MeOH	<10^{-5}	-	-
EtOH	<10^{-5}	-	-
DMF	2.20 x 10^{-3}	15.17	-12.09
AN	1.68 x 10^{-5}	27.26	0
$CHCl_3$	6.23 x 10^{-3}	11.09	-16.17

Table 5 Solubility, free energies of solution of p-*tert*-butylcalix[n]arene (n =4, 8) in various solvents at 298.15K [ref. 111]

All calixarenes are difficult to isolate, purify and characterise, but fortunately, most have sufficient solubility in chloroform, pyridine, or carbon disulfite to permit spectral determinations to be made as described above.

1.1.5.1 Synthesis

The preparation of p-*tert*-butylcalix[4]arene for a long time was a capricious event, which gave sometimes reasonable yields of the desired compound, but poor yields or even no yields were obtained in many other instances carried out under apparently identical conditions. These different results opened the access to investigate the huge number of variable involved during the condensation process between p-alkylphenols and formaldehyde. Cornforth[102] and later Gutsche[100] found that, using the procedure by Zinke, the cyclic tetramer was not always reproducible. The main reson came from the neutralization process of the precursor. It was really difficult to reproduce form one experiment to another a good quality of the tick viscous mass because its high dependent of the amount of the base. Careful investigations by Gutsche[94] later revealed that 0.03-0.04 equivalents of base represent the maximum range in which a good yield of the cyclic tetramer can be obtained, but falls fastly on both sides of this range (see Figure 69). If the amount of base present is increased, the product isolated

is instead the cyclic hexamer (i.e. calix[6]arene) which was discovered by accident when a ten-fold amount of base was used.

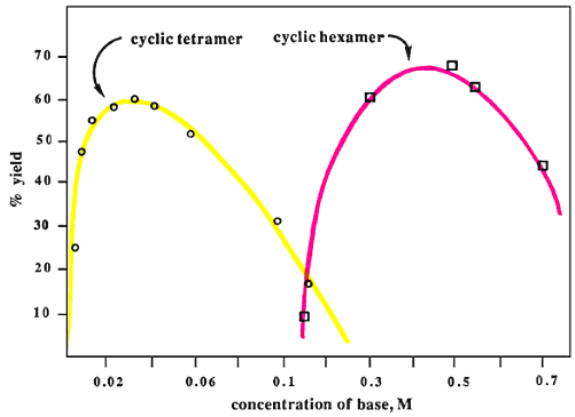

Figure 68 Effect of base concentration on the formation of p-*tert*-butylcalix[4]arene [ref. 94]

Investigations showed that the yield of tetramer reaches a maximum at and falls rapidly on both sides of this maximum Furthermore the nature of base, or rather of the cation, has a significant effect on the outcome. Using LiOH as base the yields are very low, whereas NaOH tends to give maximum yields of the cyclic octamer (which then is cracked to the cyclic tetramer), while KOH, RbOH and CsOH produce the cyclic hexamer in highest yields. The procedure for preparing the tetra(*tert*-butyl)-tetrahydroxy-calix[4]arene is given in the *Experimental Section* in detail; a mixture of p-*tert*-butylphenol, 37 % formaldehyde and NaOH (0.045 eqv. to the phenol) is heated for 2 hours at 110-120 °C to produce the "precursor". The "precursor" is then refluxed in diphenyl ether for another 2 hours, cooled and added to ethyl acetate to precipitate with 36 % yield. If the "precursor" instead is refluxed in xylene (mixture) the product collected will be the octa(*tert*-butyl)-octahydroxy-calix[8]arene in 65% yield. If the base used is KOH (0.34 eqv.), followed by reflux in xylene the product will be the hexa(*tert*-butyl)- hexahydroxy-calix[6]arene in 50 % yield. As indicated above the synthesis of the cyclic octamer and tetramer is very similar except for the

1.1.5.2 p*Ka* Values

Calixarenes have a stronger acid character than phenols, but p*K* values determination has represented a complicated task to resolve. However there are many reasons for p*K* investigations. Selective lower rim (i.e., hydroxy) modification is increasingly important in modifying calixarene function, and usually involves initial deprotonation. Comprehensive p*Ka* data would allow improved rationalization of modification methodology. In calixarene host-guest interactions many guests are potential bases for the calixarene; p*Ka* data would allow better assessment of extent of ionic (i.e. ion-pair) vs dipolar (i.e. hydrogen-bonded) complexation. Calixarenes are increasingly being used as selective hosts for neutral and cationic guests, and the strength of binding is dependent on the protonation of the calixarene; reliable p*Ka* data will allow better design of such systems. Calixarenes show a complex and varied conformational chemistry; examination of p*Ka* data can provide information about conformational effects. Finally calixarenes are ideally constructed to facilitate hydrogen bonding, both intramolecularly and as a directing force in supramolecular structural motifs. As one of the most important factors in acidity is hydrogen-bonding stabilization of an anion, a study of calixarene acidity would give insight into the wider aspects of hydrogen bonding. Recently Cunningham and Woolfall[112] have reported p*Ka* values for p-*tert*-butylcalix[n]arene (n = 4, 6, 8) in acetonitrile using a spectroscopic methods. They have used organic bases of known p*Ka*, to selectively deprotonate the calixarenes and p*Ka* values are reported in Table 6.

Calixarene tetramer	$pK_1 = 19.06$	$pK_2 > 33$	
Calixarene hexamer	$pK_1 = 15.59$	$pK_2 = 23.85$	$pK_3 > 33$
Calixarene octamer	$pK_1 = 17.20$	$pK_2 = 23.32$	$pK_3 > 33$

Table 6 pK_a values for different p-*tert*-butylcalixarenes [ref. 112]

1.1.5.3 Complexation behaviour

Many calixarenes form solid state complexes, this property having been observed even before the structures of the compounds had been established. The complexes of calixarenes with neutral molecules may be divided into three main categories: *intramolecular complexes, cage complexes* and *intermolecular complexes.*

Intramolecular complexes of calixarenes

p-*tert*-Butylcalix[4]arene forms solid state complexes with toluene, 4-picoline and p-xylene, which are stable at room temperature, whereas the complex with chloroform shows a remarkable tendency to lose the solvent. The p-*tert*-butylcalix[4]arene (1:1) toluene complex shown in (Fig. 69) was the first one whose molecular conformation in solid state was established by XRD on single crystals (Figure 69)[113-114].

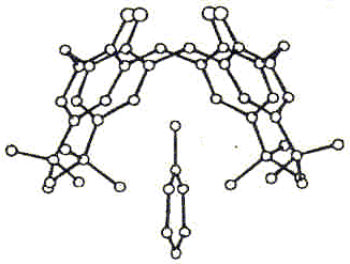

Figure 69 p-*tert*-butylcalix[4]arene (1:1) toluene complex [ref. 114]

The molecule which possesses fourfold symmetry assumes the shape designated as cone conformation dominated mainly by a cyclic array of four intramolecular hydrogen bonds. The size of the cavity is suitable to accommodate a guest molecule, in this case toluene, the C-CH_3 axis of which coincides with the fourfold axis of the macrocycle.

The guest selectivity properties towards different aromatic molecules obtained by competitive crystallization experiments in the presence of equal volumes of competing guests has shown that the presence of the cone conformation of the host is not a sufficient condition to ensure the selective complexation of an aromatic guest inside the cavity of the host, but other structural factors also play a major rule. The observation that the unsubstituted calix[4]arene never gives complexation, has led to the hypothesis of an attractive $CH_3 \cdots \pi$ interaction between the methyl group of the

toluene and the aromatic rings of the host and between guest's aromatic ring with the *tert*-butyl groups of the calixarene moiety. Other structural evidence has supported these hypotheses. Recently Ripmeester and co-workers[113] using the ^{1}H magic angle spinning (MAS) NMR spectra in combination with quantum mechanical calculations (*ab initio*) have provided important spatial information about the location of the guest molecules (toluene and pyridine) in host cavities such as p-*tert*-butylcalix[4]arene (Figure 70). For the first time a map of *complexation-induced shifts* (CIS_s) in the calixarene cavity was constructed using *ab initio* calculations.

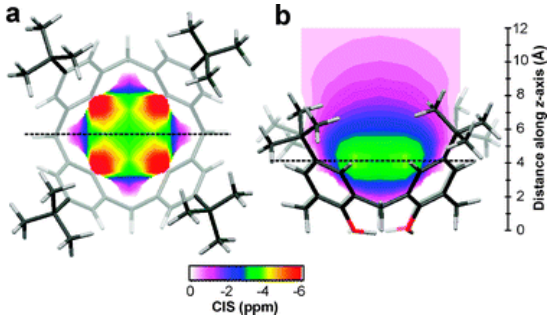

Figure 70 Complexation-induced shift maps in the p-tert-butylcalix[4]arene cavity from *ab initio* calculations [ref. 113]

These CIS maps which plot the difference in magnetic shielding between the nucleus of a "free" He atom and the "complexed" He atom, provide a useful qualitative tool for understanding the experimentally observed ^{1}H chemical shifts.

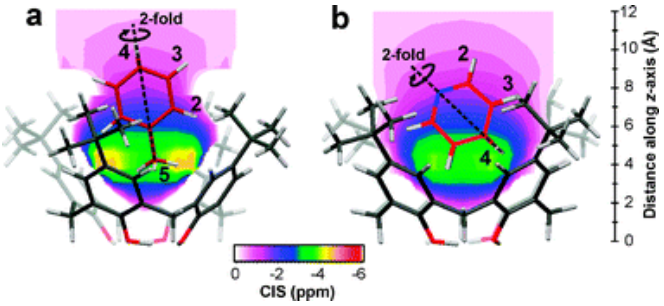

Figure 71 Complexation-induced shift maps in the p-*tert*-butylcalix[4]arene cavity from *ab initio* calculations; a) p-*tert* butylcalix[4]arene (1:1) toluene complex; b) p-*tert*-butylcalix[4]arene (1:1) pyridine complex [ref. 113]

For the toluene-calixarene complex (Fig. 71-a, b) methyl protons (H5) are located near maximum CISs, the *ortho* (H2) protons lying just slightly above the cavity show medium shifts, while the *meta* (H3) and *para* (H4) are located above the cavity regions with only small shifts. These results are in qualitative agreement with the experimentally observed CIS. This method reinforced the hypothesis of an attractive

$CH_3 \cdots \pi$ interaction between the methyl group of the toluene and the host aromatic rings and of the toluene aromatic ring protons with the *tert*-butyl groups of the calixarene moiety as described above. Intramolecular (1:1) complexes of p-*tert*-butylcalix[4]arene with 4-picoline have also been characterized by X-ray diffraction[114]. Apart from small but significant differences in the tetragonal cell parameters, the 4-picoline complex shows a molecular structure quite similar to that observed in the case of the toluene complex. The space group remains unchanged (P_4/n) and the guest molecules lie on the fourfold axis in both complexes. However, Caciuffo and co-workers[114] have shown by INS (inelastic neutron scattering) measurements that, for this complex, differences in the attractive $CH_3 \cdots \pi$ interaction between the methyl groups of the host and the aromatic π orbital of the guest could result in a different position inside the intramolecular cavity of the guest methyl group and, therefore in a different rotational barrier.

Calixarene cage complexes

In 1985 Ungaro and co-workers[115] isolated a new type of inclusion compound formed by two p-*tert*-butylcalix[4]arenes and anisole (Figure 72).

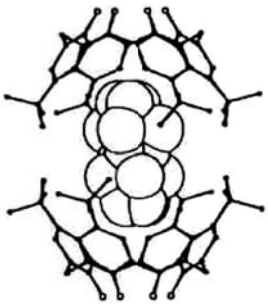

Figure 72 p-*tert*-butylcalix[4]arene (2:1) anisole complex [ref. 115]

This was the first example of an uncharged-host uncharged guest complex forming an enclosed cage structure. In the classification and nomenclature proposed by Weber and Josel[116] this inclusion compound is an example of a *cryptato-cavitate* clathrate complex. The observed solid state topology is quite different from that observed in the toluene complex reported from the same authors in 1979[85]. In the anisole complex, the lattice does not contribute to the inclusion of the anisole, whereas in the corresponding toluene (1:1) complex the guest's methyl group enters the calix cavity, and the cage is completed by the lattice bringing the p-*tert*-butyl groups of two different symmetry-related macrocyclic molecules in contact with the aromatic nucleus of the toluene.

Subsequent studies[117] have revealed that inclusion compounds involving p-*tert*-butylcalix[4]arene most often crystallize with the host molecules as bilayer structures having *low density* with (1:1) host-guest stoichiometry and *high density* with (2:1) host-guest stoichiometry. The guest either lies in a single cavity roofed by *tert*-butyl groups in the next layer, or in a capsule consisting of two opposed calixarenes molecules[107]. Several experiments exploring storage of the gasses using the *low density* have been reported[118]. However Atwood and co-workers have obtained diffraction-quality single crystals of uncomplexed p-*tert*-butylcalix[4]arene by sublimation of the compound at 280ºC under reduced pressure. The structure of this sublimed phase proves to be a polymorphic form of pure p-*tert*-butylcalix[4]arene with molecular packing in the familiar bilayer motif in which facing calixarenes are

slightly offset relative to one another. This arrangement results in the formation of skewed capsules (Figure 73-a) each with an estimated free volume of 325 Å. In several papers they have demonstrated that this *low-density* polymorph absorbs different gases (N_2, O_2, CO and CO_2) under ambient conditions.

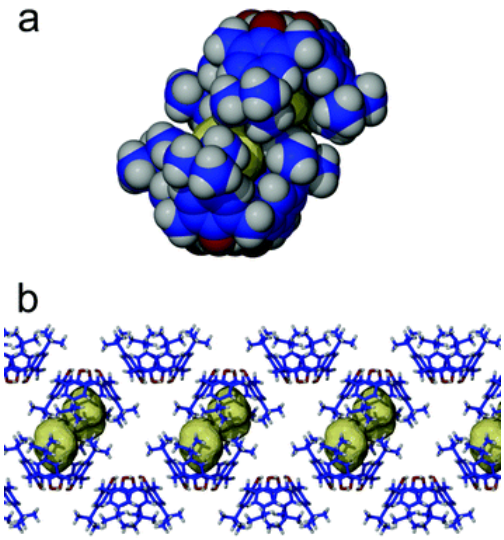

Figure 73 Representation of a bilayer packing of calixarene molecules with methane as guest [ref. 118]

They have also demonstrated the capacity of the low-density of p-*tert*-butylcalix[4]arene (Figure 73-b) to absorb methane more readily at room temperature and 1 atm pressure than do either single-wall nanotubes (SWNT) or analogous porous metal-organic frameworks (i.e. MOF-1)[118].

Intermolecular complexes

Calixarenes also have ability to form *intermolecular* complexes with aromatic molecules. In fact *p*-(1,1,3,3)-tetramethylbutylcalix[4]arene crystallizes from acetone without inclusion of solvent, wherease in the presence of toluene a 1:1 intermolecular complex has been isolated (Figure 74)[119].

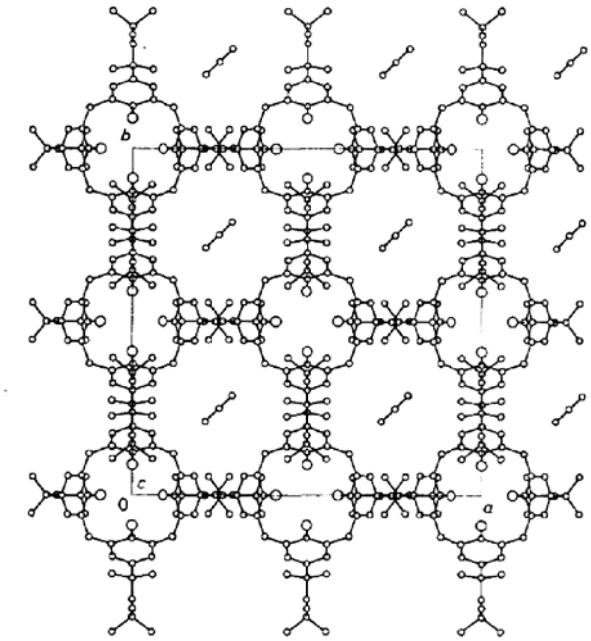

Figurem 74 Molecular packing diagram of 1,1,3,3-tetramethylbutylcalix[4]arene (1:1) toluene complex [ref. 119]

In this case the toluene molecule lies in the intermolecular cavities between the calixarene units and interacts with the terminal *t*-butyl groups in the host. Conversely, when the compound is crystallized from acetone, the crystal packing distributes the macrocycles in a quite different way which does not allow intermolecular complexation. This suggests that the toluene molecule plays a key role in the formation of the intermolecular complex because its aromatic nature can be recognized by the macrocycle and just its presence in solution drives the growth of the observed crystal structure of the complex. This is another piece of experimental evidence for coordinative interactions between the methyl groups of the host and the π electrons of the guest that determine the intermolecular character of the inclusion. However recent studies have revealed unusual properties for this calixarene derivative including storage hydrogen in its cavity. Atwood and co-workers[120] have reported that the solid state structure reveals that two *tert*-butyl moieties of distal *p*-octyl groups are

directed away from the molecular cleft, while the remaining two *tert*-butyl moieties reach into the cleft to favour the hydrogen entrapment (Figure 75-a and b).

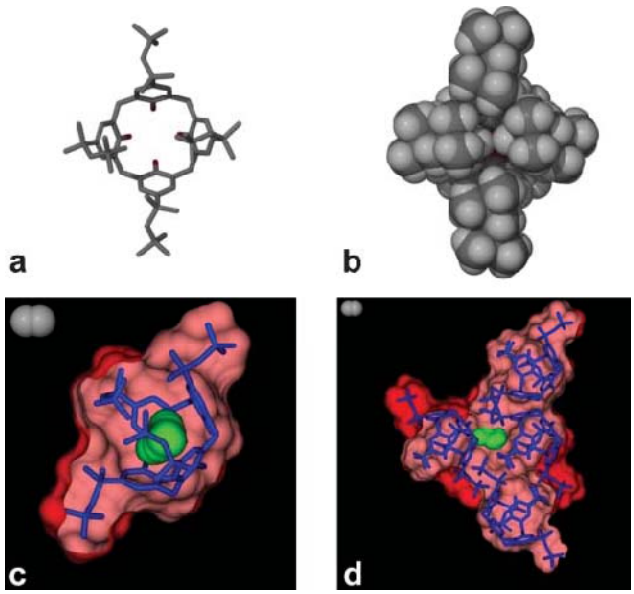

Figure 75 Representation of capped stick (a), orientation of p-*tert*-octyl moieties (b), molecular cavity (c) and additional interstitial void (d) of p-(1,1,3,3)-tetramethylbutylcalix[4]arene [ref. 120]

Thus a relatively small cavity intramolecular cavity (Figure 75-c) is formed and is completely isolated from the exterior of the calixarene molecule. An additional void is formed interstitially between six molecules (Figure 75-d).

1.1.5.4 Aims of present studies

The primary goal of the CryoMAS project, led by Prof. M. H. Levitt of the University of Southampton, is to develop the necessary technology and technique to study large biomolecules, such as proteins, using NMR at cryogenic temperatures. MAS NMR is a high resolution technique that is routinely used to solve molecular structures. By performing MAS at cryogenic temperature, the dual benefits of high resolution and increased signal-to-noise should aid in providing answers to questions that are currently beyond the scope of conventional NMR techniques. There are a broad range of scientific and technological challenges associated with achieving this goal, one of which is the development of so-called *cryorelaxors*. The target of operational temperature for CryoMAS, limited by technical challenges associated with stable rotation of the sample rotor, is around 20K. It is desirable for a cryorelaxor to have a T_1 minimum, or at least a small value of T_1 (~1s), at that temperature and at the operational field of the CryoMAS experiments. The work reported in this thesis focuses on the synthesis of a number of calixarene host-guest complexes incorporating rotationally labile methyl substituents having potential application as Cryo relaxation agents. The behaviour of the complexes prepared has been investigated by MAS and Field-cycling NMR experiments and, in some cases by INS techniques. In addition some of the complexes have been modified in order to incorporate biological “anchors” and the behaviour of some of these has been explored. Finally some work has also been carried out on the synthesis of endohedral fullerene derivatives.

2 Results and discussion

2.1 Calixarene synthesis

2.1.1 p-*tert*-Butylcalix[4]arene

For many years the preparation of the p-*tert*-butylcalix[4]arene used the Cornforth[94] procedure but this gave low yields after many crystallization cycles from a mixture of cyclic oligomers. Subsequently Gutsche and co-workers successfully developed a route to the cyclic tetramer using a "One Pot" procedure (scheme 2). This synthesis has been reported as being easy to reproduce, but for good yields careful control of many parameters is required. The reaction uses p-*tert*-butyl-phenol with formaldehyde solution in the presence of sodium hydroxide as catalyst.

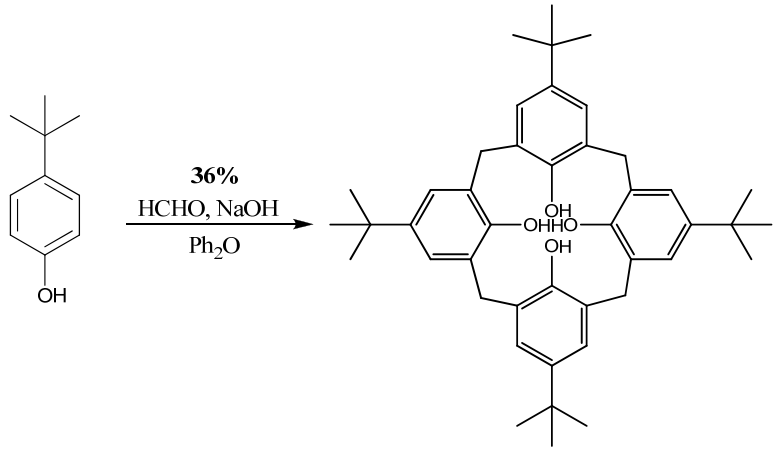

Scheme 2

In order to successfully carry out this synthesis four key factors require careful control: a) the amount of sodium hydroxide; b) the physical conditions employed c) precursor formation; and d) pyrolysis of the precursor at elevated temperatures.

As reported in the literature[94,121] the best base to give the cyclic tetramer is sodium hydroxide. The amount of the base used is also very important in order to obtain good quality precursor; this latter is a friable solid which can be ground to a powder, the particle size of which depends on the manner and extent of grinding. After careful investigation I have observed that there is an optimum amount of NaOH for which the yield of product reaches a maximum (ca. 0.03-0.04 equivalent of base) and yield falls off either side of this range. With less base the yield of cyclic tetramer falls, ultimately to zero. With more base the yield of cyclic tetramer again falls and at ca. 0.055 equivalents refluxing of the mixture becomes very dangerous because of the

development of many gas jets in the flask during the refluxing procedure at high temperature. The optimum amount of the base required to obtain a good sample of precursor and a readily filterable precipitate appears to be 0.0024mol corresponding to 0.036 equivalents of base. Under these conditions it is possible to control the reflux conditions and obtain a clean solution during the reflux procedure.

The physical parameters used are also very important in order to favour precipitation at the end of the reaction. In the first step it is better to use a big flask for three reasons: (i) the water can evaporate through the larger surface area and give a good precursor, which is yellow, friable and can be easily removed from the flask; (ii) it is very important to control the internal pressure during the pyrolysis phase; and (iii) the concentration and the pressure of the gases evolving during the reflux can be better controlled in a big flask since they can expand within a large volume. Furthermore the quality of the precursor formed is very important. To achieve a good quality intermediate, the reagents in the optimum stoichiometric ratio must be initially stirred at room temperature for 20 min, very slowly, to permit a full dissolution of the p-*tert*-butyl-phenol. Heating then at 110-120 °C gives a yellow liquid mass after 30 mins and after a further 2h the liquid mass becomes solid. Heating must be then continued for a further hour to obtain, after cooling to room temperature, a yellow thick friable material.

2.1.2 Calixarene's mechanism formation

The mechanism of base-induced oligomerization of phenol and formaldehyde has been studied for many decades. The first step is initiated by formation of phenoxide ion which acts as a carbon nucleophile, attacking the highly reactive carbonyl group of formaldehyde (scheme 3).

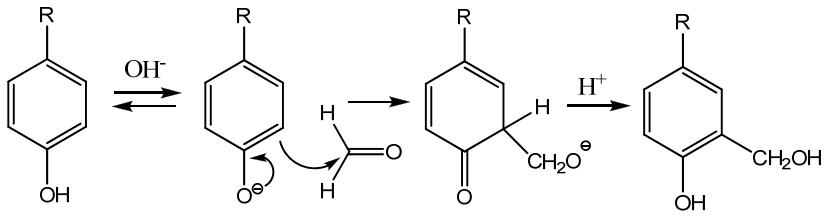

Scheme 3

Under mild conditions the reaction can be terminated at this point, but under more vigorous conditions the reaction proceeds further to give diarylmethyl adducts, involving a o-quinonemethide derivatives that can react with phenolate ions following a Michael-like addition route (Scheme 4). The idea that o-quinonemethides was involved in the formation of such linear oligomers was suggested as long ago as 1912 and was subsequently resurrected by Hultzsch, Euler, and others[94].

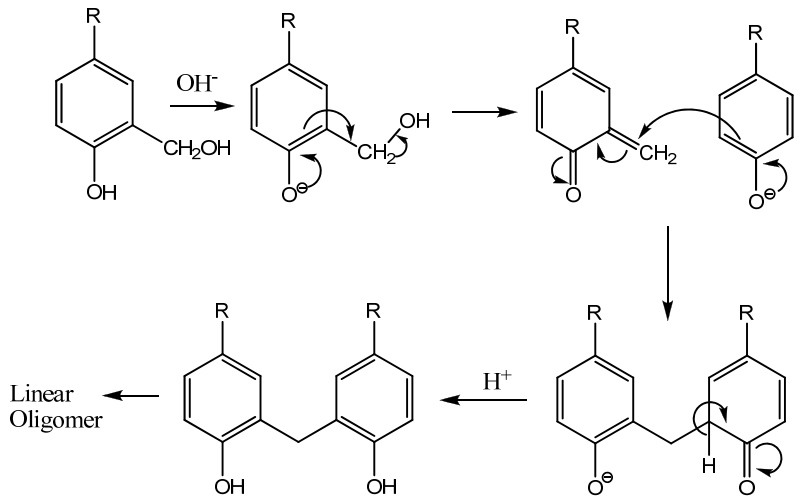

Scheme 4

The precise mechanism for the transformation from linear to cyclic oligomers remains something of a mystery, although a speculative pathway has been suggested by Gutsche and coworkers based on hydrogen-bonding considerations and oligomer interconversion reactions.

A crucial role is played by the reflux temperature for the pyrolysis of the friable intermediate. This transformation occurs at high temperature and is a very important step because, before the refluxing, the reaction gives a yellow precipitate which has been shown by Gutsche[122] to be the cyclic octamer. At high temperature this is transformed into the cyclic tetramer. This turn of events is rationalized in terms of hydrogen bonding in the cyclic as well as the linear oligomers. The presence of circularly hydrogen bonded arrays in calixarenes is supported by infrared as well as *X*-ray crystallographic data which indicate that the calix[8]arene adopts a plated loop conformation. X-ray crystallographic studies[110] of the linear tetramer show that it exists in a staggered conformation in the solid state, with intramolecular hydrogen bonding holding the phenyl groups in an almost planar, zig-zag array.

The transformation of cyclic octamer into cyclic tetramer is called "Molecular Mitosis"[94] and occurs only in a high boiling temperature solvent such as diphenyl ether at 260 °C. This solvent is very sensitive to moisture and light, and for these reasons must be stored in dark dry environment. The important conversion of p-*tert*-butylcalix[8]arene to p-*tert*-butylcalix[4]arene requires the right combination of heat and base. In this process the cyclic octamer pinches together in the middle and splits into a pair of cyclic tetramers (scheme 5)[94,97].

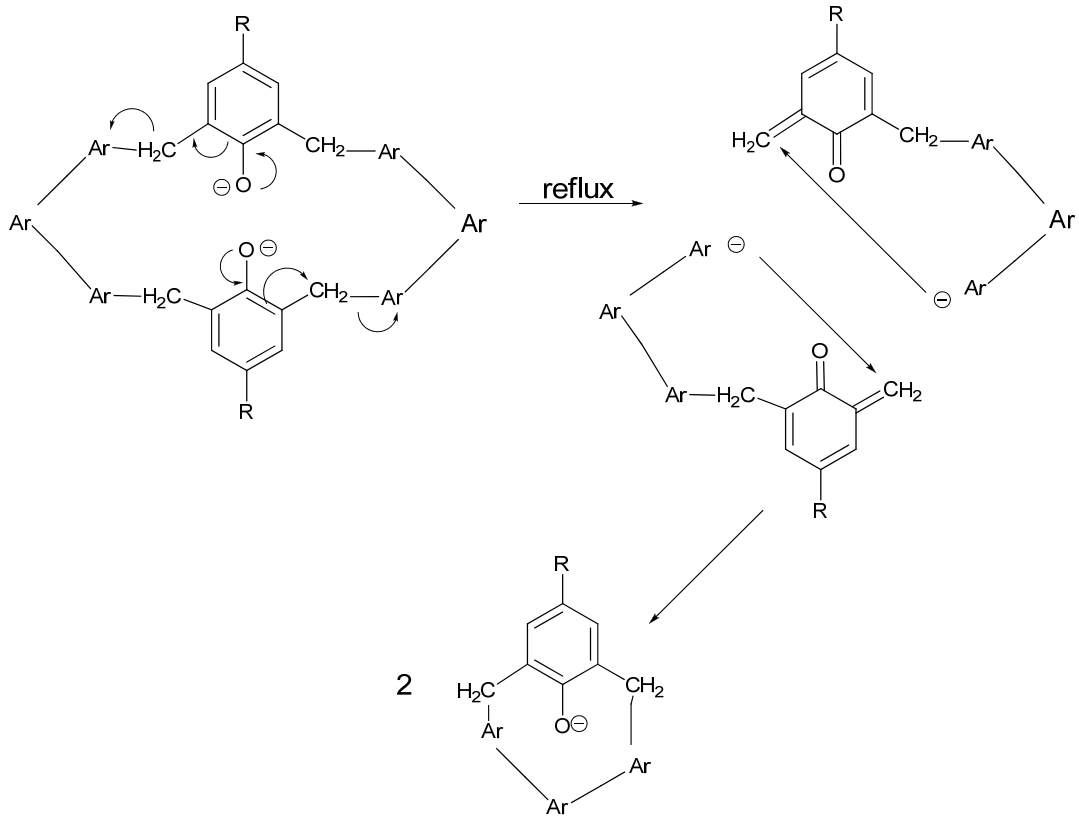

Scheme 5

The literature does not describe the exact conditions required to obtain a good "molecular mitosis" process to favour cyclic tetramer formation, but after careful investigation it has been possible optimize this procedure.

2.1.3 p-*tert*-Butyl_d_{36}-calix[4]arene

As described earlier the p-*tert*-butylcalix[4]arene can be prepared by base-catalysed condensation of p-*tert*-butylphenol and formaldehyde using a one-pot procedure in good yield.[100,102] In order to synthesize a calixarene labelled with deuterium on the *tert*-butyl groups a new strategy was required because p-*tert*-butylphenol_d_9 was not commercially available. Considerable efforts have been made to develop a good procedure for synthesis of the starting material. Friedel Crafts alkylation represented the best simplest method to introduce alkyl groups on the aromatic ring. Using phenol and *tert*-butylchloride with $AlCl_3$ as catalyst in dry chloroform, the *para*-substituted phenol can be obtained but accompanied always by smaller amounts of *ortho*-substituted and disubstituted phenols and flash chromatography is required to purify the compound[123]. It was therefore important to develop a selective method to obtain only the p-*tert*-butylphenol in high yields because the deuterated reagent (*tert*-butylchloride_d_9) is very expensive.

Using the same procedure, solvent free[124] in a preliminary experiment with non-labelled reagents, I have obtained pure p-*tert*-butylphenol in excellent yield after crystallization from petrol as showed in Scheme 6:

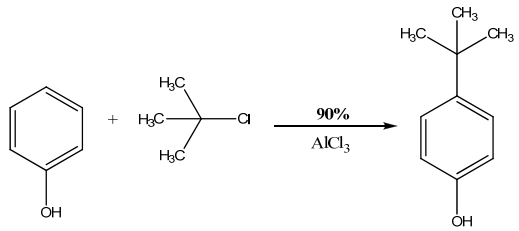

Scheme 6

The ^{1}H-NMR, ^{13}C-NMR, EIMS-GC mass spectra and the m.p. (96-98ºC) have confirmed the presence of only the *para*-substituted phenol. Therefore, it should be possible to use this method with the expensive *tert*-butyl_d_9 chloride (Scheme 7).

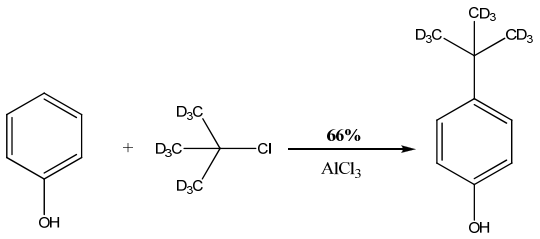

Scheme 7

The formation p-*tert*-butyl_d_9 phenol under these conditions has been confirmed by EIMS-GC, NMR and IR spectroscopy. Considerable effort has been spent obtaining a good "precursor" that must be a friable solid which can be ground to powder. It was necessary to re-crystallize the *tert*-buylphenol_d_9 from petrol to remove impurity traces and water. It has not proved easy to synthesise the p-*tert*-butylcalix[4]arene_d_{36} in micro-scale conditions, because this reaction requires the control of many physical parameters to favour the precipitation process at the end of the reaction.

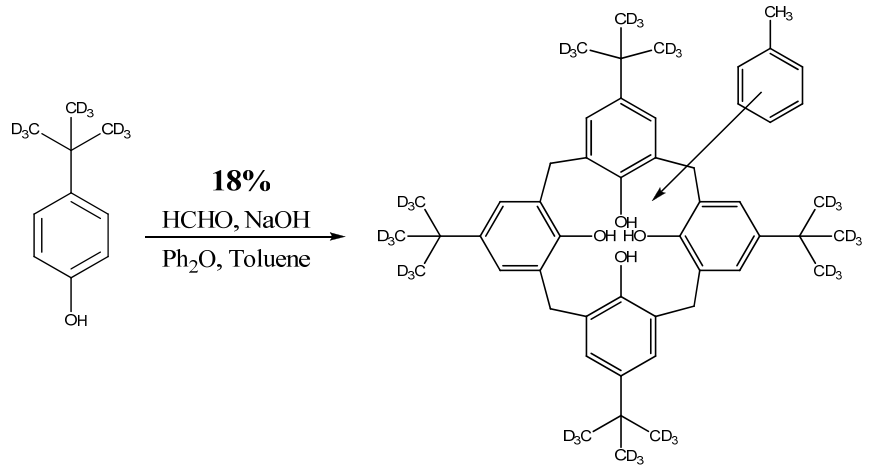

Scheme 8

After a tricky one-pot procedure the p-*tert*-butyl_d_{36} calix[4]arene (scheme 8) was synthesised, re-crystallized from toluene and its structure was confirmed by ES^- Mass spectra m/e 683, ^{1}H-NMR spectrometry (which showed aromatic protons signals and only residual protons signals in *tert*-butyl region as expected; estimated deuteration level 94.5%), and by ^{13}C-CP/MAS NMR with calculated CIS (*complexation induced chemical shift*) $\Delta\delta = \delta$ (solid state) $- \delta$ (solution) corresponding to -6.2ppm as expected for toluene guest inside the calixarene cavity (see section 2.2.2.1 of this thesis). Moreover a partially solved X-Ray structural study has confirmed the presence scaffold of the calixarene scaffold with its toluene guest molecule as indicated by the the ^{13}C-CP/MAS NMR spectra.

2.1.4 p-*tert*-Butylcalix[4]arene_d_{44}

In order to also introduce deuteration into the aromatic rings of the calixarene host the same strategy solvent free was employed as described above but using phenol_d_5 with *tert*-butylchloride_d_9 as starting materials. Pure p-*tert*-butylphenol_d_{13} was obtained in good yield after crystallization from petrol (Scheme 9).

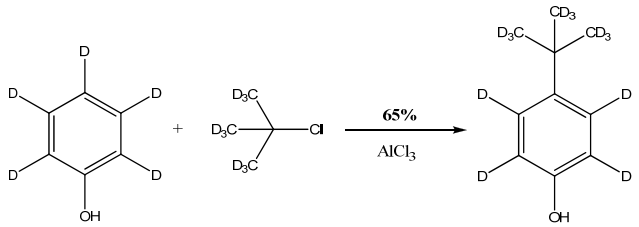

Scheme 9

The EIMS-GC Mass spectra, and ^{1}H-NMR data (showing only residual proton signals in the aromatic and *tert*-butyl region) were consistent with formation of this compound. As found previously it did not proved easy to synthesise the p-*tert*-butylcalix[4]arene_d_{44} under micro-scale conditions, because this process again requires careful control of many physical parameters (Scheme 10).

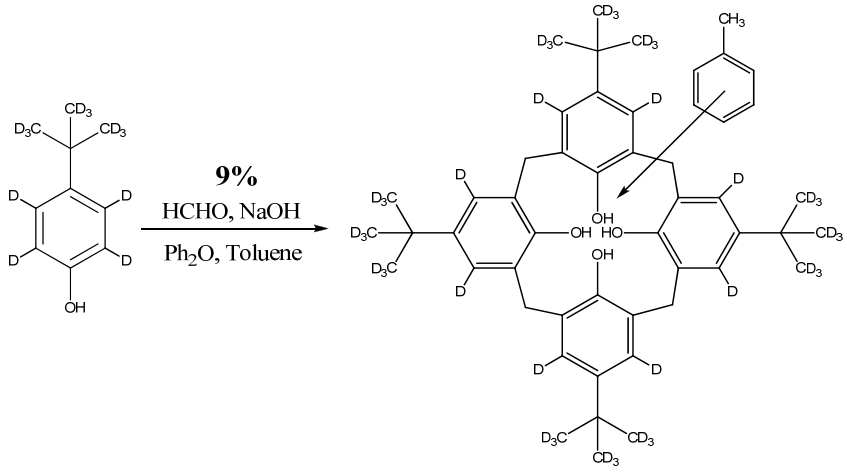

Scheme 10

After heating for 4 hours in NaOH/diphenyl ether with formaldehyde the expected yellow-orange solid ("the precursor") was formed. Molecular mitosis was then carried out as described above in a one-pot procedure and the p-*tert*-butylcalix[4]arene_d_{44} was re-crystallized from toluene and characterized by ES$^-$ Mass spectra m/e 691, ^{1}H-NMR data (with only residual proton signals being seen in the aromatic and *tert*-butyl

regions, estimated deuteration level 97.6%). The ^{13}C-CP/MAS NMR showed CIS corresponded to -6.2ppm for a toluene guest inside the calixarene cavity. (as seen for the partial deuterated calixarene)

2.1.5 p-*tert*-Butylcalix[4]arene-Biscrown3[125]

In order to increase the rigidity of a calix[4]arene, I have used the Ungaro procedure to prepare the p-*tert*-butylcalix[4]arene-Biscrown3 (Scheme 1) which capable of trapping acetonitrile inside the cavity by weak intermolecular CH···π interactions.

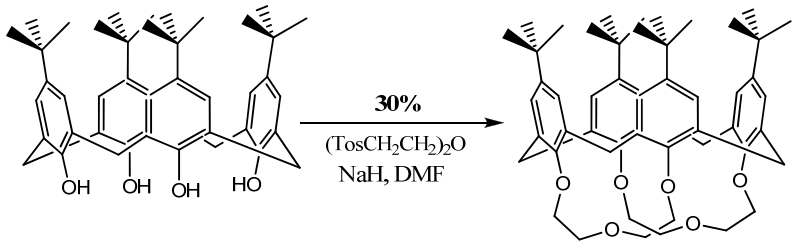

Scheme 11

By reacting p-*tert*-butylcalix[4]arene in DMF with diethylene glycol ditosylate using an excess of NaH the proximal bis-crown was obtained in 30% yield after chromatography (scheme 11).

Lower rim bridged calixarene

2.1.6 p-*tert*-Butyl-25,27-[toluene-2,6-bis(amino-carbonylmethoxy)-26,28-dihydro xycalix[4]arene

A prototype of a covalent bridged calixarene on the lower rim is the calix[4]arene-crown[94], an example of which was first synthesized in the early 1980s followed by many examples with various chain lengths[126], including calixazacrowns[127] in which one or more nitrogen atoms take place of oxygen atoms. By employing the alkylation techniques described above hemispherand moieties[128], diglycosyl moieties[129] and variety of spanners of general structure Ar-Ar or X-Ar-Z-Ar-X (X=CO or CH_2 and Z=CO) has been reported. In order to increase the control over the location of the methyl rotor within the calixarene cavity, a synthetic strategy was explored to prepare a calixarene with a covalent bridge suspended across the lower rim. Ungaro et co-workers[130] have described a method using sodium hydride and an excess of *tert*-butyl bromoacetate in tetrahydrofuran THF-N,N-dimethylformamide (DMF) to prepare a calixarene functionalized on the lower rim as tetra-esters. The functionalization of calixarenes at the lower rim can be either partial (selective) and can be carried out with a large variety of reagents. The significant differences in the p*K*a values of phenolic OH groups allow their stepwise deprotonation and their selective functionalization.

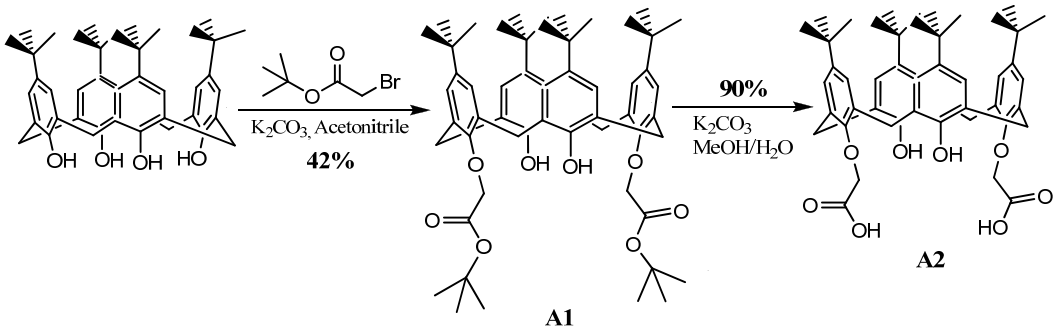

Scheme 12

Using a modification of Ungaro's procedure I have obtained in good yield 1,3-distal esters (**A1**) attached to the lower rim by performing the reaction in acetonitrile as solvent and potassium carbonate as bases, to give after simple filtration, a pure compound. NMR spectroscopy has confirmed the presence of the cone conformation

showing the characteristic AB system as a doublet at 3.18 and 4.53 ppm. Basic hydrolysis of this diester gave 1,3 distal-carboxylic acid (**A2**)[131].

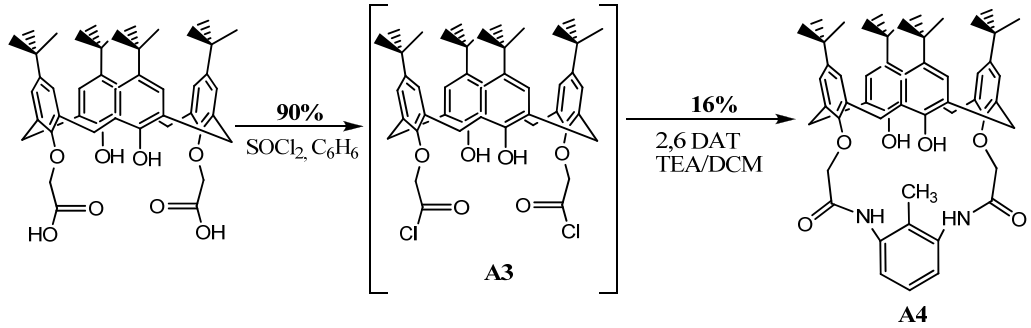

Scheme 13

This carboxylic acid was then converted into the acid chloride (**A3**) using $SOCl_2$ and used immediately for next step without further purifications (Scheme 12). Using high dilution conditions a solution of 2,6-diaminotoluene in dry dichlomethane and the bis-acid chloride (**A3**) were slowly added to a dilute solution of triethylamine (TEA) in dry dichloromethane. The poor solubility of the 2,6-diaminotoluene required a long reaction time for total dissolution. A pink solid was obtained on work up, but the NMR spectrum of this showed a complex mixture of products. All the attempts to purify the compound by column chromatography have failed, but attempts of crystallization using a mixture of hexane and dichloromethane led to precipitation of a white powder which was collected and characterized by NMR, MS and IR spectroscopy. This proved to be the desired compound (**A4**).

2.1.7 p-*tert*-Butyl-25,27-[pyridine-2.6-diylbis(aminocarbonylbutoxy)-26,28--calix[4]arene

Several groups have prepared a variety of pyridine appended calixarens, primarily for metal cation coordination[132-134]. Recently Beer and co-workers[135] have also reported a synthetic procedure to prepare 1,3-lower rim calix[4]arene pyridinium bridged analogue for anion coordination. However as described from the authors in this study attempts to use calixarenes derivatives bearing short chains on the lower rim for the quaternisation reaction with methyl iodide or dimethyl sulphate proved unsuccessfully[135] due to the steric inaccessibility of the methylation of the pyridyl

nitrogen. In order to explore the effect of the quaternisation reaction on a different structure, a calixarene derivative bearing longer chains attached on the lower rim was prepared. In the first time a calixarene derivative with di-amino-butoxy chains on the lower rim was prepared. At this proposal the key intermediate p-*tert*-butyl-25,27-[bis(cyanopropoxy)-26,28-dihydroxy]calix[4]arene (**A5**) was prepared from p-*tert*-butylcalix[4]arene following the procedure of Reinhoudt and co-workers[136] (Scheme 13) using 10 equiv of K_2CO_3 and 4-bromobutyronitrile in refluxing acetonitrile to give the di-cyano calixarene derivative as white powder after re-crystallization from $CHCl_3$/MeOH.

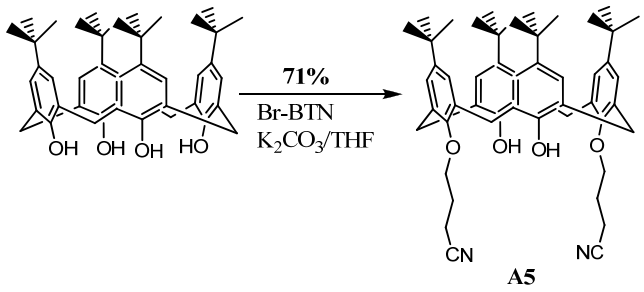

Scheme 14

Reduction of the cyano groups with $LiAlH_4$ in diethyl ether[137] gave the p-*tert*-butyl-25,26-[bis(aminopropyl)]-26,28-dihydroxycalix[4]arene (**A6**) in quantitative yield as white foam. Compound (**A6**) could not be fully characterised because of extensive solvent inclusion (see Experimental section). The calixarene-diamine (**A6**) was then reacted with 2,6-bis(chlorocarbonyl)pyridine commmercially available under high diluted conditions in dry dichloromethane in the presence of dry triethylamine (TEA) to give a pale yellow powder (Scheme 15).

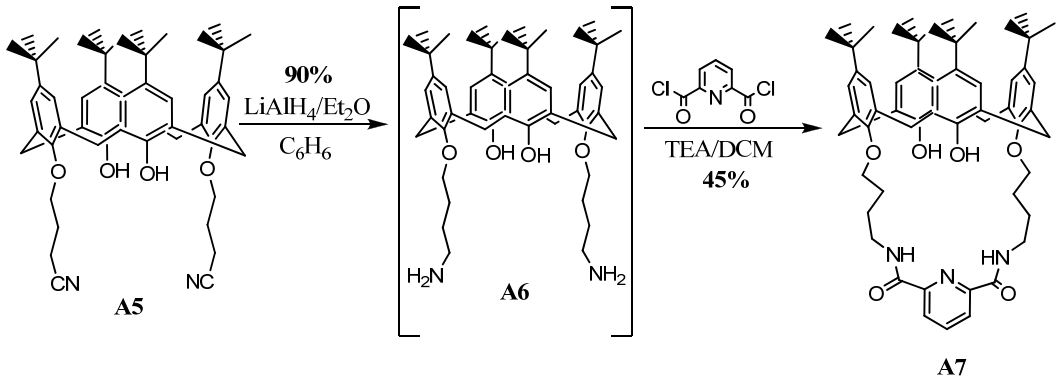

Scheme 15

All attempts to purify the product by column chromatography failed, but attempts at crystallization using hot hexane led to precipitation of (**A7**) as a white powder which was isolated and characterized by NMR, MS and IR spectra as a clean compound. Reaction of this material with an excess of methyl iodide under reflux conditions resulted in a methylation of the pyridine ring give (**A8)** as a pale-yellow solid (Scheme 16)

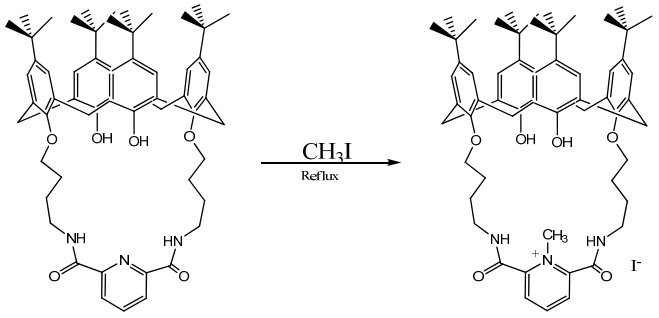

A7 **A8**

Scheme 16

However only the ^{1}H-NMR spectrum has showed a strong singlet signal at δ 3.96 confirming presumably the methylation on the pyridil nitrogen.

Lower rim functionalized calixarenes

2.1.8 p-*tert*-Butyl-25,27-bis[(maleonylmethyl)carbonylaminoethoxyethyl]-26,28-dihydroxycalix[4]arene

The biological activity of calixarenes has been well documented[138]. Cragg and Iqbal[139] have prepared transmembrane cation transporters using a calixarene-type macrocycle as scaffold. Synthetic cation channels based on lipophilic calixarens have been described by Kobuke and co-workers[140]. Recently Rogalska and co-workers[141] have reported the possibility of incorporation and translocation of three amphiphilic p-*tert*-butylcalix[4]arene derivatives bearing 6-aminopenicillanic acid or benzylpenicillin moieties on the lower rim across the bacteria membranes. To the best of our knowledge maleimide-calixarene derivatives for biological applications have not been reported. In order to prepare a bio-compatible calixarene a lower rim

functionalized maleimide calixarene was prepared. To increase the solubility and to reduce the presence of different possible conformations, a calixarene precursor with short chains was prepared. Following the McKervey[142] procedure the 1.3-distally substituted cyanomethyl calix[4]arene (**B1**) was obtained (Scheme 17)

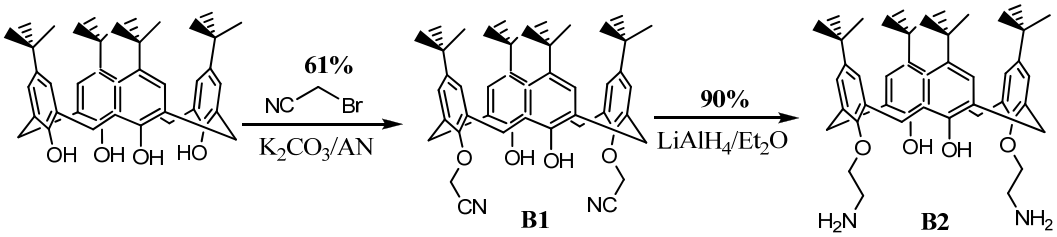

Scheme 17

A one-pot reduction with $LiAlH_4$ in dry benzene gave the corresponding diamine derivative (**B2**) in good yield. This compound could not be fully characterised because of extensive solvent inclusion (see Experimental section). The *N*-substituted maleimide (**B4**) was prepared following Rich's procedure[143]. This method involves two different steps. In the first i) formation of the maleamic acid (**B3**) from maleic anhydride and an amino carboxylic acid and ii) subsequent cyclization using dry toluene with triethylamine under reflux conditions (Scheme 18)

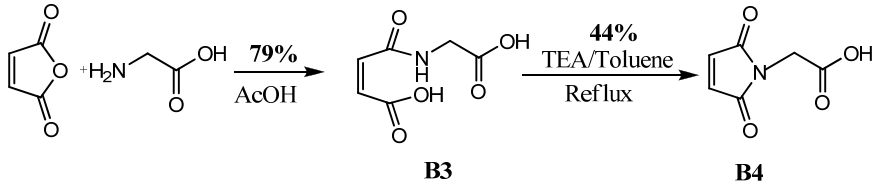

Scheme 18

The derivatization with thionyl choride of fresh sample of glycine maleimide (**B4**) gave the corresponding acyl chloride which on condensation with the p-*tert*-butyl-25,27-[bis(aminoethoxy)]-26,28-dihydroxycalix[4]arene[137] (**B2**) in high diluted conditions using dry dichloromethane gave the novel lower rim 1,3-bis-maleimide-fuctionalized calix[4]arene (**B5**) as yellow powder (Scheme 18). Mass and NMR spectroscopy together with elemental analysis has confirmed this compound. Moreover after several attempts, suitable crystals for X-ray analysis from methanol were obtained and fully resolved. These results have confirmed that calixarene adopts

a cone conformation with the maleimide groups curve-up to the lower edge of the cone (see section 2.2.5.1 of this thesis).

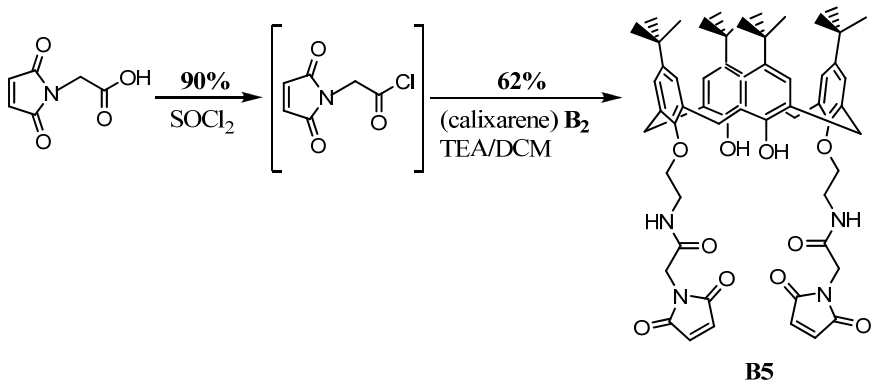

Scheme 19

2.1.9 p-*tert*-Butyl-25,27-bis[(maleonylmethyl)carbonylaminoethoxy]-26,28-dihydroxycalix[4]arene

Recently Cragg and co-workers[139] have reported the possibility to combine a calixarene and Triton-X100^{TM}, a well known surfactant used by biologist to disrupt cell membrane. The polyether-containing derivatives attached on resorcinarene system also are able to cross the cell membrane as reported from Kobuke and co-workers[144]. In order to prepare a calixarenes functionalized on the lower rim with polyether chains bearing maleimide groups, a synthetic procedure was developed. Following the Koganty[145] procedure (scheme 20) (aminoethoxy)ethanol (**C1**) was protected by phthalic anhydride to give the 2-(phthalimidoethoxy)ethanol (**C2**) in good yield. The reaction of this with p-toluensulfonic-chloride gave the corresponding (phthalamidoethoxyethyl)tosylate[146] (**C3**) which on condensation with p-*tert*-butylcalix[4]arene (Scheme 21) in dry acetonitrile and refluxed for 5 days, gave after re-precipitation from ethanol the phthalamido calixarene derivative [147] (**C4**)

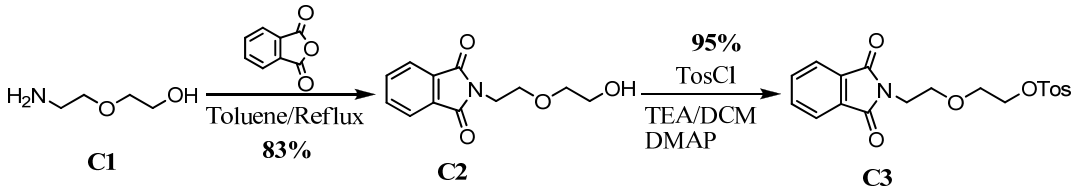

Scheme 20

De-protection using monohydrate hydrazine in refluxing ethanol gave the corresponding amino (**C5**) as white foam which was used immediately for the next step without further purification.

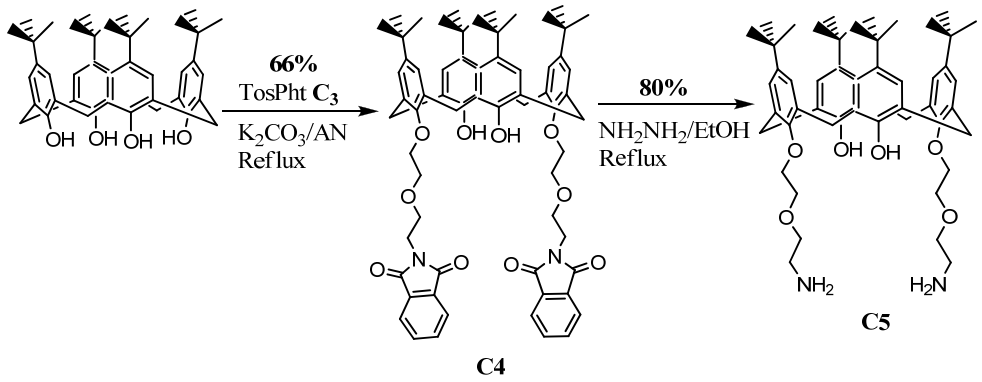

Scheme 21

Reaction with thionyl chloride of a fresh sample of maleimido glycine acid (**B4**, n = 1) gave the corresponding acyl chloride which on condensation with the amine (**C5**) in dry dichloromethane gave the novel lower rim 1,3-bis-maleimide-ethoxyethyl fuctionalized calix[4]arene (**C6**) as yellow powder (Scheme 22).

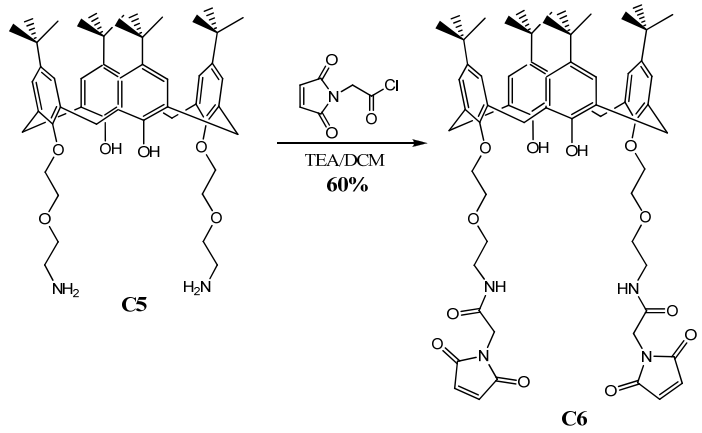

Scheme 22

Mass spectrometry has confirmed the compound m/z 1120 [M+Na], but careful investigation using NMR technique has revealed presence of starting material (**C5**) as impurity, calculated as ~25% (from NMR peak integration). All attempts to purify the compound by column chromatography and by crystallization failed (see appendix **B** of this thesis for synthetic procedure and spectroscopy results).

2- Results and Discussion: p-*tert*-butylcalix[4]arene

2.2 The behaviour of calixarene complexes with methylated aromatic guests

The major objective of this project was to explore routes to potential cryo-relaxors. One approach being the potential use of supramolecular complexes incorporating methyl rotors. Accordingly the behaviour of a number of calixarenes involving simple methylated aromatic guests has been explored. The crystallographic studies were carried out by X-ray Crystallographic Service in Southampton. The Solid-state NMR from our group (expansions can be found in appendix E and are indicated by $\mathbf{S_n}$). The Field Cycling NMR and the INS studies were carried in collaboration with Prof. A. J. Horsewill in Nottingham (see appendix C for details and mathematical models).

2.2.1 Preparation of simple calixarene complexes

For the preparation of the desired p-*tert*-butylcalix[4]arene complexes a synthetic route was employed, analogous to that used for the production of the p-*iso*-propylcalix[4]arene complexes (see experimental section). This route is summarised in scheme 23 and a full list of the compounds prepared using the p-*tert*-butylcalix[4]arene may be found in table 6.

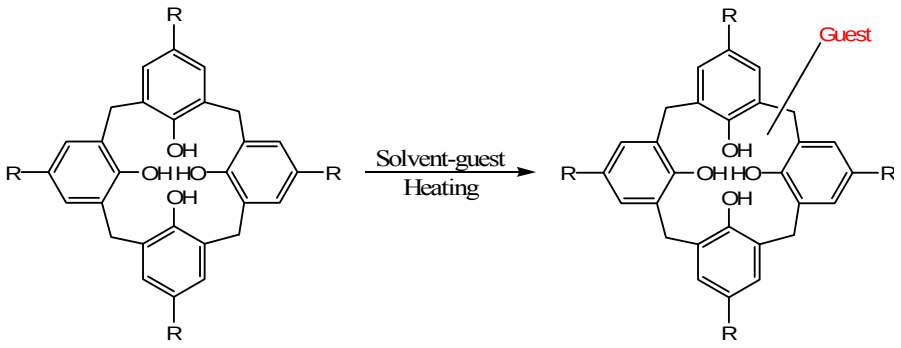

Scheme 23 Preparation of p-*tert*-butylcalix[4]arene (1:1) guest complexes

In general preparation of p-*tert*-butylcalix[4]arene complexes involved re-crystallization from the desired guest solvent, the being characterised by X-ray crystallographic studies[100]. In many cases such guests are relatively weakly held and in the solid state their location is therefore disordered hampering X-ray structural characterisation. This situation is often observed, for example, in complexes of p-*tert*-

butylcalix[4]arene with guests such as toluene and 4-picoline where the hydrogen atoms of the methyl group(s) residing inside the cavity are disordered. However, in some situations such behaviour can be advantageous since the internal barrier to methyl rotation can be extremely low allowing quantum tunnelling to occur. Several solid-state structures demonstrate that the internal cavities of calix[4]arene in the cone conformation are able to accommodate aromatic neutral molecules giving stable crystals. It has been demonstrated that intra-cavity inclusion only occurs when the calixarene is in the cone conformation[94] and furthermore the inclusion of the aromatic guest is observed only when the *para* position of the calixarene carries a *tert*-butyl group, an arrangement which is believed to provide favourable CH···π interactions between the methyl groups and the π system of the guest molecule[148]. General crystallographic data for each material (where applicable) is listed in Table 6.

	Complex Information					Crystallographic Summary				
guest structure	number	synthetic host	yield	MP °C	Lit. ref.	internal reference	data temp.	distances h/A°	d/A°	space group
Toluene	4495/36	*t-bc4*	27 %	> 300	85	06sot0765	120K	1.34	3.63	$P4/_n$
4-Picoline	4495/34	*t-bc4*	36 %	> 300	-	06sot0589	120K	1.37	3.63	$P4/_n$
4-Fluoro toluene	4474/58	*t-bc4*	49 %	> 300	-	07sot0391	120K	1.37	3.64	$P2_1/_n$
4-Chloro toluene	5180/63	*t-bc4*	62 %	> 300	-	08sot0699	120K	1.37	3.66	$P4/_n$
Acetone	4578/100	*t-bc4*	97 %	> 300	155	-	-	-	-	-

Table 6: Synthetic and crystallographic data summary for *p-tert*-butylcalix[4]arene (*t*-bc4) complexes

p-*tert*-Butylcalix[4]arene (1:1) guest complexes were obtained in different yields. As showed in table 6 the lowest yield as single crystals was founded for toluene guest while highest for the 4-chlorotoluene guest. The acetone complex prepared by simple adsorption was obtained as white powder.

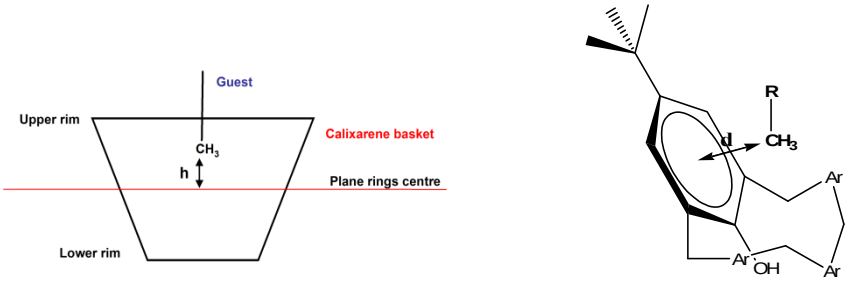

Figure 76 Definitions of geometric parameters for calixarenes complexes discussed in this thesis. **h** = distance between plane of the calix[4]arene aromatic rings centre and carbon of methyl group; **d** = distance between centroid of the calix[4]arene aromatic rings and carbon of methyl group.

2.2.2.1 p-*tert*-butylcalix[4]arene (1:1) Toluene complex

The first single crystal structures of this complex were solved at room-temperature by Andretti in 1979[85]. Following their procedure tetragonal single crystals suitable for X-ray structural analysis were obtained by slow evaporation of a saturated solution in toluene (Figure 77). However, in the present case the X-ray data was collected at 120K.

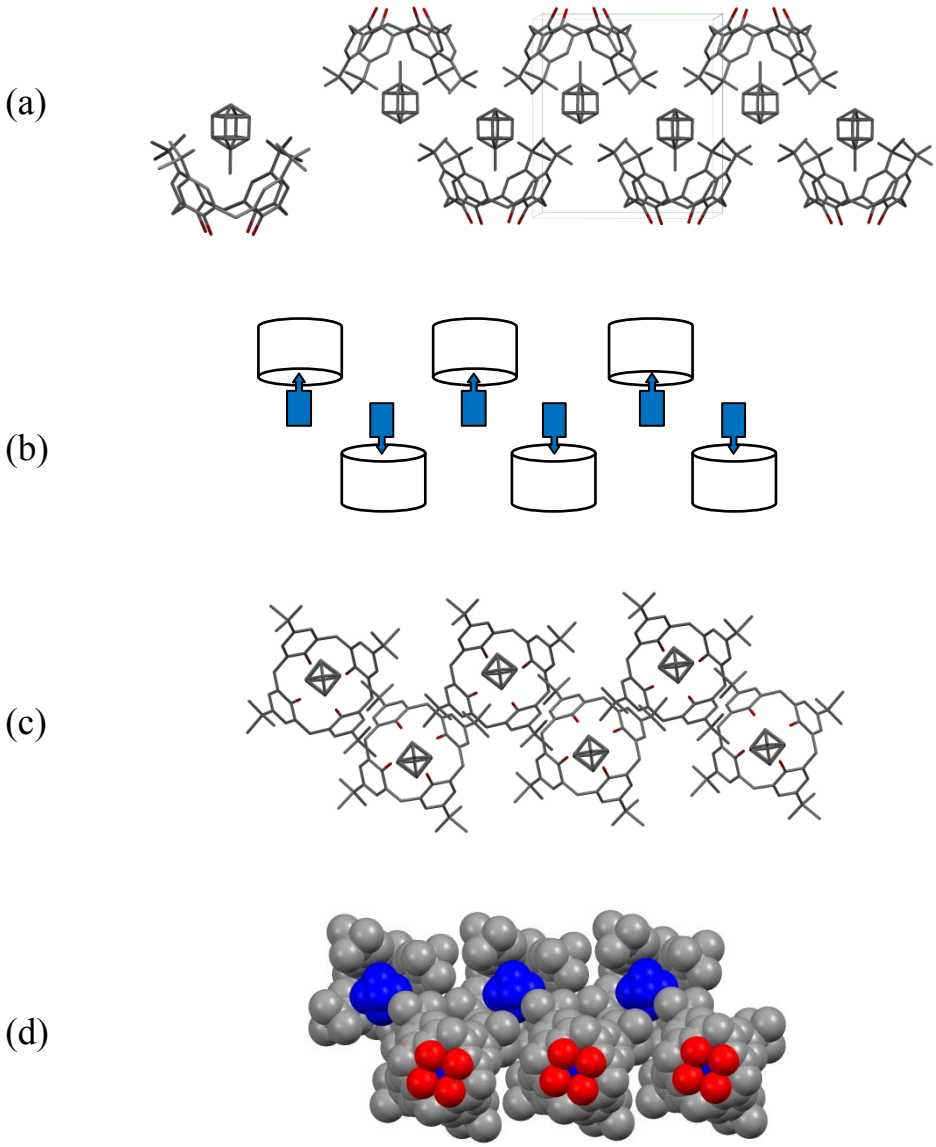

Figure 77 p-*tert*-butylcalix[4]arene (1:1) toluene complex from this work a) crystal structure and packing; b) schematic motif packing; c) crystal packing bottom view; d) space fill bottom view

As in Andretti's refinement structure, the methyl group of the guest molecule was observed to be included inside the bucket cavity of the host and to lie along a fourfold crystallographic axis. The guest molecules were found to be disordered over two equivalent sites. In addition, the *t*-butyl groups of the host molecule were also reported to be disordered over two sites. Our ^{13}C CP/MAS NMR (Figure 78 and **S_1**) showed a room temperature spectrum in agreement with the fourfold symmetric structural model inferred from our diffraction study and the Andretti's results.

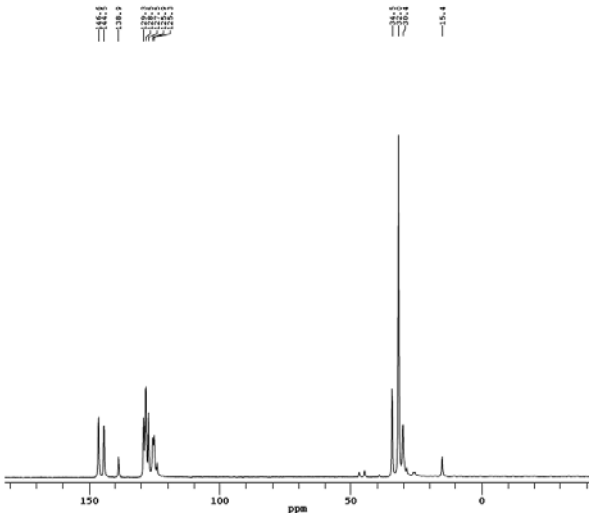

Figure 78 ^{13}C CP/MAS NMR of p-*tert*-butylcalix[4]arene (1:1) toluene complex from this work (150 MHz)

The complexation induced chemical shift (CIS) showed a value corresponded to -6.1 p.p.m for this complex also in agreement with the literature value[149] (see table 7). The thermal history of the p-*tert*-butylcalix[4]arene (1:1) toluene sample in our Field Cycling solid-state NMR studies (Figure 79) had a significant effect on the temperature dependence of T_1 at low temperatures.

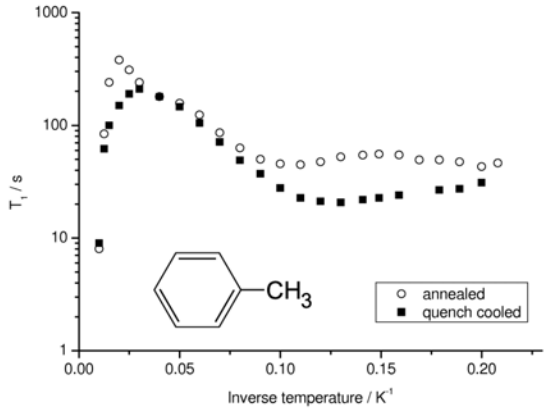

Figure 79 p-*tert*-butylcalix[4]arene (1:1) toluene, temperature dependence of T_1, B_r = 0.7T (probe **C**, field cycling). Error bars are small compared to marker size. [ref. 45]

T_1 observed to be monoexponential for both annealed and quench cooled samples. The T_1-inverse temperature curve for the quenched sample shows a shallow T_1 minimum at 7.7K ($0.13K^{-1}$). The temperature dependence of T_1 in annealed sample clearly revealed the presence of two separate methyl environments, by virtue of the presence of two low temperature minima, one at 9.1K ($0.11K^{-1}$) and other at 5.2K ($0.19K^{-1}$) as shown in Figure 79.

These results are in agreement with the INS (Inelastic Neutron Scattering) studies at low temperature reported from Caciuffo and co-workers[114] in which a number of bands were interpreted as being the result of transitions between tunnel-split librational states of the guest methyl groups (Figure 80).

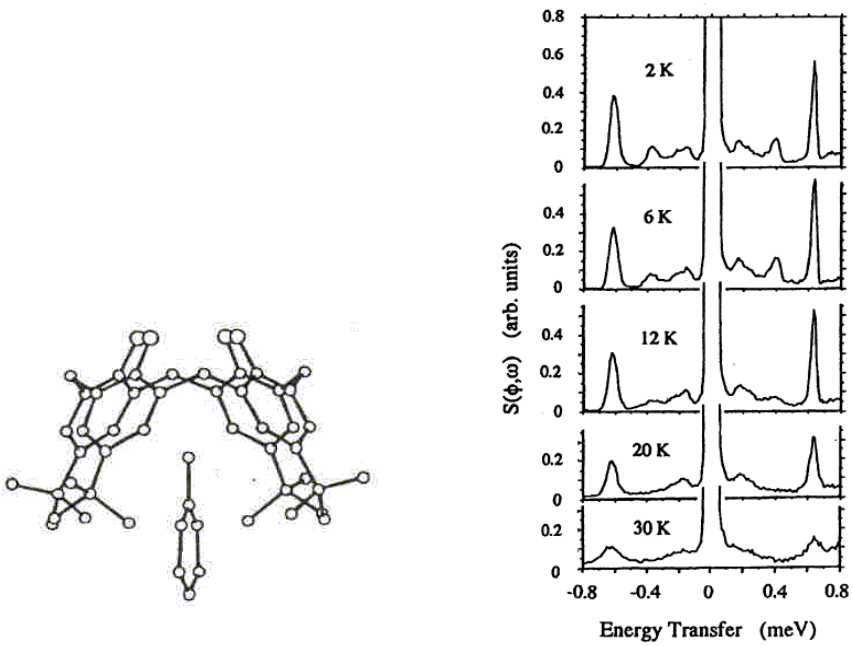

Figure 80 p-*tert*-butylcalix[4]arene/toluene 1:1 complex and Inelastic neutron scattering at low temperature from [ref. 114]

Low-temperature INS spectra for the p-*tert*-butylcalix[4]arene (1:1) toluene complex, acquired by Caciuffo and co-workers[114], are displayed in Figure 80. At temperatures below and including 6K, there is a prominent transition peak at 0.63meV, together with relatively broad excitation bands at 0.40meV and ~ 0.20meV. These features can be interpreted as the tunnelling peaks of crystallographically inequivalent methyl groups. The peak at 0.63meV indicates the presence of almost free methyl-rotors. A tunnel splitting of $\nu_t^{(0)}$ t = 0.26 ± 0.04meV is predicted by characterisation of the narrow component of the spectral density functions in sample; presumably, the narrow spectral density component that has been observed and characterised from

NMR experiments is an average of the components which give rise to the broad features in the INS spectra. The distinct methyl-group environments may be linked to the two-fold disorder of the aromatic ring observed in XRD measurements.

Atwood and co-workers have reported[149] that this complex shows a dynamic structure behaviour at room temperature that change at low temperatures into a low symmetry crystal. The ^{13}C CP/MAS NMR spectrum shows a new complex pattern in agereement with the symmetry of the calixarene complex at low temperature. In particular at temperature below 248K the peak corresponded to the carbon bearing the methyl group of the guest C-1' (Figure 81) shows a splitting in two lines.

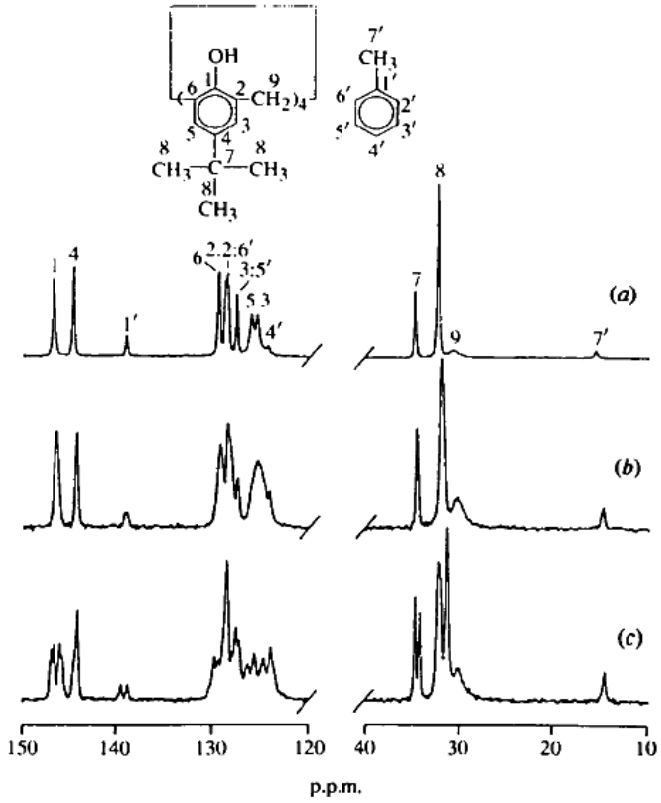

Figure 81 ^{13}C-CP/MAS NMR of p-*tert*-butylcalix[4]arene (1:1) toluene complex [ref. 149]

This suggests that the asymmetric unit in the low temperature phase contains two inequivalent calixarene toluene guest-host units. Ripmeester and co-workers[150,151] in their temperature dependent NMR study have demonstrated that a symmetry lowering transition takes place below 250K. They have studied the molecular motion of the toluene guest in detail using ^{2}H-NMR spectroscopy Figure 82. Below 250K the number of symmetry-related sites of the guest was inferred to be lower than at room temperature: the results were interpreted as a change from fourfold rotation to twofold

flips of the toluene ring (Figure 82), implying a distortion of the calixarene cavity from fourfold symmetry.

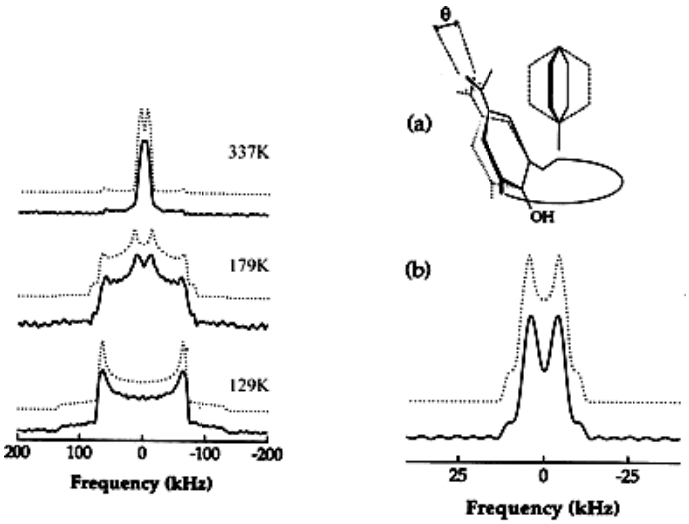

Figure 82 p-*tert*-butylcalix[4]arene (1:1) toluene complex ^{2}H-NMR studies [ref. 150]

With twofold distortion built into the structural model, they were able to refine the low-temperature structure. This improved the residual, and it resolved the disorder of the *tert*-butyl groups Figure 83.

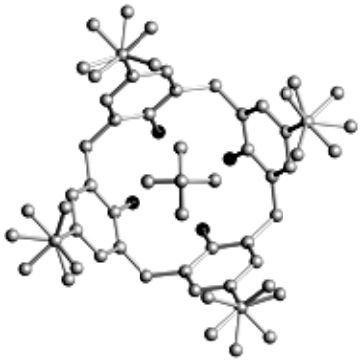

Figure 83 *t*-Bc4/toluene room-temperature structure [ref. 151]

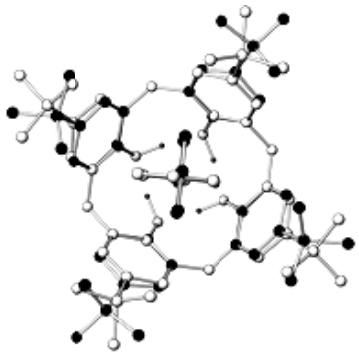

Figure 84 *t*-Bc4/toluene low-temperature structure [ref. 151]

There was a good correlation between the toluene guest orientation and the distortion of the p-*tert*-butylcalix[4]arene host molecule that locally broke the fourfold symmetry. So the lower symmetry induced in the p-*tert*-butylcalix[4]arene molecule is accompanied by a reorientation of the *tert*-butyl groups Figure 84. An interesting dilemma was also resolved by the same group. The good structural model described above was still inconsistent with the lower symmetry inferred from NMR for the low temperature. The NMR spectra suggested that the twofold distortions of the

calixarenes were correlated in some way, but the diffraction data did not pick this up. They resolved this problem as a result of some surprising observations. During their low-temperature X-ray data collections with Cu *Kα* radiation (1.54 A) additional reflections, indexed as half-integral with respect to the room temperature lattice, were observed immediately upon cooling. These clearly indicated that some sort of superstructure was present. Attempts to collect a data set based on the superlattice failed as additional reflections disappeared again over a period of about 6h. However with new CCD diffractometer and with Mo *Kα* radiation Ripmeester and co-workers[151,152] were able to observe extra reflections which proved to be persistent. Now the structural model for the low-temperature Figure 84 could be constructed that was also consistent with the NMR data.

2.2.1.2 p-*tert*-Butylcalix[4]arene (1:1) 4-methylpyridine complex

4-Methylpyridine (4-Picoline) is liquid at room temperature but solidifies at +3°C. Using the same strategy described in the previous section, tetragonal crystals were obtained from a slow evaporation of a saturated solution containing 4-picoline and p-*tert*-butylcalix[4]arene (Figure 85).

(a)

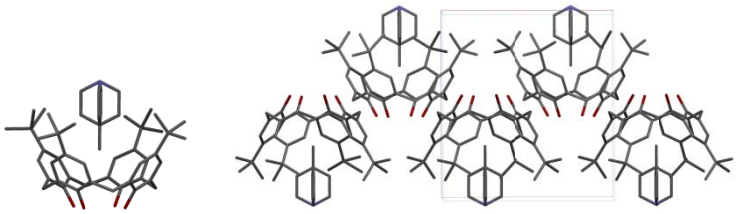

(b)

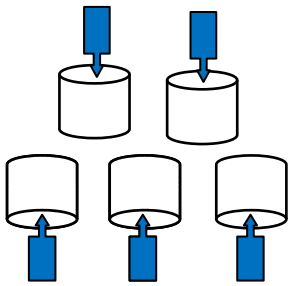

(c)

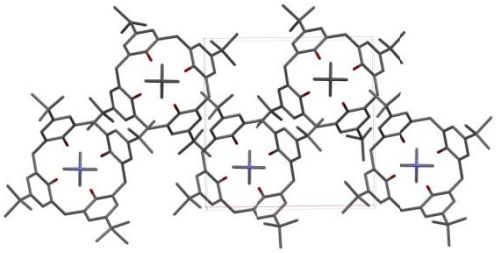

(d)

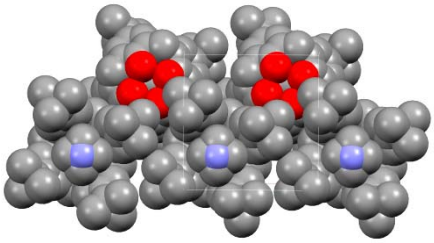

Figure 85 *p-tert*-butylcalix[4]arene (1:1) 4-methylpyridine complex from this work a) crystal structure and packing b) schematic motif packing c) crystal packing bottom view d) space fill bottom view

The crystal packing deduced from room temperature single X-ray diffraction patterns was expected to be the same as for the toluene complex but high disorder of the guest hampered full structural X-ray characterization. As previously reported for the toluene complex the best refinement model of the picoline guest molecule had it lying along a fourfold crystallographic axis with its methyl group inserted into a conical cavity of the calixarene host molecule. However, Caciuffo and co-workers[114] measuring the rotational barrier inside the cavity by INS have hypothesized that a different $CH_3 \cdots \pi$ interaction, occurs between the *t*-butyl group of the host and the aromatic π orbital of the guest. This causes a different position of the methyl group of the guest inside the bucket cavity. The ^{13}C CP/MAS NMR spectrum of this complex at room temperature shows splitting of the resonances in a manner analogous to the that seem for the toluene complex, except for the nitrogen atom (Figure 86 and **S_2**).

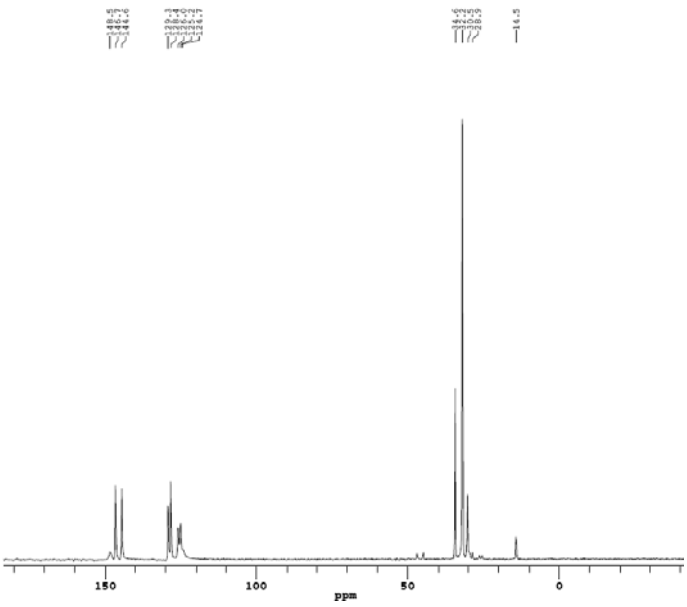

Figure 86 ^{13}C-CP MAS NMR spectrum of p-*tert*-butylcalix[4]arene (1:1) 4-methylpyridine complex from this work (150 MHz)

The peak (at δ 14.5) assigned to methyl carbon of 4-picoline in the complex, appeared to have a CIS (complexation induced chemical shift) of -6.5 p.p.m. as reported in table 7. Field Cycling solid state NMR studies show a temperature dependent mono-exponential behaviour (see Figure 87) for the quench cooled and the annealed samples, but the T1 value was dependent on the thermal history of the sample, suggesting the presence of different methyl rotors. The graphic shows a T1 minimum at low temperature 8.9K and 9.3K for the quench cooled and the annealed samples.

The existent at low temperature T1 minimum is consistent with the presence of weakly hindered groups in this sample.

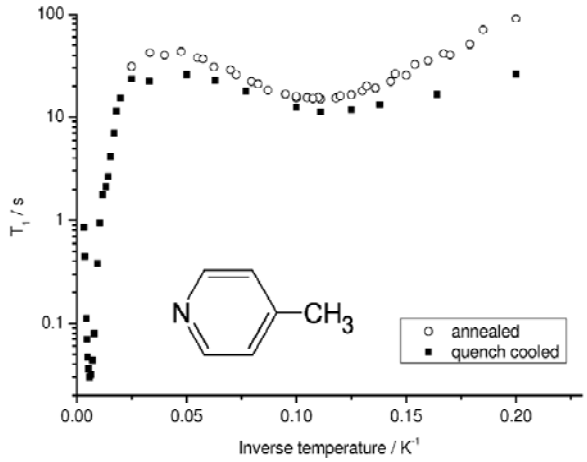

Figure 87 Temperature dependence of T_1 in p-*tert*-butylcalix[4]arene (1:1) 4-methypyridine complex, B_r = 0.7T. Quench cooled sample measured with probe **A** (constant field); annealed sample with probe **C (**field cycling). Error bars are small compared to marker size [ref. 45]

Neutron scattering measurements at low temperature reported by Caciuffo and co-workers[103] (a) showed excitation bands at approximately the same energies as had been observed for the toluene case, but with significant differences (Figure 88a).

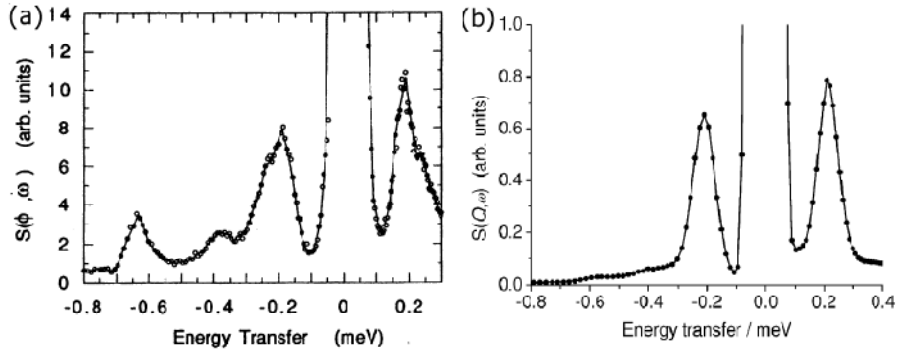

Figure 88 Inelastic neutron scattering of 4-methylpyridine complex a) literature data [ref. 103] b) [ref. 45]

There are multiple excitation bands in the range 0.17-0.63 meV, with the most intense at 0.23 meV and the bandwidths much larger than those observed for the toluene system. Furthemore the intensities of the peaks were observed being temperature dependence. These have been interpreted as being the various tunnel splitting lines for several crystallographically inequivalent methyl-group environments. INS studies on our γ-picoline complex sample have been carried out by Horsewill and co-workers Figure 88 (b) and analysed in this thesis by field-cycling NMR (figure 87). The

spectrum 88 (b) displays a single excitation at 0.210 meV but all other peaks observed in 88 (a) are absent in the spectrum 88 (b). The position of peak in 88 (a) is approximately coincident with the most intense peak in spectrum 88 (b), and is characteristic of tunnel-splitting of a methyl-group hindered by a barrier of V_3 = 105 K (E_{01} = 56 K). The presence of unhindered methyl-groups, as indicated by the broad component should be revealed by a excitation at ~ 0.65 meV. There is no trace in this reagion in the spectrum 88 (b), but there is an excitation at 0.627 meV in the spectrum 88 (a). However the number of peaks in the investigated energy range suggested the occurrence of a symmetry lowering structural distortion, leading to inequivalent crystallographic sites for the γ-picoline guest.

2.2.1.3 p-*tert*-Butylcalix[4]arene (1:1) 4-fluorotoluene comple

In order to explore the influence of the halogen atoms in *para*-position of the toluene molecule on the behaviour of methyl rotor inside the calixarene cavity of p-*tert*-butylcalix[4]arene, a series of 4-halotoluene complexes have been prepared. Tetragonal crystals suitable for X-ray analysis were obtained from a saturated solution of 4-fluorotoluene following the same procedure as described above to give the novel calixarene complex (Figure 89).

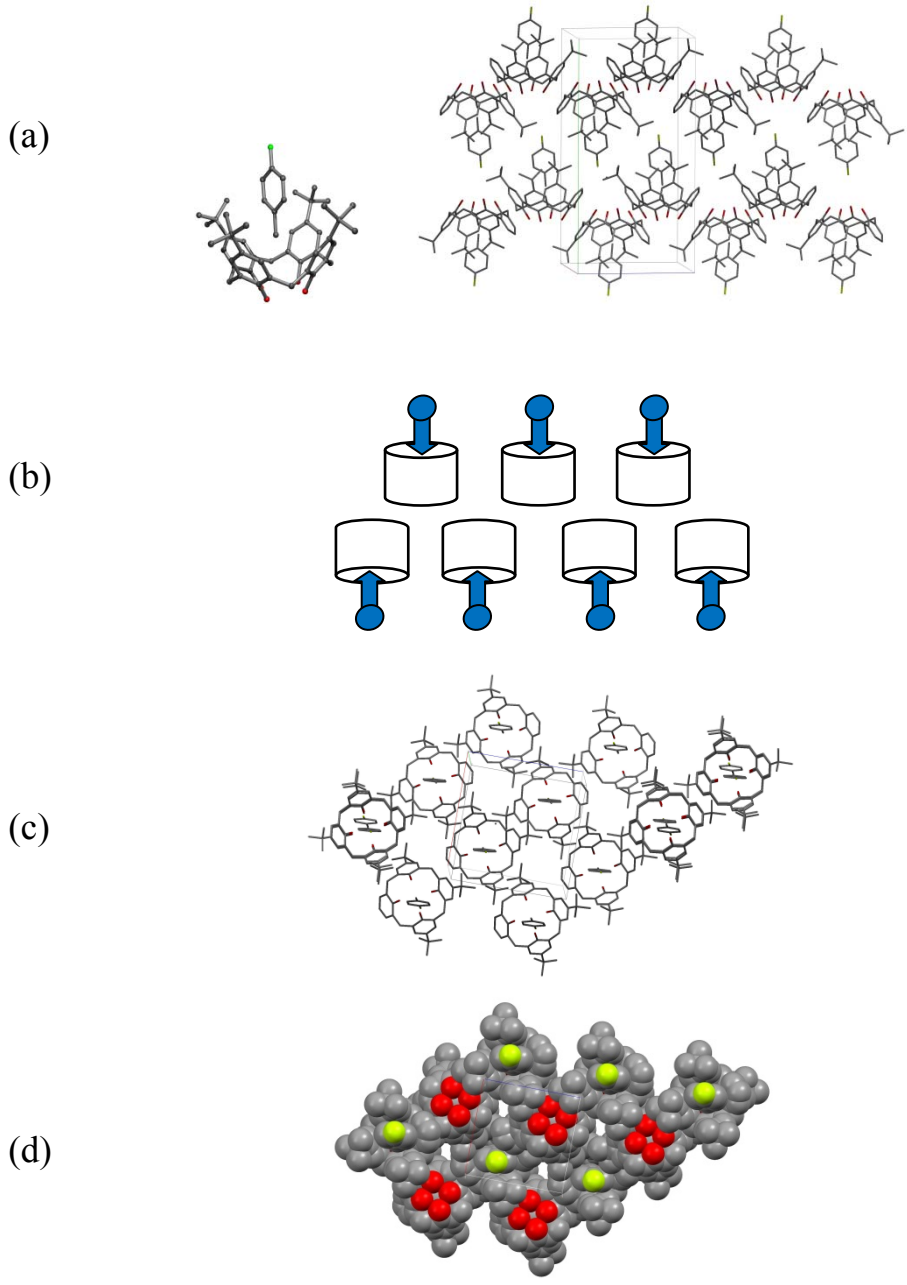

Figure 89 p-*tert*-butylcalix[4]arene (1:1) 4-fluorotoluene complex from this work a) crystal structure and packing b)schematic motif packing c) crystal packing bottom view d) space fill bottom view

Field Cycling solid state NMR studies have been carried out and the results suggest a T_1 dependence on the thermal history of the sample (Figure 90) as seen previously for the toluene complex in the present study (Figure 80). This complex shows monoexponential behaviour for both quench and annealed samples. A T_1 minimum is displayed below 28.6K ($3.5x10^{-3}K^{-1}$) for both annealed and quenched samples.

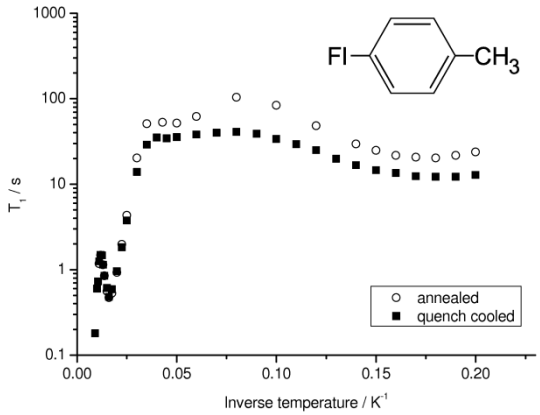

Figure 90: p-*tert*-butylcalix[4]arene (1:1) 4-Fluoro toluene complex , T_1 versus inverse temperature *Br* = 0.7T (probe **C**, field cycling). Error bars are small compared to maker size [ref. 45]

Furthermore, at very high temperatures it is possible to see a steep gradient which was the edge of the strongly hindered *tert*-butyl groups. These results are in agreement with our ^{13}C CP/MAS NMR spectrum (Figure 91 and **S3**) obtained at room temperature in which the methyl group signal for the 4-fluorotoluene appeared to have with a CIS (complexation induced chemical shift) of -6.2 p.p.m. as reported in table 7.

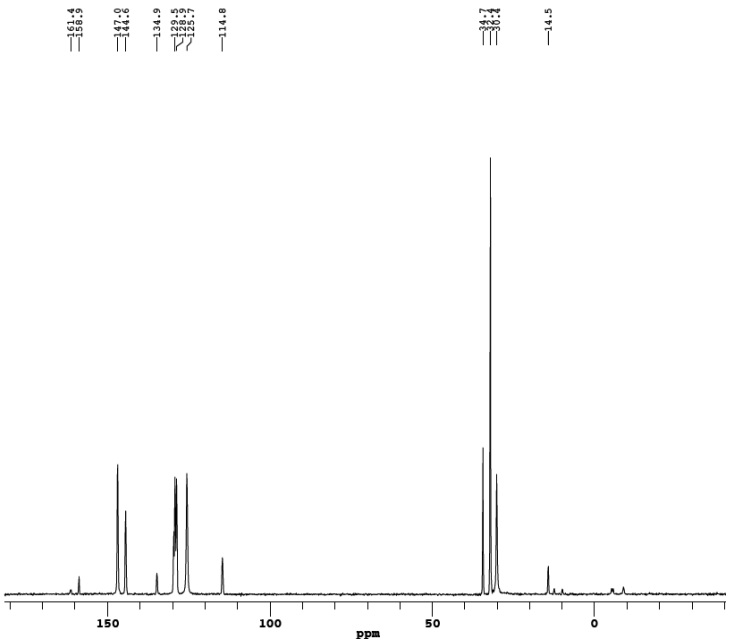

Figure 91 ^{13}C CP/MAS NMR spectrum of p-*tert*-butylcalix[4]arene (1:1) 4-fluorotoluene complex from this work (150 MHz)

Ripmeester and co-workers have reported[153] a systematic investigation which revealed a number of different structural motifs. In particular the halogens were seen to be excluded from the calixarene cavity and the general trend $CH_3 > CH_2 > CH \sim OH > Cl \sim Br$, was observed for the group most deeply included. A summary of the structure and trends is show (in Figure 92).

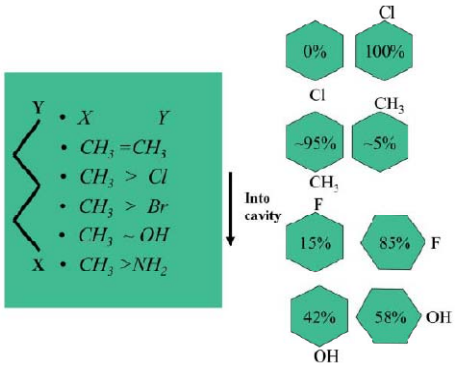

Figure 92 Recognition inside the cavity; (left) in aliphatic compounds with the preference for the deph of the cavity; (right) aromatic compounds, showing the fractional occupancy of the two sites [ref. 152, 153]

They have also observed a preference for aromatic guest, the recognition for aromatics, although the behaviour is less clear cut. The likely difference is that for an aliphatic guest the molecule can invert inside the cavity, so that the observed guest orientation is the actual equilibrium state (which may be dynamically averaged, as for pentane) whereas for the aromatic structures this process is not possible. In other studies they have investigated the behaviour of a number of aliphatic and alicyclic compounds. The results obtained suggest that π-methyl interactions may in fact not be that important in contributing to the stability of the inclusion complexes. On the other hand, for the aromatic systems, the preferred orientation likely is probably determined during the crystallization process as molecular motion that would invert the molecule within the cavity was not observed and the number of misaligned toluene molecules in the t-bc4-toluene complex was found to depend on the specific sample.

2.2.1.4 p-*tert*-Butylcalix[4]arene (1:1) 4-chlorotoluene complex

An X-ray structural study of the 4-chlorotoluene complex reveals more extensive disorder as can see in Figure 93.

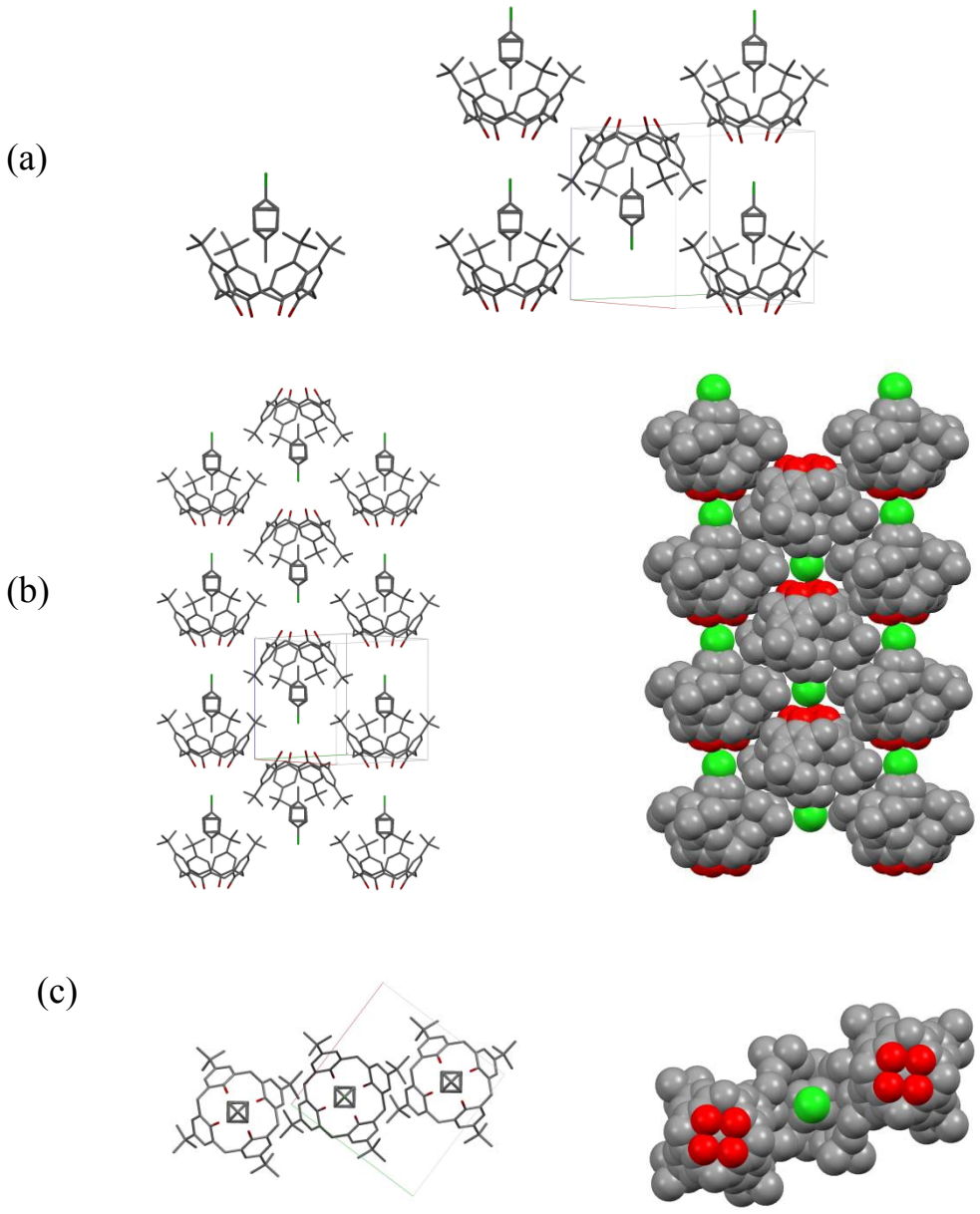

Figure 93 p-*tert*-butylcalix[4]arene (1:1) 4-chlorotoluene complex crystal packing with space fill (this work)

As showed in Fig. 93 the crystal packing reveal two similar channel motifs with each basket oriented up and a channel in the middle bearing calixarene molecule oriented down. The guest appears disordered adopting two different orthogonal orientations within the host cavity with chlorine atom (in green) lying outside the basket. The 4-chloro toluene guest molecule with the methyl group was observed to be included

inside the bucket cavity of the host and to lie along a fourfold crystallographic axis. In order to satisfy the fourfold crystallographic symmetry, the guest molecules were also disordered over two equivalent sites. The ^{13}C CP/MAS solid state NMR (Figure 94 and **S_4**) showed a room temperature spectrum in agreement with the fourfold symmetric structural model inferred from the diffraction, with a higher value of CIS (complexation induced chemical shift) of -6.8 p.p.m. as reported in table 7. This could suggest a different preference of the guest molecule for the depth of binding within the calixarene cavity.

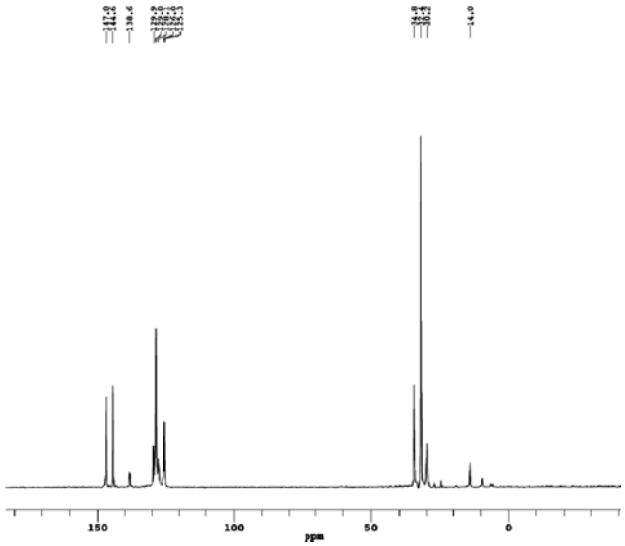

Fig ure 94 ^{13}C CP/MAS NMR of p-*tert*-butylcalix[4]arene (1:1) 4-chlorotoluene complex experimental data (150 MHz)

Again the thermal history for this complex (Figure 95) showed a considerable effect on the temperature dependence of T_1 at low temperature. The relaxation curves were monoexponential with a T_1 minimum at 15.5K ($0.0645K^{-1}$) for both thermal preparation and a hint of a minimum in the annealed sample at 6.45K ($0.16K^{-1}$).

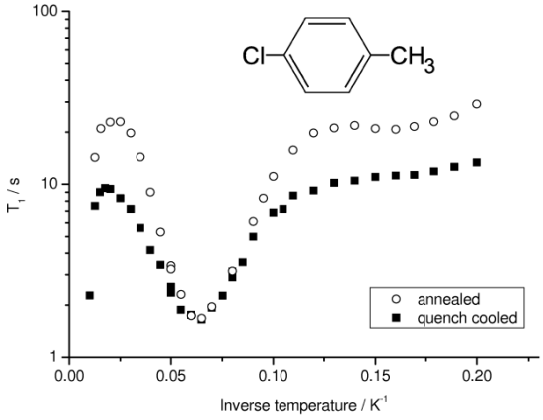

Figure 95 p-*tert*-butylcalix[4]arene (1:1) 4-Chloro toluene, T1 versus inverse temperature, B_r = 0.7T (probe **C** field-cycling). Error bars are small compared to marker size [ref. 45]

2.2.1.5 p-*tert*-Butylcalix[4]arene/acetone (1:1) complex

As discussed in the previous sections the *tert*-butyl group on the upper rim have a important function during the complexation process of the aromatic guests by creating specific attractive $CH_3 \cdots \pi$ interactions between their methyl groups and the aromatic π orbital of the guest. However in such cases the *tert*-butyl groups can decrease dramatically the solubility of the host in organic solvents. The acetone molecule is an interesting potential guest with carbonyl group bearing two methyl rotors. Klinowski and co-workers[154] using molecular calculations have hypothesized that the acetone molecule was placed with the C=O on the fourfold axis, showing a fourfold reorientation in addition to group reorientation. Subsequently Ripmeester and co-workers[155] have demonstrated by X-ray structure analysis that the best model to describe such complex has the carbonyl group point-out the cavity with one of the methyl group inside. In this work they have also shown the inclusion of guest molecules bearing electron-rich groups (soft bases) have a tendency to be rejected from the bucket cavity in favour of soft acids (CH_3~OH>CH_2>CH>F>Cl; CH_3>C=O). There is also a rapid exchanges between the methyl group trapped deeply in the cavity and the external methyl group[155]. However in the present study, attempts to grow-up crystals from a saturated solution of p-*tert*-butylcalix[4]arene in acetone failed, while ^{13}C-CP NMR spectrum from our studies was in agreement with the spectrum published from the same group, suggesting that the complex has been found (Figure 96 and **S5**).

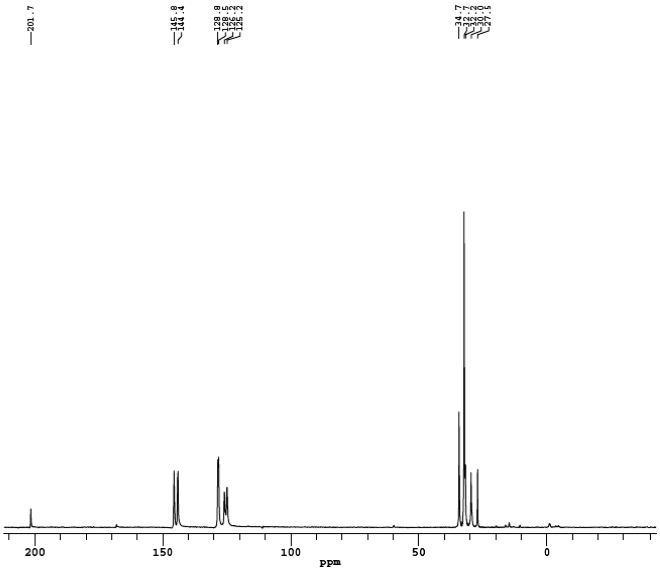

Figure 96 ^{13}C CP/MAS NMR of p-*tert*-butylcalix[4]arene (1:1) acetone complex experimental data (150 MHz)

The peak (at δ 27.5) assigned to methyl carbon of acetone in the complex, appeared to have a CIS (complexation induced chemical shift) of -2.3 p.p.m. as reported in table 7. Field Cycling solid state NMR studies have been carried out and once again the results suggest a T_1 dependence on the thermal history of the sample Figure 97.

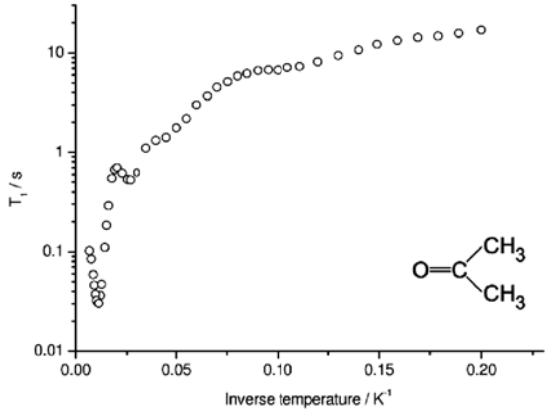

Figure 97: p-*tert*-butylcalix[4]arene (1:1) acetone, T_1 versus inverse temperature, quench cooled, B_r = 0.7T (probe **A**, constant field). Error bars are smaller compared to marker size [ref. 45]

This complex was studied only in quench cooled configuration. Below 15.3K (6.54 x $10^{-2}K^{-1}$) the relaxation was observed to be biexponential. The T1 temperature curve is relatively featureless, with exception of *tert*-butyl minimum at high temperature, there are few other clear features. An apparent minimum at 40K, but it is not distinct enough to make estimation of the environment of the methyl group that causes it.

Table 7 Selected ^{13}C-CP/MAS NMR data of p-*tert*-butylcalix[4]arene-guest complexes

Guest	Assignment	Solid	Solution	CIS*/ppm	Lit. values	ref
toluene	$PhCH_3$	15.4	21.5	-6.1	-6.2	149, 156
4-picoline	$PyCH_3$	14.5	21.0	-6.5	-	this work
4fluorotoluene	$F\text{-}PhCH_3$	14.8	21.0	-6.2	-	this work
4chlorotoluene	$Cl\text{-}PhCH_3$	14.0	20.8	-6.8	-	this work
Acetone	$CO(CH_3)_2$	27.5	29.8	-2.3	-2.3	156

*CIS (complexation induced chemical shift) = Δδ = δ (solid state) – δ (solution) [ref. 156]

2.2.2 Preparation of complexes with partially deuterated hosts

The relaxation power, of a methyl rotor is shared between all the protons in the sample, via the process of spin-diffusion. Reducing the number of protons in the complex, for example by replacing some protons with deuterons, causes the relaxivity to be shared amongst fewer protons, thereby speeding up relaxation of the system (see appendix C for further details). In the present study toluene complexes of the two partially deuterated hosts (*t*-Bcd$_{36}$) and (*t*-Bcd$_{44}$) have been prepared and have been made to characterise these. General crystallographic data for each of these materials is listed in Table 8.

Complex Information						Crystallographic Summary				
guest structure	number	synthetic host	yield	MP °C	Lit. ref.	internal reference	data temp.	distances h/Å	distances d/Å	space group
Toluene*	4651/18	*t-Bcd$_{36}$*	18 %	> 300	-	06sot0832	120K	1.33	3.0	Nd
Toluene	4651/89	*t-Bcd$_{44}$*	9%	> 300	-	J. Orton	120K	1.34	3.58	C2/c

Table 8: synthetic and crystallographic summary of deuterated p-*tert*-butylcalix[4]arene

2.2.2.1 p-*tert*-butyl_d$_{36}$-calix[4]arene (1:1) toluene complex

The p-*tert*-butyl_d$_{36}$-calix[4]arene (1:1) toluene complex (Figure 98) was prepared following the strategy described in Section 2.1.1

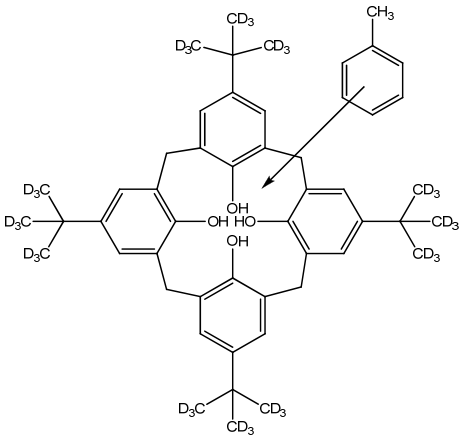

Figure 98 p-*tert*-butylcalix[4]arene_d$_{36}$ (1:1) Toluene complex (this work)

Tetragonal crystals were collected from a saturated solution of the partial deuterated host in toluene by slow evaporation and their X-ray structure was partially solved (Figure 99).

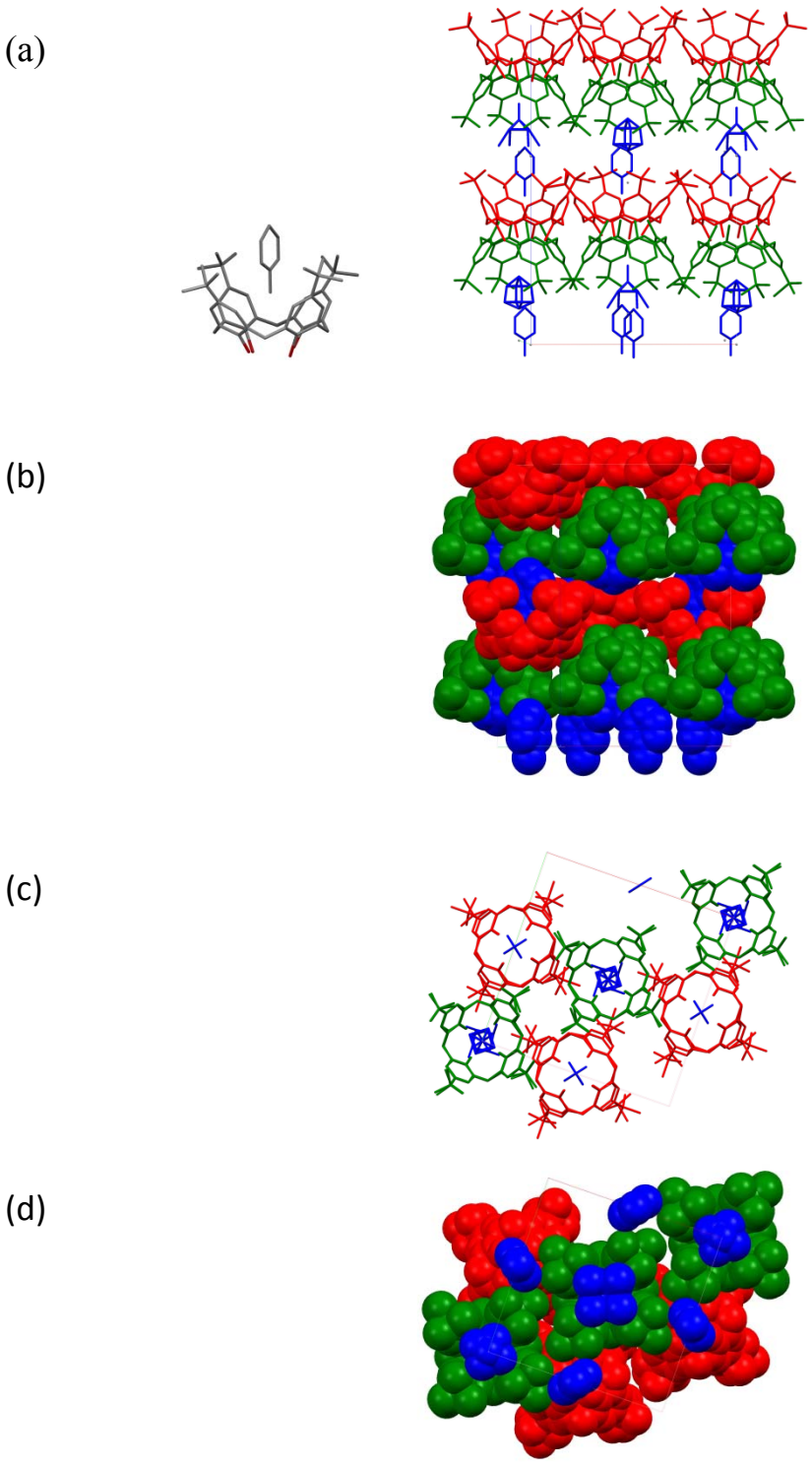

Figure 99 p-*tert*-Butyl_d_{36}calix[4]arene [green and red colour] (1:1) Toluene [blue colour] complex from this work a) crystal structure and packing b) space fill of packing front view c) crystal; packing bottom view d) space fill of packing bottom view

Space fill of the crystal structure motif revealed a heavy disorder for the guest molecule as showed in Fig. 99. The geometry of the calixarene framework is the same as that of the full protonated calixarene toluene complex (Fig. 78), but the toluene ordering changes the unit cell from tetragonal P (12,12,13) to tetragonal I (17,17,28). These two cells are very closely related – one being the primative form of the other. Unfortunately X-ray crystallography is not a good way for studying a dynamic system. The ^{13}C CP/MAS NMR of this material gives a room temperature a CIS (complexation induced chemical shift) of -2.3 p.p.m (see table 7) as reported for the non-labelled host (Figure 100 and **S$_6$**).

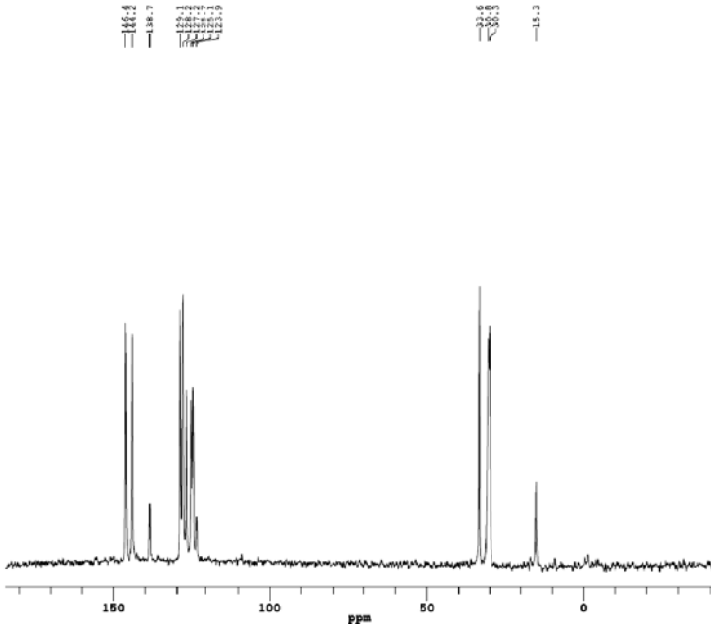

Figure 100 ^{13}C CP/MAS of p-*tert*-butyl_d_{36}-calix[4]arene (1:1) toluene complex from this work (150 MHz)

As expected an improvement in the T_1 relaxation time at low temperature is indeed observed in quench cooled samples (Figure 101).

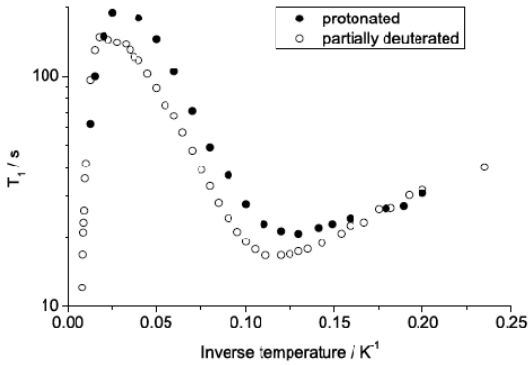

Figure 101 T1 versus inverse temperature data for fully protonated (black circles) and partially deuterated (white circles) [ref. 45] Error bars are small compared marker size.

The data shows that the T_1 minimum for the partially deuterated calixarene d_{36} host sample is deeper than that for the protonated sample, but only by factor of 1.3; similar to, but less than the predicted difference of 2.1. There is also a small shift of the minimum from ~ 8K to ~ 9K, which suggests that deuteration may cause modification of the methyl potential barrier. The *tert*-butyl protons account for over half of all the protons in the complex (72 protons out of every 128 in a unit cell; one unit cell consists of two (1:1) complexes), therefore by replacing them all with deuterons a large difference in the dipolar coupling constant, and T_1, was expected. Approximate calculations were attempted in the Quantum Dynamic laboratory of Prof. A.J. Horsewill at the University of Nottingham, to predict the effect of deuteration on the homonuclear dipolar-coupling costant, C_{HH}. The motional model was based on a model for the proton transfer in benzoic acid dimmers, which assumes hopping between two sites. The rotational motion of methyl group is somewhat more complicated than two-site hopping, but approximating the motion using the two-site hopping model can give a first approximation for how C_{HH} may change after deuteration.

2.2.2.2 p-*tert*-butylcalix[4]arene_d_{44} (1:1) Toluene complex

Using the same procedure (described in Section 2.2.2.1) the p-*tert*-butylcalix[4]arene_d_{44} (Figure 102) was prepared and crystallized from a saturated solution of toluene. Tetragonal crystals were collected by slow evaporation after several days.

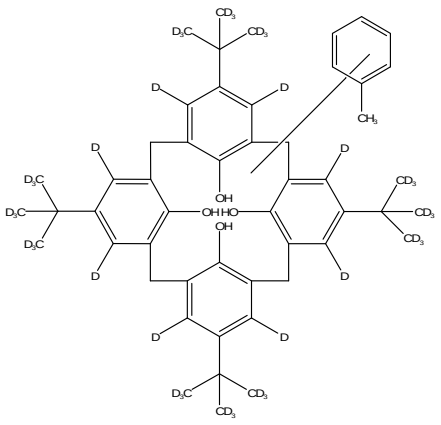

Figure 102 p-*tert*-butylcalix[4]arene_d_{44}/Toluene (1:1) complex

After considerable efforts James Orton was able to resolve the structure (Figure 103).

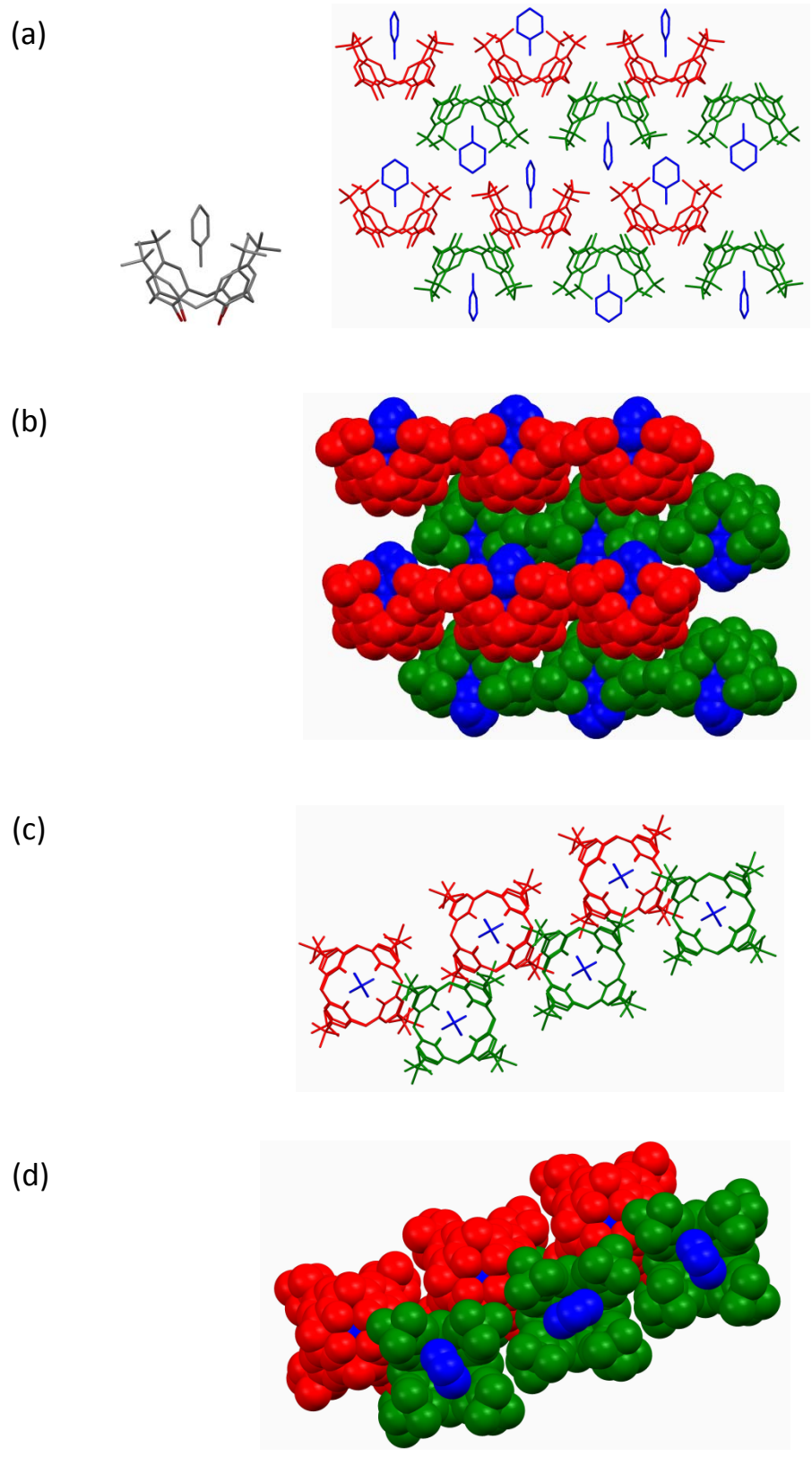

Figure 103 p-*tert*-Butylcalix[4]arene_d_{44} [green and red colour] (1:1) Toluene [blue colour] complex from this work a) crystal structure and packing b) space fill of packing front view c) crystal; packing bottom view d) space fill of packing bottom view

However the ^{13}C CP/MAS solid state NMR (Figure 104 and **S7**) showed a room temperature spectrum in consistent with the structure of the complex with CIS (complexation induced chemical shift) of -6.3 p.p.m as reported in table 9.

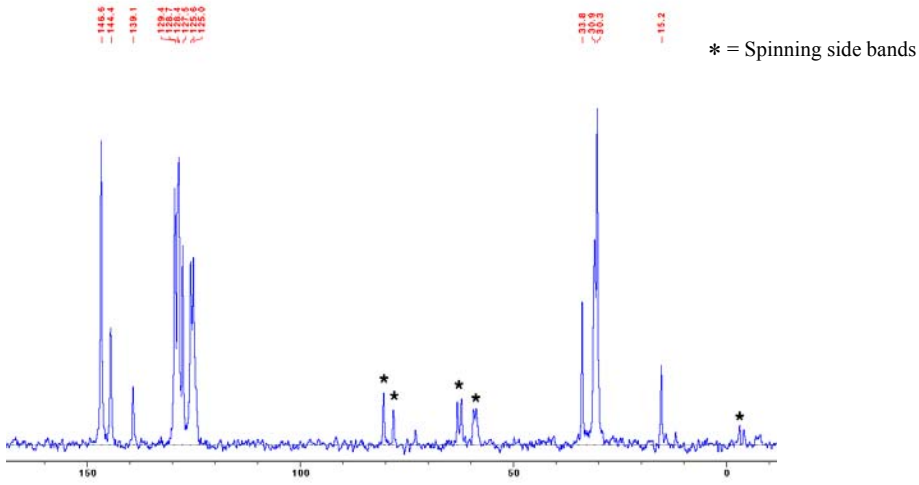

Figure 104 ^{13}C CP/MAS of p-*tert*-butylcalix[4]arene_d_{44} (1:1) toluene complex from this work (150 MHz)

As expected, an improvement of the T_1 relaxation time at low temperature (Figure 105) was observed in quench cooled samples of deuterated complexes by Field Cycling solid state NMR. The data shows that the T_1 minimum appears to become shorter with increase deuteration; the fully protonated sample has the longest T_1 20.7s (blue squares) with minimum at 7.7K, followed by partially deuterated calixarene d_{36} host sample 16.7s (red circles) with minimum at 8.8K and the partially deuterated calixarene host d_{44} 13.9s (black triangles) with minimum at 9.1K. However the dates show that the T_1 minimum differs by factor only of 2.5 but not large as initially expected.

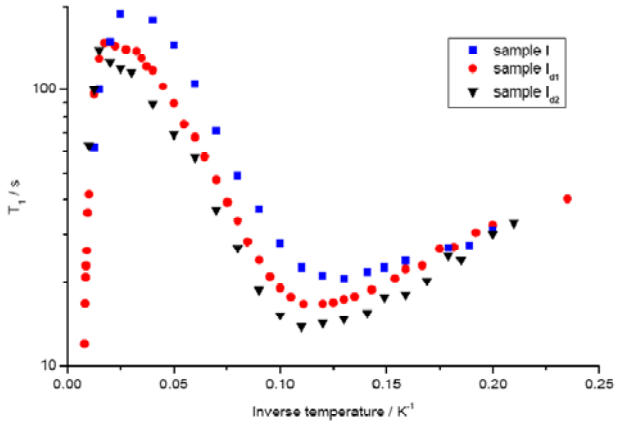

Figure 105 T_1 vs inverse temperature for p-*tert*-butylcalix[4]arene (1:1) toluene complex [ref. 45]: fully protonated calixarene host (blue squares), partially deuterated calixarene host d_{36} (red circles), partially deuterated calixarene host d_{44} (black triangles) Error bars are compatible to size of markers [from ref 45].

Based on the model described in this work, a largest positive change in the dipolar-coupling constant can be expected by reducing the number of the protons in the complex.

Table 9 Selected ^{13}C-CP/MAS NMR data of deuterated p-*tert*-butylcalix[4]arene-guest complexes

Host-Guest	**Assignment**	**Solid**	**Solution**	**CIS*/ppm**	**lit. values**	**ref**
D_{36}-toluene (1:1)	$PhCH_3$	15.3	21.5	-6.2	-	this work
D_{44}-toluene(1:1)	$PhCH_3$	15.2	21.5	-6.3	-	this work

*CIS (complexation induced chemical shift) = $\Delta\delta = \delta$ (solid state) – δ (solution) [ref. 156]

2.2.3 Preparation of complexes with p-*iso*-Propylcalix[4]arene

For the preparation of the desired p-*iso*-propylcalix[4]arene complexes a synthetic route was employed analogous to that used for the production of the corresponding p-*tert*-butylcalix[4]arene complexes (described in section 2.1.1). A full list of the compounds prepared using the p-*iso*-propylcalix[4]arene may be found in Table 10.

Complex Information						Crystallographic Summary				
guest structure	number	synthetic host	yield	MP °C	Lit. ref.	internal reference	data temp.	distances h/Å	distances d/Å	space group
p-Xylene (2:1)	4651/33	*i-pc4*	48 %	> 300	157	06sot0769	120K	1.52	3.71	$P4/_{nnc}$
Iodomethane	4651/XX	*i-pc4*	67 %	> 300	-	06sot0680	120K	1.60	3.77	$P4/_{n}$
2-Butyne	4651/18	*i-pc4*	55 %	> 300	-	06sot0756	120K	2.33	4.14	$P4/_{n}$

Table 10: synthetic and crystallographic summary of p-*iso*-propylcalix[4]arene complexes prepared in this study

2.2.3.1 p-*iso*-Propylcalix[4]arene (2:1) p-Xylene (2:1) complex

In order to explore the behaviour of a double rotor system using a 2:1 (host:guest) motif involving p-xylene it was necessary to use p-*iso*-propylcalix[4]arene as the host. However, attempts to prepare this following the procedure of Perrin[157] proved unsuccesful, only the 1:1 complex being isolated as showed in Figure 101.

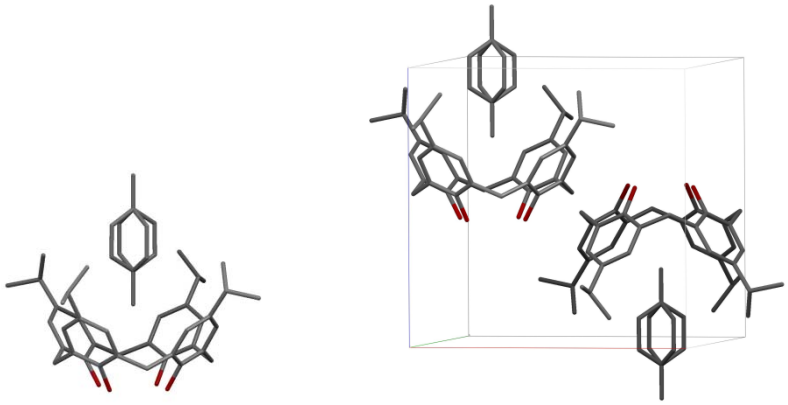

Figure 106 Molecular packing of p-*iso*-propylcalix[4]arene (1:1) p-xylene complex (this work)

Atwood and co-workers[158] in several studies have revealed that inclusion compounds involving aromatic guests most often crystallize with the host molecules packed as bilayers. Furthermore, the bilayer packing mode can be suddivided into two major categories (Figure 107):

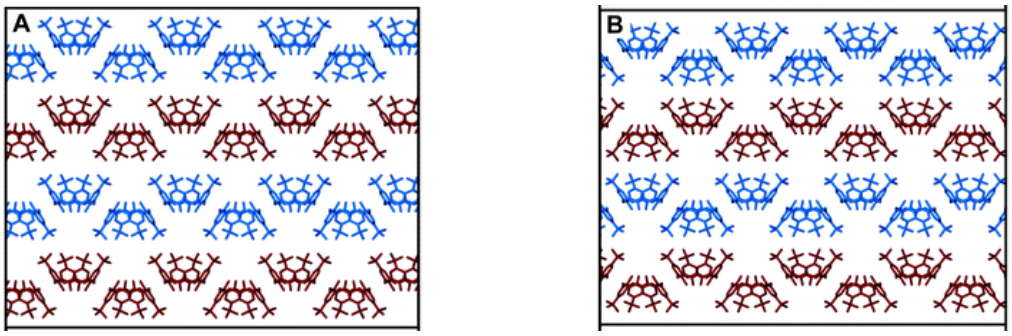

Figure 107 p-*tert*-butylcalix[4]arene bilayers packing arrangements [ref. 158]

For category **A** has space group P4/*n* host, and a host:guest ratio 1:1 and the guest is partially inserted into the calixarene cavity. For category **B** the space group is P4/*nnc* with a host:guest ratio 2:1 and two calixarene molecules face one another to form a dimeric capsule which can completely enclose the guest. In these studies Atwood and co-workers[159] have shown that thermogravimetric analysis of the t-bc4/toluene (1:1) complex indicates two distict weight-loss events, each accounting for half of the total amount of toluene originally present in the material. However Ripmeester and co-workers[152] have also shown that the thermal decomposition of various inclusion compounds exhibits quite distinct types of behaviour for different guests (Figure 108).

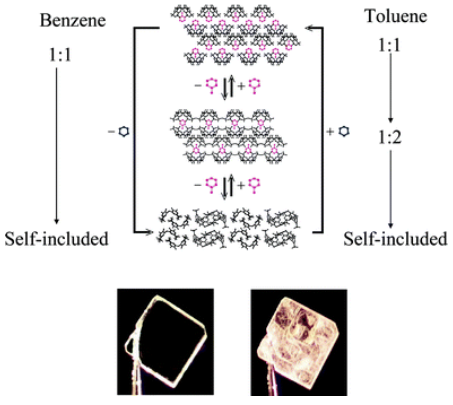

Figure 108 Scheme illustrating reversible single-crystal-to-single-crystal transition in *t*-bc4/toluene and *t*-bc4/benzene [ref. 152]

Complexes such as *t*-bc4/benzene (1:1) lose most of the guest in one step[152]; indeed in the present study the heating of a single crystal of *t*-bc4/toluene (1:1) complex showed a single-to-single-crystal transformation (Figure 109).

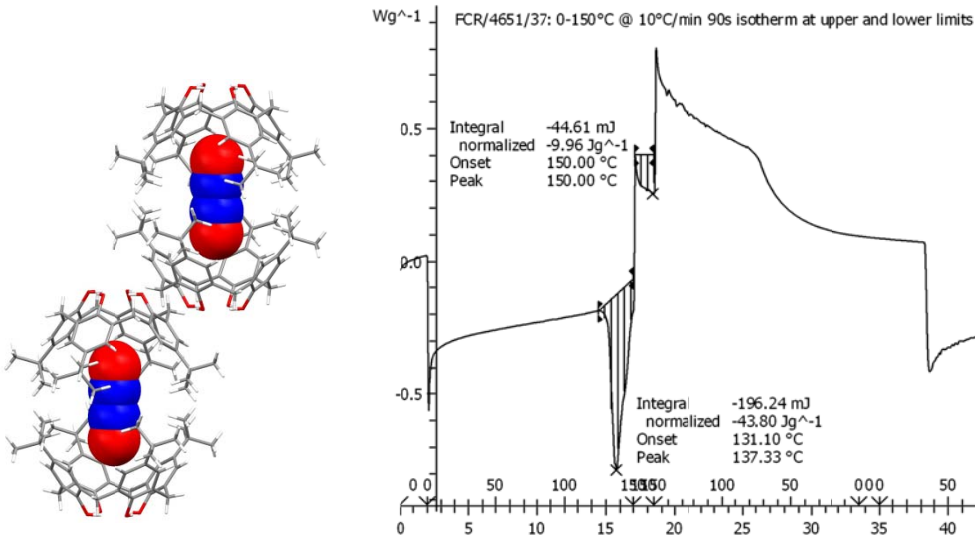

Figure 109 p-*tert*-Butylcalix[4]arene (2:1) toluene complex molecular packing and DSC analysis (this work)

Differential scanning calorimetry trace of the *t*-bc4/toluene (1:1) complex (our sample) below 200ºC was carried out and endotherms peak associated with guest loss at 137ºC was founded[159] Single porous crystals of *t*-bc4/toluene (2:1) complex prepared using this strategy were analyzed by X-ray analysis but all attempts to refine the position of the guest within the calixarene cavity failed because of the heavy disorder, so the disordered toluene molecule is indicated as van der Waals spheres/cilinders (see Figure 109 left). Following the same procedure, i-pc4/*p*-xylene (1:1) complex was successfully converted into the (2:1) *p*-xylene complex by heating single crystals at 80ºC in a sand bath for 25 minutes, during which time the space group changed from P4/n to P4/*nnc* (see Figure 110).

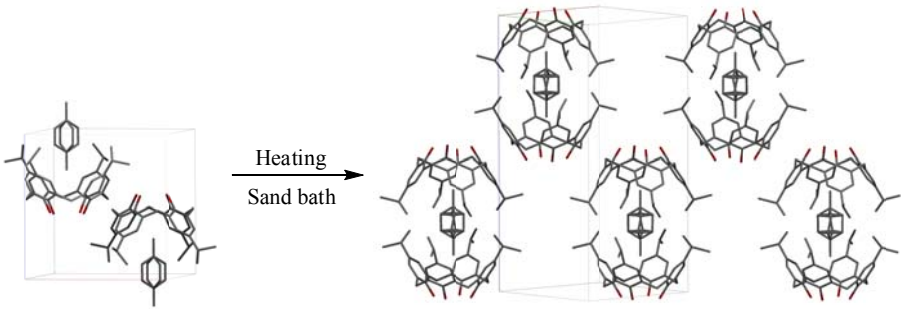

Figure 110 Single-to-single-crystal transformation of p-*iso*-propylcalix[4]arene p-xylene complex (this work)

Just as occurred for the *t*-bc4/toluene complex, this process involves as a single-to-single-crystal phase transformation and is triggered by relatively weak van der Waals interactions between host and guest molecules (Figure 111).

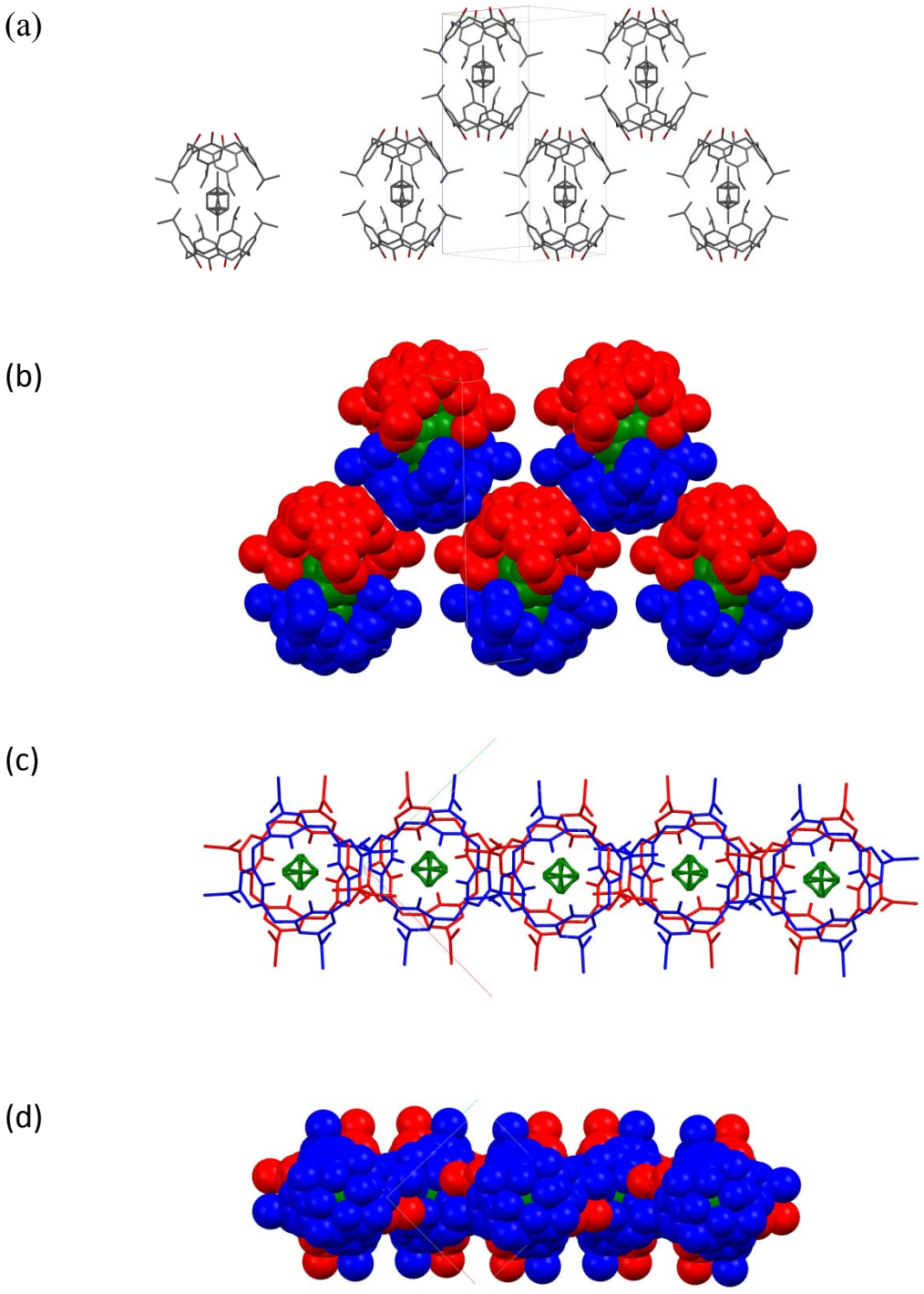

Figure 111 p-*iso*-propylcalix[4]arene (2:1) p-xylene complex from this work a) crystal structure and packing b) side view of packing of complex capsule space filled, host (red and blue colour), guest (green colour) c) bottom view of the crystal packing with each host twisted around their axis d) crystal packing space fill bottom view

We have carried out Field Cycling solid state NMR studies on this complex and a dramatic series of thermal history effects was observed (Figure 112).

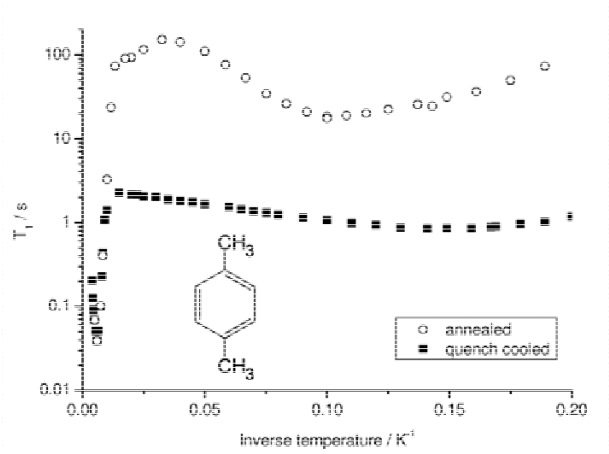

Figure 112 p-*iso*-propylcalix[4]arene (2:1) p-xylene complex, T_1 versus inverse temperature, B_r = 0.7T (probe **A**, constant field) [ref. 45]. Error bars are small compared to marker size.

Initially, the temperature dependence of T_1 was measured after the sample had been quickly cooled from room temperature. The quick cooling process begins with the sample being loaded into a cold cryostat, which can cause the temperature to drop from room temperature to temperatures as low as 220K within seconds. Further cooling is achieved by pumping the sample space with a vacuum pump, increasing the helium gas flow over the sample. With pumping, cooling rates of around $15 K min^{-1}$ are typical. T_1 was measured over a range of temperatures between 5K and 250K, in ascending order. The sample was then cooled and T_1 measurements were made at several temperatures between 190K and 120K, in descending order. After cooling to 10K, repeatition of the measurements of T_1 revealed dramatic differences from the values measured after the initial cooling. It was clear that the sample had undergone an annealing process during the temperature cycle. The flat, broad low temperature minimum is suggestive of a disordered molecular environment, in which the methyl groups experience a range of potential barriers. Attempts were made to fully anneal the sample by cooling the sample slowly ($< 1 K min^{-1}$) from 250K, however the resultant relaxation curves were observed to have bi-exponential character, (see appendix C for details) suggesting a mixed phase sample in which some of the disordered phase persisted. It was possible to separate the characteristic relaxation times of the two phases as they differed by an order of magnitude. The value of T_1 for the annealed phase (open circles, Figure 112) was found to differ by a factor of between 20 and 80 when compared with the quench- cooled sample. The low

temperature T_1 minimum is consistent with a weakly hindered methyl group, and the steep high temperature minimum at ~0.005K^{-1} is due to the motion of the strongly hindered *t*-butyl groups around the calixarene rim. Solid-state NMR studies were also carried out on this sample and all peaks in the aliphatic region and most peaks in the aromatic region of the spectrum could be assigned (Figure 113 and **S$_8$**).

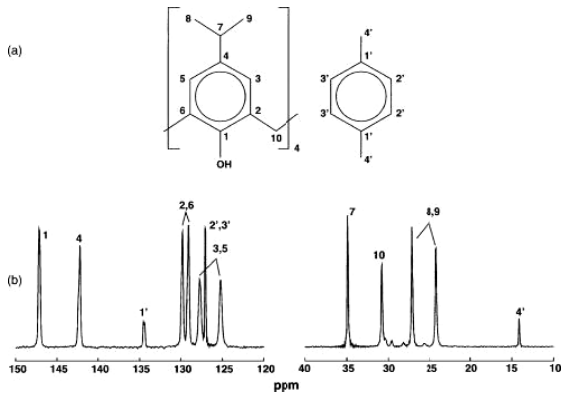

Figure 113 ^{13}C CP/MAS of p-*iso*-propylcalix[4]arene (2:1) p-xylene complex this work (150 MHz)

Partial assignments of the peaks to the host and guest molecules were obtained using the methods described by Wu and Zilm[160,161].. With this method, the assignment is complete and unambiguous for all aliphatic sites, but it is only partial in the aromatic region due to peak overlap and to the similarity of the local environments. Notice that the isopropyl methyl groups (8 and 9) are inequivalent. An almost complete assignment was achieved by means of ^{1}H-^{13}C correlation spectroscopy experiments, performed at 14.1 Tesla at a spinning frequency of 15.0 kHz. The corresponding two-dimensional spectrum is shown in Figure 114 and **S$_9$**, together with the signal projection in the two dimensions.

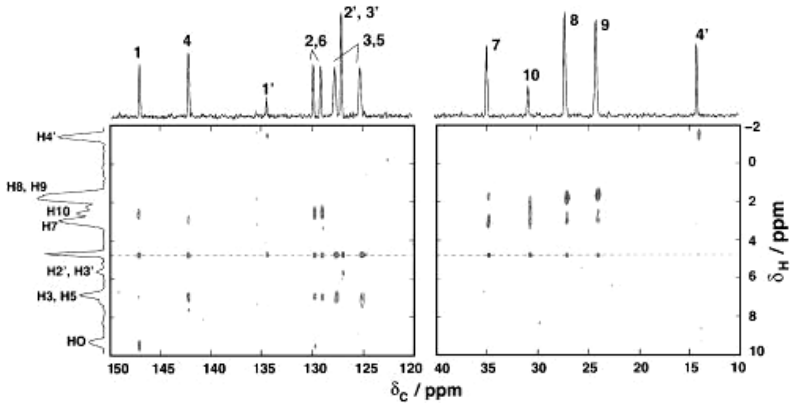

Figure 114 ^{1}H-^{13}C correlation spectrum at 14.1 T and spinning frequency of 15.0 KHz this work (150 MHz)

The presence of cross peaks connecting the ^{1}H and the ^{13}C signals indicates spatial vicinity of those sites and hence is a guide for the assignment. In particular, there are five aromatic carbon peaks coupled to an individual proton signal, (H3, H5), which are attributed to positions 2–6. The room temperature spectrum exhibits narrow lines, most of which get significantly broader at low temperature. The peak near 147 ppm is coupled to the phenolic proton and is assigned to position 1. The carbon peaks 1, 2, and 6 also show a visible interaction to H10. The peak near 134 ppm is weakly coupled to the H4' position and is assigned to position 1' of the guest, while 127 ppm sees a different proton environment and is attributed to positions 2' and 3' of the guest molecule. The only remaining ambiguities in the assignment concern positions on opposite sides of the aromatic rings, for example, positions 2 and 6, or 3 and 5. This assignment, confirmed by 2D correlation spectroscopy, is different to that proposed by Ripmeester et al[152] in closely related materials.

The effect of thermal history of the sample has been explored via proton de-coupled ^{13}C NMR spectra as shown in Figure 115.

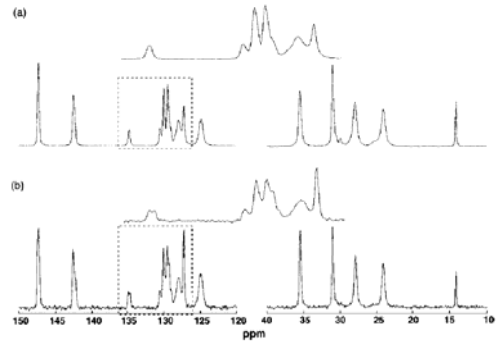

Figure 115 ^{1}H-decoupled ^{13}C-MAS NMR spectrum at 153K from this work a) Sample cooled down slowly b) Quench-cooled sample (150 MHz)

These spectra were recorded at a field of 9.4 T with a sample rotation frequency of 10.0 kHz. The room-temperature spectrum exhibits narrow lines, many of which get significantly broader at low temperature. It is interesting to compare the spectrum obtained on a sample which was cooled gradually over a time range of 12 h (Fig. 115a) with the spectrum obtained on a sample cooled rapidly from 290 to 153 K within 3 min (Fig. 115b) The larger line widths and the presence of visible shoulders on many peaks in (Fig. 115b) indicate that the structure obtained by fast cooling is more disordered. The disorder affects not only the calixarenes but also the guest

molecule, as revealed by the peak near 135 ppm, assigned to position 1' of the *p*-xylene, which displays a small splitting in the quench cooled sample. Inelastic neutron scattering studies data have not yet been reported on this complex. However, inelastic neutron scattering of the closely related *p-tert*-butylcalix[4]arene (2:1) *p*-xylene complex have been performed by Caciuffo and co-workers (Figure 116).

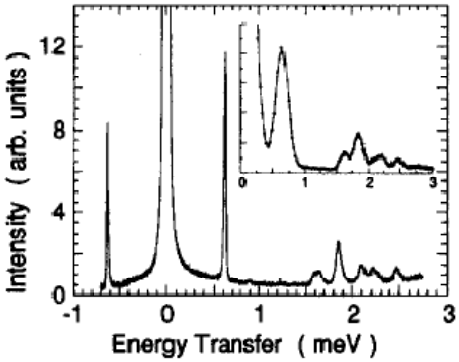

Figure 116 INS spectrum at 1.7 for p-tbc4/p-xylene deuterated complex (inset full protonated) [ref. 114]

In this case, a single tunnelling peak with energy of 626 meV was observed; this compares with the splitting of 654 meV expected for a free CH_3 rotor. The presence of almost freely rotating methyl groups is consistent with the proton spin-lattice relaxation measurements of complex (Fig. 112), especially in the quench-cooled form.

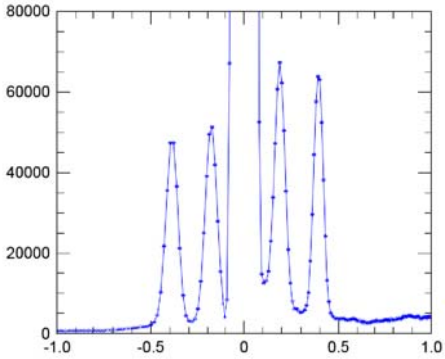

Figure 117 INS spectrum at for p-*i*bc4/p-xylene (2:1) complex [ref. 45]

However INS studies on our sample of p-*iso*-propylcalix[4]arene/p-xylene (2:1) complex have been carried out in Grenoble in collaboration with Prof. Horsewill University of Nottingham and the result is shown in Figure 117. The spectrum shows a central elastic peak and four inelastic peaks of resolution width reveals two CH_3 tunnelling peaks at 390μeV and 185μeV. Excellent quantitative agreement has been achieved between the CH_3 tunnelling splitting and the CH_3 rotational dynamics determined by field-cycling NMR relaxation data for our complex (Figure 112).

2.2.3.2 p-*iso*-propylcalix[4]arene (1:1) Iodomethane complex

Methyl iodide is a simple example of a quantum rigid rotor and exhibits quantized rotational energy levels[162]. Such rotations take place primarily about the axis aligned with the I and C atoms (see Figure 118) and can be measured by Inelastic Neutron Scattering[163].

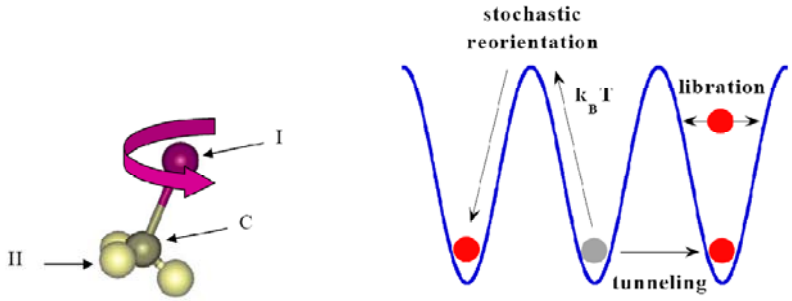

Figure 118 Methyl iodide structure and different types of methyl motions in solid state [ref. 163]

Dimeo and co-workers[162,163] have studied the rotational dynamics of the methyl group of this molecule at low temperature when confined to porous glass disks with diameters ranging from 2.5nm up to 20nm at low temperatures. They have demonstrated that the pore size has a substantial effect on the magnitude and breadth of the methyl tunnelling line shape. Therefore, it was interesting to explore the possibility of using the methyl iodide as guest inside the calixarene cavity to study such tunnelling behaviour. Crystals suitable for X-ray analysis were obtained by slow evaporation of a saturated solution after 20 days (Figure 119).

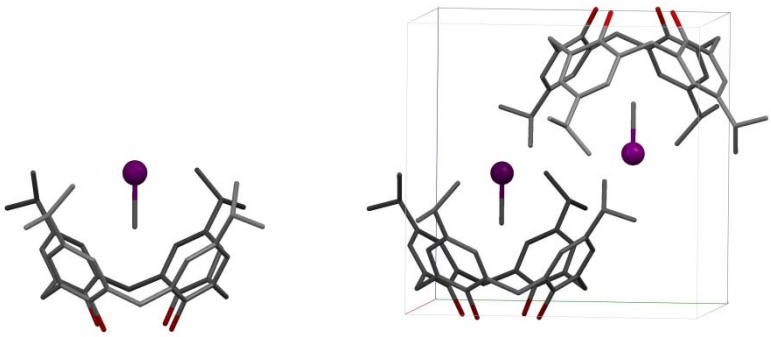

Figure 119 p-*iso*-propylcalix[4]arene (1:1) iodomethane crystal structure and packing (this work)

As previously reported for the *t*-bc4/toluene complex the best refinement model for the iodomethane guest molecule was found to lie along a fourfold crystallographic axis with its methyl group inserted into a conical cavity of the calixarene host

molecule. However, as for the toluene case the presence of a different $CH_3 \cdots \pi$ interaction, occurs between the *t*-butyl group of the host and the aromatic π orbital of the guest. This causes probably a different position of the methyl group of the guest inside the bucket cavity.

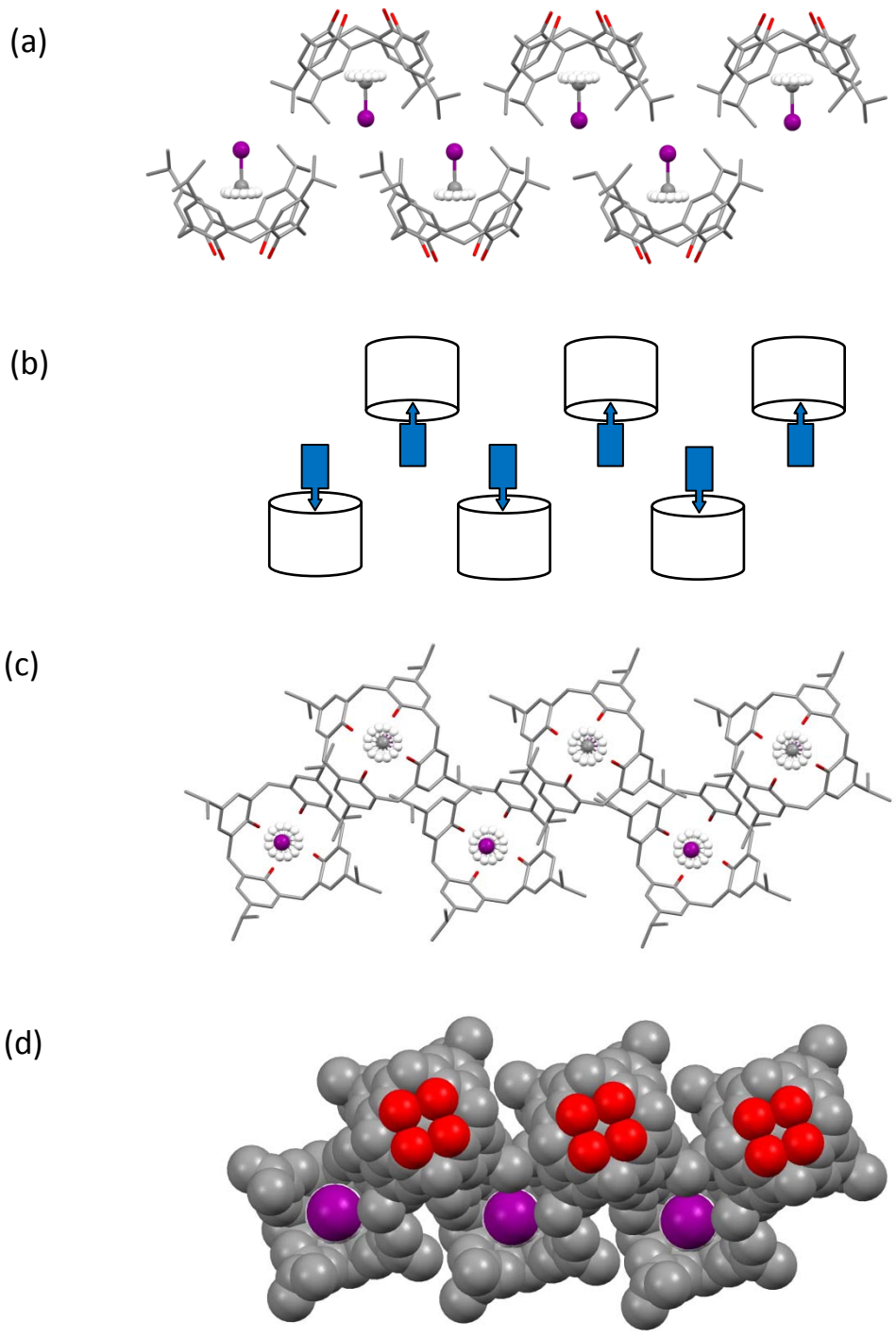

Figure 120 *p-iso*-propylcalix[4]arene (1:1) iodomethane complex from this work a) crystal structure and packing b) schematic motif packing c) crystal packing bottom view d) space fill bottom view

The ^{13}C CP/MAS NMR at room temperature (see Figure 121 and **S_{10}**) for the iodomethane complex revealed two signals for the *iso*-propyl groups confirming that these are inequivalent with a CIS (complexation induced chemical shift) of -5.6 p.p.m. as reported in table 11.

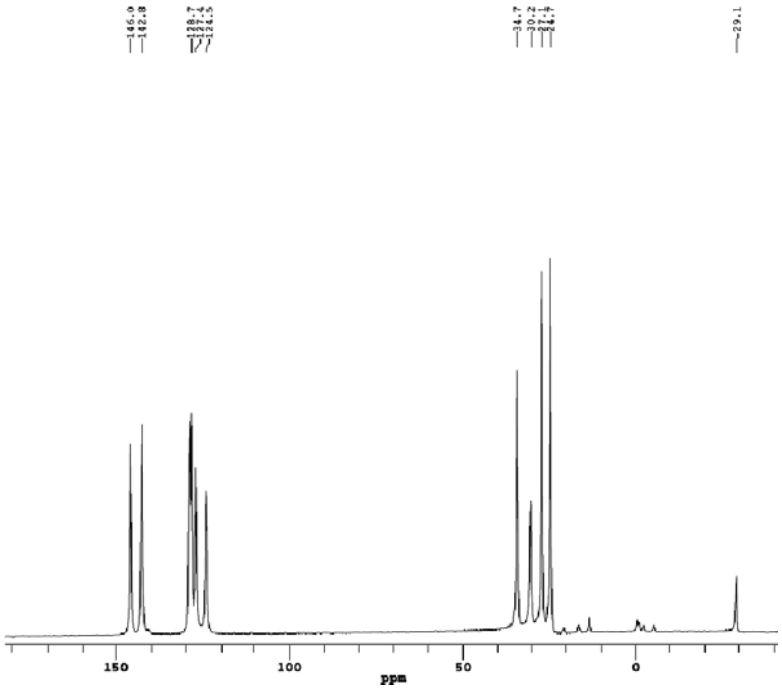

Figure 121 ^{13}C CP-MAS NMR spectrum of p-*iso*-propylcalix[4]arene (1:1) iodomethane complex from this work (150 MHz)

Field cycling solid state NMR experiments have been carried out on this material. These show temperature dependent bi-exponential behaviour that was mantained right up to high temperature (see Figure 122).

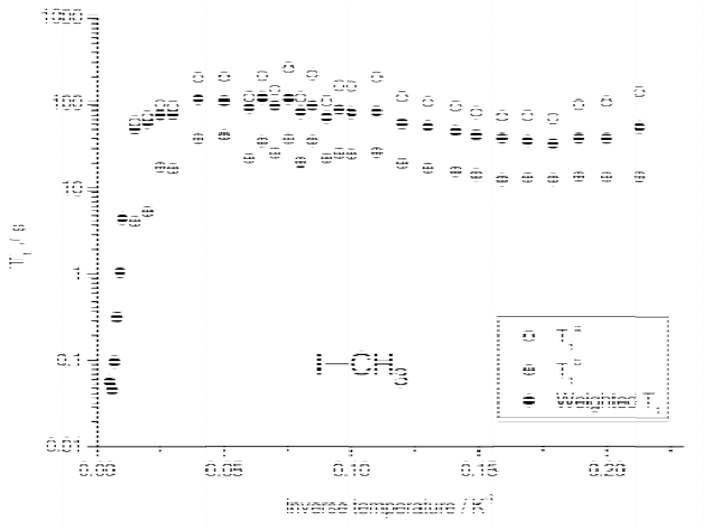

Figure 122 p-*iso*-propyl[4]arene/Iodomethane (1:1) complex, T1 versus inverse temperature B_r = 0.7T (probe **A**, constant field) [ref. 45] Error bars are smaller compare to marker size.

The relaxation was bioexponential up to 66.7K; at temperatures greater than this the relaxation was monoexponential. At low temperature the relaxation curves were dominated by the T_1^b component. With the increasing temperature, the ratio gradually favoured the slower T_1^a component. The change in the relative proportions of the components could be indicative of gradual structural changes in the sample. In the figure 122 the relaxation components are plotted, along with the weighted value of T_1 (T_1^w) which is a measure of the average relaxation time of the system (equation *XV*).

$$T_1^w = \frac{\left(M_0^{(a)}.T_1^a + M_0^{(b)}.T_1^b\right)}{M_0^{(a)} + M_0^{(b)}} \qquad XV$$

Data points show an appreciable degree of scatter, perhaps suggesting disorder. The T_1^w versus inverse temperature curve is very flat and broad at low temperature, showing a shallow minimum at 5.6K ($0.18K^{-1}$) attributed to iodomethane methyl rotor. Neutron scattering studies for this methyl iodide complex confined in calixarene cavity have not been carried out as yet, but Dimeo and co-workers[163] have discussed the tunnelling and librational dynamics of CH_3 group (Figure 123) in their porous disc complexes.

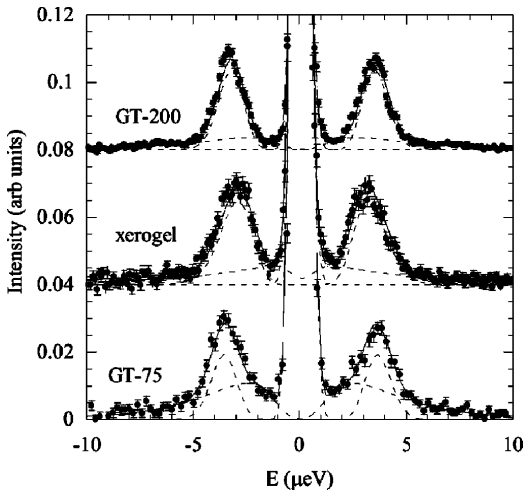

Figure 123 Rotational Tunneling spectra for methyl iodide confined in tree porous materials with different diameters [ref. 163]

In that case the methyl iodide's behaviour can be analysed using a simple two component model composed of weakly and strongly disordered molecules. They have found no simple correlation between the mean diameters and the barrier height. These results suggest that a more complex behaviour dominate the tunnelling line, therefore calixarene cavity approximation can be taken.

2.2.3.3 p-*iso*-propylcalix[4]arene (1:1) 2-Butyne complex

2-Butyne or (dimethylacetylene, DMA) is a potentially the simplest compound containing at the same time two symmetrical methyl rotors. DMA melts at 241K and thus is a liquid at ambient temperature. Attempts to prepare ipc4/2-butyne (1:1) complex at room temperature failed because of the high volatility of the alkyne which impedes slow crystallization but performing the crystallization process at low temperature, rhombic crystals suitable for X-ray analysis were obtained (Figure 124).

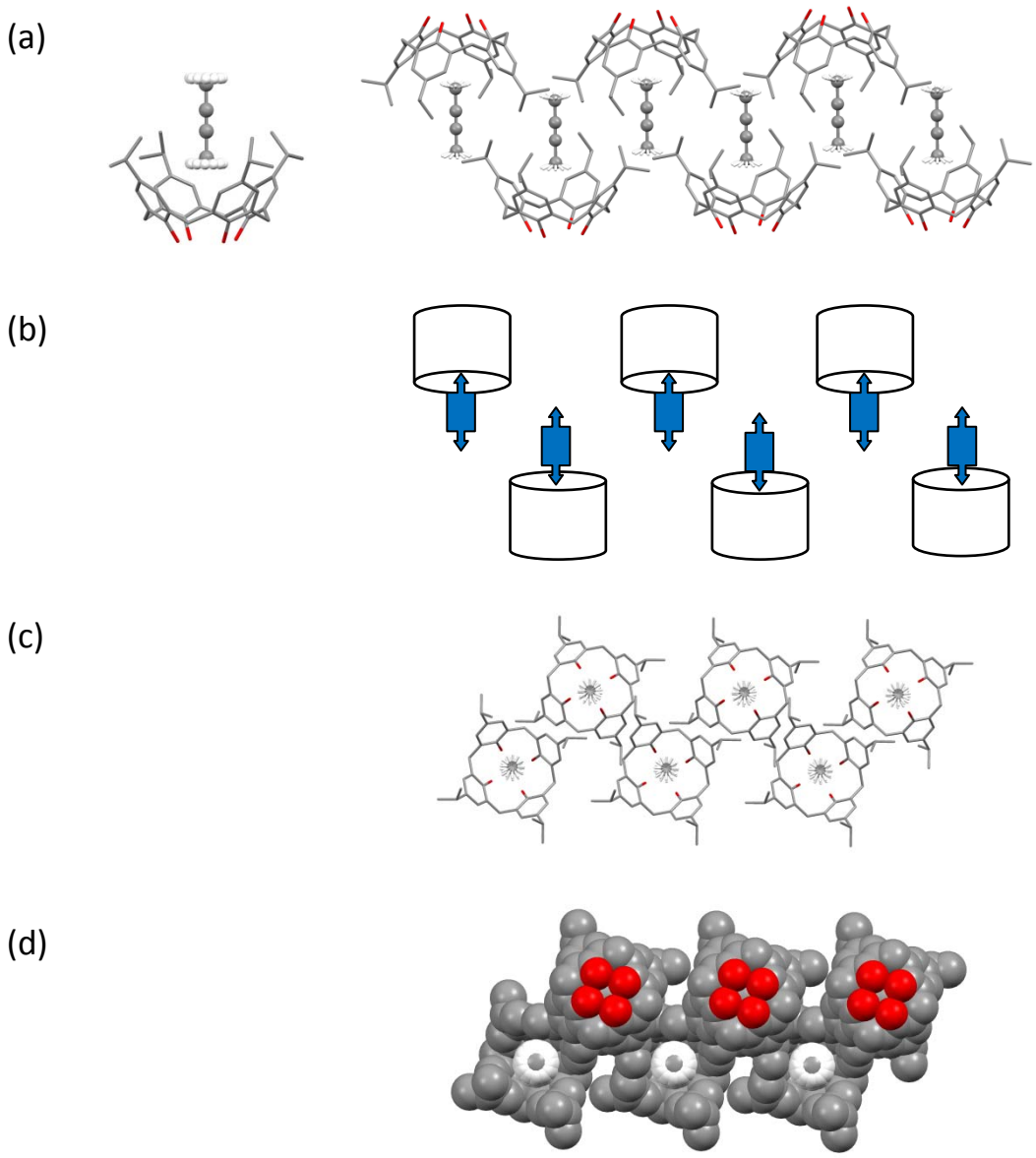

Figure 124 *p-iso*-propylcalix[4]arene (1:1) 2-butyne complex from this work a) crystal structure and packing b) schematic motif packing c) crystal packing bottom view d) space fill bottom view

A surprisingly a good refinement was obtained and no many disorder affecting the molecular packing was observed in contrast to that seen in previous complexes. A bottom view of crystal packing shows one methyl group in the bucket cavity and the other outside Figure 124. The ^{13}C CP/MAS NMR at room temperature is shown in Figure 125 and **S_{11}**. This spectrum again reveals a CIS (complexation induced chemical shift) of -4.6 p.p.m. as reported in table 11 with again two distinct signals for the *iso*-propyl groups confirming that the methyl groups of these are inequivalent.

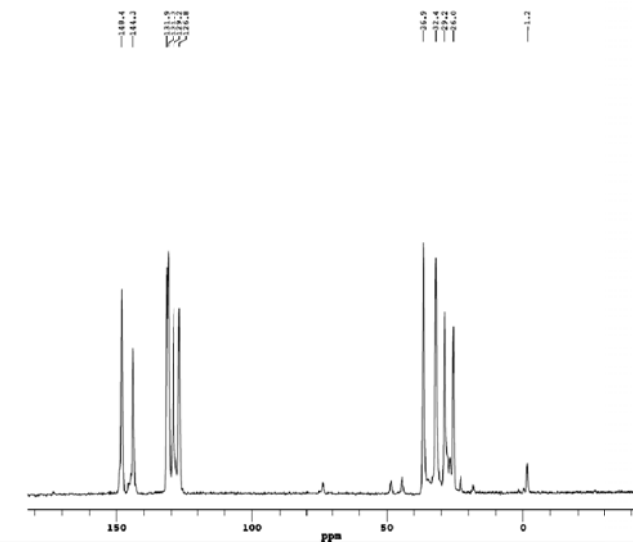

Figure 125 ^{13}C CP-MAS NMR spectrum of p-*iso*-propylcalix[4]arene (1:1) 2-butyne complex from this work (150 MHz)

An up-field shift (-1.2 ppm) for the methyl group of the 2-butyne (see Figure 125) was observed. Field Cycling solid state NMR studies at room temperature have shown a very high T_1 minima and so further low temperature experiments were not performed (Figure 126).

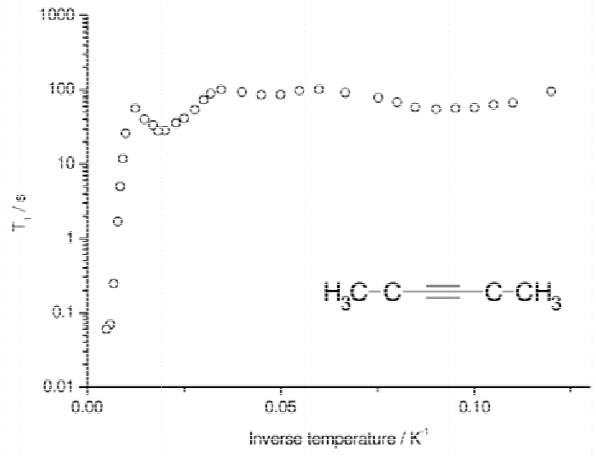

Figure 126 p-*iso*-propyl[4]arene (1:1) 2-butyne complex, T_1 versus inverse temperature B_r = 0.86T (probe **B**, constant field) [ref. 45] Error bars are smaller compared to marker size

The apparent minima at 10.6K ($9.4\times10^{-2}K^{-1}$) and 21.4K ($4.7\times10^{-2}K^{-1}$) could be due to the inequivalent methyl rotors. Presumably, the methyl group within the calixarene cavity is the less hindered rotor, giving rise to the low temperature minimum. This assignment could be tested perhaps measuring the temperature dependence of T_1 in a (2:1) complex of calixarene and 2-butyne, analogous to sample (Fig. 111), if indeed it is possible for such a complex to be crystallised. Prager and co-workers[164] in several studies have reported the methyl rotational excitations of free 2-butyne using neutron scattering techniques (Figure 127).

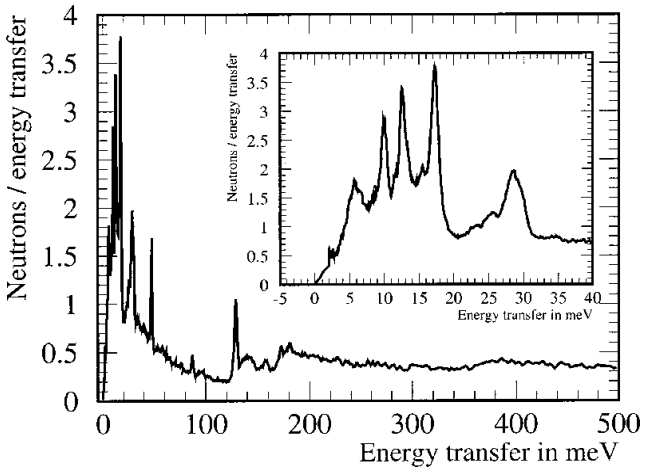

Figure 127 Neutron spectrum of free 2-butyne at temperature T<15K [ref. 164]

The 2-butyne was the primary system where rotational tunnelling was studied by high resolution neutron spectroscopy. Further low temperature INS studies were carried out from Prager and co-workers after the crystal structure became known[165] (Fig 127). The neutron spectrum is characterized by four peaks at 6, 9.9, 12.6 and 17.3 meV. There are two regimes: above 20 meV which corresponds to the internal molecular vibrations, higher harmonic and combination bands and below 20 meV which are characterized by regime of phonons Fig 127. In the present work INS for the new complex *i*-pc4/2-butyne has not been investigated but it would be very interesting to explore the physical behaviour of the methyl rotor confined inside a calixarene cavity.

Table 11 Selected ^{13}C-CP/MAS NMR data of p-*iso*-propylcalix[4]arene-guest complexes

Guest	**Assignment**	**Solid**	**Solution**	**CIS*/ppm**	**lit. values**	**ref**
p-xylene (2:1)	$Ph(CH_3)_2$	13.7	20.9	-7.2	-7.2	this work
iodomethane (1:1)	$I\text{-}CH_3$	-29.1	-23.5	-5.6	-	this work
2-butyne (1:1)	$(CCH_3)_2$	-1.2	3.40	-4.6	-	this work

*CIS (complexation induced chemical shift) = $\Delta\delta = \delta$ (solid state) – δ (solution) [ref. 156]

2.2.4 Preparation of simple complexes

Several approaches accordingly to functionalization of calixarenes on the lower-rim were investigated and different complexes were obtained. A full list of the crystals obtained is given in Table 12.

Complex Information						Crystallographic Summary				
guest structure	number	host	synthetic yield	distance h/A	Lit. ref.	internal reference	data temp.	distances d_1/Å	d_2/Å	space group
Nitromethane	4495/51	*t-btc*	12 %	-	-	06sot0751	120K	3.79	3.65	P-1
Acetonitrile	4651/80	*t-bcw*	10 %	-	168	08sot0650	120K	3.55	3.12	P-1

Table 12: synthetic and crystallographic summary of other p-*tert*-butylcalix[4]arene derivative complexes

An important characteristic of the calixarenes is the low solubility in organic solvents. Just as the p-alkylgroups in a calixarene affect its melting point so too they affect solubility, and it is no surprise that long chain alkyl group in the p-position increases their solubility in organic solvents. Analogous attachment of esters or ethers generally increases the solubility in organic solvents, and these differences can sometimes be used to separate the component of a mixture. Geometric parameters of calixarenes complexes with view from the top are displayed in figure 128.

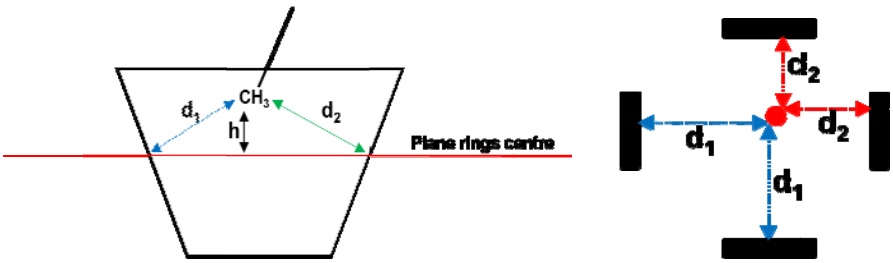

Figure 128 Definitions of geometric parameters for calixarenes complexes discussed in this section. **h** = distance between plane of the calix[4]arene aromatic rings centre and carbon of methyl group; $\mathbf{d_1}$ = major distance between centroid of the calix[4]arene aromatic rings and carbon of methyl group; $\mathbf{d_2}$ = minor distance between centroid of the calix[4]arene aromatic rings and carbon of methyl group.

2.2.4.1 p-*tert*-butylcalix[4]arene-tetracarbonate (1:1) nitromethane complex

McKervey and co-workers[142] have reported the synthesis of a calixarene functionalized on the lower rim with four ester groups using ethyl-chloroformate in basic conditions. This was then crystallised by slow evaporation of a saturated

solution of p-*tert*-butylcalix[4]arene-tetracarbonate in nitromethane, needles crystals suitable for X-ray analysis were obtained and fully characterized (Figure 129).

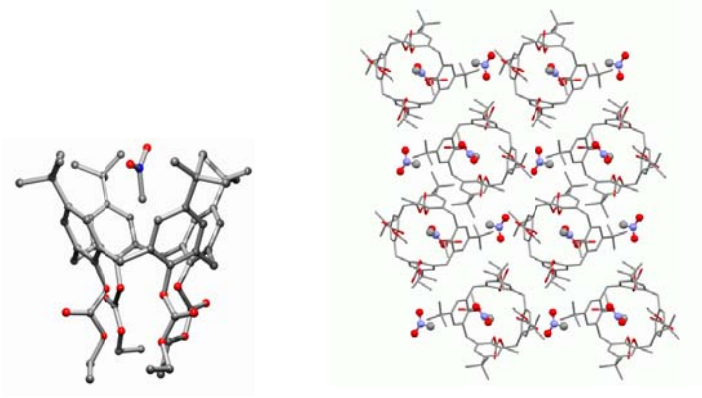

Figure 129 p-*tert*-butylcalix[4]arene-tetracarbonate/nitromethane (1:1) complex crystals structure and packing (this work)

The X-ray diffraction study established that the tetracarbonate calixarene possesses a perfect cone conformation with a fourfold crystallographic symmetry. The guest molecule appeares displaced from the center of the cavity (red circle) following a diagonal line towards the aromatic rings of the basket (black rectangles) Figure 128. The pendant ester groups are maximally extended and each carbonyl group is directed away from the calixarene cavity. The ^{13}C CP/MAS solid state NMR spectrum at room temperature reveals disordered for the methyl group of the guest and multiple resonances for the calixarene structure in the aromatic region and for the carbonyl groups of tetracarbonate units on the lower rim (Figure 130 and **S_{12}**).

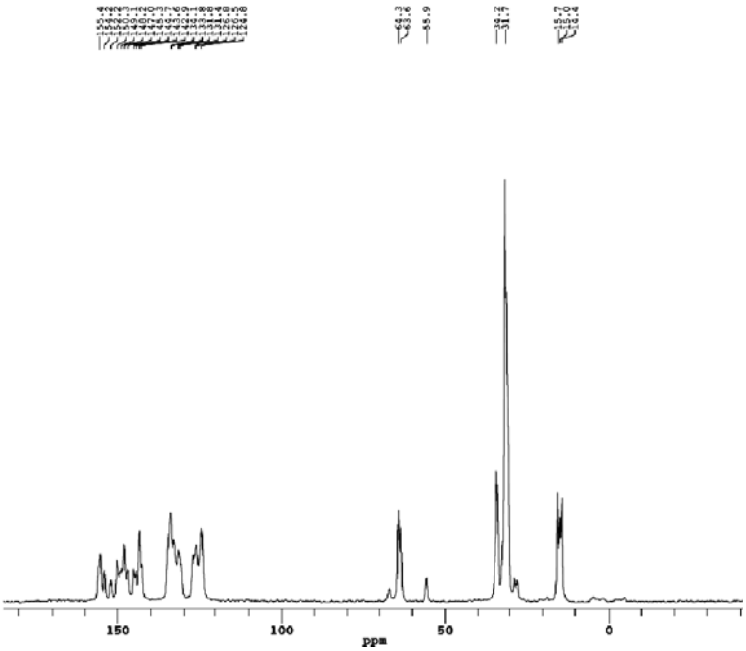

Figure 130 ^{13}C-CP NMR spectrum of p-*tert*-butylcalix[4]arene-tetracarbonate (1:1) nitromethane complex (150 MHz this work)

Furthermore the solid state NMR spectrum showed several peaks for the methyl group of nitromethane in agreement with the calixarene-nitromethane clathrate crystal structure. As show in (Figure 128) these are two nitromethane guests in different environments. Field Cycling solid state NMR studies showed biexponential character temperature dependent after quench cooling as illustrated (Figure 131).

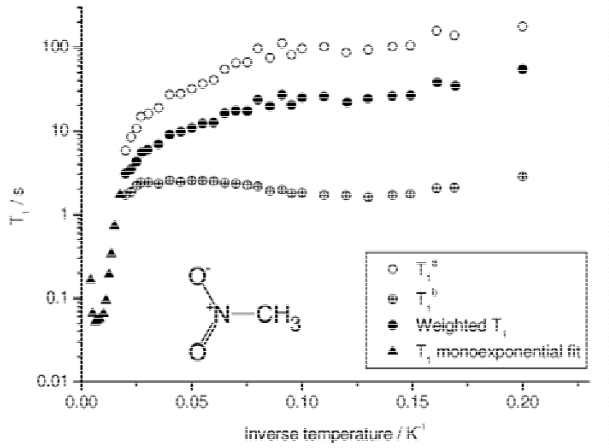

Figure 131 Field Cycling NMR of p-*tert*-butylcalix[4]arene-tetracarbonate (1:1) nitromethane complex, quench cooled, B_r = 0.7T (probe **A**, constant field) [ref. 45].

The ethyl groups each have one methyl rotor, which is expected to be strongly hindered in this complex. The biexponential nature of the relaxation persists up to 50K ($0.02K^{-1}$), and unlike the previous samples, the relative amount of each component remained fairly constant. The short component, T_1^b, dominates the relaxation curve and between 5-50K the average value of M_0^a/M_0^b was 0.34 with a standard deviation of 0.04. Above 50K the relaxation curves appeared less biexponential, and were fitted using the monoexponetial expression (see equation *XIX* in appendix D). In figure 131 the two relaxation components are plotted, along the weighted value of T1 (T_1^w) as for the p-*iso*-propylcalix[4]arene/iodomethane (1:1) complex using the expression *XV*. Above 50K, the T1 value from monoexponential fits of the relaxation curves are plotted. At low temperatures, there are no distinct features in the T_1 dependence that can be attributed to guest methyl group dynamics. T_1^w becomes shorter at high temperatures and the change is gradual. The T_1 minimum at 138K (7.25×10^{-3}) due to the strongly hindered methyl groups of the calixarene host is the only clear feature. In the present study INS for this novel calixarene-nitromethane complex has not been investigated. However interesting results has been reported from Trevino and co-workers[166,167] by the inelastic neutron scattering of the free nitromethane crystal structure.

2.2.4.2 p-*tert*-butylcalix[4]arene-bisCrown3 (1:1) acetonitrile complex

In order to increase the rigidity of a calix[4]arene, the introduction of lower rim bridges has been explored. Following the procedure Arduini and co-workers [168] the p-*tert*-butylcalix[4]arene-Bicrown3 capable of trapping acetonitrile inside the cavity by was prepared. Suitable crystals for X-ray structural analysis were obtained from slow evaporation of acetonitrile solution as reported previously from the authors (Fig. 132).

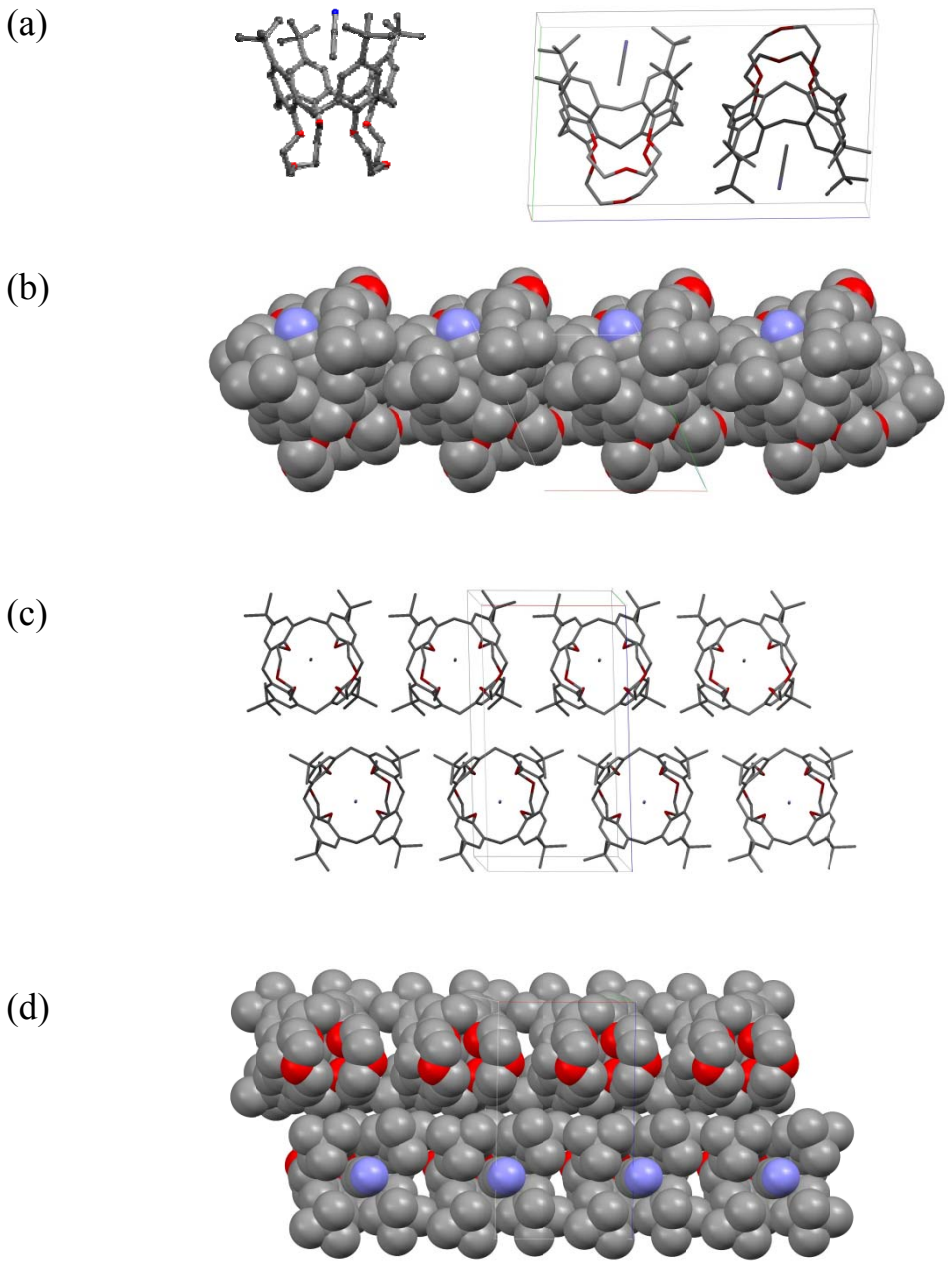

Figure 132 p-*tert*-butylcalix[4]arene-Biscrown3/Acetonitrile (1:1) complex a) crystal structure and packing b) schematic motif packing c) crystal packing bottom view d) space fill bottom view

Arduini and co-workers have reported detailed geometrical descriptions which define the host's geometry and the orientation of the guests in the complexes[168]. The shape of the host cavity, and consequently its symmetry, was defined through the angle between the benzene ring and the plane defined by the bridging methylene carbons of the calixarene[116] (Figure 132). The ^{13}C CP/MAS solid state NMR at room temperature revealed a strong up-field shift for the methyl group of the guest and several splitting peaks for the calixarene structure in the aromatic region and the ether bridges groups on the lower rim (Figure 133 and **S_{13}**).

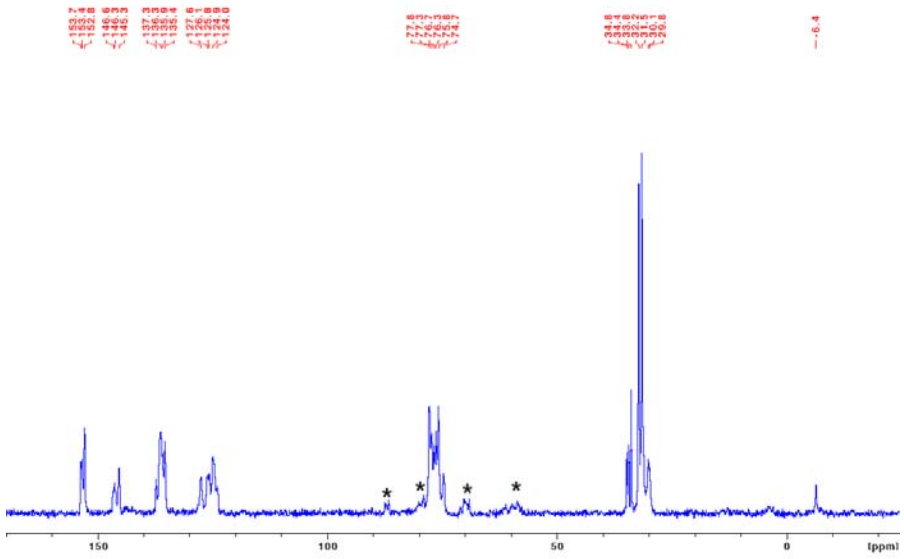

Figure 133 ^{13}C-CP NMR spectrum of p-*tert*-butylcalix[4]arene-bis-crown (1:1) acetonitrile complex 150 MHz (this work)

2.2.4.3 p-*tert*-butylcalixarene bridge

In order to increase the control over the location of the methyl rotor within the calixarene cavity a synthetic strategy to prepare a calixarene with a covalent bridge suspended across the lower rim has been developed (see section 2.1.6) and the desired compound was obtained in good yield (Figure 134)

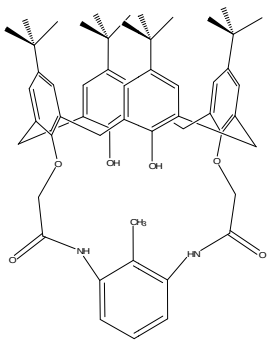

Figure 134 p-tert-butylcalix[4]arene bridge structure

Unfortunately all attempts to grown crystals suitable for X-ray analysis failed. The results of Field cycling solid state NMR experiments on this material are shown in Figure 135.

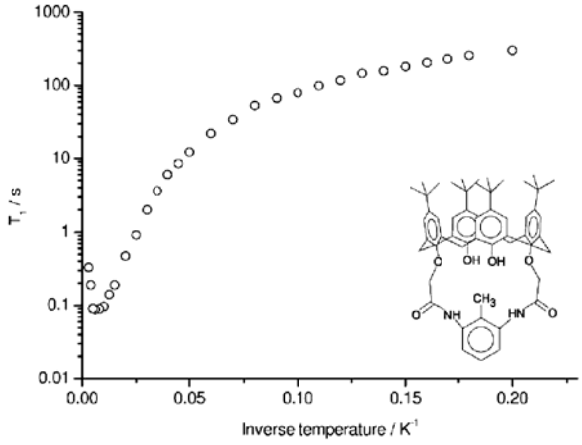

Figure 135 ^{13}C CP/MAS NMR of p-*tert*-butylcalix[4]arene bridge, quench cooled, B_r = 0.91T (probe **C**, constant field) [ref. 45] Error bars are smaller compared to marker size

The temperature dependence of T_1 was measured only for a quench-cooled sample of complex. The relaxation curves collected were of mono-exponential character, and remained as such even after cycling back down to low temperature after an initial batch of measurements. As with several of the other samples, the only distinct feature

of the T_1 vs. T^{-1} curve is the high temperature minimum, which for that sample is located at 150K. The high temperature minimum cannot be described as the previous samples due a superposition of minima from the two types of methyl group present i.e. the groups that comprise the *tert*-butyl groups, and those bonded to the aromatic ring on the 'bridge' of the molecule. There is not enough information to determine the contribution of these components, however measurement of the temperature dependence of T_1 at different field strengths, and measurement of the dispersion of T_1 could aid in separation of the components. The ^{13}C CP/MAS solid state NMR at room temperature is showed in (Figure 136 and **S_{14}**).

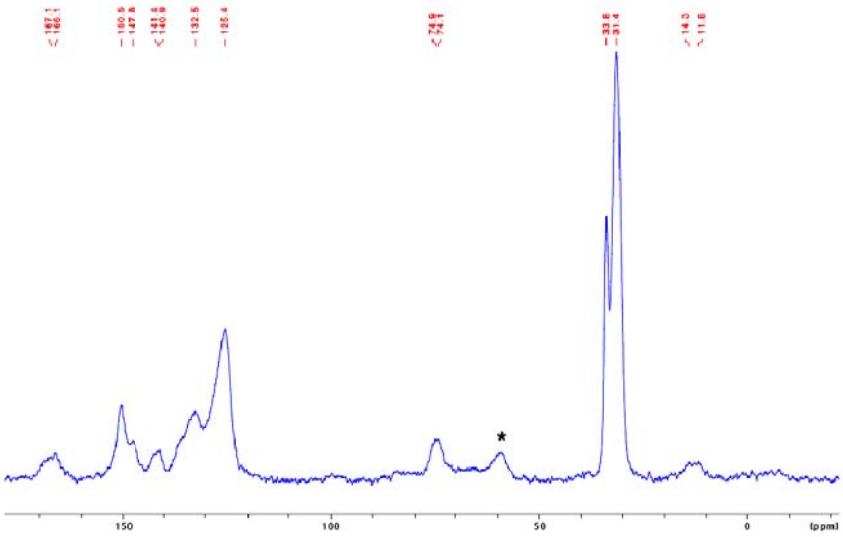

Figure 136 ^{13}C-CP NMR spectrum of p-*tert*-butylcalix[4]arene-bridge 150 MHz (from this work)

The broad peaks showed in the spectrum reflect the complexity of the methyl rotors motion in this complex.

Table 13 Selected ^{13}C-CP/MAS NMR data of p-*tert*-butylcalix[4]arene-derivatives guest complexes

Guest	Assignment	Solid	Solution	CIS*/ppm	lit. values	ref
nitromethane (1:1)	CH_3NO_2	55.8	62.8	-7	-	This work
acetonitrile (1:1)	CH_3CN	-6.4	+1.2	-5.2	-	This work

*CIS (complexation induced chemical shift) = $\Delta\delta = \delta$ (solid state) – δ (solution) [ref. 156]

Approach to potential Cryorelaxors bearing active biological anchors

2.2.5.1 *p-tert*-Butyl-[25,27-bis(maleonylmethyl-carbonylaminoethoxy)]-26,28-dihydroxycalix[4]arene preliminary biological tests

To demonstrate the potential of CryoMAS NMR spectroscopy for the characterization of biomolecular structures, a model membrane-bound protein system namely GlpT was chosen. GlpT is a typical member of the major facilitator superfamily (MFS) of transport proteins found in all types of organisms from cyano-bacteria to man Figure 137.

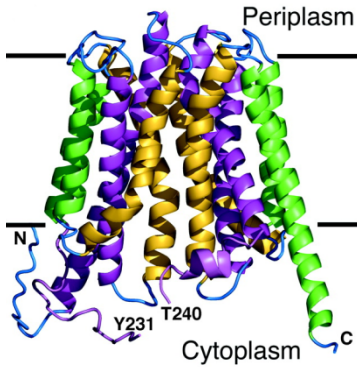

Figure 137 Ribbon representation of GlpT [ref 169]

GlpT transports glycerol-phosphate and phosphate across the inner membrane of *E. coli* in an obligatory exchange-diffusion. This class of membrane-bound proteins, in particular galactose-H^+ membrane-transport protein (GalP) of *Escherichia coli* Figure 138 has been studied extensively by the Henderson group (University of Leeds)[170].

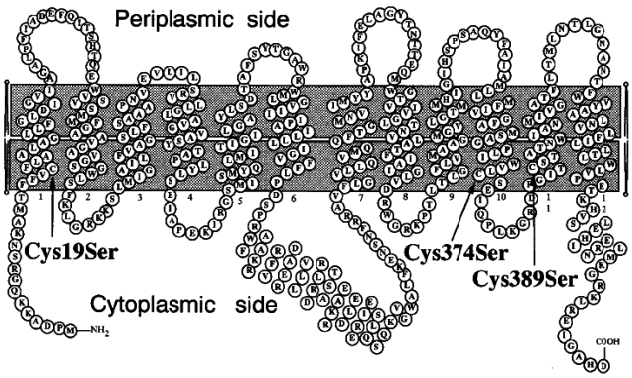

Figure 138 Two dimensional model of the galactose-H^+ symport protein [ref. 170]

This protein is similar in substrate specificity and susceptibility to cytochalasin B and foskolin, to the human GLUT1 sugar transport protein; furthermore, these proteins have about 30% identical amino acid sequence. Transport activities of both GalP and GLUT1 are inhibited by the thiol-group-specific reagent, N-ethylmaleimide Figure 139.

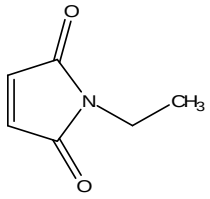

Figure 139 N-ethylmaleimide [ref. 171]

Henderson and co-workers[171] have shown that only the Cys^{374} reacts with *N*-ethylmaleimide. This compound has been used as probe to determinate of the depth of sulphydryl groups within the membranes. Beechey and co-workers[172] have synthesised a series of *N*-polymethylenecarboxymaleimides for use as membrane-impermeant sulphydryl reagents. The position of some of the essential sulphydryl groups of the phosphate-transporter protein of insect flight muscle and rat liver mitochondria have been determined using these compounds. The chain-length and the partition coefficient of *N*-polymethylenecarboxymaleimides are listed in Table 14.

Compound	Partition coefficient	Distance (Aº)
R-CH_2COOH	0.03	5.9
R-$(CH_2)_2$COOH	0.03	7.1
R-$(CH_2)_3$COOH	0.03	8.3
R-$(CH_2)_4$COOH	0.03	9.6
R-$(CH_2)_5$COOH	0.03	10.8
R-$(CH_2)_7$COOH	0.03	13.2

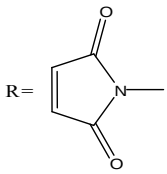

Table 14 Properties of N-polymethylenecarboxymaleimides [ref. 172]

The introduction of extra methylene groups causes an increase in the overall hydrophobicity as measured by the partition coefficient of the compounds between octanol and phosphate buffer (pH 8.0). In order to facilitate attachment of potential cryorelaxors to biological structures new calixarene-maleimide derivatives were prepared and preliminary tests on GalP were carried out. The biological applications of calixarenes have been well documented, thought it has been largely overlooked using several strategies[173]. Several strategies to attach the maleimide groups on the

lower rim have investigated. In this project attempts to use maleimide linked using a long-chain of methylene groups resulted in a complex and inseparable mixture, but performing the coupling reaction between diamino-calixarene and the acyl-chloride of the maleimido-acetic acid under high dilution conditions gave the desired compound in good yield (see section 2.1.8) and after considerable efforts crystals from methanol solution were obtained and the molecular structure was fully resolved (figure 140).

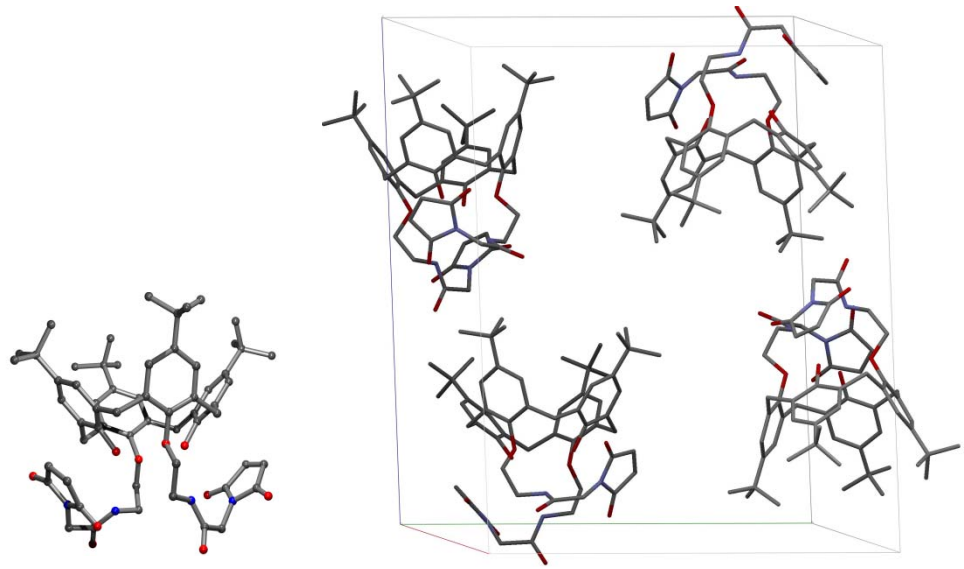

Figure 140 Calixarene-maleimide crystal structure and packing (this work)

This structure has $P2_1/c$ crystal symmetry with intramolecular hydrogen bonds between the hydroxyl protons confirming that this calixarene adopts a *cone* conformation and the maleimide groups curve-up to the lower edge of the cone. This result in the solid state is in accordance with solution state. The cone conformation was reflected in the characteristic AB system for the methylene groups bridging the aromatic rings in the ^{1}H-NMR spectra. Its solubility in different solvents like chloroform, dimethylsulphoxide and particularly in methanol left a good reason to investigate its behaviour in the GalP system.This compound was tested in the biological laboratory of Prof. Henderson for binding to GalP in whole-cell transport measurements, where its reaction with cysteine should have blocked the uptake of [3H]galactose into the cells. The compound was tested alongside positive controls using competition by an alternative substrate, D-glucose, and by blockage of the transport by reaction with *N*-ethylmaleimide. The results are summarised in Fig. 141

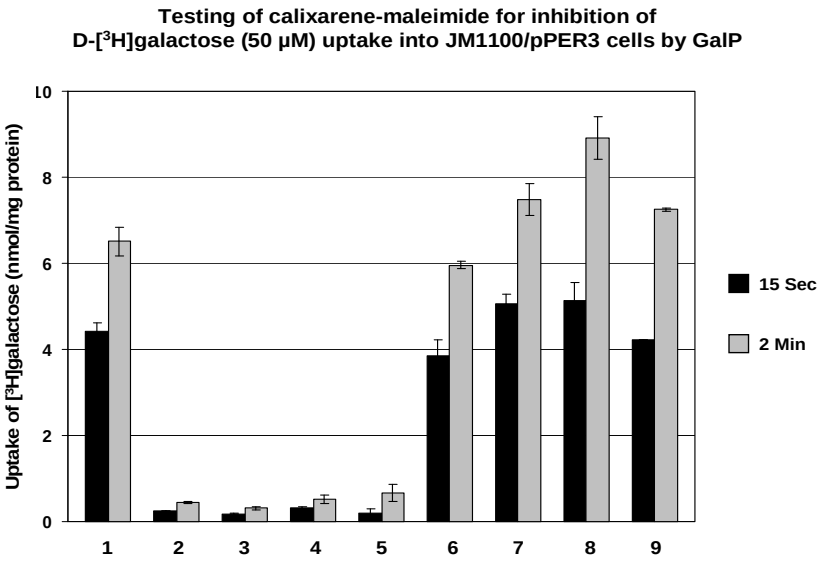

1. Uncompeted (+ 2% DMSO)
2. + 1 mM D-Glucose
3. + 0.4 mM N-ethylmaleimide
4. + 0.2 mM N-ethylmaleimide
5. + 0.1 mM N-ethylmaleimide
6. + 0.4 mM calixarene-maleimide
7. + 0.2 mM calixarene-maleimide
8. + 0.1 mM calixarene-maleimide
9. Uncompeted (+ 2% DMSO)

The cells were pre-incubated with the competing compounds or DMSO for 45 min at room temperature before performing the assay.

All competing compounds were added from a stock solution in 100% DMSO to give a final concentration of 2% DMSO with the cells.

Some of the calixarene-maleimide compound appeared to come out of solution in the cell suspension.

(MW of NEM = 125.1, MW of calixarene-maleimide = 1009.4)

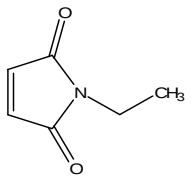

N-Ethylmaleimide (NEM)

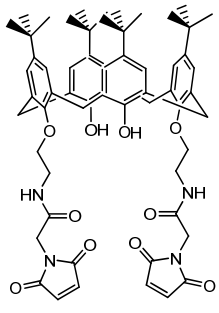

Calixarene-maleimide

Figure 141 N-Ethyl-maleimide and calixarene-maleimide: biological tests and chemical structures (this work)

As shown in the histogram no definitive inhibition of sugar transport was observed in the presence of the calixarene-maleimide compound, although there may be a slight effect at a concentration of 0.4 mM. It therefore appears that the calixarene-maleimide is not reacting with cystein in GalP under these assay conditions.

A possible reason for this is due to the size of the compound itself which may be too large to cross the cell wall or the outer membrane of the cell, so that it does not even reach GalP inthe inner membrane for reaction to take place wherease whilst the smaller *N*-ethylmaleimide is able to do this. Alternatively, if the calixarene-maleimide is able to reach the inner membrane, another possibility for non-reaction is that it is too large to enter the substrate-binding cavity in the protein, and so cannot reach the cysteine. A further issue is the poor solubility of the calixarene-maleimide compound.

2.2.5.2 p-*tert*-butyl-[25,27-bis(maleonylmethylcarbonyl-aminoethoxyethyl)]-26,28-dihydroxycalix[4]arene

In order to increase the solubility of calixarenes functionalized on the lower rim by maleimide groups, a procedure was developed to prepare hydrophilic chains to attach to the lower rim (see section 2.1.9) and the desired compound was obtained in good yield as yellow powder but contaminated with traces of start material Figure 142.

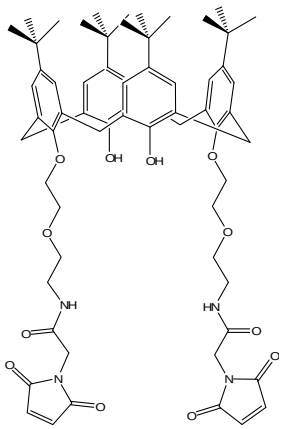

Figure 142 Calixarene-maleimide glycol-chains

All attempts to purify the compound by column chromatography or crystallization failed and no biological tests on this new structure are carried out. Further work is required to purify and to investigate its biochemical properties and to insert by

chemical approach a methyl rotor inside the calixarene cavity (or to suspend it over the cavity). As discussed in previous sections of this thesis, none of the calixarene complexes studied here appear to satisfy the criteria to have a T_1 minimum, or at least a small value of T_1 (~ 1s), at the operational field of the CryoMAS experiments with the exception perhaps of i-pC4/p-xylene (2:1) complex in the quench cooled state. Currently complexes of molecular hydrogen trapped in fullerene cages (see section 3 and 4) appear to display more promise in the context of applications as cryorelaxors.

2.2.5.3 (Maleonyl-methylcarboxy-ethoxyethyl)-fullero-pyrrolidine

In order to attach a maleimide group to a fullerene surface the following synthetic procedure was developed. Starting from *tert*-butyl bromo acetate and using an excess of the (aminoethoxy)-etahnol in presence of triethylamine, *tert*-butylglycine ethylene-glycol was obtained after purification by column chromatography (Scheme 25)

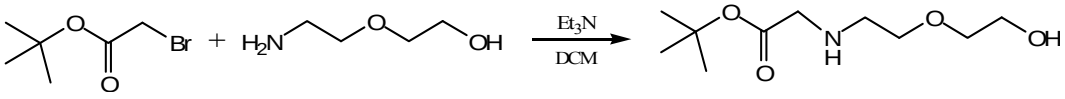

Scheme 25

De-protection of *tert*-butyl group using basic hydrolysis in refluxing conditions with NaOH 1M gave the corresponding glycine ethoxyethanol in high yield (Scheme 26)

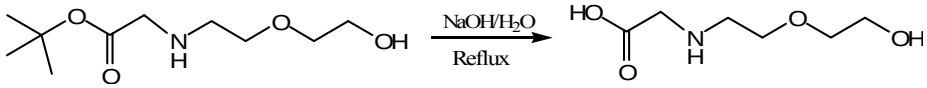

Scheme 26

Following Prato's procedure[174] the fulleropyrrolidine alcohol chain was obtained by 1,3-cicloaddition of the azomethidine ylide (generate by condensation of ethoxyethyl glycine with para-formaldehyde) into fullerene C_{60} in toluene (Scheme 27)

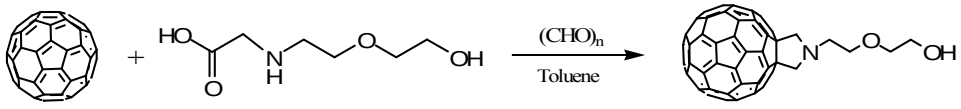

Scheme 27

Subsequent condensation with maleonyl glycine using dicyclohexylcarbodiimide as a coupling reagent as in dry dichloromethane gave, after purification, the fulleropyrrolidine maleimide in good yield and this was characterised by Maldi Tof LD^+, IR and NMR spectroscopy (Scheme 28)

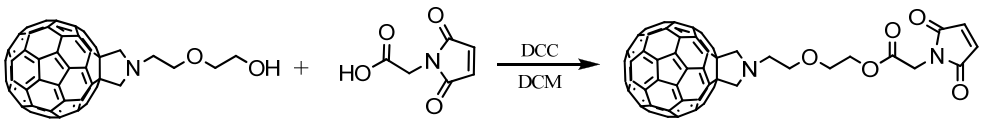

Scheme 28 (Maleonyl-methyl-carboxy-ethoxy-ethyl)-fullero-pyrrolidine synthesis

This new compound could potentially represent a good carrier for delivering the $H_2@C_{60}$ fullerene complex onto protein systems, the maleimide group (**C**) providing a potential anchor to bind the complex to aminoacid thiol groups in the protein chain (**D**), while the glycol chain (**B**) helps to improve its solubility in polar solvents. The $H_2@C_{60}$ complex (**A**) should show cryo-relaxor behaviour its molecular surroundings at very low temperature (Figure 143)

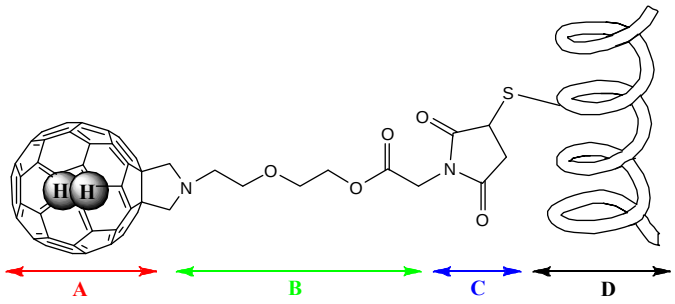

Figure 143 Maleimide-fulleropyrrolidine

Further work is required in order to improve the solubility of this material in polar solvents such as water and explore its biochemical and NMR relaxation properties.

2.3 Endohedral Fullerene C_{60} Synthesis

2.3.1 Endohedral fullerene complexes

Since the fullerenes became available in macroscopic quantities in 1990, an enormous number of studies have been carried out in many fields of science. Of particular interest in the present project is the ability to entrap inside the cage small molecules such as He, Ne, Ar, Kr, Xe[175-176] such complexes being known as endohedral fullerenes. Noble-gas atoms can be inserted into fullerene cages in ca. 0.1% incorporation yield by heating the fullerene powders under forcing conditions (650ºC) under 3000 atmosphere of the noble gas[177-178]. The mechanism for the incorporation of these noble-gas atoms postulated that one or two of the carbon fullerene bounds are cleaved under such extremely high pressure to open a temporary hole on the surfaces which allows the noble gas atoms to enter the fullerene interior[179]. The creation of a large and permanent orifice on the fullerene surface by organic synthesis could provide a great opportunity to introduce ideally any atom or small molecule inside the cage. In order to realize the chemical synthesis of such endohedral fullerenes using this approach, named "molecular surgery", Komatsu and co-workers[177] have established a synthetic route to open an orifice (Figure 144) large enough for a hydrogen molecule to enter the cage, and to then regenerate the original fullerene structure[180-182] with retention of the encapsulated gas (Figure 145) this complex being known as "$H_2@C_{60}$".

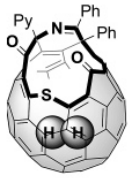

H_2@ATOCF

Figure 144

$H_2@C_{60}$

Figure 145

Levitt and co-workers[11] have demonstrated that in this complex the relaxation of the endohedral hydrogen is very rapid at cryogenic temperatures. Such a structure is therefore a very promising agent for use as a "cryorelaxor", the robust cage protecting the hydrogen molecular rotor from external interference.

2.3.2 Endohedral fullerene synthesis: "The molecular surgery"

In order to synthesize the **H_2@C_{60}** complex (Figure 145) via the open-cage fullerene complex **H_2@ATOCF** (Figure 144) the "Molecular Surgery" approach following Komatsu's procedure has been explored (Scheme 29).

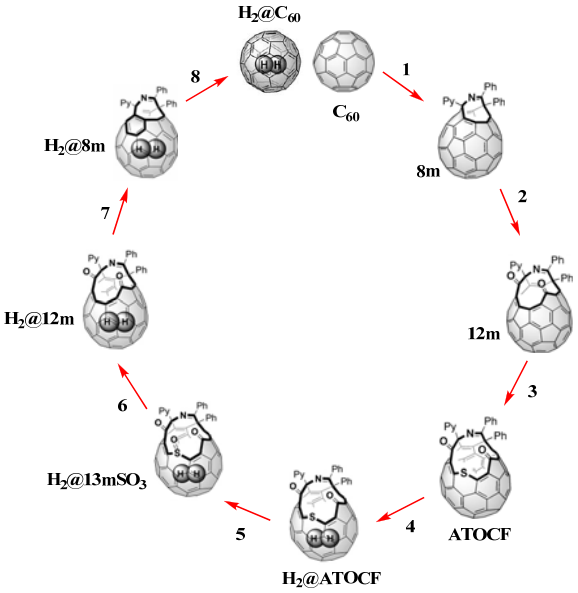

Scheme 29 Synthesis of H_2@C_{60}

Each step has been carefully investigated in a small scale, in order to develop properly the skills required to scale up these reactions. Furthermore in order to clarify ambiguous fragmentations observed by Maldi Tof-LD^+ spectrometry analysis, ESI-MS^+ technique was used for each fullerene derivative (Table 15).

Table 15

Fullerene	Maldi-Tof LD^+	ESI-MS^+
8m 1003m/e	720 [C_{60}], 1003 [M], 1057 [M+Na+MeOH]	1003 [12%M+H]$^+$, 1025 [100% M+Na]$^+$, 1042 [14% M+K]$^+$, 1057 [18% M+Na+MeOH]$^+$
12m 1035m/e	1035 [M], 1057 [M+Na]	1035 [13%M+H]$^+$,1057 [100% M+Na]$^+$, 1074 [40% M+K]$^+$
13mATOCF 1067 m/e	960 [M-Py-C=O], 1067 [M$^{+\cdot}$], 1089 [Na], 1105 [M+K]	1067 [52%M+H]$^+$,1089 [100% M+Na]$^+$, 1105 [16% M+K]$^+$
H_2@ATOCF 1069 m/e	960 [M-py-C=O], 1039 [M-S], 1069 [M$^{+\cdot}$], 1091 [M+Na], 1107 [M+K]	1069 [23%M+H]$^+$, 1091 [100% M+Na]$^+$, 1107 [25% M+K]$^+$
H_2@13mSO_3 1084 m/e	960 [M-py-C=O], 1084[M$^{+\cdot}$], 1107 [M+K]	Too poor solubility
H_2@12m 1037 m/e	1005 [H_2@8m], 1037[M$^{+\cdot}$], 1059[M+Na], 1075 [M+K]	1037 [14%M+H]$^+$, 1059 [100% M+Na]$^+$, 1075 [24% M+K]$^+$
H_2@8m 1005m/e	722 [H_2@C_{60}], 1005 [M$^{+\cdot}$]	1005[100% M+H]$^+$, 1027 [20%M+Na]$^+$
H_2@C_{60} 722 m/e	722 [M$^{+\cdot}$]	Not possible to analyse by ESI-MS

In the first step (**1**, in scheme 30) a thermal cycloaddition reaction was carried out by heating a solution of fullerene C_{60} with one equivalent of 5,6-diphenyl-3-(2-pyridyl)-1,2,4-triazine in o-dichlorobenzene (ODCB) at 180ºC for 17h. The reaction proceeded smoothly to afford one major product, exhibiting a purple colour in solution, together un-reacted C_{60} (ca. 50% recovery) (Scheme 30).

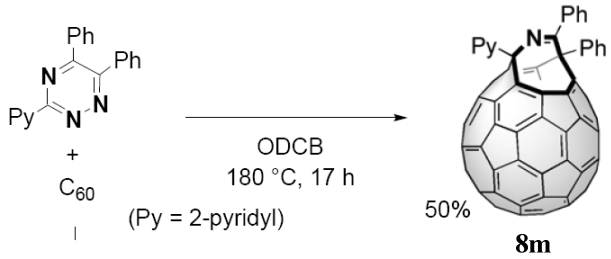

Scheme 30 Synthesis of 8m

The product was highly soluble in organic solvents such as chloroform, toluene, *o*-dichlorobenzene due to the presence of phenyl and pyridyl substituent as reported in the literature[180]. Characterisation of the open-cage 8-membered ring (**8m** see Table 15) fullerene product was based on mass spectral information. Maldi-Tof LD^+ showed the peak at m/e 1003 [M] formed by addition of triazine to C_{60} together with a strong peak at 720 m/e which corresponds with fullerene C_{60}. Further investigation of the same sample by $ESI\text{-}MS^+$ revealed no evidence for the peak corresponding to the empty fullerene C_{60}. This confirms that the laser power used during Maldi-Tof LD^+ technique is able to induce the complete re-closure of the open-cage 8-membered-ring into fullerene.

When a saturated oxygen-solution of **8m** in carbon tetrachloride (step **2**) was irradiated with visible light using a high-pressure Hg-lamp overnight at room temperature, the colour turned from purple to brown. Separation of the reaction product using flash column chromatography afforded two photo-oxidation isomeric products which were characterised by Maldi-Tof LD^+ as m/e 1035 and $ESI\text{-}MS^+$ (Scheme 31).

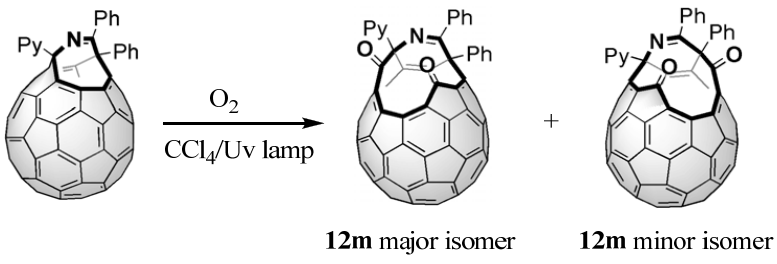

Scheme 31 Synthesis of endohedral fullerene 12m isomers

These two oxidation products major and minor isomers (Scheme 32) are produced by the reaction of **8m** with photochemically generated singlet oxygen. Komatsu and co-workers[180] have shown that the 12-membered-ring orifice (**12m**) is rather small allow introduction of even a small atom based on the results of theoretical calculations. In order to further enlarge the 12-memember-ring orifice (**12m** major isomer**)**, the Toda reaction[183] was used to insert a sulphur atom into an activated C-C single bond on the orifice (step **3**). As described in the literature refluxing conditions, and presence of base such as tetrakis-(dimethylamino)ethylene (TDAE 1 equiv) is required to activate the C-C single bond[181-182]. In this reaction, TDAE, a typical π-electron donor, is supposed to activate **12m** either by one-electron transfer or by complexation. However we have found that a slight excess of base and prolonged refluxing conditions produce a significant improvement in the yield (87%) (Scheme 32).

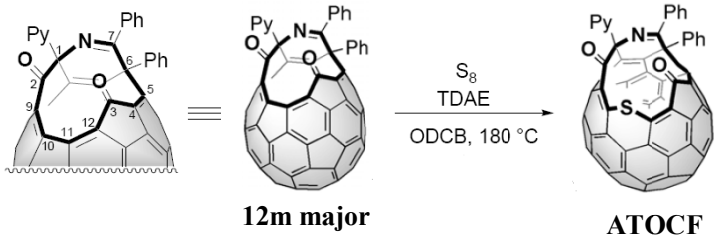

Scheme 32 Synthesis of ATOCF

The open-cage fullerene **ATOCF** (aza-thio-open-cage-fullerene) has been fully characterised using Maldi-TOF LD^+ (m/e 1067), ESI-MS^+ and IR spectroscopy. A strong peak at 960 m/e was found due the laser power of Maldi-TOF LD^+ technique inducing the extrusion of pyridine ring and the two carbonyl groups, but no evidence for that peak was founded by ES-MS^+. Rubin and co-workers[184] succeeded in introducing a helium atom (475 atm, 288-305 ºC, 7.5h) and hydrogen molecule (100 atm, 400 ºC, 48h) into a open-cage fullerene derivative **B** (Scheme 33)

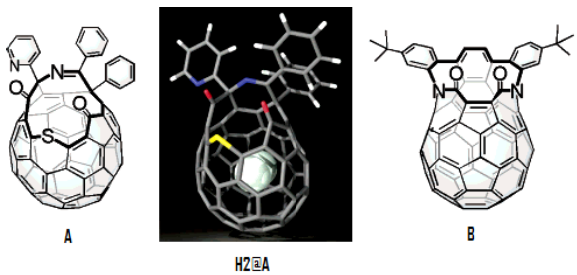

Scheme 33 open-cage fullerenes [ref 180]

However, this compound is somewhat unstable at such temperatures, and about 30% of **B** decomposed during the insertion of the molecular hydrogen. Thus, in order to achieve 100% encapsulation of these gaseous molecules, it is necessary to synthesize an open-cage fullerene derivative having a larger orifice with sufficient thermal stability. Compound **ATOCF** has an orifice, the diameter of which is 5.64 Å along the long axis and 3.75 Å along the short axis (Figure 146), and is thermally stable up to 250 ºC. Calculated activation barriers for insertion and escape have been carried out[185]. The activation energies (Figure 147) required for the insertion of He, Ne, H_2 and Ar into A were calculated to be 19.0, 26.2, 30.1 and 97.8 kCal mol^{-1}, respectively. These values are considerable lower than the corresponding energies calculated for **B** (2.45, 40.6, 41.4, 136.3 Kcal mol^{-1}) indicating that insertion of atoms or molecule such as He, Ne, and H_2 in **A** is quite feasible.

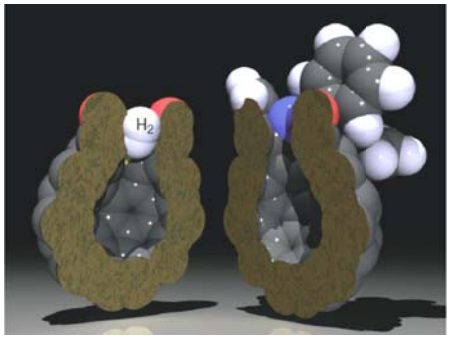

Figure 146 Cut-out view of open-cage fullerene cavity [ref 186]

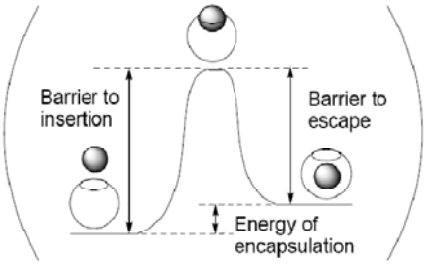

Figure 147 energy barrier insertion [ref 185]

The encapsulation following the Komatsu's procedure of hydrogen into **A** was attempted by treatment of a powder of **A** with a high pressure of hydrogen gas (800 bar) at 200 ºC in a special autoclave made for this project (Figure 148).

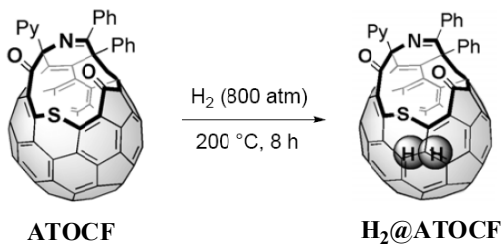

ATOCF **H_2@ATOCF**

Scheme 34 ATOCF hydrogen insertion

Figure 148 Autoclave for hydrogen insertion [ref 187]

After 8h, formation of the endohedral complex H_2@**A** without decomposition of **A** was confirmed by Maldi-Tof LD^+ and NMR spectroscopy as described from the literature[180]. The Maldi-Tof LD^+ mass analysis showed the molecular ion peak of **H_2@ATOCF** (m/e 1069) was clearly observed, along with a peak for the empty cage **ATOCF** (m/e 1067) formed by release of the hydrogen molecule upon laser irradiation. The ^{1}H-NMR spectrum of the resulting material showed a new sharp signal at very high field (δ -7.25 ppm) as previously reported in addition to the signals for aromatic protons appearing with exactly the same chemical shifts as those for **A** itself. This additional signal is assigned to the resonance of the incorporated molecular hydrogen, which is subjected to strong shielding by the fullerene cage. The encapsulation rate was highly dependent on the pressure of hydrogen gas: the yield of **H_2@ATOCF** was 90% under 560 atm and 51% under 180 atm of H_2, with all other conditions kept the same[188]. In order to reduce the size of the orifice to produce H_2@C_{60} without loss of the encapsulated hydrogen oxidation of the sulphide unit (step **5**) of the **H_2@ATOCF** by *m*-choroperbenzoic acid (m-CPBA) is required to make the sulphur atom readily removable (Scheme 35).

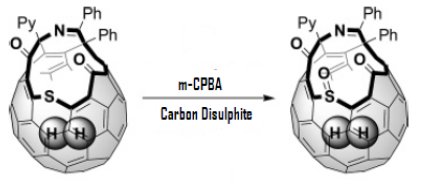

H_2@ATOCF **H_2@13mSO$_3$**

Scheme 35 Synthesis of H_2@13mSO$_3$

Attempts to follow the literature procedure by using of toluene as solvent failed, but the oxidation reaction, in carbon disulphide under argon atmosphere, proceeded at room temperature smoothly to give the corresponding sulfoxide **H_2@13mATOCF** in quantitative yield after simple filtration through silica gel. After MS investigation due the extremely poor solubility in organic solvents, the compound was identified by Maldi-Tof LD^+ technique as molecular peak at m/e 1084 (M^+) with series of other different peaks m/e 1069, m/e 960 and m/e 1107. These different fragmentations were explained as follows. The peak at m/e 1084 corresponds to sulfoxide open cage structure; while the peak at m/e 1069 is derived by decomposition of the sulfoxide group of the open cage during the laser irradiation as reported by McCabe and co-workers[189-190] and the m/e 960 as results of extrusion of pyridine ring with the two

carbonyl groups. No evidence of crystal structure was reported in the literature for this compound, so attempted to prepare suitable crystal for X-ray investigation were attemped. By slow evaporation of a saturated solution of the **H_2@13mSO_3** in toluene brown crystals were obtained and fully resolved by X-Ray structural analysis (Figure 149 on the right).

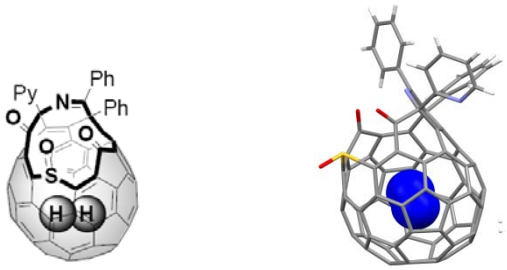

H_2@13mSO_3 **H_2@13mSO_3 crystal structure**

Figure 149 Crystal structure of open-cage H_2@13mSO_3 (from this work)

The sulfoxide group was found to point out from the rim of the cage (exo) as predicted by Komatsu et al[182]. Furthermore larger distance between the two carbonyl groups was found when compare, with the **H_2@ATOCF**. This new crystal structure (as yet un-published) represents a valuable opportunity to gain further insight into the physical behaviour of hydrogen inside the cage. Full details of the data collection and solution can be found in Appendix A. In order to chemically remove the SO unit the literature procedure was initially explored by irradiation of a toluene solution, but there was practically no reaction because of the poor solubility of the open cage **H_2@13mSO_3**. In contrast, simple irradiation of a solution of **H_2@13mSO_3** in benzene/ethyl acetate 20:1 with visible light trough a Pyrex glass flask by use of a high pressure xenon-Hg lamp, afforded to desired product H_2@12m in 26% yield (Scheme 36) together with recovery of un-reacted **H_2@13mSO_3** (10%) (Scheme 36).

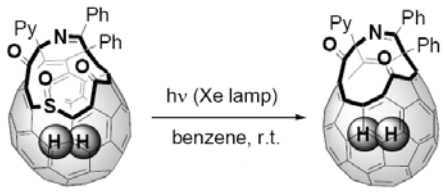

H_2@13mSO_3 **H_2@12m**

Scheme 36 Synthesis of H_2@12m

The structure **H_2@12m** was confirmed by Maldi-Tof LD^+ analysis showing m/e 1037 and m/e 1005 corresponded to H_2@8m due the re-closure by laser irradiation. Again

no evidence of that peak was founded by ES-MS$^+$. To produce **H_2@C_{60}**, further reduction of the orifice size is required. For this purpose the Mc-Murry reaction[191-193] for reductive coupling of the two carbonyl groups around the orifice of **H_2@12m** is used. This leads to the formation of the open-cage fullerene derivative **H_2@8m** which has an eight-membered-ring orifice, a process which was optimised after extensive investigation at 89% yield (Scheme 37).

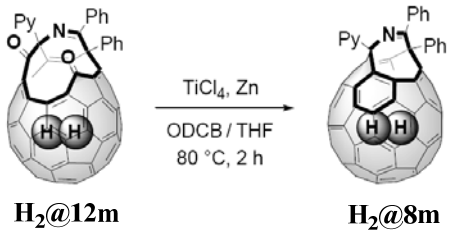

H_2@12m **H_2@8m**

Scheme 37 Synthesis of H_2@8m

The high efficiency of this reaction is quite reasonable since the carbonyl groups of H_2@12m are fixed in a parallel orientation and in a close proximity. The structure was confirmed by Maldi-Tof LD$^+$ with a peak at m/e 1005. There was also a peak at m/e 722 which corresponds to H_2@C_{60} due the re-closure of the cage by laser irradiation. No evidence for that peak was found using ESI-MS$^+$ which showed m/e 1005 and m/e 1027 (M+Na). The final step to completely reclose the orifice was accomplished by heating the H_2@8m in a vacuum-sealed glass tube placed in an electric furnace at 400ºC for 3h (Scheme 38).

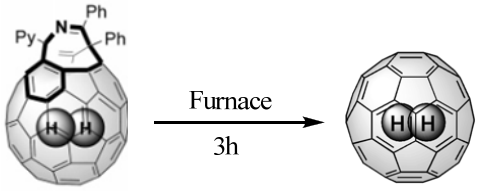

H_2@8m **H_2@C_{60}**

Scheme 38 Synthesis of H_2@C_{60}

The resulting black material completely dissolved in carbon disulfite and was analyzed by HPLC on a Cosmosil Buckyprep column eluted with toluene (two directly connected columns). After 20 recycles, H_2@C_{60} was completely separated as confirmed by Maldi-Tof LD$^+$, IR and TLC. The adsorption mechanism of the Buckyprep column is based on a π-π interaction with the pyrenyl groups in the stationary phase[194-195]. Therefore, a very weak but appreciable van der Waals

interaction must be operating between the inner hydrogen molecule and the π-electron cloud of outer C_{60}, and this must have contributed to this separation.

3 Endohedral fullerenes C_{60} derivatives

A number of the endohedral H_2 fullerene intermediates prepared in this work have been studied by several techniques[196-197]. T_1 measurements were carried out from our group; Inelastic Neutron Scattering were provided in collaboration with Prof. Horsewill and Infrared Spectrum from our group.

3.1 The behaviour of hydrogen confined in fullerene cage derivatives

The properties of these trapped hydrogen complexes have a great interest for several reasons: a) confined hydrogen is a good potential candidate for a cryorelaxor; b) study of the behaviour of hydrogen as a quantum rotor encapsulated in fullerene cages of different size and symmetry is itself theoretically interesting; c) an understanding of how the cage symmetry and the size affect the T_1 relaxation of H_2 will help in the development of new cryorelaxors: d) it is also interest to understand how the cage symmetry and the cage size affect other observables (e.g. ^1H and ^{13}C line-shape, dipole-dipole interactions). Several solid-state NMR studies of endohedral H_2-fullerene complexes, including ^1H and ^{13}C spin relaxation studies, have been carried out in collaboration with various members of the Cryo-MAS consortium. These studies have involved three different endohedral H_2-fullerene complexes, studied over a wide range of temperatures and applied magnetic fields.

I = H_2@13m **II = H_2@C_{60}** **III = H_2@mal**

Scheme 39 Endohedral fullerenes derivatives [ref 182]

The effect of the size and symmetry of the cage on some NMR properties are exemplified in Figure 150, where the intramolecular ^1H-^1H dipole-dipole coupling as a fuction of temperature for H_2 is plotted for the three samples. The details of these experiments are beyond the scope of this thesis. For a perfect isotropic rotation the intramolecular dipole-dipole coupling within the H_2 molecule is expected to vanish

exactly. As symmetry of the environment is lowered, the dipolar coupling smoothly increases.

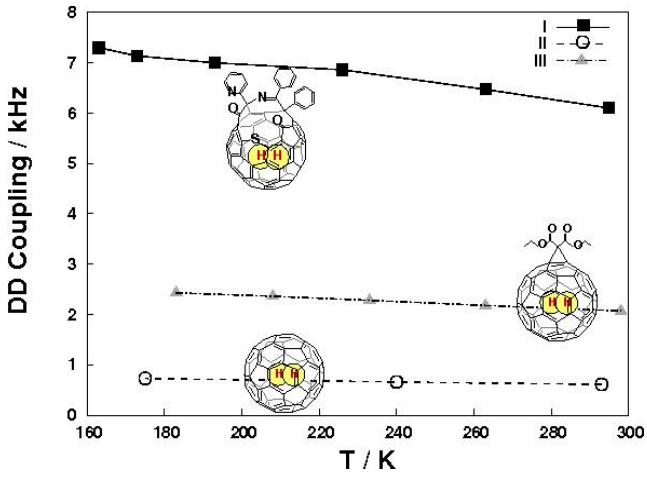

Fig 150 Plot of the dipole-dipole 1H-1H couplings with respect to temperature for sample I-III.

As for the dipolar interaction, also the spin-lattice relaxation time constants T_1 appears to smootly change with the size and shape of the environment. The T_1 data as a function of the temperature for the compounds **I-III** displayed intriguing behaviour (Figure 151).

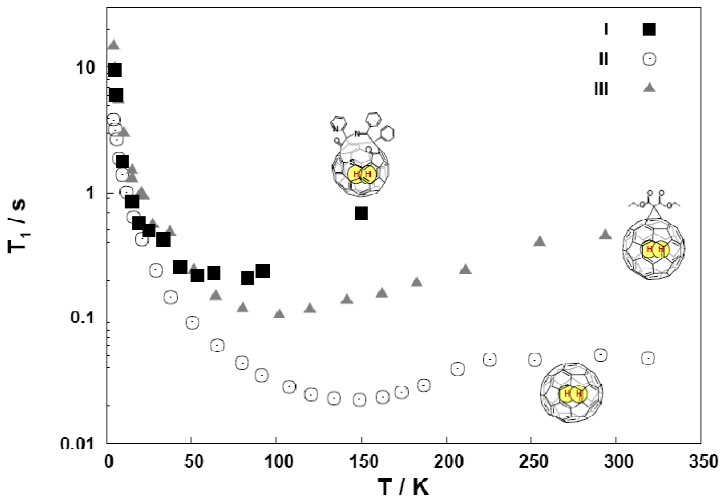

Figure 151 T_1 measurement of endohedral fullerene derivatives performed under static conditions, at 8.5 T, using a 2.5 mm single channel static probe with an horizontal coil. The samples were placed in 2.5 mm pyrex tube (not sealed)

The T1 data in Fig. 151 were recorded under static conditions, hence they are a weighted average of the T1 of the endohedral and exohedral protons, which equilibrate with each other through, spin diffusion. This leads to overall T1 values which are longer for **I** than for **III** and **II** respectively, to reflect the larger number of

exohedral hydrogen atoms. T1 measurements on spinning samples indicate that the intrinsic T1 value for H_2 in these systems is typically of the order of ten of milliseconds[198].

The spin-lattice relaxation time constant for the sample with lowest symmetry, **I** has broad minimum at a temperature of around 60-70 K. Sample **III** and sample **II** have respectively their T1 minima near 100 K and 150 K. The results of these three compounds suggest a correlation between the symmetry of the cage and the temperature of the T1 minima. In particular reducing the symmetry of the cavity leads to a shift in the T1 minimum towards higher temperatures. A complete theory that fully describes this behaviour is currently under development. Nevertheless, this important observation will guide the future design of the complex with T1 minima at temperatures lower that 50 K.

3.2 Quantum rotation of endohedral hydrogen confined within a fullerene cage

Inelastic Neutron Scattering (INS) studies of the H_2@ATOCF were carried out in collaboration with Prof A. J. Horsewill (University of Nottingham) (Figure 152).

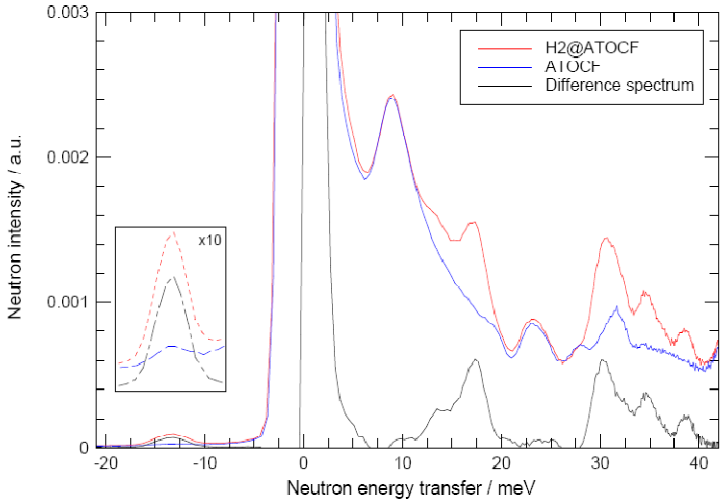

Figure 152 INS of H_2@ATOCF (in red), empty cage ATOCF (in blue) and difference spectrum (in black) from this work

In ATOCF the presence of the orifice causes the spherical symmetry of the fullerene cage to be broken. The cavity can be approximated as a scalene ellipsoid. For the proposes of analysis it is useful to approximate the ellipsoidal cavity to a spherical box. Scaling of the ATOCF spectra was necessary because of the larger mass of

sample available (510mg, compared to 492mg of H_2@ATOCF). In order to isolate the INS spectrum of the endohedral hydrogen molecule it is necessary to remove any contributions arising from the scattering from exohedral hydrogen atoms (the protons attached to the aromatic groups at the orifice). This was achieved by acquiring a spectrum from a sample of ATOCF with an unoccupied cavity (empty cage), and subtracting this from the spectrum of H_2@ATOCF. Figure 152 shows the spectra collected at T=2.5K, (neutron wavelength 1.24Å). The energy axis shows the neutron energy transferred to the sample [where energy > 0 corresponds to neutron energy lost and energy < 0 corresponds to neutron energy gained]. The peak at -13.3meV can immediately be indentified as ortho-para transition ($J = 1 \rightarrow 0$) of the endohedral hydrogen. At 2.5K the only possible excited state that may impart energy to a neutron is the population of the ortho-hydrogen. An equivalent peak is observed at +13.3meV, corresponding to the $J = 0 \rightarrow 1$ transition. In H_2 gas this transition is expected to be at 14.8meV. The difference suggests that the rotation of the endohedral hydrogen molecule is coupled to other degrees of freedom. In the present work INS behaviour for the H_2@C_{60} complex has not been investigated because of the tricky procedure of scale-up, but it would be very interesting to explore the physical behaviour of the hydrogen confined inside symmetrical fullerene C_{60} cage.

3.3 Infrared spectroscopy of an endohedral hydrogen-fullerene complex

The dynamics of the hydrogen confined in cages of fullerene C_{60} was also studied by solid state IR spectroscopy in our group and the observed spectra were compared with previous studies of the endohedral fullerene complex (Figure 153).

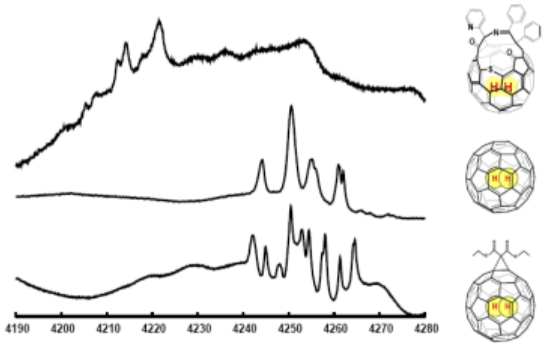

Figure 153 Infrared spectrum on different endohedral fullerene complexes [from this work]

The features and complexity of the spectra reflect the different degree of symmetry of the potential experienced by the constrained H_2 molecule in the different cage architecture. In general, isolated homonuclear diatomics (H_2) have no infrared activity [199]. However, H_2 does diplay IR activity in situations where there are intermolecular interactions present, such as in the solid and liquid phase[200,201], in contrained environments[202-205], and in pressurized gases[206,207]. IR spectra of such systems are usually broad due to inhomogeneities in the system the result of random collisions. As an exception, narrow lines are observed in semiconductor crystals[208] and solid hydrogen[209]. Similarly we expected narrow lines in the solid $H_2@C_{60}$, where the broadening of IR lines is suppressed by homogeneous distribution of trapping potentials provided by C_{60} molecules and by van der Waals interactions between the molecules. The low temperature IR absorbtion peaks of $H_2@C_{60}$ are located in four narrow a spectral bands between 4060 and 4810 cm^{-1} as shown in Figure 154.

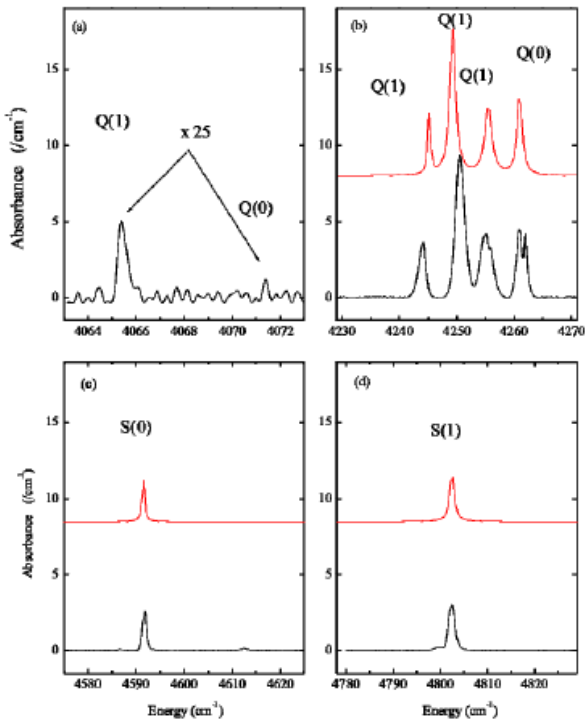

Figure 154 IR absorbtion spectra of $H_2@C_{60}$ at 6K (black) and the best fit theoretical spectrum (red) from this work

Peaks at around 4250, 4600 and 4800 cm^{-1} (Figures 154b-d) are assigned to vibrational excitations of H_2 accompained by translation and/or rotational excitation. It is the translation-rotation coupling that splits the Q(1) line into three peaks. Weak transitions around 4070 cm^{-1} (Figure 154a) represent pure vibrational excitations of the H_2 molecule

3.4. Overview of results

In this project several calixarene complexes have been prepared and their behaviour has been analysed by NMR-relaxometry techniques used for studying molecular motion in organic complexes. These experiments have clearly demonstrated that, at cryogenic temperatures, the spin-lattice relaxation of protons within this class of complexes is affected their by thermal history. Proton T_1 values measured in samples that are cooled quickly from room temperature are consistently shorter than T_1 values measured in slowly cooled samples. The difference has been attributed to the level of structural disorder present in the sample. Presumably, quick cooling "*freezes-in*" metastable configurations of the lattice, which gives rise to highly mobile, unhindered molecular species. The target operational temperature for CryoMAS, limited by the technical challenges associated with stable rotation of the sample rotor, is around 20K. It is desirable for a cryorelaxor to have a T_1 minimum, or at least a small value of T_1 (~ 1s), at this temperature and at the operational field of the CryoMAS experiments.

None of calixarene complexes studied here appear to satisfy these criteria with the exception perhaps of p-xylene (2:1) complex in the quench cooled state. Currently complexes of molecular hydrogen trapped in fullerene cages appear to display more promise in the context of applications as cryorelaxors.

4 Conclusion and further work

The work of this thesis has focussed on two approaches to develop Cryorelaxors for low temperature solid-state NMR applications.

The first approach has explored the dynamic behaviour of a number of calixarene host-guest complexes. These have been structurally characterised and eleven calixarene complexes have been studied in order to determine their suitability as cryorelaxors in cryo-MAS NMR. Field-cycling NMR has been used to study the rotational motion of methyl-groups in the complexes involving p-xylene, toluene, and 4-picoline, as guest molecules. Measurements of the T_1 relaxation have revealed the presence of crystallographically inequivalent methyl groups in these samples. The rotational potential barriers determined by NMR measurements agree very well with those obtained from INS spectra for samples 4-picoline and p-xylene. Measurement of the temperature dependence of T_1 at range of field strengths has revealed the existence of an additional motional process that contributes to the proton spin-lattice relaxation at low temperatures. Further work is required in order to characterise this motion, and identify its origins. Further work will also be required in order to gain better understanding of the thermal history effects observed in the calixarene samples. The work here suggests that the disorder of the molecular crystal is a very important factor for the proton spin-lattice relaxation at cryogenic temperatures. However, preliminary INS measurements on sample p-xylene sample suggest that the efficient relaxation in quench cooled samples is not solely caused by methyl groups with a distribution of hindering barriers, as was originally hypothesized. In the complexes studied, the methyl-groups of the guest molecules remain mobile at cryogenic temperature due to quantum tunnelling.

The second approach involved an investigation of the synthesis of endohedral C_{60} complexes of H_2, following the procedures of Komatsu, and also a study of approaches to attach to them surface groups in order to design a method to attach the C_{60} moiety to biological samples. In order to explore potential anchoring of the cryorelaxors, calixarenes and fullerene moieties bearing maleimide groups have been prepared. Further work is required to explore the binding of cryorelaxor complex to larger molecules, in order to evaluate their potential applications as NMR enhancement agents. However, the present study has shown that despite the existence

of freely rotating methyl-groups in some of the calixarene samples, the proton T_1 values at low temperatures are too long, by at least an order of magnitude, for these complexes to be used practically as cryorelaxors. Deuteration of the host molecule has been shown to increase the efficiency of proton relaxation and reduce T_1, however the reduction is small. Molecular hydrogen confined to the cavity of aza-thia-open-cage fullerene has proved to be a very interesting model system for studying quantum dynamics, as demonstrated by a range of high profile publications using NMR, INS and IR. The INS investigations described in this thesis have clearly demonstrated the feasibility of studying samples of relatively low mass and limited availability. It is hoped that this investigation will be the first in a line of studies on similar systems, including HD@ATOCF and H_2 confined in the spherical cavity of C_{60} ($H_2@C_{60}$). The endohedral H_2 fullerene complexes have very short T1 in a wide temperature range; hence they are potentially very promising as cryorelaxors. Their role as cryorelaxors will be addressed in future studies.

5 Experimental

5.1 Procedures and equipment summary

Methods for purification of reagents and solvents

Commercial compounds were purchased from Acros, Avocado, Fluka, Lancaster or Sigma-Aldrich; unless otherwise stated all materials were reagent grade and used without further purification. When necessary solvents and reagents were purified and dried according to known literature procedures and whenever possible solvents were freshly distilled immediately before use:

- dichloromethane (DCM) was dried over calcium hydride and distilled at 40ºC
- chloroform ($CHCl_3$) was dried over calcium hydride and distilled at 61ºC
- acetonitrile (MeCN) was dried over activated 4Å molecular sieves, and was freshly decanted before use.
- diethyl ether (Et_2O) was dried over sodium wire and was freshly decanted
- ethanol (EtOH) was dried over calcium sulphate and distilled at 78ºC
- methanol (MeOH) was dried over calcium sulphate and distilled at 65ºC
- *o*-diclorobenzene was dried over calcium hydride and distilled under vacuum
- tetrahydrofuran (THF) was dried over sodium wire with benzophenone indicator and distilled at 65ºC
- toluene was dried over calcium hydride and distilled at 111ºC

Characterisation methods

- **Melting points** were measured on an Electro-thermal melting point apparatus and are uncorrected.
- **IR spectra** were obtained using a Golden Gate Attenuated Total Reflection (ATR) sampling attachment on a Mattson Satellite 3000 FTIR spectrometer.
- **^{1}H, and ^{13}C NMR** solution spectra were recorded on a Bruker 600 and 300 spectrometer at 600, 300 and 75 MHz respectively.

- ^{1}H NMR data is displayed in the following manner (<integral coefficient> H, <multiplicity>, J= <coupling constant>, **H** <**inference**>)
- Multiplicities are quoted as **s**-singlet, **d**-doublet, **t**-triplet, **q**-quartet, **qu**-quintet, **sx**-sextet, sp-septet, **o**-octet, **n**-nontet, **m**-multiplet, etc.; coupling constants (J) are quoted in Hz.
- **All ^{1}H-NMR spectrum were calibrated at 7.26 ppm ($CDCl_3$) and for ^{13}C-NMR at 77.00 ppm ($CDCl_3$)**

- **^{13}C-CP/MAS NMR** solution spectra were recorded on a Bruker AM600 spectrometer at 400.13MHz respectively
- **Elemental analysis** of the calixarens samples resulted in *C* values 2% to 7% lower than the calculated values (see Boehmer, V.; Jung, K.; Schoen, M.; Wolff, A. *J.Org. Chem.***1992**, 57, 790-792)
- **Electrospray mass spectra** were recorded on a Micromass Platform II single quadrapole mass spectrometer.
  - The instrument is calibrated with a mixture of sodium and caesium iodide, the operating conditions were capillary 3.50kV, HV lens 0.5kV, cone voltage 20V, source temperature 110ºC, ES eluent: 100% acetocyano at 100µl min^{-1}, nitrogen drying gas 3001h^{-1} and nebulising gas 201h^{-1}
  - 10µl injections of c.a. 1-10 µl ml^{-1} solutions were made using a Hewlett-Packard HP1050 auto-sampler.
  - Negative ion data were recorded under identical conditions except for different polarity voltages and capillary voltages of 3.0 kV.
- **Single Crystal X-ray structural analyses** were made using a Nonius Kappa CCD diffractometer and Nonius FR591 rotating anode X-ray generator.
  - The data was processed using the *Collect*, *HKL* and *maXus* software

- Structures were solved using *SIR* and/or *SHELX* in the *WinGX* suite of programs.
- Crystals were analysed using Mercury and Crystal explorer.

- **Field Cycling NMR** analysis were obtained from Prof. Horsewill School of Physics and Astrophysics in Nottingham

Crystallographic data

These compounds (calixarene complexes) often form a beautiful prismatic crystals but this outward perfection often masks internal crystallographic disorder of both the host and guest. In many cases diffraction is only observed at low theta values and is accompanied by areas of diffuse scattering. This makes interpretation for the crystallographer of the structure problematic; in some cases it's only possible to indentify the gross structure and connectivity and observed that there is a disordered molecule in the cavity. The Cambridge database reveals that these types of structures have R values commonly within the range 3-12% but with a significant number above 18%. An electronic copy of the relevant crystallographic data for all the compounds structurally investigated within this study may be found upon the compact disc included with this document and in the appendix. This data includes: cif files, tables of fractional atomic co-ordinates; selected inter-atomic distances, bond and torsion angles.

6:1 Synthetic methods and characterisation

p-*tert*-Butylcalix[4]arene (1:1) Toluene complex

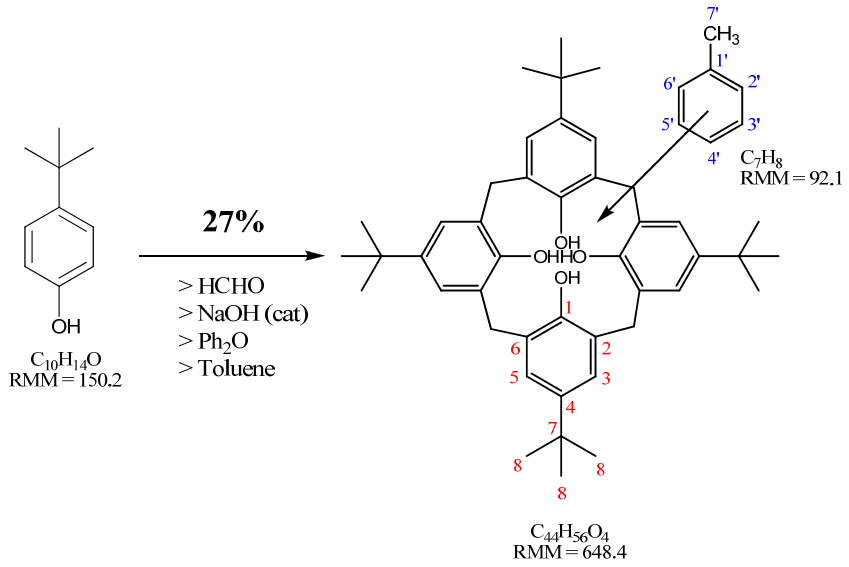

To a 3-necked flask of 500mL were added (10g, 0.066mol) of p-*tert*-butylphenol, (6.2 mL, 0.0830mol) of formaldehyde 37% and (96mg, 0.0024mol) of sodium hydroxide corresponding at 0.036 equivalent of base, stirred slowly for 20 min at room temperature to obtain a partial dissolution of the p-*tert*-butyl phenol. Then it was heating at 120 °C for 2h to give after 30 min a homogeneous solution light yellow and in the end a viscous mass yellow. When the magnetic stirrer was stopped, this condition were maintained for other 1h to gave in the end after cooled at room temperature a friable solid yellow thick mass “the precursor”. It was broken in small pieces, then under nitrogen diphenyl ether was added and heated at 120 °C with a condenser. During this time the precursor went in solution after ca. 10 min and when it was completely dissolved the condenser was removal. In this phase the nitrogen flow was increase to remove the water trapped in the precursor grid. A yellow turbid solution was obtained in ca. 2 min and these conditions were maintained for ca. 15 min. The solution was carried at 150-160 °C an after ca. 2 min a precipitate started to form. This step was very critical because must favour the cyclic octamer formation and for this conditions it was need ca. 10 min during which the precipitate increase was observed. The mixture was carried at 180 °C to give much foam

and in the end at reflux temperature ca. 260 °C for 2h under a gentle flow of nitrogen with a condenser. This temperature was very important because in this phase the cyclic octamer was transformed in cyclic tetramer observable through a colour and chemical physical changed of the solution from turbid at clean brown. The reaction mixtures remained clear at the reflux temperature, and only upon cooling does precipitate once again appear. (Those two final parameters are very important, because if the temperature conditions are insufficiently strenuous or too rapid a flow of nitrogen the cyclic octamer can be reported as the major product). The reaction solution was cooled to room temperature, treated with 150mL of ethyl acetate, stirred for 30 min and allowed to stand for 30 min to obtain a white precipitate at the bottom of the flask. Filtration of yields material which was washed twice with 10mL of ethyl acetate, once with 20mL of acetic acid and 10mL of water to yield after dried (5.01g 47%) of crude compound as white powder. TLC *Rf* = 0.65 (Petrol/Dichlorometane 1:1). This material was treated with 90 mL of boiling toluene and filtered at hot to give after cooling to room temperature for 48h and filtration on buchner funnel, (3.34g 27%) of product as glistening white plates, corresponding to 1:1 complex with toluene.

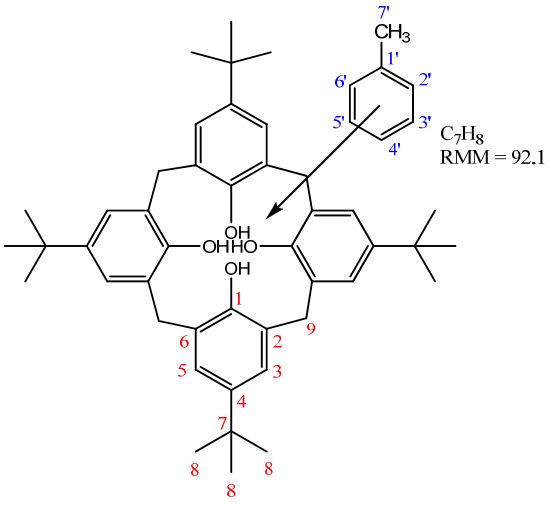

$C_{44}H_{56}O_4$
RMM = 648.4

XRD (single crystal)**:** 2006Sot0765

MP: > 300ºC (reported: > 344-346ºC)[102]

MS/ES$^-$ (M/Z): 647.8 [100% M-H]$^-$

Elemental Analysis: Attempts to have satisfactory elemental analysis failed.

^{1}H NMR ($CDCl_3$)**:** 10.33 (1H, s, **OH**), 7.28-7.15 (6H, m, **Ar guest** + **$CDCl_3$**), 7.05 (2H, s, **H3, H5**), 4.25 (1H, d, J=13.2, **H9**), 3.51 (1H, d, J=13.2, **H9**), 2.36 (3H, s, **H7'**), 1.21 (9H, s, **H8**)

^{13}CP-MAS NMR: 146.6 (**C1**), 144.5 (**C4**), 138.9 (**C1'**), 129.4 (**C6**), 128.5 (**C2**, **C2'**, **C6'**) 127.5 (**C5'**, **C3'**), 125.9 (**C5**), 125.3 (**C3**), 124.2 (**C4'**), 34.5 (**C7**), 32.0 (**C8**), 30.4 (**C9**), 15.4 (**C7'**) **{21.5 CH_3 free Toluene}**

FTIR ν_{max} (cm^{-1})**:** 3163 (stretch **OH**), 2951-2866 (stretch **CH**), 1200 (stretch **C-O**)
(solid state, selected)

p-*tert*-Butylcalix[4]arene (1:1) 4-Picoline complex

To a solution of 60mL of 4-picoline heated at ca. 100 °C in a 3-necked flask of 150mL were added (5.28g, 0.033mol) of p-*tert*-butyl-calix[4]arene in a small portions until completely dissolution. The content of the flask was filtered hot to give after cooling at room temperature for and filtration, (3.62g, 29%) of white glistening crystals.

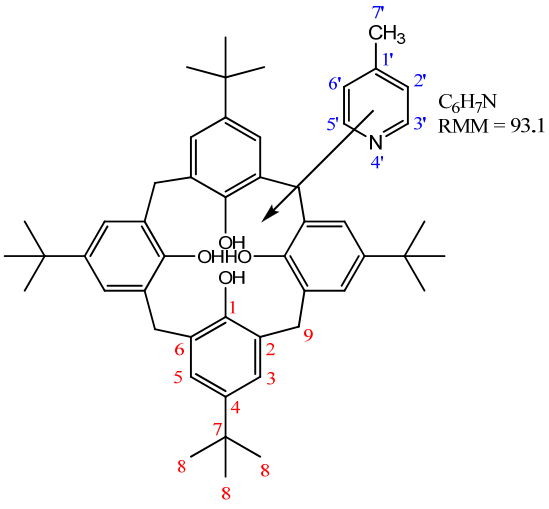

$C_{44}H_{56}O_4$
RMM = 648.4

XRD (single crystal)**:** 2006Sot0589

MP: > 300ºC

Anal. Calcd. for $C_{44}H_{56}O_4 + C_7H_7N$: C 80.93, H 8.56, N 1.89, Found: C80.76, H 8.60, N 1.55.

^{1}H NMR ($CDCl_3$)**:** 10.33 (1H, s, **OH**), 8.58 (2H, d, J=7.6), 7.62 (2H, d, **H5**), 7.05 (2H, s, **H3**, **H5**), 4.25 (1H, d, J=13.2, **H9**), 3.49 (1H, d, J= 13.2, **H9**), 2.64 (3H, s, **H7'**), 1.21 (9H, s, **H8**)

^{13}CP-MAS NMR: 148.5 (**C1**), 146.7 (**C4**), 144.6 (**C1'**), 129.4 (**C6**), 128.4 (**C2**, **C2'**, **C6'**) 126.0 (**C5'**, **C3'**), 125.2 (**C5**, **C3**), 34.6 (**C7**), 32.0 (**C8**), 30.5 (**C9**), 14.5 (**C7'**) **{21.0 CH_3 free 4-picoline}**

FTIR ν_{max} (cm^{-1})**:** 3161 (stretch **OH**), 2952-2866 (stretch **CH**), 1200 (stretch **C-O**)
(solid state, selected)

p-*tert*-Butylcalix[4]arene (1:1) 4-Fluoro toluene complex

To a solution of 60mL of 4-Fluoro toluene heated at ca. 110 °C in a flask of 100mL were added (1.0g, 1.54mol) of p-*tert*-butyl-calix[4]arene in a small portions until completely dissolution. The content of the flask was filtered hot to give after cooling at room temperature for 2 days and filtration on Buchner funnel, (517mg, 49%) of white glistening crystals corresponding to 1:1 complex.

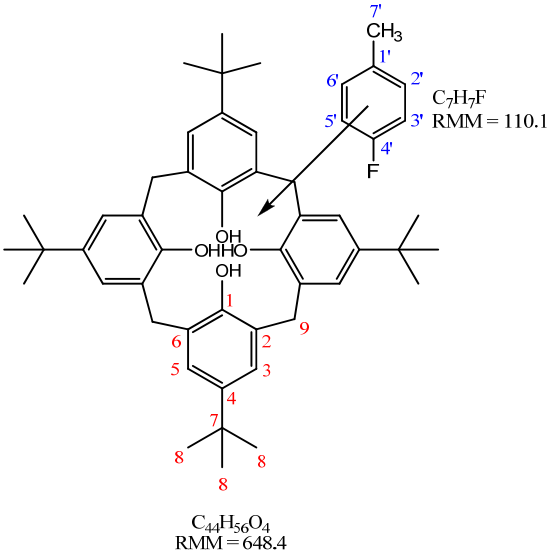

XRD (single crystal)**:** 2007Sot0391

MP: > 300ºC

Anal. Calcd. for $C_{44}H_{56}O_4 + C_7H_7F$: C 80.70, H 8.37, Found: C80.88, H 8.45.

^{13}CP-MAS NMR: 161.4 (**C4'**), 158.9 (**C4'**), 147.0 (**C1**), 144.6 (**C4**), 134.9 (**C1'**), 129.5 (**C2**, **C2'**), 128.9 (**C6**, **C6'**) 128.8 (**C5**), 125.7 (**C3**), 114.8 (**C3'**, **C5'**), 34.7 (**C7**), 32.4 (**C8**), 30.5 (**C9**), 14.8 (**C7'**) **{21.0 CH_3 free 4-fluoro toluene}**

FTIR ν_{max} (cm^{-1})**:** 3163 (stretch **OH**), 2951-2866 (stretch **CH**), 1200 (stretch **C-O**)
(solid state, selected)

p-*tert*-Butylcalix[4]arene (1:1) 4-Chloro toluene complex

At 60 mL of 4-Chlorotoluene heated at ca. 140 °C in a flask of 100 mL were added (1.0g, 1.54mol) of p-*tert*-butyl-calix[4]arene in a small portions until completely dissolution. The content of the flask was filtered hot to give after cooling at room temperature for 2 days and filtration on Buchner funnel, (796mg, 67%) of white glistening crystals corresponding to 1:1 complex.

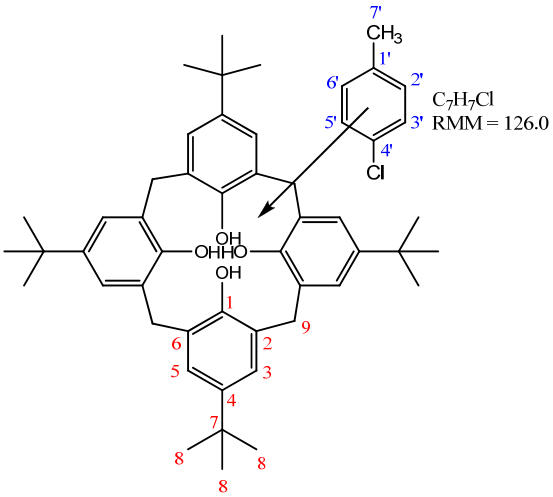

$C_{44}H_{56}O_4$
RMM = 648.4

XRD (single crystal)**:** 2008Sot0699

MP: > 300ºC

Anal. Calcd. for $C_{44}H_{56}O_4 + C_7H_7Cl$: C 78.99, H 8.19, Found: C79.17, H 8.35.

^{13}CP-MAS NMR: 147.0 (**C1**), 144.6 (**C4**), 134.6 (**C1'**), 129.9 (**C6**), 129.0 (**C2**, **C2'**, **C6'**, **C4'**) 128.1 (**C3'**, **C5'**), 126.0 (**C5**), 125.3 (**C3**), 34.8 (**C7**), 32.4 (**C8**), 30.2 (**C9**), 14.0 (**C7'**) **{20.8 CH_3 free chloro toluene}**

FTIR ν_{max} (cm^{-1})**:** 3163 (stretch **OH**), 2951-2866 (stretch **CH**), 1200 (stretch **C-O**)
(solid state, selected)

p-*tert*-Butylcalix[4]arene (1:1) acetone complex

To 5mL of acetone at r.t. in a flask of 100 mL were added (406mg, 0.63mmol) of p-*tert*-butylcalix[4]arene in a small portions until white suspension appeared. The content of the flask was stirred overnight. Then the solvent was removed by slow evaporation to give after 2 days (431mg, 97%) of white powder corresponding to 1:1 complex.

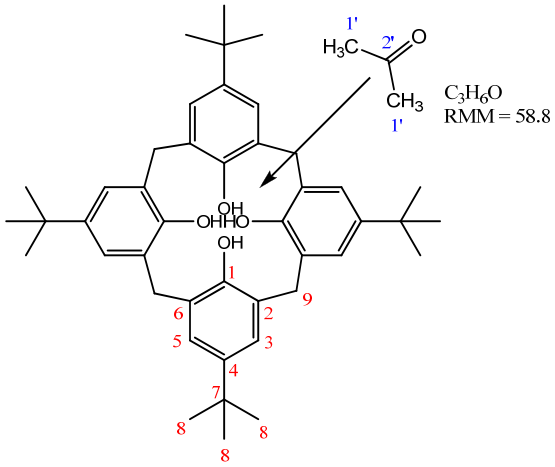

MP: > 300ºC

^{13}CP-MAS NMR: 201.7 (**C2'**), 145.8 (**C1**), 144.4 (**C4**), 128.8, 128.5, 126.2, 125.2 (**C2, C3, C5, C6**), 34.7 (**C7**), 32.7 and 32.7 (**C8**), 30.0 (**C9**), 27.5 (**C1'**) **{20.8 CH_3 free acetone}**

FTIR ν_{max} (cm^{-1})**:** 3163 (stretch **OH**), 2951-2866 (stretch **CH**), 1200 (stretch **C-O**)

(solid state, selected)

p-*tert*-Butylphenol

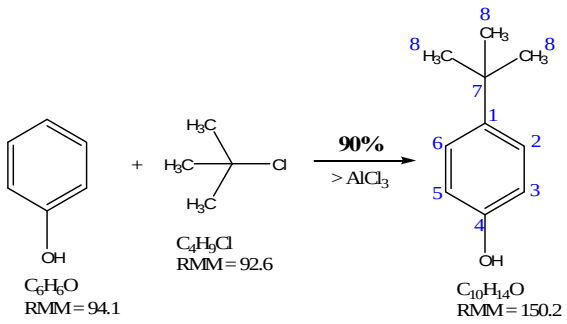

To a flask of 10mL flame dried and purged with nitrogen equipment with HCl trap were added (470mg, 5.0mmol) of phenol and (553mg, 6.0mmol) 0.65mL of *tert*-butylchloride stirring under gentle flow of nitrogen. Rapidly it was added (50mg, 0.38mmol) of Alumium chloride in portions (cooled the flask in ice-bath). After 15 minutes a white off solid was formed in bottom flask, washed with water and the tick mass broken in small pieces to give after filtration on buchner funnel and dried in vacuum pump (677mg, 90%) of white powder. TLC *Rf* = 0.55 (Hexane/Ethyl Acetate 4:1).

MP: > 96-98ºC

EIMS/GC (M/Z): 150 [$M^{+\cdot}$ 39.7%], 135 [100%], 119 [9.2%], 107 [71.8%], 95 [21%]

^{1}H NMR ($CDCl_3$)**:** 7.30-7.25 (2H, m, **H2, H6**), 6.82-6.76 (2H, m, **H3, H5**), 4.70 (1H, sbr, **OH**), 1.32 (9H, s, **H8**)

^{13}C-NMR ($CDCl_3$)**:** 153.1 (**C4**), 143.5 (**C1**), 126.4 (**C2, C6**), 114.7 (**C5, C3**), 34.0 (**C7**), 31.5 (**C8**)

FTIR ν_{max} (cm^{-1})**:** 3219 (stretch **OH**), 2960 (stretch **CH**), 1234 (stretch **C-O**)

(solid state, selected)

p-*tert*-Butyl_d_9 phenol

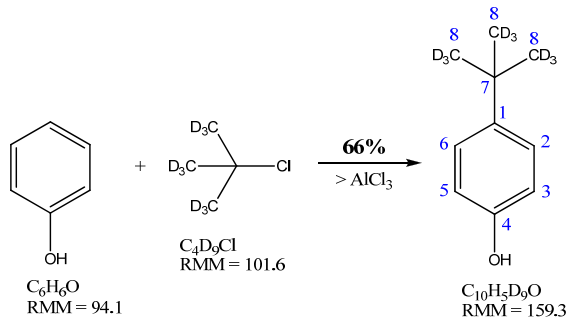

To a flask of 10 mL flame dried and purged with nitrogen equipment with HCl trap were added (772mg, 8.2mmol) of phenol and (1.0g, 9.84mmol) 1.07mL of *tert*-butylchloride_d_9 stirring under gentle flow of nitrogen. Rapidly it was added (149mg, 1.04mmol) Alumium chloride in portions (cooled the flask in ice-bath). After 25 minutes a light pink solid was formed in bottom flask, washed with 2 mL of water and the tick mass broken in small pieces to give after filtration on buchner funnel and dried in vacuum pump (1.13g, 90%) of crude as white powder. The crude powder was crystallised by Petrol filtered at hot and cooled at room temperature in conical flask for 1 night to give after filtration on buchner and dried in vacuum pump white needle crystals (864mg, 66%). TLC *Rf* = 0.43 (Hexane/Ethyl Acetate 4:1).

MP: 94-95ºC

EIMS/GC (M/Z): 159 [$M^{+\cdot}$ 22%], 141[100%], 109 [22%], 94 [7.83%]

^{1}H NMR ($CDCl_3$)**:** 7.04-7.00 (2H, m, **Ar**), 6.57-6.52 (2H, m, **Ar**), 4.49 (1H, sbr, **OH**), 1.03-1.02 (1.4H, **residual proton signals after *tert*-butyl deuteration**) **[estimated deuteration 98.6%]**

^{13}C-NMR ($CDCl_3$)**:** 153.1 (**C4**), 143.6 (**C1**), 126.4 (**C2, C6**), 114.8 (**C5, C3**), 34.0 (**C7**), 30.7, 30.4, 30.2 (**C8**)

FTIR ν_{max} (cm^{-1})**:** 3164 (stretch **OH**), 2214 (stretch **C-D**), 1232 (stretch **C-O**)

(solid state, selected)

p-*tert*-Butyl_d_{36} calix[4]arene (1:1) Toluene complex

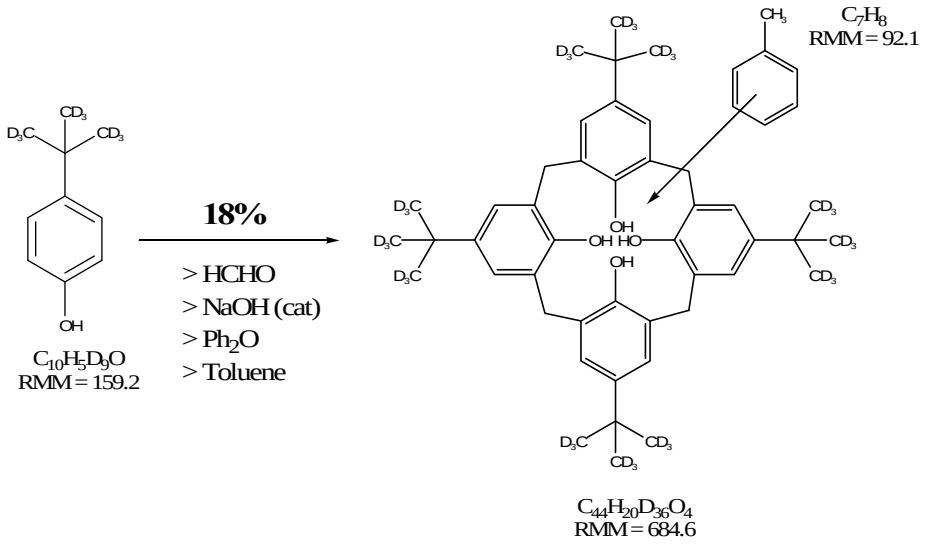

To a 3-necked flask of 50mL flame dried and purged with nitrogen were added (850mg, 5.34mmol) of p-*tert*-butylphenol_d_9, (0.53mL, 6.60mmol) of formaldehyde 37% and (7.67mg, 0.20mmol) of sodium hydroxide dissolved in a minimum amount of water. It was heating at 120 °C for 2h to give after 10 min a colourless liquid. After 2h a viscous orange mass appeared. When the magnetic stirrer was stopped, this condition were maintained for other 1:30h to give in the end after cooled at room temperature a friable solid orange thick mass “the precursor”. It was broken in small pieces, then under nitrogen diphenyl ether was added and heated at 120 °C with a condenser. During this time the precursor went in solution after ca. 10 min and when it was completely dissolved the condenser was removal. In this phase the nitrogen flow was increase to remove the water trapped in the precursor grid. A yellow turbid solution was obtained in ca. 4 min and these conditions were maintained for ca. 15 min. The solution was carried at 150-160 °C an after ca. 2 min a precipitate started to form. This step was very critical because must favour the cyclic octamer formation and for this conditions it was need ca. 10 min during which the precipitate increase was observed. The mixture was carried at 180 °C to give much foam and in the end at reflux temperature ca. 260 °C for 2h under a gentle flow of nitrogen with a condenser. This temperature was very important because in this phase the cyclic octamer was transformed in cyclic tetramer observable through a colour

and chemical physical changed of the solution from turbid at clean red-brown solution. The reaction mixtures remained clear at the reflux temperature, and only upon cooling does precipitate once again appear. The reaction solution was cooled to room temperature for 1h, to give a deep brown solution. It was treated with 15mL of ethyl acetate, stirred for 30 min and allowed to stand for 30 min to obtain a white precipitate at the bottom of the flask. Filtration of yields material which was washed twice with two once of ethyl acetate, to give after dried after dried on vacuum pump (220mg, 26%) of crude compound as white powder. TLC *Rf* = 0.75 (Petroleum ether/Dichlorometane 1:1). This material was treated with 27mL of boiling toluene and filtered at hot to give after cooling to room temperature for 2 days and filtration on buchner funnel, (171mg, 18%) of product as rhombic crystals, corresponding to 1:1 complex with toluene.

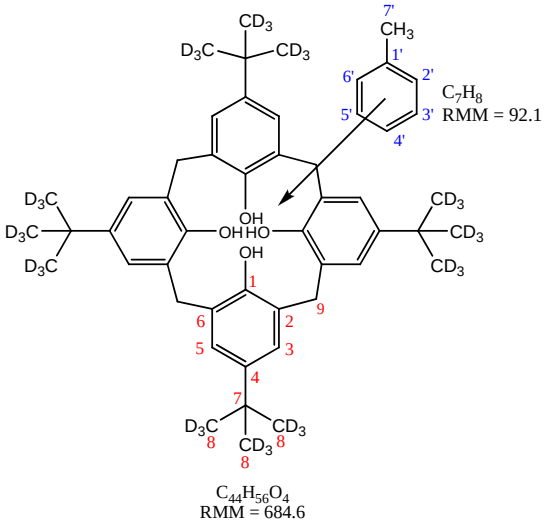

XRD (single crystal)**:** 2006Sot0832

MP: > 300ºC

MS/ES$^-$ (M/Z)**:** 683.8 [100% M-H]$^-$

Accurate Mass: required 707.6321 [M+Na]$^+$ founded 707.6322 [M+Na]$^+$

^{1}H NMR ($CDCl_3$)**:** 10.34 (1H, s, **OH**), 7.28-7.16 (6H, m, **Ar guest + $CDCl_3$**), 7.04 (2H, s, **H3, H5**), 4.26 (1H, d, J=13.2, **H9**), 3.49 (1H, d, J=13.2, **H9**), 2.36 (3H, s, **H7'**), 1.26-1.13 (5.47H, **residual proton signals after *tert*-butyl deuteration**) [**estimated deuteration: 94.5%**]

^{13}CP-MAS NMR: 146.3 (**C1**), 144.2 (**C4**), 138.6 (**C1'**), 129.1 (**C6**), 128.2 (**C2**, **C2'**, **C6'**), 127.2 (**C3'**, **C5'**), 125.7 (**C5**), 125.0 (**C3**), 124.0 (**C4'**), 33.6 (**C7**), 30.7 (**C8**), 30.2 (**C9**), 15.2 (**C7'**) **{21.5 CH_3 free toluene}**

FTIR ν_{max} (cm^{-1})**:** 3156 (stretch **OH**), 2212 (stretch **C-D**), 1476 & 1462 (stretch **C-C**)

(solid state, selected)

p-*tert*-Butylphenol_d_{13}

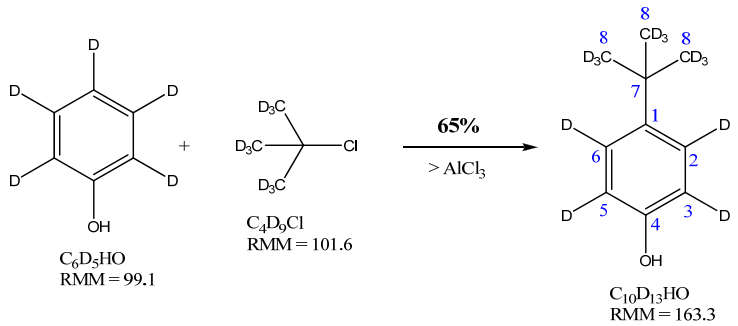

Into a 10mL flask which had been flame dried and purged and attached to an HCl trap were added phenol_d_5 (0.821g, 8.2mmol) and (1.0g, 9.84mmol) 1.07mL of *tert*-butylchloride_d_9 stirring under a gentle flow of nitrogen. (0.149g, 1.04mmol) of Alumium chloride was rapidly added in portions (cooling the flask in ice-bath). After 25 minutes a yellow solid was formed in bottom flask. This was washed with deuterated water (3mL) cooled in ice bath and the result thick mass was then broken into small pieces to give after filtration and drying in vacuum pump (1.2g, 90%) a crude as off-white (1.2g, 90%). The crude powder was crystallised from Petrol filtered and after cooling overnight gave white needles (0.716g, 54%). TLC *Rf* = 0.50 (Hexane/Ethyl Acetate 4:1).

MP: 81-82ºC

EIMS/GC (M/Z)**:** 163

^{1}H NMR ($CDCl_3$)**:** 6.79 (**residual proton signal after aromatic deuteration**), 5.03 (1H, s, **OH**), 1.27-1.26 (**residual proton signal after *tert*-butyl deuteration**)

^{13}C-NMR 153.0 (**C4**), 143.4 (**C1**), 126.3, 126.0, 125.7 (**C2, C6**), 114.7, 114.4, 114.0 (**C5, C3**), 33.0 (**C7**), 30.8, 30.6, 30.4, 30.1, 29.9 (**C8**)

FTIR ν_{max} (cm^{-1})**:** 3214 (stretch **OH**), 2215 (stretch **C-D**), 1578 (stretch **C-C**)

(solid state, selected)

p-*tert*-Butylcalix[4]arene_d_{44} (1:1) Toluene complex

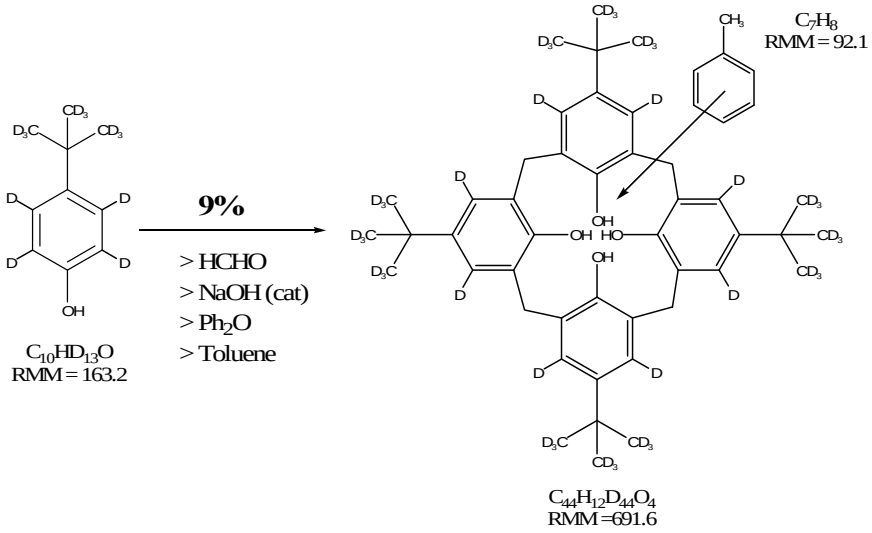

To a 3-necked flask of 50mL flame dried and purged with nitrogen were added (0.716g, 4.39mmol) of p-*tert*-butylphenol_d_{13}, (0.44mL, 5.43mmol) of formaldehyde 37% and (0.0061 g, 0.16mmol) of sodium hydroxide dissolved in a minimum amount of water. It was heating at 120 °C for 2h to give after 10 min a yellow liquid. After 2h a viscous orange mass appeared. Stirring was then stopped, and heating was maintained for a further 2h to give after cooling to room temperature a friable solid orange thick mass "the precursor". This was broken in to small pieces, and then under nitrogen of diphenyl ether (8mL) was added and the mixture was heated at 120 °C under a condenser. During this time the precursor went in solution after ca. 10 min and when it was completely dissolved. In this phase the nitrogen flow was increase to remove the water trapped in the precursor grid. A yellow-orange turbid solution was obtained in ca. 4 min and these conditions were maintained for ca. 15 min. The solution was then heated to 150-160 °C an after ca. 2 min a precipitate started to form. The mixture was then heated at 180 °C to

give foam which changed colour to dark brown and finally it was refluxed at ca. 260 °C for 2h under a gentle flow of nitrogen. In this phase the solution changed from turbid to clear red-brown. The reaction mixture remained clear at the reflux temperature, and only upon cooling did a precipitate once again appear. The reaction solution was cooled at room temperature for 1h, to give a deep brown solution. This was then treated with ethyl acetate (15mL), and then stirred for 30 min. It was allowed to stand for 30 min after which time a white precipitate had formed. Filtration gave a material which was washed twice with two once of ethyl acetate, to give after dried after drying a white powder (85 mg, 12%). TLC *Rf* = 0.67 (Petrol/Dichlorometane 1:1). This material was treated with boiling toluene (14mL) and filtered hot to give after standing at room temperature for 2 days rhombic crystals (68mg, 9%), corresponding to 1:1 calixarene_d_{44}/toluene complex.

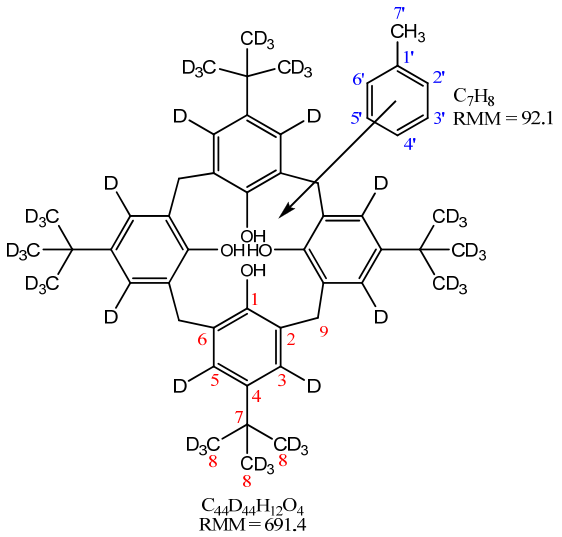

MP: > 300ºC

MS/ES$^-$ (M/Z): 691.7 [100% M-H]$^-$

Accurate Mass: required 715.6822 [M+Na]$^+$ founded 715.6823 [M+Na]$^+$

^{1}H NMR ($CDCl_3$)**:** 10.34 (1H, s, **OH**), 7.28-7.16 (6H, m, **Ar guest+ $CDCl_3$**), 4.26 (1H, d, J=13.2, **H9**), 3.49 (1H, d, J=13.2, **H9**), 2.36 (3H, s, **H7'**), 1.25-1.16 (2.42H, **residual proton signal after *tert*-butyl deuteration**) [**estimated deuteration: 97.6%**]

^{13}CP-MAS NMR: 146.6 (**C1**), 144.4 (**C4**), 139.1 (**C1'**), 129.3 (**C6**), 128.7 (**C2, C2', C6'**), 128.4 (**C3', C5'**), 127.4 (**C5**), 125.7 (**C3**), 125.0 (**C4'**), 33.8 (**C7**), 30.9 (**C8**), 30.3 (**C9**), 15.3 (**C7'**) **{21.5 CH_3 free Toluene}**

FTIR ν_{max} (cm^{-1}): 3164 (stretch **OH**), 2212 (stretch **C-D**), 1486 (stretch **C-C**)

(solid state, selected)

***p-iso*-Propylcalix[4]arene**

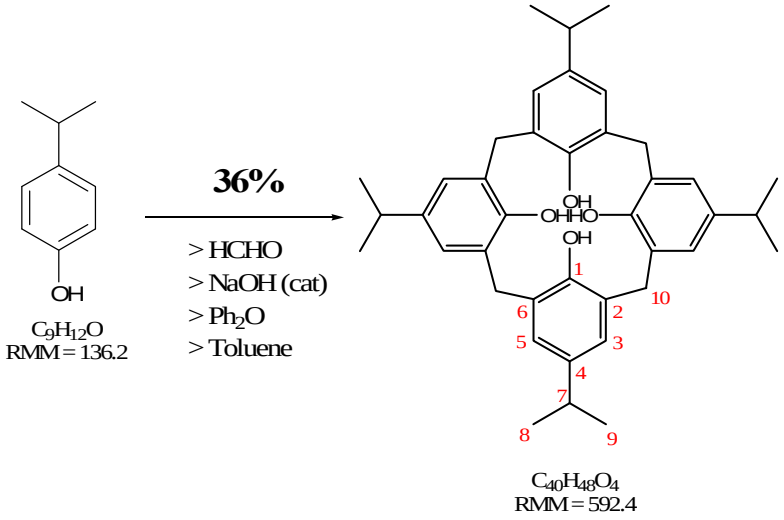

To a 3-necked flask of 500mL were added (9g, 0.067 mol) of p-*iso*-propylphenol, (6.2 mL, 0.0830mol) of formaldehyde 37% and (95.6mg, 0.0024mol) of sodium hydroxide corresponding at 0.036 equivalent of base, stirred slowly for 20 min at room temperature to obtain a partial dissolution of the p-*tert*-butyl phenol. Then it was heating at 120 °C for 2h to give after 30 min a homogeneous solution light yellow and in the end a viscous mass yellow. When the magnetic stirrer was stopped, this condition were maintained for other 1h to gave in the end after cooled at room temperature a friable solid yellow thick mass "the precursor". It was broken in small pieces, then under nitrogen diphenyl ether was added and heated at 120°C with a condenser. During this time the precursor went in solution after ca. 10 min and when it was completely dissolved the condenser was removal. In this phase the nitrogen flow was increase to remove the water trapped in the precursor grid. A yellow turbid solution was obtained in ca. 2 min and these conditions were maintained for ca. 15 min. The solution was carried at 150-160°C an after ca. 5min

a precipitate started to form. This step was very critical because must favour the cyclic octamer formation and for this conditions it was need ca. 15min during which the precipitate increase was observed. The mixture was carried at 180°C to give much foam and in the end at reflux temperature ca. 260°C for 2.5h under a gentle flow of nitrogen with a condenser. The reaction mixtures remained light-turbid at the reflux temperature, and only upon cooling does precipitate once again appear. The reaction solution was cooled to room temperature, treated with 150mL of ethyl acetate, stirred for 30 min and allowed to stand for 30 min to obtain a white precipitate at the bottom of the flask. Filtration of yields material which was washed twice with 10mL of ethyl acetate, once with 20mL of acetic acid and 10mL of water to yield after dried (5.01g 47%) of crude compound as white powder (3.60g, 36%). TLC *Rf* = 0.60 (Petrol/Dichlorometane 1:1).

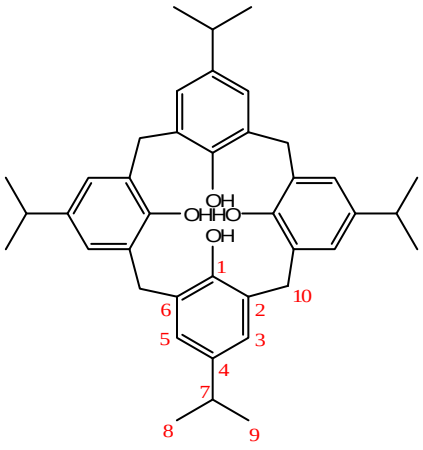

$C_{40}H_{48}O_4$
RMM = 592.4

MP: > 300ºC

MS/ES$^-$ (M/Z): 591.8 [100% M-H]$^-$

^{1}H NMR ($CDCl_3$)**:** 10.27 (1H, s, **OH**), 6.90 (2H, s, **Ar**), 4.21 (1H, s, **H10**), 3.50 (1H, s, **H10**), 2.72 (1H, sept, **H7**), 1.17 (3H, s, **H8**), 1.14 (3H, s, **H9**)

^{13}C-NMR: 146.9 (**C1**), 142.2 (**C4**), 128.1 (**C2, C6**), 126.9 (**C3, C5**), 33.2 (**C7**), 32.2 (**C8**), 24.0 (**C9**)

***p-iso*-Propylcalix[4]arene (2:1) *p*-xylene complex**

At 16mL of p-xylene heated at ca. 100°C in a flask of 100 mL were added (400mg, 10.67mmol) of p-*iso*-propyl-calix[4]arene in a small portions heating at 140°C until completely dissolution. The content of the flask was filtered hot to give after cooling at room temperature for 3 days and filtration on Buchner funnel, (274mg, 59%) of glistening rhombic crystals corresponding to 1:1 complex (X-ray results corresponded to structure Cambridge database YARXOE). 271mg of this p-*iso*-propylcalix[4]arene (1:1) p-xylene complex crystals was heated at 85°C for 25min in a sand bath to make the (2:1) complex (244mg 48%) white porous crystals.

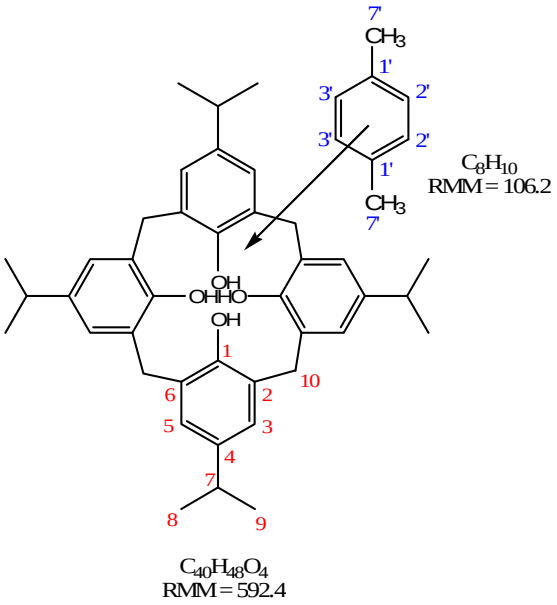

XRD (single crystal)**:** 2006Sot0769

MP: > 300ºC (reported: > 300ºC)[157]

^{1}H NMR ($CDCl_3$)**:** 10.30 (1H, s, **OH**), 7.08 (4H, m, **H2'**, **H3'**), 6.90 (2H, s, **Ar**), 4.22 (1H, dbr, J=13.2, **H10**), 3.51 (1H, d, J=13.2, **H10**), 2.72 (2H, sept, **H7**), 2.32 (6H, s, **H7'**), 1.17 and 1.14 (12H, s, **H8**, **H9**)

^{13}CP-MAS NMR: 146.7 (**C1**), 141.8 (**C4**), 134.0 (**C1'**), 129.3, 128.6 (**C2**, **C6**), 127.6, 124.8 (**C3**, **C5**) 126.6 (**C2'**, **C3'**), 34.8 (**C7**), 30.4 (**C10**), 26.6 (**C8**), 23.7 (**C9**), 13.7 (**C7'**) **{20.9 CH_3 free p-xylene}**

FTIR ν_{max} (cm^{-1})**:** 3154 (stretch **OH**), 2954, 2870 (stretch **CH**), 1243 (stretch **C-O**)

(solid state, selected)

***p-iso*-Propylcalix[4]arene (1:1) iodo-methane complex**

At 60 mL of 4-Chlorotoluene heated at ca. 140 °C in a flask of 100mL were added (1.0g, 1.54mol) of p-*tert*-butyl-calix[4]arene in a small portions until completely dissolution. The content of the flask was filtered hot to give after cooling at room temperature for 2 days and filtration on Buchner funnel, (796mg, 67%) of white glistening crystals corresponding to 1:1 complex.

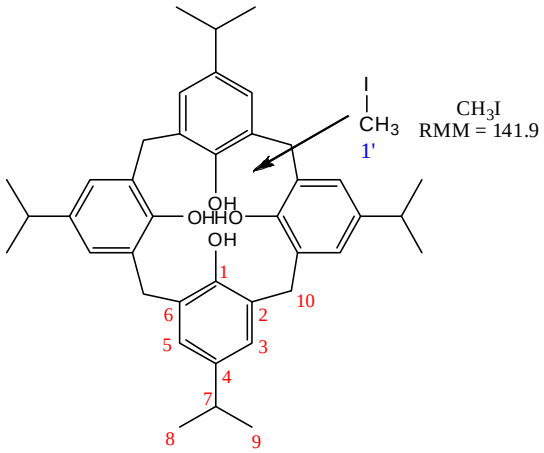

$C_{40}H_{48}O_4$
RMM = 592.4

XRD (single crystal)**:** 2006Sot0680

MP: > 300ºC

^{1}H NMR ($CDCl_3$)**:** 10.26 (1H, s, **OH**), 6.89 (2H, s, **Ar**), 4.22 (1H, dbr, J=13.2, **H10**), 3.51 (1H, dbr, J=13.2, **H10**), 2.71 (2H, sept, **H7**), 2.16 (3H, s, **H1'**), 1.16 (3H, s, **H8**), 1.14 (3H, s, **H9**)

^{13}CP-MAS NMR: 146.0 (**C1**), 142.8 (**C4**), 128.7 and 127.6 (**C2**, **C6**), 124.5 (**C3**, **C5**), 34.7 (**C7**), 30.2 (**C10**), 27.1 (**C8**), 24.7 (**C9**), -29.1.7 (**C1'**) **{-23.5 CH_3 free iodomethane}**

FTIR ν_{max} (cm^{-1})**:** 3154 (stretch **OH**), 2954, 2870 (stretch **CH**), 1243 (stretch **C-O**)

(solid state, selected)

***p-iso*-Propylcalix[4]arene (1:1) 2-butyne complex**

At 2.5mL of 2-butyne at r.t. in a flask of 5mL were added (20mg, 0.034mmol) of p-*isot*-propyl-calix[4]arene in a small portions until completely dissolution. The content of the flask was stored in the fridge at 4ºC 24h to give after filtration on Buchner funnel, (12mg, 54%) of white glistening crystals corresponding to 1:1 complex.

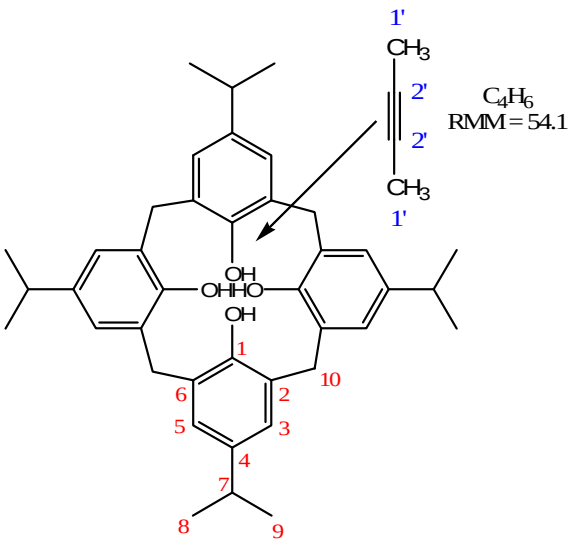

XRD (single crystal)**:** 2006Sot0756

MP: > 300ºC

^{1}H NMR ($CDCl_3$)**:** 10.26 (1H, s, **OH**), 6.89 (2H, s, **Ar**), 4.22 (1H, dbr, J=13.2, **H10**), 3.51 (1H, dbr, J=13.2, **H10**), 2.71 (1H, sept, **H7**), 1.75 (3H, s, **H1'**), 1.16 (3H, s, **H8**), 1.14 (3H, s, **H9**)

^{13}CP-MAS NMR: 148.4 (**C1**), 144.3 (**C4**), 131.9 and 129.2 (**C2**, **C6**), 131.3 and 126.8 (**C3**, **C5**), 76.8 (**C2'**), 36.9 (**C7**), 32.4 (**C10**), 29.2 (**C8**), 26.0 (**C9**), -1.2 (**C1'**) **{3.4 CH_3 free 2-butyne}**

FTIR ν_{max} (cm^{-1})**:** unable to collect IR spectrum

(solid state, selected)

***p-tert*-Butyl-calix[4]arene-25,26,27,28-tetracarbonate (1:1) nitromethane complex**

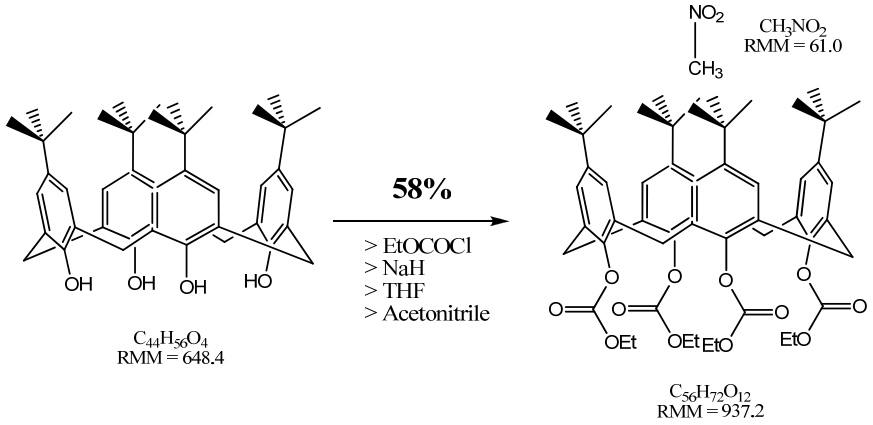

Into a 3 neck flask which had been flame dried and purged with nitrogen were added dry tetrahydrofuran 50mL (distilled over CaH_2 and stored on molecular sieves). The p-*tert*-butylcalix[4]arene (648mg, 1mmol) and sodium hydride (1.16g, 48mmol) were added stirring for 10 minutes. After this time, ethyl chloroformate (3.1ml, 0.032mmol) were added and the grey suspension refluxed at 80-81°C for 3 days. Excess of sodium hydride was removed by dropwise addition of water, and the solvent and excess of ethyl formate were removed at reduced pressure. The residue was taken up in chloroform (60mL) washed with water (x 30mL) and dried over magnesium sulphate. Removal of the solvent followed re-precipitation of residue from dichloromethane/ethanol gave the tetracarbonate as colourless powder (203mg, 21%). Crystallization of saturated solution of calixarene-tetracarbonate in nitromethane (16mL) left a microcrystalline white powder (118mg, 12%)

XRD (single crystal)**:** 2006Sot0751

MP: > 300ºC

^{1}H NMR ($CDCl_3$)**:** 6.93 (2H, s, **Ar**), 4.38 (2H, q, J=12.1, **CH_2 ester**), 4.31 (1H, s, **CH_3 guest**), 3.93 (1H, d, J=12.5, **CH_2**), 3.29 (1H, d, J=12.5, **CH_2**), 1.46 (3H, t, J=12.8, **CH_3 ester**), 1.09 (9H, s, ***tert*-Butyl**)

^{13}C-NMR ($CDCl_3$)**:** 155.3, 147.7, 144.1, 133.0, 125.3, 64.0, 34.0, 31.2, 14.4

^{13}CP-MAS NMR: 155.4, 154.2, 152.2, 150.3, 149.1, 148.2, 147.0, 145.3, 144.7, 143.6, 134.1, 133.8, 131.8, 131.4, 126.8, 126.5, 124.8, 64.3, 63.6, 55.8, 34.2, 31.7, 28.8, 27.9, 15.7, 15.0, 14.4

***p-tert*-Butyl-25,26,27,28-[tetra(ethyloxyglycol)]-calix[4]arene (1:1) acetonitrile complex**

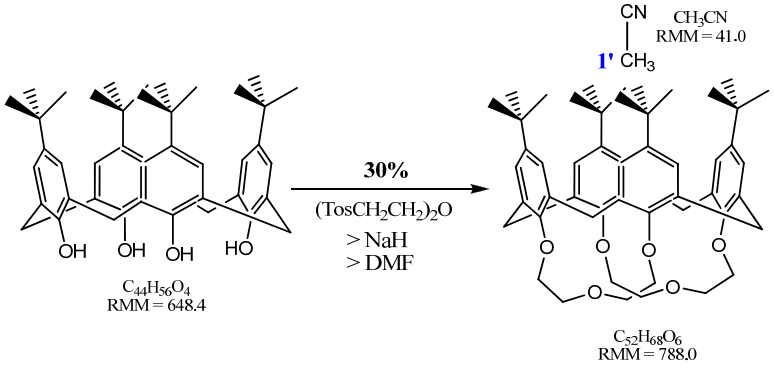

Into a 3 neck flask which had been flame dried and purged with nitrogen dry dimethylformamide 83mL p-*tert*-butylcalix[4]arene (504mg, 0.78mmol) and NaH (60%) mineral oil (251mg, 10.4mmol) were added heating at 80°C. Diethylene glycol ditosylate (828mg, 2.0mmol) dissolved in 1 mL of DMF was added and the mixture refluxed for 4 h to give a light yellow solution. Solvent evaporation gave a white-yellow residue that was taken up with HCl 10% (20mL) extracting with ethyl acetate (x 20mL). The organic phase was dried over Na_2SO_4 to give 588mg of white off solid. This material was purified by column chromatography using Hexan/EtOAc 7:3 to give (189mg, 30%) as white solid. TLC *Rf* = 0.57 (Hexane/Ethyl Acetate 4:1). This material was re-crystallised from saturated solution of acetonitrile to give needle crystals (88mg, 10%)

XRD (single crystal)**:** 2008Sot0650

LRMS/ES$^-$ (M/Z): 812.0 [100% M+Na]$^+$, 828 [10% M+AN]$^+$

MP: > 300ºC (reported: > 300ºC)[125]

^{1}H NMR ($CDCl_3$)**:** 6.93 (4H, d, J=2.40, Ar**H**), 6.88 (4H, d, J=2.40, Ar**H**), 5.03 (2H, d, J=12.30, Ar**CH_2**Ar), 4.45 (2H, d, J=12.1,), 4.33-3.88 (16H, m), 3.17 (2H, d, J=12.35, Ar**CH_2**Ar), 3.14 (2H, d, J=12.12, O**CH_2CH_2**O), 1.09 (36H, s, t-**But**)

^{13}C-NMR ($CDCl_3$)**:** 153.0, 145.0, 134.8, 134.3, 125.6, 124.6, 75.8, 74.1, 33.9, 31.4, 31.2

^{13}CP-MAS NMR: 153.7, 153.4, 152.8, 146.6, 146.3, 145.3, 137.3, 136.3, 135.9, 135.4 127.6, 126.1, 125.8, 124.9, 124.0, 77.8, 77.3, 76.7, 76.3, 75.8, 74.7, 34.8, 34.4, 33.8, 32.2, 31.5, 30.1, 29.8, -6.8 (**C1'**), **{1.75 CH_3 free acetonitrile}**

p-*tert*-Butyl-25,27-bis(tertbutylcarboxymethoxy)-26,28-dihydroxycalix[4]arene

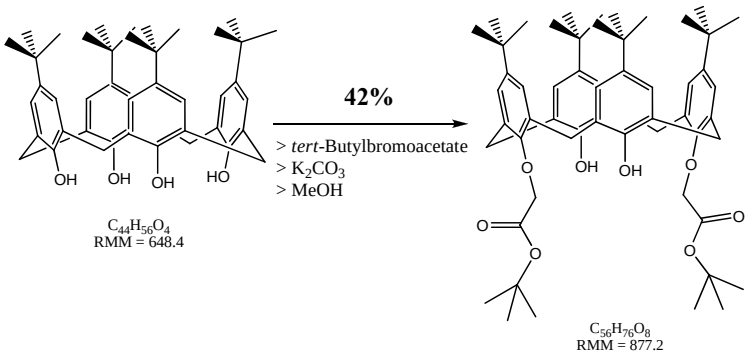

Into a 3 neck flask which had been flame dried and purged with nitrogen dry acetonitrile 12mL, p-*tert*-butylcalix[4]arene (500mg, 0.77mmol), potassium carbonate (116mg, 0.84 mmol) and of *tert*-Butylbromoacetate (0.23mL, 1.54mmol) were added and the white suspension heating at 81-82°C for 3 days. After this time dichloromethane (20mL) was added washing with portions of brine (10mL). The organic phase was dried over Na_2SO_4 filtered and evaporated on buchi to give 680mg of light yellow oil. This material was added of MeOH (10mL) to give after filtration a white powder (281mg 42%). TLC *Rf* = 0.71 (DCM/MeOH 99:1).

MP: > 180-183ºC

LRMS/ES$^-$ (M/Z): 876 [100% M-H]$^-$

^{1}H NMR ($CDCl_3$)**:** 7.07 (2H, s, **OH**), 7.03 (4H, s, Ar**H**), 6.79 (4H, s, Ar**H**), 4.58 (4H, s, O**CH_2**CO), 4.45 (4H, d, J=13.0, Ar**CH_2**Ar), 3.30 (4H, d, J=13.2, Ar**CH_2**Ar), 1.54 (18H, s, ***t*-But lower rim**), 1.28 (18H, s, ***t*-But**), 0.96 (18H, s, ***t*-But**)

^{13}C-NMR ($CDCl_3$)**:** 168.2, 150.8, 150.5, 146.9, 141.4, 132.5, 127.9, 125.6, 125.0, 82.2, 73.2, 33.9, 33.8, 31.8, 31.7, 31.0, 28.2

FTIR ν_{max} (cm^{-1})**:** 3154 (stretch **OH**), 2954, 2870 (stretch **CH**), 1243 (stretch **C-O**)

(solid state, selected)

***p-tert*-Butyl-25,27-bis(carboxymethoxy)-26-28-dihydroxycalix[4]arene**

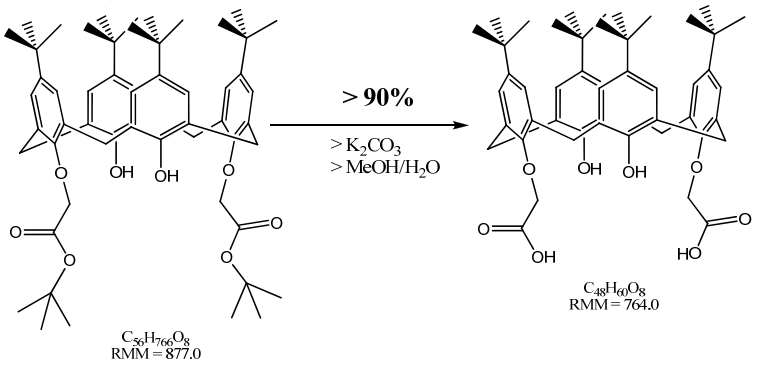

Into a 3 neck flask methanol 7mL and p-*tert*-butylcalix[4]arene (100mg, 0.11mmol) were added heating at reflux T. A solution of potassium carbonate (158mg, 1.14mmol) dissolved in 1 mL of water was added stirring for 2h in reflux condition. After this time the white mix was cooled at R.T. and the solvent removed to give a white powder. The residue was taken up using 35ml of water and the pH adjusted to about 2 with HCl 1M., extracting twice with dichloromethane and the solution evaporated to give a white powder in quantitative yield. TLC *Rf* = (DCM/MeOH 99:1).

MP: > 220ºC (decomp.) (reported: > 220ºC decomp.)

LRMS/ES$^-$ (M/Z): 763 [100% M-H]$^-$

^{1}H NMR ($CDCl_3$)**:** 7.07 (4H, s, Ar**H**), 6.79 (4H, s, Ar**H**), 4.70 (4H, s, O**CH_2**COOH), 4.13 (4H, d, J=13.0, Ar**CH_2**Ar), 3.47 (4H, d, J=13.2, Ar**CH_2**Ar), 1.28 (18H, s, ***t*-But**), 1.08 (18H, s, ***t*-But**)

^{13}C-NMR ($CDCl_3$)**:** 169.5, 149.0, 148.7, 132.4, 127.1, 126.4, 125.7, 72.1, 150.8, 34.2 33.9, 32.3, 31.5, 31.0

FTIR ν_{max} (cm^{-1})**:** 2954, 2868, 2923 cm^{-1} (Stretch **OH**), 1738 cm^{-1} (stretch **C=O**), (solid state, selected) 1191 cm^{-1} (stretch **C-O**)

p-*tert*-Butyl-25,27-bis(chloroformylmethoxy)-26,28-dihydroxycalix[4]arene

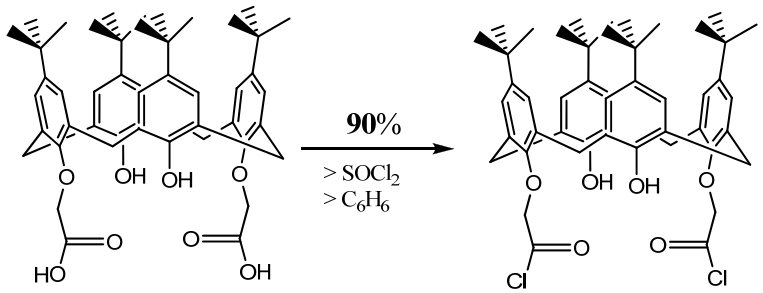

$C_{48}H_{60}O_8$
RMM = 764.0

$C_{48}H_{58}O_6Cl_2$
RMM = 801.9

Into a 3 neck flask which had been flame dried and purged with nitrogen were added dry benzene 35mL (distilled over CaH_2 and stored on molecular sieves). The p-*tert*-butylBis[(Carboxymethyl)dihydroxy]calix[4]arene (700mg, 0.91mmol), and the thionyl chloride (2.0g, 16.5mmol) were added with vigorous stirring. The colourless suspension was heated at reflux (80-81°C) for 3.5 h. Then the solvent was evaporated and the off-white microcrystalline solid (a tedious and long evaporation was observed). The product contain benzene (<u>all attempts to remove benzene failed</u>) was used immediately for the next step without any other purification (682mg, > 90%)

LRMS/ES$^-$ (M/Z)**:** 801.3 [100% M-H]$^-$

^{1}H NMR ($CDCl_3$)**:** 7.09 (4H, s, Ar**H**), 6.79 (4H, s, Ar**H**), 6.18 (2H, s, **OH**), 5.04 (4H, s, O**CH_2**CO), 4.34 (4H, d, J= 12.5, Ar**CH_2**Ar), 3.40 (4H, d, J= 12.6, Ar**CH_2**Ar), 1.30 (18H, s, ***t*-But**), 0.94 (18H, s, ***t*-But**)

^{13}C-NMR ($CDCl_3$)**:** 170.0, 149.9, 149.8, 147.8, 142.2, 131.8, 128.3, 127.8, 126.1, 125.3, 78.9, 33.9, 33.8, 31.9, 31.6, 31.5

FTIR ν_{max} (cm^{-1})**:** 3480 cm^{-1} (stretch **C-H**), 1810 cm^{-1} (stretch **C-O acyl-chloride**)

(solid state, selected)

***p-tert*-Butyl-25,27-[toluene-bis(2,6-aminocarbonylmethoxy)]-26,28-dihydroxy calix[4]arene**

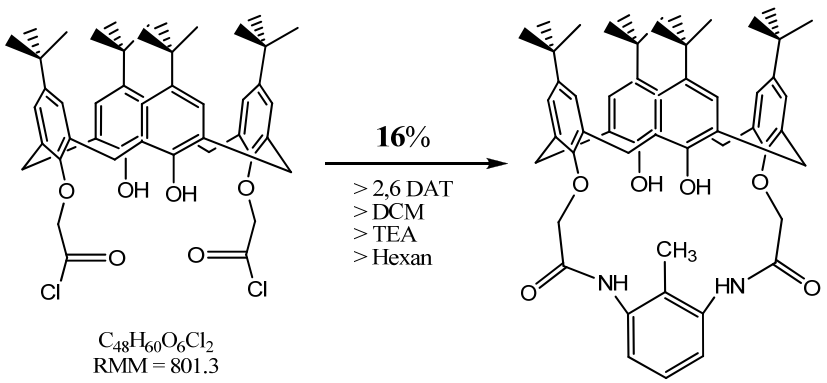

$C_{48}H_{60}O_6Cl_2$
RMM = 801.3

$C_{55}H_{66}N_2O_6$
RMM = 851.1

Into other 3 neck flask which had been flame dried and purged with nitrogen were added dry dichloromethane 90mL (fresh distilled over CaH_2) and the p-*tert*-butylBis[(Chloromethoxy)dihydroxy]calix[4]arene (700mg, 0.87mmol) with vigorous stirring under N_2. A second solution 2,6 diamino-toluene (106mg, 0.87mmol) and triethylamine (177mg, 1.75mmol) in dichloromethane 90 mL was added dropwise and the brown mixture was left to stir for 2 days. Then the solvent was evaporated and the brown residue was taken up with dichloromethane (100mL) washing twice with HCl 1M (30 mL). The organic phase was separated washed with brine (3 X 30mL) and dried over

Na_2SO_4, filtered and evaporated to give a brown-pink material (651 mg). This solid was precipitated using hexan/DCM (5mL) to give after filtration a white powder (142mg, 16%). TLC *Rf* = 0.31 (EtOAc/EtOH 9:1).

MP: > 252-254ºC

LRMS/ES$^-$ (M/Z): 874 [100% M+Na]$^+$

^{1}H NMR ($CDCl_3$)**:** 9.17 (2H, s, Ar**NH**CO), 7.49 (2H, dd, J=8.1, Ar**H**), 7.16 (4H, s, Ar**H**), 7.11 (1H, t, J=8.2, Ar**H**), 6.72 (4H, s, Ar**H**), 6.11 (2H, s, **OH**), 4.61 (4H, s, O**CH$_2$**CO), 4.25 (4H, d, J=13.5, Ar**CH$_2$**Ar), 3.45 (4H, d, J=13.5, Ar**CH$_2$**Ar), 2.22 (3H, s, **CH$_3$**), 1.35 (18H, s, ***t*-But**), (18H, s, ***t*-But**)

^{13}C-NMR ($CDCl_3$)**:** 166.1, 149.6, 148.7, 148.1, 143.2, 135.2, 131.3, 128.0, 126.7, 126.0 125.5, 123.8, 120.6, 74.80, 33.98, 33.90, 31.64, 30.80, 13.68

^{13}CP-MAS NMR: 167.1, 166.1, 150.5, 147.8, 141.4, 140.9, 132.5, 125.4, 74.9, 74.1, 33.5, 31.4, 14.3, 11.5

FTIR ν_{max} (cm^{-1})**:** (solid state, selected) 3350 and 3320 cm^{-1} (stretch **NH**), 1680cm^{-1} (stretch **C=O**), 1590 cm^{-1} (bending **NH**)

***p-tert*-Butyl-[25,27-bis(cyanopropoxy)]-26,28-dihydroxy]calix[4]arene**

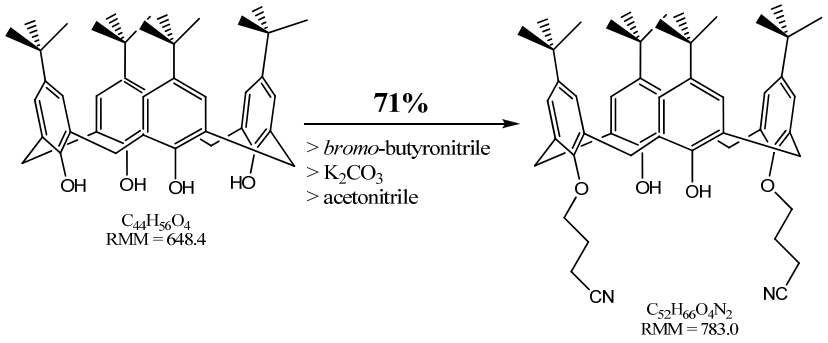

$C_{44}H_{56}O_4$
RMM = 648.4

$C_{52}H_{66}O_4N_2$
RMM = 783.0

Into a 3 neck flask which had been flame dried and purged with nitrogen dry acetonitrile 32mL, p-*tert*-butylcalix[4]arene (2g, 3.08mmol), potassium carbonate (514mg, 3.72 mmol) and of bromobutyrronitrile (960mg, 6.48mmol) were added and the white suspension heating at 81-82°C for 5 days. After this time the solvent was removed and the residue taken up in dichloromethane 100mL washing with portions of HCl 1M (3x20mL) and brine (3x20mL). The organic phase was dried over Na_2SO_4 filtered and evaporated to give (2.19g, 91%) of white-off powder. Re-crystallization of this material from $CHCl_3$/MeOH (2:1) gave white crystals (1.72g 71%). TLC *Rf* = 0.33 (DCM/MeOH 99:1).

MP: > 300ºC (reported: > 300ºC)[136]

LRMS/ES$^+$ $_{(M/Z)}$: 806.9 [100% M+Na]$^+$

^{1}H NMR $_{(CDCl_3)}$**:** 7.32 (2H, s, OH), 7.06 (4H, s, Ar**H**), 6.85 (4H, s, Ar**H**), 4.17 (4H, d, J=12.5, Ar**CH_2**Ar), 3.37 (4H, d, J=12.5, Ar**CH_2**Ar), 4.10 (4H, t, CN**CH_2**CH_2), 3.03 (4H, t, O**CH_2**CH_2), 2.38-2.30 (4H, m, CH_2**CH2**CH2),1.28 (18H, s, **t-But**), 0.96 (18H, s, **t-But**)

^{13}C-NMR $_{(CDCl_3)}$**:** 150.3, 148.8, 147.6, 142.1, 132.5, 127.5, 125.8, 125.3, 119.4, 73.3, 34.0, 33.8, 31.8, 31.6, 31.0, 26.6, 14.2

FTIR ν_{max} $_{(cm^{-1})}$**:** 2246 (stretch **CN**)

(solid state, selected)

***p-tert*-Butyl-[25,27-bis(aminobutoxy)]-26,28-dihydroxycalix[4]arene**

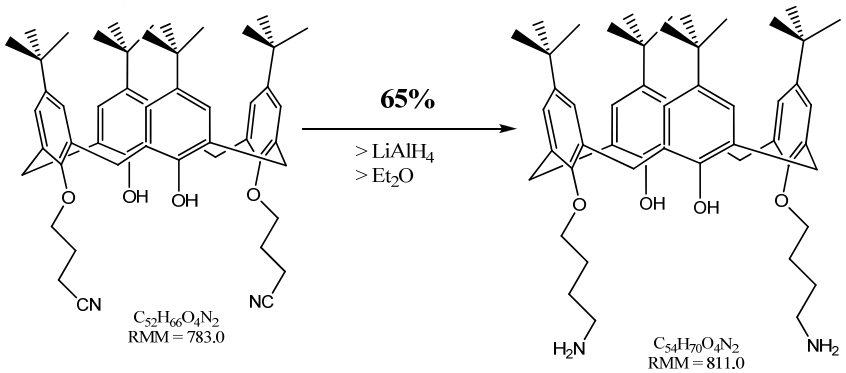

Into a 3 neck flask which had been flame dried and purged with nitrogen were added dry diethyl ether 50mL (stored over sodium wire) and the p-*tert*-butyl Bis[(Cyanopropoxy) dihydroxy]calix[4]arene (1.0g, 1.28mmol). Slurry of lithium aluminium hydride (700mg, mmol) in diethyl ether (5mL) was slowly added with vigorous stirring and the white suspension was heated at reflux (40°C) overnight. Then the reaction flask was immersed into an ice-water bath, the excess $LiAlH_4$ destroyed by careful addition of wet benzene (70mL) and water (10mL). The organic layer was decanted and the inorganic aluminium salts were rinsed with benzene (20mL) and evaporated to give (658mg, 65%) as white foam. (All attempts to removed benzene failed and was used immediately for the next step without further purification)

This compound could not be fully characterized because the extensive solvent inclusion!

^{1}H NMR ($CDCl_3$)**:** 7.36 (2H, s, **Benzene ~35%**), 7.04 (2H, s, Ar**H**), 6.82 (2H, s, Ar**H**), 4.30 (2H, d, J=13.0, Ar**CH_2**Ar), 3.99 (2H, t, J=12.8, CH_2**CH2**O), 3.31 (4H, d, J=13.2, Ar**CH_2**Ar), 2.86 (2H, t, J=4.5, CH_2**NH_2**), 2.10-2.01 (2H, m, CH_2**CH_2**CH_2), 1.89-1.79 (2H, m, CH_2**CH_2**CH_2), 1.28 (9H, s, **t-But**), 0.98 (9H, s, **t-But**)

^{13}C-NMR ($CDCl_3$)**:** 150.7, 149.9, 146.7, 141.4, 132.7, 128.3, 127.7, 125.4, 125.0, 76.2, 42.0, 33.9, 33.8, 31.7, 31.7, 31.0, 30.3, 27.4

***p-tert*-Butyl-25,27-[pyridine-bis(2,6-carbonylaminobutoxy)]-26,28-dihydroxy calix[4]arene**

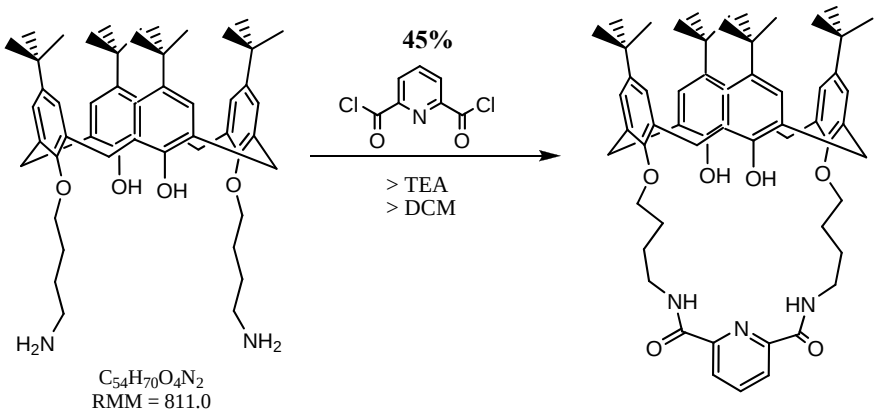

$C_{54}H_{70}O_4N_2$
RMM = 811.0

$C_{59}H_{75}O_6N_3$
RMM = 922.2

Into a 3 neck flask which had been flame dried and purged with nitrogen dry dichloromethane 70mL (fresh distilled over CaH_2) and the p-*tert*-butylBis[(Aminobutoxy)dihydroxy]calix[4]arene (500mg, 0.64mmol) were added with vigorous stirring. A second solution pyridine-2,6-dicarbonyl dichloride (130mg, 0.64mmol) and triethylamine (130mg, 1.28mmol) 0.24mL in dichloromethane 70mL was added dropwise and the brown mixture was left to stir for 2 days. Then the solvent was evaporated and the brown residue was taken up with dichloromethane (100mL) washing twice with HCl 1M (20mL). The organic phase was separated washed with brine (3 x 20mL) and dried over Na_2SO_4, filtered and evaporated to give a brown-pink material (498 mg). This solid was precipitated using hot hexan (25mL) to give after filtration a white powder (263 mg, 45%). TLC *Rf* = 0.70 (EtOAc/MeOH 9:1).

MP: > 300ºC

LRMS/ES$^+$ (M/Z): 944 [100% M+Na]$^+$

HRMS: Required 944.5545 founded 944.5545

^{1}H NMR ($CDCl_3$)**:** 8.37 (2H, d, J=7.68, Py**H**), 8.20 (2H, br t, J=6.03, N**H**), 8.02 (1H, t, J=8.05, Py**H**), 7.05 (4H, s, Ar**H**), 6.96 (2H, s, **OH**), 6.70 (2H, s, Ar**H**), 4.22 (4H, d, J=13.0, Ar**CH_2**Ar), 3.96 (4H, t, J=6.22, O**CH_2**CH_2), 3.67 (4H, q, J=6.60, CH_2**CH_2**NH), 3.28 (4H, d, J=13.1, Ar**CH_2**Ar), 2.16-1.98 (8H, m, (x2) CH_2**CH_2CH_2**CH_2), 1.30 (18H, s, t-**But**), 0.89 (18H, s, t-**But**)

^{13}C-NMR ($CDCl_3$)**:** 163.4, 150.4, 149.9, 148.7, 146.8, 141.7, 139.1, 132.0, 127.8, 125.4, 125.0, 124.8, 76.2, 39.3, 33.8 (x2), 31.7, 31.4, 31.0, 30.9, 27.8, 26.1

FTIR ν_{max} (cm^{-1})**:** 3355 (stretch **NH**), 1678 and 1665 (stretch **C=O**), 1530 (bend **NH**)

(solid state, selected)

***p-tert*-Butyl-[25,27-bis(cyanomethoxy)]-26,28-dihydroxycalix[4]arene**

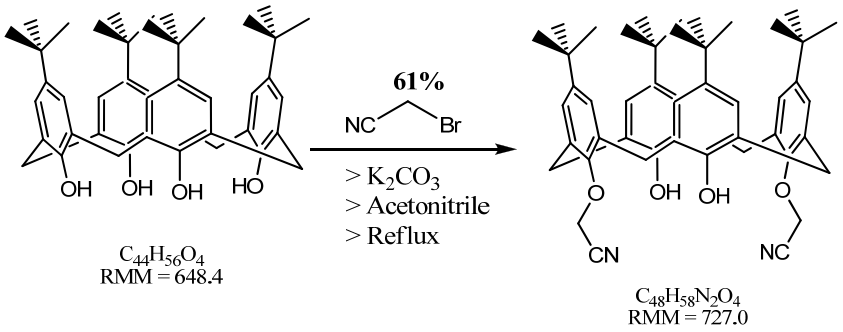

$C_{44}H_{56}O_4$
RMM = 648.4

$C_{48}H_{58}N_2O_4$
RMM = 727.0

Into a 3 neck flask which had been flame dried and purged with nitrogen were added dry acetonitrile 32mL (distilled over CaH_2 and stored on molecular sieves). The p-*tert*-butylcalix[4]arene (2.0g, 3.1mmol), potassium carbonate (515mg, 3.7mmol) and the bromo-acetonitrile (814mg, 6.8mmol) were added with vigorous stirring. The white suspension was heated at reflux (81-82°C) for 2 days. Then the solvent was evaporated and the brown residue was taken up with dichloromethane (80mL) washing twice with HCl 1M (20mL). The organic phase was separated washed with brine (3 X 20mL) and dried over Na_2SO_4, filtered and evaporated to give a light brown material (1.68g). This solid was precipitated using EtOH (60mL) to give after filtration a white powder (1.38g, 61%) (Lit[134] 57%). TLC *Rf* = 0.31 (DCM/MeOH 99:1).

MP: 270-272°C (reported > 290°C)[142]

LRMS/ES$^-$ (M/Z): 745 [100% M+H_2O], 789 [M+Na+AN]

^{1}H NMR ($CDCl_3$)**:** 7.12 (4H, s, Ar**H**), 6.72 (4H, s, Ar**H**), 5.55 (2H, s, **OH**), 4.81 (4H, s, O**CH_2**CN), 4.23 (4H, d, J=13.0, Ar**CH_2**Ar), 3.45 (4H, d, J=13.2, Ar**CH_2**Ar), 1.33 (18H, s, t-**But**), 0.88 (18H, s, t-**But**)

^{13}C-NMR ($CDCl_3$)**:** 149.9, 148.7, 148.5, 142.5, 131.8, 127.8, 126.2, 125.3, 115.0, 60.4, 33.9, 33.8, 31.7, 31.6, 30.8, 30.7

FTIR ν_{max} (cm^{-1})**:** 2286 cm^{-1} (stretch CN)

(solid state, selected)

p-*tert*-butyl-[25,27-bis(aminoethoxy)]-26,28-dihydroxycalix[4]arene

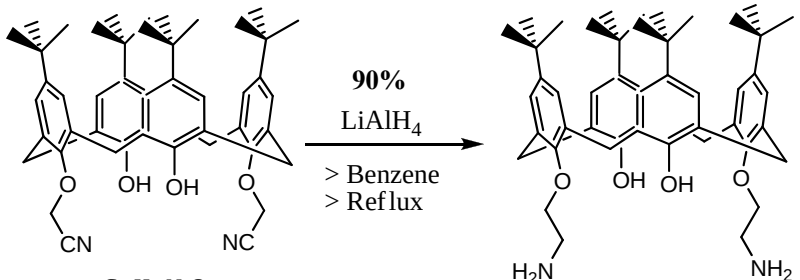

$C_{48}H_{58}N_2O_4$
RMM = 727.0

$C_{48}H_{66}N_2O_4$
RMM = 735.0

Into a 3 neck flask which had been flame dried and purged with nitrogen were added dry diethyl ether 68mL (stored over sodium wire) and the p-*tert*-butyl bis[(cyanomethoxy) dihydroxy] calix[4]arene (1.30g, 1.79mmol). Slurry of lithium aluminium hydride (536mg, 15.7mmol) in diethyl ether (5mL) was slowly added with vigorous stirring and the white suspension was heated at reflux (40°C) for 5h. Then the reaction flask was immersed into an ice-water bath, the excess $LiAlH_4$ destroyed by careful addition of wet benzene (70mL) and water (10mL). The organic layer was decanted and the inorganic aluminium salts were rinsed with benzene (20 mL) and evaporated to give a white foam (1.23g, 85%) (Lit.[129] 96%). TLC *Rf* = 0.1 (DCM/MeOH 99:1).

This compound could not be fully characterized because the extensive solvent inclusion!

^{1}H NMR ($CDCl_3$)**:** 8.34 (2H, s, **OH**), 7.35 (**Benzene** ~45%), 7.04 (4H, s, Ar**H**), 6.72 (2H, s, Ar**H**), 4.34 (4H, d, J=12.0, Ar**CH_2**Ar), 4.08 (4H, t, J=12.8, O**CH_2**), 3.37 (4H, d, J=12.9, Ar**CH_2**Ar), 3.31(4H, t ,J=4.6, **CH_2**NH_2) 1.25 (18H, s, t-**But**), 1.10 (18H, s, t-**But**).

^{13}C-NMR ($CDCl_3$)**:** 150.4, 149.2, 147.4, 141.9, 133.2, 128.3, 127.6, 125.8, 125.4, 78.7, 42.6, 34.1, 33.8, 32.1, 31.6, 31.5, 31.1

FTIR ν_{max} (cm^{-1})**:** unable to collect IR spectra because extensive solvent inclusion

(solid state, selected)

Glycine maleamic acid

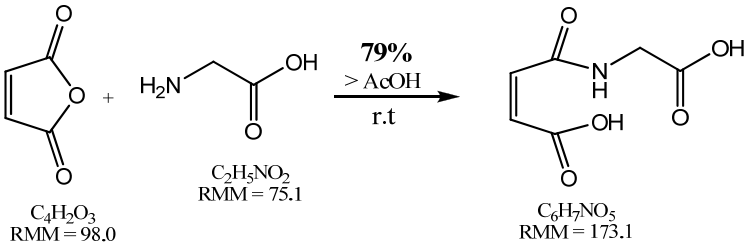

Into a flask acetic acid 48mL and glycine (3.0g, 41mmol) were added stirring at r.t. for 10 minutes. After this time maleic anhydride (4.0g, 41mmol) dissolved in 18mL of acetic acid was added stirring for 3 h at room temperature. A white precipitate was formed that was filtered off, washing with portion of water to give after dried in vacuum pump overnight (5.43g, 79%) (Lit[143] 96%) as white powder. TLC *Rf* = 0.10 ($CHCl_3$/MeOH 1:1).

MP: 191-192°C (reported > 187-188°C)[143]

LRMS/ES$^-$ (M/Z): 172.1 $(M-H)^-$

^{1}H NMR ($CDCl_3$)**:** 13.6 (2H, br s, **COOH**), 9.22 (1H, br t, **NH**), 6.46 (1H, d, J=12.4, CO**CH**=CH), 6.33 (1H, d, J=12.4, CH=**CH**COOH), 3.94 (2H, d, 5.8, NH**CH_2**COOH)

^{13}C-NMR ($CDCl_3$)**:** 171.3 (**COOH**), 170.0 (**C-1**), 166.2 (**C-4**), 134.2 (**C-3**), 131.0 (**C-2**), 41.9 (**C-5**)

FTIR ν_{max} (cm^{-1})**:** 3203 cm^{-1} (stretch **NH**), 1699 (stretch **C=O**), 1514 (bend **NH**)

(solid state, selected)

Preparation of maleimido glycine acid

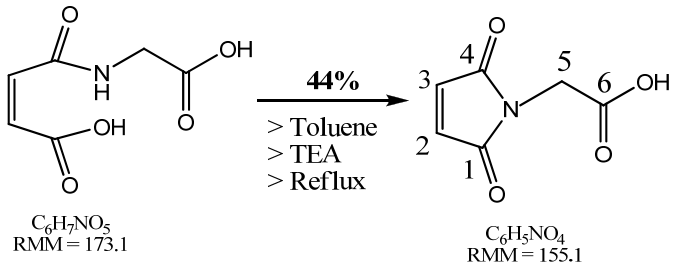

$C_6H_7NO_5$
RMM = 173.1

$C_6H_5NO_4$
RMM = 155.1

Into a 3 neck flask flame dried and purged with nitrogen 350mL of toluene (fresh distilled), glycine maleamic acid (2.0g, 12mmol) and triethylamine (3.5g, 35mmol) were added. This solution was refluxed with vigorous overhead stirring for 7 h with concomitant removal of formed water using a Dean-Stark separator, to give orange oil in bottom flask. The toluene was decanted away from the oil and evaporated to give light yellow oil 1.02g. It was washed with HCl 1M (20mL) until pH 2 extracted with portions of EtOAc (35mL x 3), dried over Mg SO_4 and filtered to give (0.818g 44%) (Lit[143] 46%) as white solid. TLC *Rf* = 0.46 ($CHCl_3$/MeOH 1:1).

MP: 93-95°C (reported 113-113.5°C)[143]

LRMS/ES$^-$ (M/Z)**:** 154.1 $[100\% M-H]^-$

^{1}H NMR ($CDCl_3$)**:** 10.2 (1H, br s, COOH), 6.80 (2H, s, **H-2,3**), 4.33 (2H, s, **H-5**)

^{13}C-NMR ($CDCl_3$)**:** 171.3 (**C-6**), 169.7 (**C-1,4**), 135.8 (**C-2,3**), 39.4 (**C-5**)

FTIR ν_{max} (cm^{-1})**:** 2282 cm^{-1} (stretch **OH**), 1681 (stretch **C-O conjugated**)

(solid state, selected)

***p-tert*-Butyl-[25,27-bis(maleonylmethyl-carbonylaminoethoxy)]-26,28-dihydroxy calix[4]arene**

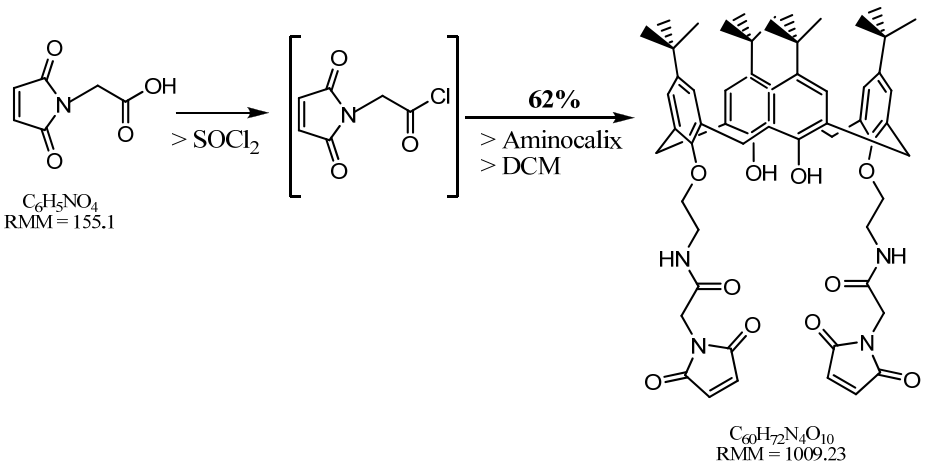

$C_6H_5NO_4$
RMM = 155.1

$C_{60}H_{72}N_4O_{10}$
RMM = 1009.23

Into a 3 neck flask which had been flame dried and purged with nitrogen thionyl chloride 5mL and maleonyl-glycine (120mg, 0.70mmol) were added. The yellow mixture was carried out to reflux T for 30 minutes. The solvent was removed and the yellow oil dissolved in dry dichloromethane 20mL. In second flask (flame dried and purged with nitrogen) dry dichloromethane 20mL and diamino-calix[4]arene (250mg, 0.34mmol), were added (solution B). Drop-wise, both solution A and B, were added in a flask containing dry dichloromethane 30mL and triethylamine (71mg, 0.097mL) in 1h stirring overnight. After the solvent was removed and the yellow material (523mg) taken up with dichloromethane 70mL washing with HCl 1M (2x25mL) and brine (2x25mL) dried over Na_2SO_4, filtered and evaporated to give a pale-yellow solid (213mg, 62%). TLC *Rf* = 0.94 (DCM/MeOH 1:1).

XRD (single crystal)**:** 2007Sot1687

MP: 238°C (decomposition)

Anal. Calcd. for $C_{60}H_{72}N_4O_{10}$: C 71.41, H 7.19, N 5.55, Found: C68.18, H 7.11, N 5.35.

LRMS/ES$^-$ (M/Z): 1032 $[100\% M+Na]^+$

^{1}H NMR ($CDCl_3$)**:** 9.03 (2H, s, **OH**), 8.51 (2H, br t, J=6.0, **NH**), 7.03 (8H, s, x2, **Ar**), 6.25 (4H, s, **CH=CH**), 4.28 (4H, s, CO**CH$_2$**N), 4.14-4.16 (8H, m, CH_2**CH$_2$**O and Ar**CH$_2$**Ar overlap), 3.98-3.97 (4H,m, CH_2**CH$_2$**NH), 3.38 (4H, d, J=13.1, Ar**CH$_2$**Ar), 1.22 (18H, s, **t-But**), 1.17 (18H, s, **t-But**)

^{13}C-NMR ($CDCl_3$)**:** 170.4, 166.7, 149.0, 148.6, 148.3, 143.1, 133.4, 133.2, 128.0, 126.3, 126.0, 76.1, 41.0, 39.5, 34.3, 34.0, 32.4, 31.5, 31.1

FTIR ν_{max} (cm^{-1})**:** 3355 (stretch **OH**), 1678 & 1665 (stretch **NHCO**), 1530 (bend **NH**)

(solid state, selected)

Ethoxyethyl-phtalamide

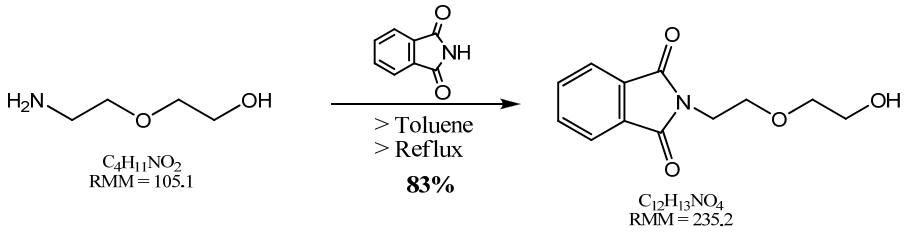

Into a 3 neck flask which had been flame dried and purged with nitrogen dry toluene 450 mL (fresh distilled over CaH_2) was added. The 2-(2-aminoethoxy)-ethanol (10.5 g, 0.1 mol), and phtalic anhydride (14.8 g, 0.1 mol) were added with vigorous stirring. The white suspension was heated at reflux (81-82°C) for 4 h and the water collected by dean-stark separator. Then the solution was cooled at room temperature, the solvent evaporated and dried in vacuum to give yellow oil (24.1 g). Crystallization from chloroform gave a pale yellow solid (20 g, 83%) (Lit[145] 85%). TLC *Rf* = 0.7 (DCM/MeOH 4:1).

MP: 64°C

LRMS/ES$^-$ (M/Z): 252 [100% M+H_2O]$^+$

^{1}H NMR ($CDCl_3$)**:** 7.81-7.66 (4H, m, Ar**H**), 3.88-3.84 (2H, m, **CH_2**N), 3.72-3.68 (2H, m, O**CH_2**CH_2N), 3.65-3.64 (2H, m, **CH_2**OH), 3.63-3.54 (2H, m, **CH_2**CH_2OH)

^{13}C-NMR ($CDCl_3$)**:** 168.2, 133.8, 131.7, 123.1, 72.1, 68.0, 61.3, 37.3

FTIR ν_{max} (cm^{-1})**:** 3200-3400 (stretch **OH**), 1701 (stretch **C=O**),

(solid state, selected)

Tosyl-ethoxyethyl-phtalamide

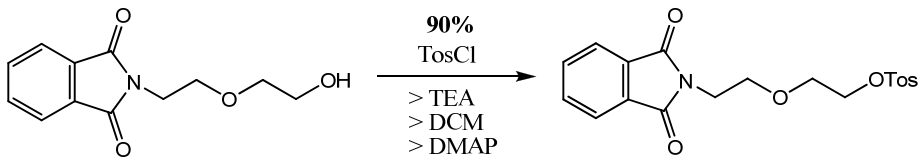

$C_{12}H_{13}NO_4$
RMM = 235.2

$C_{19}H_{20}NO_6S$
RMM = 390.1

Into a 3 neck flask which had been flame dried and purged with nitrogen were added dry dichloromethane 180mL (distilled over CaH_2 and stored on molecular sieves) and the (ethoxyethyl)-phtalamide (15g, 0.064mol). The triethylamine (10g, 0.1mol), tosyl chloride (12.2g, 0.064mol) and dimethyl-amino pyridine in catalytic amount (260mg, 0.002mol) were added with vigorous stirring. The pale yellow solution was refluxed for 16 h. After this time the mixture was washed with citric acid 10% (80 mL) and water (3 X 80 mL). The organic phase was separated dried over $MgSO_4$, filtered and evaporated to give a light orange solid (26.4g). This solid was precipitated using EtOH (70 mL) to give after filtration a white powder (24.9g, quantitative) (Lit[146] quantitative). TLC *Rf* = 0.85 (DCM/MeOH 4:1).

MP: 64-66°C (reported[146] not stated)

LRMS/ES$^-$ (M/Z): 412 [100% M+Na]$^+$

^{1}H NMR ($CDCl_3$)**:** 7.84-7.71 (2H, m, Pht**H**), 7.70-7.69 (2H, m, Ar**H**), 7.32-7.29 (2H, m, Tos**H**), 4.11-4.08 (2H, m, **CH_2**OSO_2), 3.84-3.80 (2H, m, **CH_2**N), 3.65 (4H, m, CH_2OCH_2), 2.42 (4H, s, **CH_3**)

^{13}C-NMR ($CDCl_3$)**:** 168.1, 144.7, 133.9, 132.9, 132.0, 129.7, 127.9, 123.1, 69.1, 68.0, 67.9, 37.0, 21.6

FTIR ν_{max} (cm^{-1})**:** 1346 (stretch **S=O**), 1002 (stretch **S-O**), 1705 (stretch **C=O**)

(solid state, selected)

***p-tert*-butyl-25,27-[bis(phtalamide-ethoxyethyl)]-26,28-dihydroxycalix[4]arene**

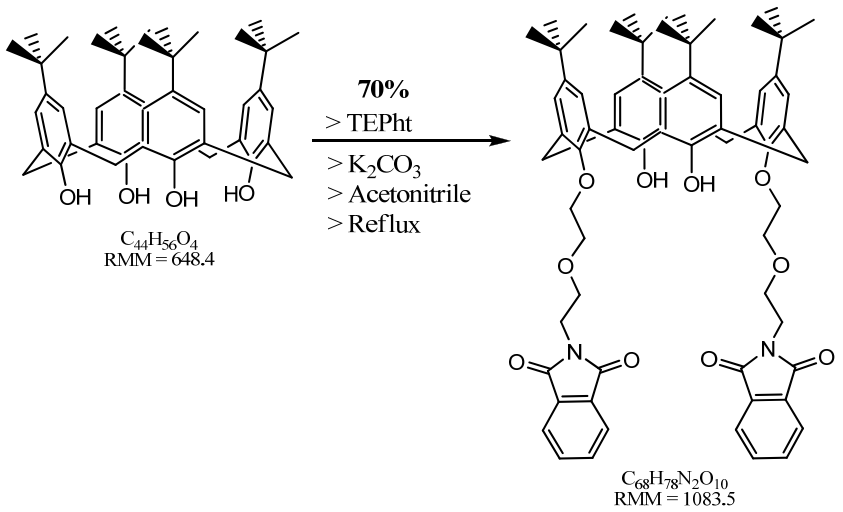

Into a 3 neck flask which had been flame dried and purged with nitrogen dry acetonitrile 32mL (distilled over CaH_2 and stored on molecular sieves) was added. The p-*tert*-butylcalix[4]arene (1.0g, 1.54mmol), potassium carbonate (434mg, 3.14mmol) and the tosyl-ethoxyethyl-phtalamide (1.6g, 3.85mmol) were added with vigorous stirring. The white suspension was heated at reflux (81-82°C) for 4 days. Then the solvent was evaporated and the off-white residue was taken up with HCl 1M (20 mL) extracting with dichloromethane (3 X 30 mL). The organic phase was separated washed with brine (3 X 20mL) and dried over Na_2SO_4, filtered and evaporated to give a light yellow material

(1.87 g). This solid was precipitated using EtOH (25mL) to give after filtration a white powder (1.17g, 70%) (Lit[147] 68%). TLC *Rf* = 0.68 (DCM/MeOH 4:1).

MP: 125-127°C

LRMS/ES$^-$ (M/Z): 1106.5 [100% M+Na]$^+$

^{1}H NMR ($CDCl_3$)**:** 7.54-7.46 (4H, m, Pht**H**), 7.45-7.43 (2H, m, Pht**H**), 6.81 (4H, s, calixAr**H**), 6.79 (4H, s, calixAr**H**), 4.07-3.97 (20H, m, 3xO**CH$_2$**, N**CH$_2$** and Ar**CH$_2$**Ar), 3.03 (4H, d, J=13.1, Ar**CH$_2$**Ar), 1.21 (18H, s, t-**But**), 1.01 (18H, s, t-**But**)

^{13}C-NMR ($CDCl_3$)**:** 168.5, 149.8, 149.4, 146.8, 140.9, 133.3, 131.8, 127.7, 125.3, 124.7 122.6, 74.9, 69.9, 68.4, 38.1, 33.9, 33.7, 31.6, 31.5, 31.0

FTIR ν_{max} (cm^{-1})**:** 3200-3300 (stretch **O-H**), 1708 (stretch **C=O**),

(solid state, selected)

***p-tert*-butyl-[25,27-bis(aminoethoxyethyl)]-26,28-dihydroxy]calix[4]arene**

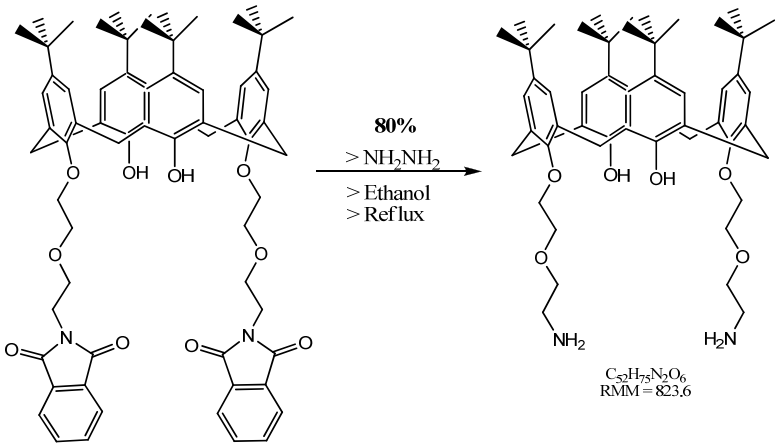

Into a 3 neck flask which had been flame dried and purged with nitrogen ethanol 25mL, the p-*tert*-butyl-Bis[(phtalamide-ethoxyethyl)dihydroxy]calix[4]arene (1.13g, 1.04mmol) and hydrazine monohydrate (516mg, 10.3mmol, 0.5mL) were added. The white suspension was heated at reflux (80°C) for 15h. Then the reaction flask was immersed into an ice-water bath, the excess hydrazine destroyed by careful addition of water (70

mL) extracting with dichloromethane (3 X 40 mL). The organic phase was dried over Na2SO4 filtered and evaporated leave white foam (6.81 mg, 80%) (Lit[147] 100%). TLC *Rf* = 0.69 (Chloroform/MeOH 1:1).

MP: 178-180°C (reported[147] not stated)

LRMS/ES$^+$ (M/Z): 824 [100% M+H]$^+$, 412 [58% M/2]$^+$

^{1}H-NMR ($CDCl_3$): 7.04 (4H, s, Ar**H**), 6.79 (4H, s, Ar**H**), 4.36 (4H, d, J=13.0 Hz, Ar**CH_2**Ar), 4.18-4.16 (4H, m, OCH_2**CH_2**O), 3.96-3.93 (4H, m, OCH_2**CH_2**O), 3.68 (4H, t, J=4.6 Hz, O**CH_2**CH_2NH_2), 3.29 (4H, d, J=13.0 Hz, Ar**CH_2**Ar), 2.96 (4H, br t, **CH_2**NH_2), 1.29 (18H, s, t-**But**), 0.95 (18H, s, t-**But**)

^{13}C-NMR ($CDCl_3$)**:** 150.4, 149.7, 146.8, 141.4, 132.6, 127.8, 125.5, 125.0, 75.2, 73.3 69.7, 41.9, 33.9, 33.8, 31.7, 31.5, 31.0

FTIR ν_{max} (cm^{-1})**:** 3321 (stretch **N-H**), 1483 (bend **N-H**), 1122 (stretch **C-N**)

(solid state, selected)

Open-cage fullerene 8 membered-ring (8m)

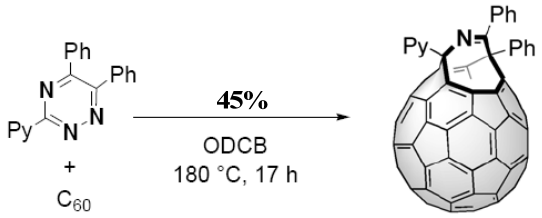

$C_{80}H_{15}N_2$
RMM = 1003.2

Into a 3 neck flask which had been flame dried and purged with nitrogen were added dry *o*-dichlorobenzene 120mL (distilled over CaH_2 and stored on molecular sieves) fullerene C60 (1.5g, 2.08mol) and 3-(2-pyridil)-5,6-diphenyl-1,2,4-triazine (656mg, 2.11mol) were added refluxing for 17h. The solvent was removed and subject to flash column chromatography over silica gel. Elution with toluene gave un-reacted C60 (883mg, 42%) while the following elution with Toluene/Ethyl acetate 30:1, 25:1 and 20:1 gave open-cage fullerene derivative with 8-membered ring (980mg, 47%) as brown powder (Lit[180] 50%). TLC *Rf* = 0.47 (Toluene/Ethyl acetate 9:1).

MP: > 300°C

MS/Maldi Tof-LD$^+$ 1003 [$M^{+\cdot}$], 720 [C_{60} *laser re-closure*], 1057 [M+K]$^+$,

MS/ES$^+$ (M/Z): 1003 [12% M+H]$^+$, 1025 [100% M+Na]$^+$, 1057 [M+Na+MeOH]$^+$

^{1}H NMR ($CDCl_3$)**:** 8.68 (1H, m), 8.0-7.90 (2H, m), 7.76-7.69 (2H, m), 7.44-7.37 (2H, m)

HPLC (Toluene)**:** (retention time: 16 min)

FTIR ν_{max} (cm^{-1})**:** 1750 (stretch **C=N**)

(solid state, selected)

Open-cage fullerene 12 membered-ring (12m Major isomer)

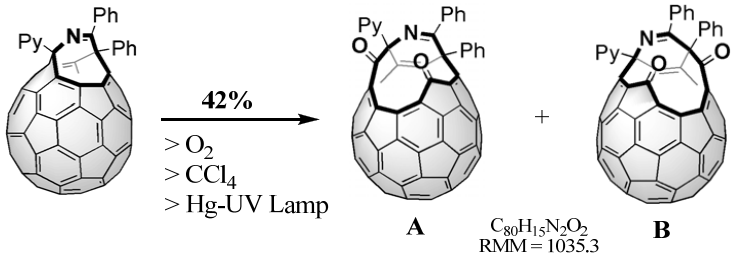

Into a special flask carbon tetrachloride 500mL was added and saturated with oxygen stream for 2h. After this time open-cage 8-membered ring (8m) (500mg, 0.5mmol) was added and the purple mixture irradiated by high-pressure mercury lamp (500W) from distance of 20 cm for overnight under air. The brown solution was evaporated and the black solid subject to flash column chromatography over silica gel. Elution with toluene/Ethyl acetate 30:1 gave minor isomer (**B**) open-cage 12-membered-ring (12m) (220mg, 38%) while the following elution with Toluene/Ethyl acetate 20:1 gave open-cage fullerene derivative major isomer (**A**) 12-membered ring (242mg, 47%) as brown powder (Lit[180] 42%). TLC major isomer *Rf* = 0.45 (Toluene/Ethyl acetate 9:1).

MP: > 300°C

MS/Maldi Tof-LD$^+$ 1035 [$M^{+\cdot}$], 1057 [M+Na]$^+$, 1073 [M+K]$^+$

MS/ES$^+$ (M/Z): 1035 [13% M+H]$^+$, 1057 [100% M+Na]$^+$, 1074 [40% M+K]$^+$

^{1}H NMR ($CDCl_3$)**:** 8.52 (1H, m), 8.37 (1H, m), 8.07-7.98 (3H, m), 7.82 (1H, m), 7.37-7.03 (8H, m)

HPLC (Toluene)**:** (retention time: 23 min)

FTIR ν_{max} (cm^{-1})**:** 1747, 1700 (stretch **C=O**)

(solid state, selected)

Open-cage fullerene 13 membered-ring (13m ATOCF)

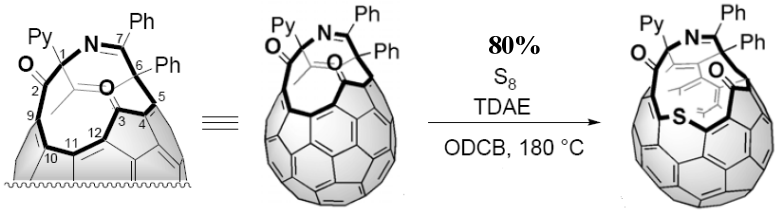

$C_{80}H_{15}N_2O_2$
RMM = 1035.3

$C_{80}H_{15}N_2O_2S$
RMM = 1067.1

Into a 3 neck flask which had been flame dried and purged with nitrogen dry *o*-dichlorobenzene 180mL (distilled over CaH_2 and stored on molecular sieves) open-cage fullerene 12-membered ring (12m) (434mg, 0.42mmol) heating until 180°C. Then tetrakis(dimethylamino)ethylene (84mg, 0.42mmol) were added and refluxed for 2h resulting in a dark red solution. The solvent was removed and the brown powder subject to flash column chromatography over silica gel. Elution in gradient with Toluene/Ethyl acetate 100:1, 30:1, 25:1 and 20:1 gave open-cage fullerene derivative with 13-membered ring (aza-thio-open-cage-fullerene ATOCF) (324mg, 72%) as brown powder (Lit[180] 73%). TLC *Rf* = 0.48 (Toluene/Ethyl acetate 9:1).

MP: > 300°C

MS/Maldi Tof-LD$^+$ 1067 [$M^{+\cdot}$], 960 [M-Py-CO (x2)], 1089 [M+Na]$^+$, 1105 [M+K]$^+$

MS/ES$^+$ (M/Z): 1067 [51% M+H]$^+$, 1089 [100% M+Na]$^+$, 1105 [14% M+K]$^+$

FTIR ν_{max} (cm^{-1})**:** 1740 (stretch C=O)

(solid state, selected)

Open-cage fullerene H_2@13 membered-ring (H_2@ATOCF)

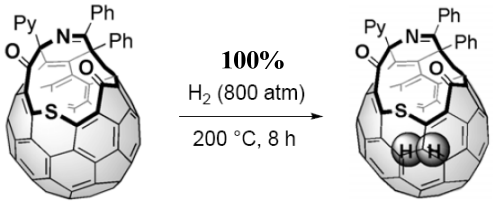

$C_{80}H_{15}N_2O_2S$
RMM = 1067.1

$C_{80}H_{17}N_2O_2S$
RMM = 1069.3

A powder of ATOCF (1000mg, 0.94mmol) light wrapped in a aluminium foil was placed in a special high pressure cell (see Figure 146) and left overnight under hydrogen at 800 bar and 200ºC. After this time it was cooled at room temperature to give quantitative H_2@ATOCF. The same result was obtained using a different high pressure cell (insertion performed from Prof. Yasujiro Murata in Japan sending our sample) at 1,410 atm 200ºC for 12h as brown powder (Lit[182] 100%). TLC *Rf* = 0.48 (Toluene/Ethyl acetate 9:1).

MP: > 300°C

MS/Maldi Tof-LD$^+$ 1069 [$M^{+\cdot}$], 1091 [M+Na]$^+$, 1107 [M+K]$^+$, 960 [M-Py-CO (x2)]

MS/ES$^+$ (M/Z)**:** 1069 [22% M+H]$^+$, 1091 [100% M+Na]$^+$, 1107 [23% M+K]$^+$

^{1}H NMR ($ODBC\_d_4$)**:** 8.60 (1H, m), 8.23 (1H, m), 8.18-8.15 (2H, m), 8.02 (1H, m), 7.53 (1H, m), 7.36 (7H, m), 7.30-7.25 (3H, m), 7.04-6.88 (4H, m) **-7.23 (2H, s, Hydrogen in C_{60})**

FTIR ν_{max} (cm^{-1})**:** 1740 (stretch C=O)

(solid state, selected)

Open-cage fullerene 13 membered-ring sulfoxide (H_2@13mSO_3)

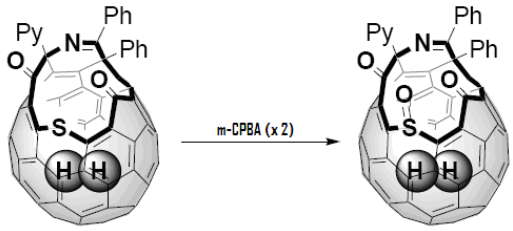

$C_{80}H_{17}N_2O_2S$
RMM = 1067.1

$C_{80}H_{17}N_2O_3S$
RMM = 1084.2

Into a 3 neck flask which had been flame dried and purged with nitrogen carbon disulphite 250mL, open-cage fullerene H_2@13-membered ring (H_2@13m) (200mg, 0.19mmol) and m-chloroperbenzoic acid (86.7mg, 0.5mmol) were added and stirred at room temperature overnight. The solvent was removed and the brown powder subject to flash column chromatography over silica gel. Elution in gradient toluene/EtOAc 30:1, 20:1 and 10:1 gave the open-cage fullerene derivative H_2@13-membered ring (H_2@13mSO_3) (182mg, 89%) as dark brown powder (Lit[180] 100%). TLC *Rf* = 0.18 (Toluene/Ethyl acetate 9:1).

Compound extremely insoluble in all organic solvents, characterized only by MS/Maldi Tof-LD$^+$ and X-ray crystal structure!

XRD (single crystal)**:** 2008Sot1189

MP: > 300°C

MS/Maldi Tof-LD$^+$ 1084 (m/z)

MS/ES$^+$ (M/Z): 1084 $(M+H)^+$, 1107 $(M+Na)^+$, 1123 $(M+K)^+$ (***poor solubility***)

FTIR ν_{max} (cm^{-1})**:** 1746 (stretch **C=O**) and 1073 (stretch **S=O**)

(solid state, selected)

Open-cage fullerene H_2@12 membered-ring (H_2@12m)

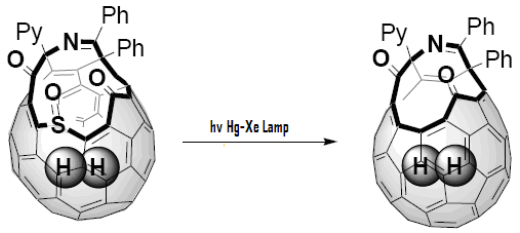

$C_{80}H_{17}N_2O_3S$
RMM = 1084.1

$C_{80}H_{17}N_2O_2$
RMM = 1037.3

Into a special flask benzene/Ethyl acetate 20:1 250mL was added degassing with nitrogen for 2h. After this time open-cage H_2@13-membered ring (H_2@13mSO_3) (50mg, 0.046mmol) was added and the brown mixture irradiated by high-pressure mercury lamp (500W) for 4h. The brown solution was evaporated and subject to flash column chromatography over silica gel. Elution with Toluene/Ethyl acetate 25:1 gave the desired compound (H_2@12m) (17mg, 36%) while the following elution with Toluene/Ethyl acetate 10:1 gave un-reacted open-cage fullerene derivative (H_2@13mSO_3) (10mg, 21%) as brown-red powder (Lit[182] 42%). TLC *Rf* = 0.45 (Toluene/Ethyl acetate 9:1).

MP: > 300°C

MS/Maldi Tof-LD$^+$ 1037 (m/z)

MS/ES$^+$ (M/Z): 1037 $(M+H)^+$, 1059 $(M+Na)^+$, 1175 $(M+K)^+$

^{1}H NMR (ODBC_d_4)**:** 8.57 (1H, m), 8.40 (1H, m), 8.10-7.99 (3H, m), 7.82 (1H, m), 7.40-7.35 (4H, m), 7.27-7.07 (4H, m), **-5.78 (2H, s, Hydrogen in C_{60})**

HPLC (Toluene)**:** (retention time: 23 min)

FTIR ν_{max} (cm^{-1})**:** 1747, 1700 (stretch C=O)

(solid state, selected)

Open-cage fullerene 8-membered-ring (H_2@8m)

$C_{80}H_{17}N_2O_2$
RMM = 1037.3

$C_{80}H_{17}N_2$
RMM = 1005.1

Into a 3 neck flask which had been flame dried and purged with argon zinc as sandy (300mg, 4.87mmol) and dry tetrahydrofuran 10mL. Cooling at 0ºC titanium chloride (IV) dropwise (250µL, 2.28mmol) was added and heated at 81-82ºC for 2h. A tenth portion of the black slurry 0.4mL was added to a stirred solution of H_2@12m (20mg, 0.019mmol) in 4mL of *o*-dichlorobenzene at room temperature under argon atmosphere. After heating at 80ºC for 1.5h the brown-red mixture was diluted with carbon disulphite (50mL) washing with $NaHCO_3$ saturated solution (20mL), brine (20mL). The organic layer was dried over $MgSO_4$ and evaporated under vacuum to give a brown solid and subject to flash column chromatography over silica gel. Elution with Toluene/Ethyl acetate 20:1 gave open-cage fullerene derivative with 8-membered ring H_2@8m (19mg, 89%) as brown powder (Lit[182] 88%). TLC *Rf* = 0.38 (Toluene/Ethyl acetate 9:1).

MP: > 300°C

MS/Maldi Tof-LD$^+$ 1005 (m/z)

MS/ES$^+$ (M/Z): 1005 $(M+H)^+$, 1027 $(M+Na)^+$, 1105 $(M+K)^+$

^{1}H NMR (ODBC_d_4)**:** 8.74 (1H, m), 8.04-7.92 (2H, m), 7.80 (1H, m), 7.72 (4H, m), 7.48-7.39 (2H, m), 7.29-7.12 (7H, m), **-2.93 (2H, s, Hydrogen in C_{60})**

HPLC (Toluene)**:** (retention time: 16 min)

FTIR ν_{max} (cm^{-1})**:** 1748 (stretch **C=N**)

(solid state, selected)

Fullerene ($H_2@C_{60}$)

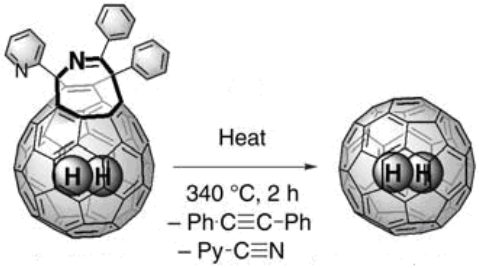

A powder of $H_2@8m$ (20mg, 0.020mmol) light wrapped in a aluminium foil was placed in a long glass-ware tube which was vacuumed for 2h. After this time it was heated with an electric furnace at 350-400C for 2h. The resulting sticking powder was dissolved with carbon disulphite and passed through a glass tube packed with silica gel to afford $H_2@C_{60}$ (8.3mg, 58%) contaminated with empty fullerene C_{60}. The compound was dried and dissolved in 10mL of toluene for recycling HPLC (two columns connected in series with toluene as mobile phase) purification to give pure $H_2@C_{60}$ (3mg, 21%) as brown powder (Lit[182] 90%). TLC *Rf* = 0.92 (Toluene/Ethyl acetate 9:1).

MP: > 300°C

MS/Maldi Tof-LD$^+$ 722 (m/z)

MAS/NMR: -1.3 ppm (**Hydrogen in C_{60}**)

HPLC (Toluene)**:** (retention time: 26 min)

tert-Butyl-(hydroxyethoxy)-ethylamino acetate

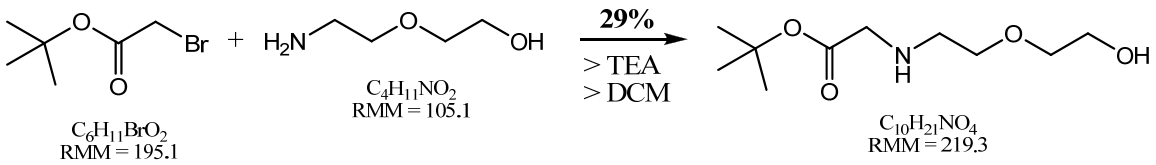

$C_6H_{11}BrO_2$
RMM = 195.1

$C_4H_{11}NO_2$
RMM = 105.1

$C_{10}H_{21}NO_4$
RMM = 219.3

Into a 3 neck flask which had been flame dried and purged with nitrogen dry dichloromethane 90mL (distilled over CaH_2 and stored on molecular sieves) was added. 2-(2-Aminoethoxy)-ethanol (2.63g, 35mmol), and triethylamine (2.53g, 18mmol) were added with vigorous stirring. Then *tert*-butylbromoacetate (3.10g, 15.9mmol) dissolved in 10mL of dry dichloromethane were added dropwise in 1h stirring at room temperature for 4h. The solvent was evaporated washing with water (3x40 mL) and brine (2x50mL) dried over Na_2SO_4, filtered and evaporated to give yellow oil (2.60g). Purification by flash column chromatography using Ethyl acetate/Methanol 4:1 gave clear colourless oil (1.56g, 29%). TLC *Rf* = 0.32 (EtOAc/MeOH 4:1).

HRMS: Required 242.1363 Founded 242.1364

MS/ES$^-$ (M/Z): 220.3 $(M+H)^+$

^{1}H NMR ($CDCl_3$)**:** 3.71-3.68 (2H, m), 3.60-3.54 (4H, m), 3.31 (2H, s), 2.80-2.77 (4H, m), 1.44 (9H, s)

^{13}C-NMR ($CDCl_3$)**:** 171.5, 81.3, 72.3, 70.2, 61.6, 51.3, 48.7, 28.0

FTIR ν_{max} (cm^{-1})**:** 3500-3100 (stretch **OH**), 1731 (stretch **C=O**)

(solid state, selected)

N-2-(2-aminoethoxy-ethanol)-glycine

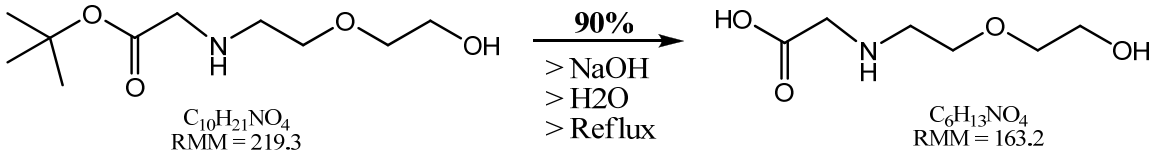

$C_{10}H_{21}NO_4$
RMM = 219.3

$C_6H_{13}NO_4$
RMM = 163.2

Into a 1 neck flask NaOH 1M solution 5mL *tert*-butylalchool (200mg, 0.91mmol) were added refluxed overnight. After this time the solution was acidify by HCl 1M until pH=2 and the solvent removed to leave a off-white solid. The white material was washed with cold ethanol and evaporated in buchi to leave a white powder (134mg, 90%) which was used for the next step without further purification. TLC *Rf* = 0.32 (EtOAc/MeOH 4:1).

HRMS: Required 164.0917 Founded 164.0918

MS/ES$^-$ (M/Z): 162 $(M-H)^-$

^{1}H NMR ($DMSO.d_6$)**:** 9.26 (1H, br s), 3.91 (2H, s), 3.74 (2H, t, J=5.6), 3.57-3.46 (4H, m), 3.18 (2H, t, J=4.9)

^{13}C-NMR ($CDCl_3$)**:** 168.9, 73.1, 66.3, 60.9, 47.9, 47.2

FTIR ν_{max} (cm^{-1})**:** 3250 (stretch **NH** II amine), 1726 (stretch **C=O**), 1056 (stretch **C-O**)

(solid state, selected)

Fullero pyrrolidine ethoxyethanol

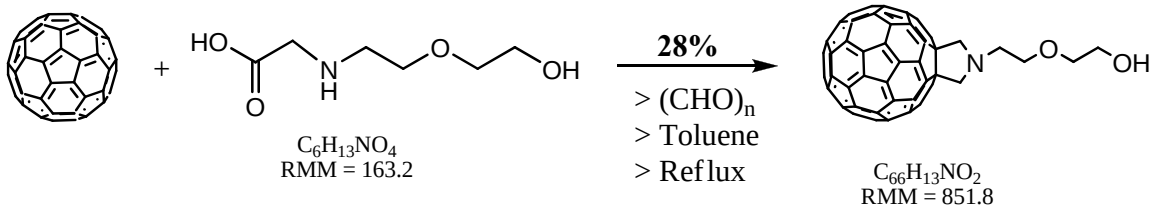

$C_6H_{13}NO_4$
RMM = 163.2

$C_{66}H_{13}NO_2$
RMM = 851.8

Into a 3 neck flask which had been flame dried and purged with nitrogen dry toluene 90mL (distilled over CaH_2 and stored on molecular sieves) and fullerene C_{60} (125mg, 0.17mmol), ethoxyethanol glycine (29mg, 0.18mmol) and *para*-formaldehyde (16mg, 0.54mmol) were added refluxing for 2h. The brown solution was loaded in a column and purified by flash chromatography using toluene to remove the un-reacted fullerene C_{60} and toluene/ethyl acetate 1:1 to isolate the desiderate compound as brownish powder (41mg, 28%). (Lit[174] 39%). TLC *Rf* = 0.36 (Toluene/EtOAc 1:1).

MS/Maldi Tof-LD$^+$: 851.8 ($M^{\cdot+}$)

^{1}H NMR ($CDCl_3$)**:** 4.53 (4H, s), 4.09 (2H, t, J=5.5), 3.89-3.80 (4H, m), 3.39 (2H, t, J=5.5)

FTIR ν_{max} (cm^{-1})**:** 2957 cm^{-1} (stretch **OH**), 1036 (stretch **C-O ether**)

(solid state, selected)

Fullero-pyrrolidine maleimide ethylenglycol

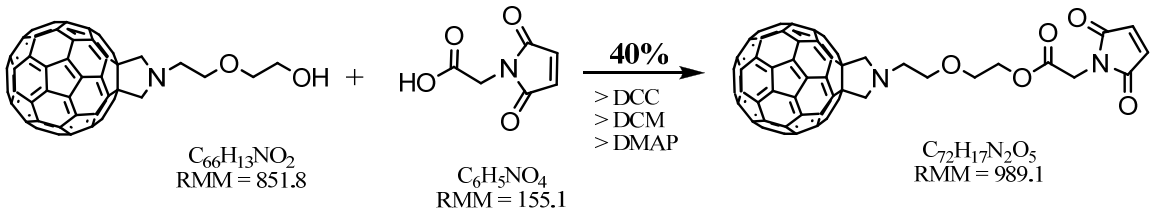

Into a 3 neck flask which had been flame dried and purged with nitrogen dry DCM 20mL (distilled over CaH_2 and stored on molecular sieves) maleonyl-glycine (15.7mg, 0.0.094mmol) and *DCC* (19.7mg, 0.094mmol) were added stirring for 30 min. A solution of fulleropyrrolidine (20mg, 0.023mmol) and DMAP (1.17mg, 0.009mmol) in 40mL of dry DCM was added drop-wise stirring overnight. After this time the brown-red mix was evaporated to give a brown solid 48mg that was loaded in a column and purified by flash chromatography using toluene/EtOAc 4:1 to isolate the desiderate compound as brownish powder (9mg, 40%). TLC *Rf* = 0.61 (Toluene/EtOAc 1:1).

MS/Maldi Tof-LD$^+$: 989.0 [$M^{+\cdot}$]

^{1}H NMR ($CDCl_3$)**:** 6.78 (2H, s, **CH=CH**), 4.52 (4H, s, **CH_2-N pyrrolidine**), 4.46-4.43 (2H, m, **CH_2**CH_2), 4.07-4.03 (2H, t, J=5.5, **CH_2**CH_2), 3.90-3.87 (2H, s, **CH_2**COO), 3.36 (2H, t, J=5.5, **CH_2**CH_2)

^{13}C-NMR ($CDCl_3$)**:** unable to collect NMR spectrum.

FTIR ν_{max} (cm^{-1})**:** 3200-3300 (stretch **OH**), 1708 (stretch **C=O**)

(solid state, selected)

6 References

(1) Bloch, F. *Phys. Rev.* **1946**, *70*, 460.

(2) Duer, M. *Introduction to Solid-State NMR Spectroscopy*; WileyBlackwell, **2004**.

(3) Castellani, F.; van Rossum, B.; Diehl, A.; Schubert, M.; Rehbein, K.; Oschkinat, H. *Nature* **2002**, *420*, 98.

(4) Pektova, A. T. *Proc. Natl. Acad. Sci.* **2002**, *99*, 16742.

(5) Panesar, K. S.; Horsewill, A. J.; Cuda, F.; Carravetta, M.; Mamone, S.; Danquigny, A.; Grossel, M. C.; Levitt, M. H. *J. Chem. Phys.* **2008**, *128*, 144512.

(6) Navon, G.; Song, Y. Q.; Room, T.; Appelt, S.; Taylor, R. E.; Pines, A. *Science* **1996**, *271*, 1848.

(7) Hall, D. A.; Maus, D. C.; Gerfen, G. J.; Inati, S. J.; Becerra, L. R.; Dahlquist, F. W.; Griffin, R. G. *Science* **1997**, *276*, 930.

(8) Abragam, A. *Principles of Nuclear Magnetism*; Oxford Press, **1961**.

(9) Runge, V. M.; Clanton, J. A.; Lukehart, C. M.; Partain, C. L.; James, A. E. *Am. J. Roentgenol.* **1983**, *141*, 1209.

(10) Levitt, M. H.; Carravetta, M., *GB Patent*, WO/2005/101044, **2005.**

(11) Carravetta, M.; Johannessen, O. G.; Levitt, M. H.; Heinmaa, I.; Stern, R.; Samoson, A.; Horsewill, A. J.; Murata, Y.; Komatsu, K. *J. Chem. Phys.* **2006**, *124*.

(12) Caciuffo, R.; Galeazzi, R.; Horsewill, A. J.; Ikram, A.; Ugozzoli, F. *Phys. Rev. B* **1999**, *60*, 11867.

(13) Tanaka, K.; Takamoto, N.; Tezuka, Y.; Kato, M.; Toda, F. *Tetrahedron* **2001**, *57*, 3761.

(14) Fillaux, F.; Nicolai, B.; Paulus, W.; Kaiser-Morris, E.; Cousson, A. *Phys. Rev. B (Condensed Matter and Materials Physics)* **2003**, *68*, 224301-1-13.

(15) Murata, M.; Maeda, S.; Morinaka, Y.; Murata, Y.; Komatsu, K. *J. Am. Chem. Soc.* **2008**, *130*, 15800

(16) Szejtli, J. *Cyclodextrin Technology*, **1988**, Springer: New York.

(17) Lagona, J.; Mukhopadhyay, P.; Chakrabarti, S.; Isaacs, L. *Angew. Chem., Int. Ed.* **2005**, *44*, 4844.

(18) Gale, P. A.; Pavel, A. Jr.; Sessler, J. L. *Coord. Chem. Rev.* **2001**, *222*, 57.

(19) Gale, P. A.; Bates, G. W.; Light, M. E. *CrystEngComm* **2006**, *8*, 300.

(20) Rebek, J. *Angew. Chem., Int. Ed.* **2005**, *44*, 2068.

(21) Ripmeester, J. A.; Bagryanskaya, E. G.; Polovyanenko, D. N.; Coleman, A. W.; Udachin, K. A.; Ananchenko, S. A. *Chem. Commun.* **2008**, 223.

(22) Carravetta, M.; Levitt, M. H. In *Cryo-MAS Open Day* **2007**.

(23) Tamer, U.; Hanna, S. G.; Tonelli, A. E.; Marcus, A. H. *Cryst. Growth Des.* **2006**, *6*, 1113.

(24) Atwood, J. A.; Davies, J. E.; MacNicol, D.; Vogtle, D.; Lehn, J. M. *Comprehensive Supramolecular Chemistry*; Pergamon: Oxford, **1996**; Vol. 3.

(25) Plazanet, M.; Bartolini, P.; Torre, R. *J. Phy.: Condens. Matter.* **2007**, *19*, 205108.

(26) Freeman, W. A. *Acta Crystallogr., Sect. B: Struct. Sci.* **1984**, *40*, 382.

(27) Huang, W. H.; Zavalij, P. Y.; Isaacs, L. *Acta Crystallogr., Sect. E: Struct. Rep. Online* **2008**, *64*, O1321-U2425.

(28) Hoffmann, R.; Knoche, W.; Fenn, C.; Buschmann, H. J. *J. Chem. Soc. Faraday Trans.* **1994**, *90*, 1507.

(29) Gale, P. A.; Sessler, J. L.; Kral, V. *Chem. Commun.* **1998**, 1.

(30) Gale, P. A.; Sessler, J. L.; Lynch, V.; Sansom, P. I. *Tetrahedron Lett.* **1996**, *37*, 7881.

(31) Atwood, J. A.; MacGillivray, L. R. *Chem. Commun.* **1999**, 181.

(32) Manifar, T.; Rohani, S.; Jennings, M.; Hairsine, D.; Dance, I. *CrystEngComm* **2006**, *8*, 59.

(33) Chen, Y. S.; Hart, H. *J. Org. Chem.* **1989**, *54*, 2612.

(34) Song, Q. L.; Ho, D. M.; Pascal, R. A. *J. Am. Chem. Soc.* **2005**, *127*, 11246.

(35) Gomes, J.; Mallion, R. B. *Chem. Rev.* **2001**, *101*, 1349.

(36) Cizmeciyan, D.; Yonutas, H.; Karlen, S. D.; Garcia-Garibay, M. *Solid State Nucl. Magn. Reson.* **2005**, *28*, 1.

(37) Lecalve, N.; Pasquier, B.; Braathen, G.; Soulard, L.; Fillaux, F. *J. Phys. C Solid State* **1986**, *19*, 6695.

(38) Kaiser-Morris, E.; Cousson, A.; Paulus, W.; Fillaux, F. *Acta Crystallogr., Sect. E: Struct. Rep. Online* **2001**, *E57*, o1113.

(39) Kirstein, O.; Prager, M.; Johnson, M. R.; Parker, S. F. *J. Chem. Phys.* **2002**, *117*, 1313.

(40) Bloemberger, N.; Purcell, E. M.; Pound, R. V. *Phys. Rev.* **1948**, *73*, 679.

(41) Sharp, R. R. *Paramagnetic NMR*; The Royal Society of Chemistry, **2003**; Vol. 32.

(42) Bretonniere, Y.; Mazzanti, M.; Pecaut, J.; Dunand, F. A.; Merbach, A. E. *Inorg. Chem.* **2001**, *40*, 6737.

(43) Aime, S.; Botta, M.; Crich, S. G.; Giovenzana, G. B.; Jommi, G.; Pagliarin, R.; Sisti, M. *J. Chem. Soc. Chem. Comm.* **1995**, 1885.

(44) Brasch, R. *Radiology* **1983**, *147*, 781.

(45) Panesar, S. K. PhD Thesis, University of Nottingham, **2008** (Data Used with Permission).

(46) Levitt, M. H. *Spin Dynamics: Basic of Nuclear Magnetic Resonance*; Wiley, **2001**.

(47) Press, W. *Single-Particle Rotations in Molecular Crystals*; Springer-Verlag, **1981**.

(48) Miyazaki, T. *Atom Tunnelling Phenomena in Physics, Chemistry and Biology*; Spinger-Verlag Berlin, **2004**.

(49) Bell, R.P. *The Tunnel Effect in Chemistry;* Chapman and Hall, Inc. London, **1980**.

(50) Goldanskii, V.I.; Trakhtenberg, L.I.; Fleurov, V.N. *Tunneling Phenomena in Chemical Physics,* Gordon and Breach Sci. Publ., New York, **1989.**

(51) Kittel, C. *Introduction to Solid State Physics*, John Wiley & Sons, New York, **1966**.

(52) Cohen-Tannoudji C, Diu B, Laloe F. *Quantum Mechanics*, Wiley-VCH, Paris, **2005**.

(53) Horsewill, A. J. *Prog. Nucl. Magn. Reson. Spectrosc.* **1999**, *35*, 359.

(54) Horsewill, A. J.; Panesar, K. S.; Rols, S.; Johnson, M. R.; Murata, Y.; Komatsu, K.; Mamone, S.; Danquigny, A.; Cuda, F.; Maltsev, S.; Grossel, M. C.; Carravetta, M.; Levitt, M. H. *Phys. Rev. Lett.* **2009**, *102*, 4.

(55) Horsewill, A. J. *Prog. Nucl. Magn. Reson. Spectrosc.* **2008**, *52*, 170.

(56) Smyth, C. P. *Chem. Rev.* **1936**, *19*, 326.

(57) Purcell, E. M.; Torrey, H. C.; Pound, R. V. *Phys. Rev.* **1946**, *69*, 37.

(58) Haupt, J. *Naturforsch* **1971**, *26a*, 1578.

(59) Haupt, J. *Phys. Lett. A* **1972**, *A 38*, 389

(60) Prager, M.; Heidemann, A. *Chem. Rev.* **1997**, *97*, 2933.

(61) Haupt, J. *Zeitschrift Fur Naturforschung Part a-Astrophysik Physik Und Physikalische Chemie* **1971**, *A 26*, 1578.

(62) Nair, S.; Dimeo, R. M.; Neumann, D. A.; Horsewill, A. J.; Tsapatsis, M. *J. Chem. Phys.* **2004**, *121*, 4810.

(63) Heidemann A.; Magerl A.; Prager M.; Richter D.; and Springer T. *Quantum Aspects of Molecular Motions in Solids,* Springer-Verlag, Berlin Heidelberg **1987.**

(64) Tomaselli, M.; Degen, C.; Meier, B. H. *J. Chem. Phys.* **2003**, *118*, 8559.

(65) Colmenero, J.; Moreno, A. J.; Alegria, A. *Progr. Polym. Sci.* **2005**, *30*, 1147.

(66) Pedersen, C. J. *Angew. Chem., Int. Ed. Engl.* **1988**, *27*, 1021.

(67) Pedersen, C. J. *Fed. Proc.* **1968**, *27*, 1305.

(68) Lehn, J. M. *Supramolecular Chemistry: Concepts and Prospectives*; VCH, 1995.

(69) Francesconi, O.; Ienco, A.; Moneti, G.; Nativi, C.; Roelens, S. *Angew. Chem., Int. Ed.* **2006**, *45*, 6693.

(70) Atwood, J. L.; Steed, J. W. *Supramolecular Chemistry*; John Wiley & Sons, 2000.

(71) Cram, D. J. *Angew. Chem., Int. Ed.* **1988**, *27*, 1009.

(72) Davies, J. E. D. *J. Incl. Phenom. Mol.* **1998**, *32*, 499.

(73) Powell, H. M. *Research (London)* **1948**, *1*, 353.

(74) Vogtle, F.; Lohr, H. G.; Franke, J.; Worsch, D. *Angew. Chem., Int. Ed.* **1985**, *24*, 727.

(75) Severin, K. Image used with permission

(76) Frey, A. Image used with permission

(77) Metzeger, A.; Lynch, V.; Aslyn, E. V. *Angew. Chem., Int. Ed.* **1997**, *8*, 862.

(78) Severin, K. Image used with permission

(79) Severin K. Image used with permission

(80) Schneider, H.J.; Yatsmirsky, A. *Principles and Methods in Supramolecular Chemistry*, **1999**, Wiley-Blackwell: Chichester.

(81) Chang, S.K.; Hamilton, A.D. *J. Am. Chem. Soc.* **1988**, 110, 1318

(82) Severin, K. image used with permission

(83) Sarri, P.; Venturi, P. S. F.; Cuda, F.; Roelens, S. *J. Org. Chem.* **2004**, *69*, 3654.

(84) Hunter, C. A.; Sanders, J. K. M. *J. Am. Chem. Soc.* **1990**, *112*, 5525.

(85) Andreetti, G. D.; Ungaro, R.; Pochini, A. *J. Chem. Soc.,Chem. Commun.* **1979**, 1005.

(86) Schaefer, T. P.; Schneider, W. G. *J. Chem. Phys.* **1960**, *32*, 1218.

(87) Fujiwara, S.; Nakagawa, N. *Bull. Chem. Soc. Jpn.* **34**, *34*, 143.

(88) Grossel, M. C.; Cheetham, A. K.; Hope, D. A. O.; Lam, K. P.; Perkins, M. J. *Tetrahedron Lett.* **1979**, 1351.

(89) Klopman, G. *Chemical Reactivity and Reaction Paths*; Wiley-interscience New York, **1974**.

(90) Ungaro, R.; Pochini, A.; Andreetti, G. D.; Sangermano, V. *J. Chem. Soc., Perkin Trans. 2* **1984**, 1979.

(91) Andretti, G.; Ori, O.; Alfieri, A.; Pochini, A.; Ungaro, R. *J. Incl. Phenom.*, **1988**, 6, 523

(92) Nishio, M.; Umezawa, Y.; Hirota, M.; Takeuchi, Y. *Tetrahedron*, **1995**, 32, 88678

(93) Ungaro, R.; Pochini, A.; Andretti, G.D.; Domiano, P. *J. Chem. Soc., Perkin Trans. 2*, **1985**, 197.

(94) Gutsche, D. C. *Calixarenes: An Introduction*; RSC Publishing, 2nd edition, **2008**.

(95) Asfari, Z.; Bohmer, V.; Harrowfield, J.; Vincens, J. *Calixarenes 2001*; Kluwer Accademic Publishers, **2001**.

(96) Mandolini, L.; Ungaro, R. *Calixarenes in Action;* Imperial College Press, **2000**.

(97) Bohmer, V.; Vincens, J. *A Versatile Class of Macrocycle Compounds (Topic in Inclusion Science)*; Springer, **1990**.

(98) Meijere, d. A. *Angew. Chem., Int. Ed. Engl.* **2005**, *44*, 7836.

(99) Bretslow, R.; Dong, S. D. *Chem. Rev.* **1998**, *98*, 1997.

(100) Gutsche, C. D.; Iqbal, M.; Stewart, D. *J. Org. Chem.* **1986**, *51*, 742.

(101) Gutsche, C. D.; Muthukrishnan, R. *J. Org. Chem.* **1978**, *43*, 4905.

(102) Gutsche, C. D.; Dhawan, B.; No, K. H.; Muthukrishnan, R. *J. Am. Chem. Soc.* **1981**, *103*, 3782.

(103) Gutsche, D. C.; Dhawan, B.; Levine, J. L.; Hynun No, K.; Bauer, L. J. *Tetrahedron* **1983**, *39*, 409.

(104) Gutsche, D. C.; Bauer, L.J. *J. Am. Chem. Soc.* **1985**, 107, 6052.

(105) Kammerer, S.; Happel, G.; Caesar, F. *Makromol. Chem.* **1972**, *162*, 179.

(106) Bauer, L. J.; Gutsche, C. D. *J. Am. Chem. Soc.* **1985**, *107*, 6063.

(107) Arduini, A.; Pochini, A.; Reverberi, S.; Ungaro, R. *J. Chem. Soc., Chem. Comm.* **1984**, 981.

(108) Gutsche, C. D.; Bauer, L. J. *Tetrahedron Lett.* **1981**, *22*, 4763.

(109) Andreetti, G. D.; Calestani, G.; Ugozzoli, F.; Arduini, A.; Ghidini, E.; Pochini, A.; Ungaro, R. *J. Incl. Phenom. Macro.* **1987**, *5*, 123.

(110) Gutsche, C. D.; Gutsche, A. E.; Karaulov, A. I. *J. Incl. Phenom. Macro.* **1985**, *3*, 447.

(111) De Namor, D.; Angela, F. *Pure & Appl. Chem.* **1993**, *65*, 193.

(112) Cunningham, I. D.; Woolfall, M. *J. Org. Chem.* **2005**, *70*, 9248.

(113) Ripmeester, J. A.; Brouwer, D. H.; Alavi, S. *Phys. Chem. Chem. Phys.* **2008**, *10*, 3857.

(114) Caciuffo, R.; Amoretti, G.; Carlile, C. J.; Fillaux, F.; Francescangeli, O.; Prager, M.; Ugozzoli, F. *Physica B* **1994**, *202*, 279.

(115) Ungaro, R.; Pochini, A.; Andreetti, G. D.; Domiano, P. *J. Chem. Soc., Perkin. Trans. 2* **1985**, 197.

(116) Weber, E.; Josel, H. P. *J. Incl. Phenom. Macro.* **1983**, *1*, 79.

(117) Atwood, J. L.; Barbour, L. J.; Agoston, j.; Shottel, B. L. *Science* **2002**, *298*, 1000.

(118) Atwood, J. L. *Chem. Commun.* **2005**, 4420.

(119) Andretti, G. D.; Ungaro, R. *J. Chem. Soc., Perkin Trans. 2* **1983**, 1773-1779.

(120) Atwood, J. L. *Chem. Commun.* **2005**, 5272.

(121) Gutsche, D. C.; Iqbal, M.; Stewart, D. *J. Org. Chem.* **1986**, *51*, 742.

(122) Gutsche, D. C.; Munch, J. H. *Org. Synth.* **1990**, *68*, 243.

(123) Zheng, Y. S.; Huang, Z. T. *Synth. Commun.* **1997**, *27*, 1237.

(124) L., W. k. *Macroscale and Microscale Organic Experiment* Houghton Mifflin: Boston, **1994**.

(125) Arduini, A.; Fabbi, M.; Mantovani, M.; Mirone, L.; Pochini, A.; Secchi, A.; Ungaro, R. *J. Org. Chem.* **1995**, *60*, 1454.

(126) Gutsche, C.D.; *Calixarenes Revisited*; RSC Publishing, **1998**

(127) Ouselati, I. *Tetrahedron* **2007**, *63*, 10840.

(128) Dijkstra, P.J.; Brunink, J.A; Bugge, K.E.; Reinhoudt, D.N.; Harkema, S.; Ungaro, R.; Ugozzoli, F.; Ghidini, E. *J. Am. Chem. Soc.* **1989**, 111, 7567

(129) Dondoni, A.; Hu, X.; Marra, A.; Banks, H.D. *Tetrahedron Lett.* **2001**, 42, 3295

(130) Arduini, A.; Pochini, A.; Reverberi, S.; Ungaro, R. *J. Chem. Soc., Chem. Commun.* **1984**, 981.

(131) Arnaud-Neu, F.; Barboso, S.; Casnati, A.; Pinalli, A.; Schwing-Weill, M. J.; Ungaro, R. *New J. Chem.* **2000**, *24*, 967.

(132) Bottino, F.; Giunta, L.; Pappalardo, S. *J. Org. Chem.* **1989**, 54, 5407.

(133) Papparardo, S.; Giunta, L.; Foti, M.; Ferguson, G.; Gallagher, J.F.; Kaiter, B. *J. Org. Chem.* **1992**, 57, 2611.

(134) Beer, P. D.; Gale, P. A.; Smith, D. K. *Supramolecular Chemistry*; Oxford University Press, **1999**

(135) Beer, P. D.; Drew, M. G. B.; Gradwell, K. *J. Chem. Soc., Perkin Trans. 2* **2000**, 519.

(136) Scheerder, J.; Fochi, M.; Engbersen, J. F. J.; Reinhoudt, D. N. *J. Org. Chem.* **1994**, *59*, 7815.

(137) Szemes, F.; Hesek, D.; Chen, Z.; Dent, S. W.; Drew, M. G. B.; Goulden, A. J.; Graydon, A. R.; Grieve, A.; Mortimer, R. J.; Wear, T.; Weightman, J. S.; Beer, P. D. *Inorg. Chem.* **1996**, *35*, 5868.

(138) Iqbal, K. S. J.; Allen, M. C.; Fucassi, F.; Cragg, P. J. *Chem. Commun.* **2007**, 3951.

(139) Iqbal, K. S. J.; Cragg, P. J. *Dalton T.*, **2007**, 26.

(140) Tanaka, Y.; Miyachi, M.; Kobuke, Y. *Angew. Chem. , Int. Ed.* **1999**, *38*, 504.

(141) Korchowiec, B.; Ben Salem, A.; Corvis, Y.; de Vains, J. B. R.; Korchowiec, J.; Rogalska, E. *J. Phys. Chem. B* **2007**, *111*, 13231.

(142) Collins, E.M.; Mckervey, A. M.; Madingan, E.; Moran, M.B.; Owens, M.; Ferguson, G.; Harris, S.J. *J. Chem. Soc. Perkin. Trans. I* **1991**, *51*, 3137.

(143) Rich, D. H.; Gesellchen, P. D.; Tong, A.; Cheung, A.; Buckner, C. K. *J. Med. Chem.* **1975**, *18*, 1004.

(144) Tan, S. D.; Chen, W. H.; Satake, A.; Wang, B.; Xu, Z. L.; Kobuke, Y. *Org. Biomol. Chem.* **2004**, *2*, 2719.

(145) Lown, J. W.; Koganty, R. R.; Joshua, A. V. *J. Org. Chem.* **1982**, *47*, 2027.

(146) Botros, S.; Lipkowski, A. W.; Takemori, A. E.; Portoghese, P. S. *J. Med. Chem.* **1986**, *29*, 874.

(147) Lankshear, M. D.; Cowley, A. R.; Beer, P. D. *Chem. Comm.* **2006**, 612.

(148) Bott, S.G.; Coleman, A.W.; Atwood, J. L. *J. Am. Chem. Soc.* **1986**, 108, 1709

(149) Facey, G. A.; Dubois, R. H.; Zakrzewski, M.; Ratcliffe, C. I.; Atwood, J. L.; Ripmeester, J. A. *Supramolecular Chemistry* **1993**, *1*, 199.

(150) Ripmeester, J. A.; Ratcliffe, C. I.; Enright, G.; Brouwer, E. *Acta Crystallogr., Sect. B. Struct. Science* **1995**, *51*, 513.

(151) Enright, G.; Brouwer, E.B.; Udachin, C.; Ratcliffe, I.; Ripmeester, J. *Acta Crystallogr., Sect. B.* **2002**, B58, 1032.

(152) Ripmeester, J. A.; Enright, G. A.; Ratcliffe, C. I.; A., U. K.; Moudrakovski, I. L. *Chem. Commun.* **2006**, 4986.

(153) Brouwer, E.; Enright, G.D.; Ripmeester, J.A. *Supramol. Chem.*, **1996**, 7, 143

(154) Benevelli, F.; Kolodziejski, W.; Wozniak, K.; Klinowski, J. *Phys. Chem. Chem. Phys.* **2001**, 3, 1762

(155) Udachin, K. A.; Enright, G. D.; Ratcliffe, C. I.; Ripemeester, J. A. *ChemPhyChem* **2003**, *4*, 1059.

(156) Schatz, J.; Schildbach, F.; Lentz, A.; Rastatter, S. *J. Chem. Soc., Perkin Trans. 2* **1998**, 75.

(157) Perrin, M.; Gharnati, F.; Oehler, D.; Perrin, R.; Lecocq, S. *J. Inclus. Phenom. Mol.* **1993**, *14*, 257.

(158) Atwood, J. L.; Barbour, L. J.; Jerga, A. *Chem. Comm.* **2002**, 2952.

(159) Dalgarno, S. J.; Thallapally, P. K.; Barbour, L. J.; Atwood, J. L. *Chem. Soc. Rev.* **2007**, *36*, 236.

(160) Wu, X.L. and Zilm, K. W. *J. Magn. Reson.*, Ser. A **1993**, 102, 205

(161) Wu, X.L. and Zilm, K. W. *J. Magn. Reson.*, Ser. A **1993**, 104, 119

(162) Dimeo, R. M. *Am. J. Phy.* **2003**, *71*, 885.

(163) Dimeo, R. M.; Neumann, D. A. *Phys. Rev. B (Condensed Matter)* **2001**, *63*, 014301/1.

(164) Prager, M.; Kirstein, O.; Johnson, M. R.; Parker, S. F. *J. Chem. Phys.* **2002**, *117*, 1313.

(165) Prager, M.; Ibberson, R. M. *Acta Crystallogr., Sect. B: Struct. Sci.* **1995**, *51*, 71.

(166) Trevino, S. F.; Choi, C. S.; Neumann, D. A. *J. Chem. Phys.* **1993**, *98*, 78.

(167) Trevino, S. F.; Prince, E.; Hubbard, C. R. *J. Chem. Phys.* **1980**, *73*, 2996.

(168) Arena, G.; Contino, A.; Longo, E.; Spoto, G.; Arduini A.; Pochini, A.; Secchi, A.; Massera, C and Ugozzoli, F. *New. J. Chem.* **2004**, 28, 56.

(169) Abramson, J. Image used with permission

(170) Henderson, P. J. F.; Marsh, D. *Biochim. Biophys. Acta* **2001**, *1510*, 464.

(171) Henderson, P. J. F.; McDonald, P. *Biochem, J.* **2001**, *353*, 709.

(172) Griffiths, D. G.; Partis, M. D.; Sharp, R. N.; Beechey, R. B. *Febs Letters* **1981**, *134*, 261.

(173) Ben Sdira, S.; Felix, C.; Giudicelli, M. B.; Vocanson, F.; Perrin, M.; Lamartine, R. *Tetrahedron Lett.* **2005**, *46*, 5659.

(174) Maggini, M.; Scorrano, G.; Prato, M. *J. Am. Chem. Soc.* **1993**, *115*, 9798.

(175) Herrmann, A.; Diederich, F.; Thilgen, C.; Meer, H.-U.; Muller, W. H. *Helv. Chim. Acta* **1994**, *77*, 1689.

(176) Wilson, S. R.; Lu, Q. J. *J. Org. Chem.* **1995**, *60*, 6496.

(177) Hirsch, A.; Bettreisch, M. Fullerenes, **2005**, Wiley-VCH: Weinheim

(178) Saunders, M.; Jimenez-Vazquez, H. A. *Science* **1993**, 259, 1428

(179) Saunders, M.; Cross, R. J.; Jimenez-Vazquez, H. A.; Shimshi, R.; Khong, A. *Science* **1996**, 271, 1693

(180) Murata, Y.; Murata, M.; Komatsu, K. *J. Am. Chem. Soc.* **2003**, *125*, 7152.

(181) Komatsu, K.; Murata, M.; Murata, Y. *Science* **2005**, *307*, 238.

(182) Murata, M.; Murata, Y.; Komatsu, K. *J. Am. Chem. Soc.* **2006**, 128, 8024.

(183) Toda, F.; Tanaka, K.; Tsukada, H.; Shimanouchi, H.; Sasada, Y. *Chem. Lett.* **1979**, 1381.

(184) Rubin, Y. *Chem. Eur. J.* **1997**, *3*, 1009.

(185) Chuang, S. C.; Murata, M.; Murata, Y.; Komatsu, K. *J. Org. Chem.* **2007**, 72, 6447.

(186) Sawa, H.; Wakabayashi, Y.; Murata, Y.; Murata, M.; Komatsu, K. *Angew. Chem., Int. Ed.* **2005**, 44, 1981

(187) Strata Ltd Image used with permission

(188) Staniski, C. M.; Cross, R. J.; Saunders, M.; Murata, M.; Murata, Y.; Komatsu, K. *J. Am. Chem. Soc.* **2005**, 127, 299

(189) Nelson, C.; McCabe, P. H. *Tetrahedron Lett.* **1978**, 19, 2819.

(190) Kobayashi, K.; Mutuai, K. *Tetrahedron Lett.* **1981**, 22, 5201.

(191) McMurry, J. E. *Chem. Rev.* **1989**, 89, 1513.

(192) Mukaiyama, T.; Sato, T.; Hanna, J. *Chem. Lett.* **1973**, 1041.

(193) D. Yu, D.; Forman, B. M. *J. Org. Chem.* **2003**, 68, 9489.

(194) Syamala, M. S.; Cross, R. J.; Saunders, M.; Tanaka, N. *J. Am. Chem. Soc.* **2002**, 124, 6216.

(195) Yamamoto, K.; Saunders, M.; Khong, A.; Cross, R. J.; Grayson, M.; Gross, M. L.; Benedetto, A. F.; Weisman, R. B. *J. Am. Chem. Soc.* **1999**, 121, 1591.

(196) Carravetta, M.; Danquigny, A.; Mamone, S.; Cuda, F.; Johannessen, O. G.; Levitt, M. H.; Heinmaa, I.; Stern, R.; Grossel, M. C.; Samoson, A.; Murata, Y.; Murata, Y.; Komatsu, K.; Levitt, M.H. *J. Chem. Phys.* **2006**, *124*.

(197) Mamone, S.; Ge, M.; Huvonen, D.; Nagel, U.; Danquigny, A.; Cuda, F.; Maltsev, S.; Grossel, M. C.; Murata, Y.; Murata, Y.; Komatsu, K.; Levitt, M. H.; Room, T.; Carravetta, M. *J. Chem. Phys.* **2009**, 130, 081103.

(198) Carravetta, M.; Danquigny, A.; Mamone, S.; Cuda, F.; Johannessen, O. G.; Heinmaa, I.; Panesar, K.; Stern, R.; Grossel, M. C.; Horsewill, A. J.; Samoson, A.; Murata, Y.; Murata, Y.; Komatsu, K.; Levitt, M.H. *J. Chem. Chem. Phys.* **2007**, 9, 4879.

(199) Herzberg, G, *Molecular Spectra and Molecular Structure, I. Spectra od Diatomic Molecules*, 2nd ed. Van Nostrand, Princeton, **1950**

(200) Allin, E. J.; Hare, F. J.; MacDonald, R. E. *Phys. Rev.* **1955**, 98, 554.

(201) Hare, W. F. J.; Allin, E. J.; Welsh, H. L. *Phys. Rev.* **1955**, 99, 1887.

(202) Hourahine, B.; Jones, R. *Phys. Rev. B* **2003**, 67, 121205.

(203) FiztGerald, S. A.; Forth, S.; Rinkoski, M. *Phys. Rev. B* **2002**, 65, 140302.

(204) FiztGerald, S. A.; Churchill, H. O. H.; Korngut, P. M.; Simmons, C. B.; Strangas, Y. E. *Phys. Rev. B* **2006**, 73, 155409.

(205) Herman, R. M.; Lewis, J. C.; *Phys. Rev.* **2006**, 73, 155408.

(206) Kudian, A.; Welsh, M. *J. Can. J. Phys.* **1971**, 49, 230.

(207) McKellar, A. R. W.; Welsh, H.L. *J. Can. J. Phys.* **1974**, 52, 1082.

(208) Chen, E. E.; Stavola, M.; Fowler, W. B.; Walters, P. *Phys. Rev. Lett.* **2002**, 88, 105507.

(209) Oka, T. *Annu. Rev. Phys. Chem.* **1993**, 44, 299.